

Reconstructions of Neotropical Hydroclimate: A Compound-Specific Deuterium Isotope Approach.

Thesis submitted for the degree of

Master of Philosophy

At the University of Leicester

By

Genevieve Tyrrell

School of Geography, Geology and the Environment

University of Leicester

2019

Abstract

Reconstructions of Neotropical Hydroclimate: A Compound-Specific Deuterium Isotope Approach.

Genevieve Tyrrell.

The hydrogen isotope composition of leaf wax (δD_{wax}) has been found to successfully record the isotopic composition of precipitation (δD_{p}) and as a result has been used extensively in palaeohydrological research. Although widely applied across the globe, δD_{wax} records remain scarce within the tropics, most specifically in northern South America. To resolve this gap in the literature, the δD_{wax} values of three sediment cores obtained from Colombia – two from the Amazon Basin and the third from the high-altitude Páramo ecosystem of the Andes - were analysed to reconstruct past rainfall in northern South America. In the Amazonian sites, microbial degradation limited the extent of palaeohydrological data obtained from the cores, providing a precipitation record for the past ~2000 years. The records showed increased precipitation during the Little Ice Age and Medieval Climate Anomaly, contradicting other northern South American records. In contrast, the high-Andean δD_{wax} record spanned ~85,000 years. δD_{wax} values decrease by ~4‰ during the Last Glacial Maximum suggesting the rainfall slightly increased during this time. Additionally, δD_{wax} during the Younger Dryas increased suggesting a slight reduction in precipitation. δD_{wax} values indicate the climate became progressively drier throughout the early-to-mid-Holocene, with the highest δD_{wax} occurring at 4200 cal yr BP (the 4.2 event). This was then followed by a dramatic reduction in δD_{wax} into the Late Holocene, before increasing again into the youngest 2000 cal yr BP of the record. Interestingly, higher precipitation, inferred through a decrease in δD_{wax} , coincides with a southward displacement of the ITCZ during the LGM and the LIA. The records suggest that, in northern South America, ITCZ movements may not be the sole cause of changes in precipitation.

Acknowledgments

First and foremost, I would like to thank my supervisors Arnoud Boom and Andy Carr for their continued support throughout the MPhil, reading and rereading drafts of the thesis, and explaining isotope theory (multiple!) times to ensure I fully understood the research. You both have made me feel like I am than capable of completing a research project, even when I do not believe it myself, and even if I have not said this, you have made the MPhil an enjoyable and (mostly!) stress-free process!

Thanks to Bill Hickin for employing me throughout the MPhil. I am so grateful, and have really appreciated your support, kindness and humour over the last 18 months.

To the tearoom crew - Gemma, Kerry, Lisa, Hayley and Gary. I really needed all the random discussions and laughter at lunchtime. Also massive thanks to my office colleagues – Pengyuan, Ahmed, Mohammed, Natalia and Chris. It has been so lovely to share a workspace with you all.

Lastly and most importantly I wish to thank my family (Mum, Dad, Madelaine, Murphy) and Krishna for their constant emotional and financial support throughout the MPhil. I would dedicate the thesis to you, but I know you won't read it!

Table of Contents

| | |
|---|------|
| Abstract..... | ii |
| Acknowledgments..... | iii |
| List of Figures..... | vii |
| List of Tables..... | xii |
| List of Abbreviations..... | xiii |
| List of definitions..... | xv |
| Chapter 1: Introduction..... | 1 |
| Chapter 2: Literature Review..... | 3 |
| 2.1 The Importance of Stable Isotopes..... | 3 |
| 2.1.1. Stable Isotopes – An Overview..... | 3 |
| 2.1.2. Fractionation..... | 4 |
| 2.1.3. The Stable Isotopes of Water..... | 5 |
| 2.1.4. Isotopes in Tropical South America..... | 9 |
| 2.1.5 Conclusions..... | 11 |
| 2.2. Isotopes in South American Paleoclimate Studies..... | 11 |
| 2.2.1 The Last Glacial Maximum (LGM)..... | 12 |
| 2.2.2 Younger Dryas (YD)..... | 13 |
| 2.2.3 Dansgaard-Oeschger (D/O) and Heinrich Events..... | 14 |
| 2.2.4 The Holocene..... | 15 |
| 2.2.5 The Medieval Climate Anomaly (MCA) and the Little Ice Age (LIA)..... | 16 |
| 2.2.6 Limitations and Conclusions..... | 17 |
| 2.3. Leaf Wax <i>n</i> -Alkanes as a Paleoclimatic Proxy..... | 19 |
| 2.3.1. Leaf Wax Structure and Use..... | 19 |
| 2.3.2. <i>n</i> -alkanes..... | 20 |
| 2.3.2.1. Using <i>n</i> -alkanes in scientific study – taxonomic indicators or environmental biomarkers?..... | 21 |
| 2.3.2.2. Characterising distributions within <i>n</i> -alkanes..... | 23 |
| 2.4 Hydrogen Isotopes in Leaf Wax..... | 27 |
| 2.5. The use of <i>n</i> -alkanes in Palaeohydrological Research..... | 31 |
| 2.5.1 Conclusions..... | 34 |
| Chapter 3: Materials and Methods..... | 35 |
| 3.1. San Pedro de Tipisca – Aguajal Agua Blanca and Aguajal del Loretillo..... | 36 |
| 3.1.1. Background..... | 36 |

| | |
|---|----|
| 3.1.2. Site Description | 36 |
| 3.1.3. Core Description | 41 |
| 3.2. Guatavita – Pantano de Martos..... | 43 |
| 3.2.1. Background | 43 |
| 3.2.2. Site Description | 43 |
| 3.2.3. Pantano de Martos Core | 45 |
| 3.3. Sample Preparation..... | 48 |
| 3.3.1 Radiocarbon Analysis | 48 |
| 3.4. Total Organic Carbon and Total Nitrogen Analysis | 48 |
| 3.5. Lipid Extraction..... | 49 |
| 3.5.1. Obtaining the lipid content of the sample | 49 |
| 3.5.2. Gas Chromatography Mass Spectrometry | 49 |
| 3.5.3. Deuterium Analyses..... | 50 |
| Chapter 4: Results..... | 51 |
| 4.1. Aguajal Agua Blanca..... | 51 |
| 4.1.1. Total Organic Carbon (TOC), Total Nitrogen (TN) and the TOC/TN Ratio..... | 51 |
| 4.1.2. Bulk Isotope Data - $\delta^{13}\text{C}$ and $\delta^{15}\text{N}$ | 52 |
| 4.1.3. Leaf wax <i>n</i> -alkane distributions | 53 |
| 4.1.4. Leaf wax <i>n</i> -alkane δD | 56 |
| 4.2. Aguajal del Loretillo..... | 58 |
| 4.2.1. Total Organic Carbon (TOC), Total Nitrogen (TN) and the TOC/TN Ratio..... | 58 |
| 4.2.2. Bulk Isotope Data - $\delta^{13}\text{C}$ and $\delta^{15}\text{N}$ | 59 |
| 4.2.3. Leaf wax <i>n</i> -alkane distributions | 60 |
| 4.2.4. Leaf wax <i>n</i> -alkane δD | 63 |
| 4.3. Pantano de Martos | 65 |
| 4.3.1 Total Organic Carbon (TOC), Total Nitrogen (TN) and the TOC/TN Ratio..... | 65 |
| 4.3.2. Bulk Isotope Data - $\delta^{13}\text{C}$ and $\delta^{15}\text{N}$ | 66 |
| 4.3.3. Leaf wax <i>n</i> -alkane distributions | 67 |
| 4.3.4. Leaf wax <i>n</i> -alkane δD | 71 |
| Chapter 5: Discussion. | 73 |
| 5.1. TOC, TN, TOC/TN and the isotopic values of bulk organic matter ($\delta^{13}\text{C}$) | 73 |
| 5.1.1 TOC..... | 73 |
| 5.1.2. TN..... | 74 |
| 5.1.3. TOC/TN | 74 |

| | |
|---|-----|
| 5.1.4. Bulk $\delta^{13}\text{C}$ | 76 |
| 5.2. Leaf wax <i>n</i> -alkane distributions | 83 |
| 5.2.1. Leaf wax <i>n</i> -alkane distributions | 83 |
| 5.2.1.1. Carbon Preference Index (CPI)..... | 83 |
| 5.2.1.2. Average Chain Length (ACL) | 85 |
| 5.2.1.3. P_{aq} and Norm31 | 86 |
| 5.3. Leaf wax <i>n</i> -alkane δD | 90 |
| 5.3.1 Leaf wax origin and reliability in palaeohydrological reconstruction | 90 |
| 5.3.2. Water source..... | 91 |
| 5.4. Interpreting the $\delta\text{D}_{\text{wax}}$ record - Aguajal Agua Blanca and Aguajal del Loretillo..... | 93 |
| 5.4.1. Aguajal Agua Blanca | 93 |
| 5.4.2. Aguajal del Loretillo | 94 |
| 5.3.2 Longevity of the records | 96 |
| 5.5. Interpreting the $\delta\text{D}_{\text{wax}}$ record - Pantano de Martos | 98 |
| 5.5.1. Ice volume correction on the Pantano de Martos record | 98 |
| 5.5.2 Glacial climate variability | 103 |
| 5.5.3 Holocene climate variability | 104 |
| 5.6 Factors controlling the changes in precipitation | 108 |
| Chaper 6: Conclusions. | 111 |
| 6.1. Aguajal Agua Blanca and Aguajal del Loretillo | 111 |
| 6.2. Pantano de Martos | 112 |
| 6.3. Overall Conclusions | 113 |
| Appendix A – Age-depth modelling..... | 114 |
| Appendix B – Supplementary Pollen Data | 126 |
| References..... | 130 |

List of Figures

Figure 1. The morphology and chemistry of leaf epicuticular waxes through a) a diagram of the epidermal cells of intracellular and epicuticular wax and b) the structure of long-chain *n*-alkanes and fatty acids which are typical compounds found within terrestrial higher plants. Taken from Eley and Hren (2018).

Figure 2. The relative abundance of *n*-alkanes from a) fresh plants and b) soils taken from Howard et al. (2018). The results are displayed as an average percentage for each chain length, with the error bars representing standard deviation.

Figure 3. The net apparent fractionation for a) *Eriophorum vaginatum*, a C₃ monocot and b) *Betula nana* a C₃ shrub. Taken from Daniels et al. (2017).

Figure 4. Map showing South America and also the locations of Pantano de Martos, Aguajal Agua Blanca and Aguajal del Loretillo – the three records used in this study within Colombia.

Figure 5. The location of the Tipisca cores Aguajal Agua Blanca and Aguajal del Loretillo. Map includes information regarding the proximity to the Rio Loretoyacu and the forest types found close to the palm swamp.

Figure 6. The Loretoyacu River close to where both Aguajal Agua Blanca and Aguajal del Loretillo were sampled.

Figure 7. The closed canopy environment of where the cores were sampled.

Figure 8. The environment where the cores were obtained. Note the large amounts of organic matter on the ground, originating from the surrounding vegetation.

Figure 9. Combined image displaying the Aguajal Agua Blanca core.

Figure 10. Combined image displaying the Aguajal del Loretillo core.

Figure 11. The Location of the Pantano de Martos core, with reference to Bogota and the Cordillera Oriental

Figure 12. The location of the Pantano de Martos core.

Figure 13. Local vegetation where the core was sampled. Note, the top of the core was obtained from a blanket of *Sphagnum* moss.

Figure 14. Combined image of the Pantano de Martos core, taken in 50 cm increments.

Figure 15. Down-core trends in total organic carbon (TOC), nitrogen (TN) and the TOC/TN ratio for Aguajal Agua Blanca.

Figure 16. Down-core trends in $\delta^{13}\text{C}$ and $\delta^{15}\text{N}$ for Aguajal Agua Blanca obtained by elemental analysis.

Figure 17. *n*-alkane distributions for a) -90 cal yr BP (0 cm), b) 246 cal yr BP (48 cm) and c) 535 cal yr BP (90 cm) of the Aguajal Agua Blanca core.

Figure 18. The average chain length (ACL_{23-33}) and the carbon preference index (CPI_{23-33}) for Aguajal Agua Blanca.

Figure 19. The P-aqueous (P_{aq}) ratio and Norm31 values for Aguajal Agua Blanca.

Figure 20. δD values for the C_{27} , C_{29} and C_{31} *n*-alkanes for the Aguajal Agua Blanca core.

Figure 21. Down-core trends in total organic carbon, nitrogen and the TOC/TN ratio for Aguajal del Loretillo.

Figure 22. Down-core trends in $\delta^{13}\text{C}$ and $\delta^{15}\text{N}$ for Aguajal del Loretillo obtained by elemental analysis.

Figure 23. *n*-alkane distribution graphs for samples at a) 84 cal yr BP and b) 2400 cal yr BP

Figure 24. The average chain length (ACL_{23-33}) and the carbon preference index (CPI_{23-33}) for Aguajal del Loretillo.

Figure 25. The P-aqueous (P_{aq}) ratio and Norm31 values for Aguajal del Loretillo.

Figure 26. The $\delta\text{D}_{\text{wax}}$ values for the C_{27} , C_{29} and C_{31} *n*-alkanes obtained from the Aguajal del Loretillo core.

Figure 27. Total organic carbon (TOC), total nitrogen (TN) and the TOC/CN ratio for the Pantano de Martos core.

Figure 28. Down-core trends in the $\delta^{13}\text{C}$ and $\delta^{15}\text{N}$ for the Pantano de Martos core

Figure 29. *n*-alkane distributions for samples a) 0cm, b) 50cm, c) 100cm, d) 150cm, e) 178cm and f) 198cm (-348, 440, 13,000, 29,500, 39,800 and 44,800 cal yr BP).

Figure 30. Down core trends in the average chain length (ACL_{23-33}) and the carbon preference index (CPI_{23-33}) of the Pantano de Martos core.

Figure 31. *n*-alkane distributions for the samples with the highest (a) and lowest (b) CPI_{23-33} values at 7000 cal yr BP and 21,000 cal yr BP respectively.

Figure 32. The P-aqueous (P_{aq}) ratio and Norm31 ($C_{31} / (C_{31} + C_{29})$) for the Pantano de Martos core.

Figure 33. δD measurements for the C_{27} , C_{29} and C_{31} n-alkanes in Pantano de Martos core.

Figure 34. TOC/TN vs. $\delta^{13}C$ diagram, taken from Sifeddine et al (2004).

Figure 35. TOC/TN vs. $\delta^{13}C$ diagram for a) Aguajal Agua Blanca and, b) Aguajal del Loretillo. Clusters of samples are grouped into algae, C_3 land plants and C_4 land plants.

Figure 36. Bulk $\delta^{13}C$ values and TOC/TN against age for the Aguajal Agua Blanca core. Figure 34a depicts the clusters of samples within the Aguajal Agua Blanca core. Combining the parameters with the age of the core shows that the samples that fall into the algae cluster of samples occur at ~600 cal yr BP until the end of the core. Therefore, it is suspected that from this point, the source of organic matter within the sediment is not of C_3 , or even possible terrestrial origin.

Figure 37. Bulk $\delta^{13}C$ values and TOC/TN against age for the Aguajal del Loretillo core. TOC/TN values throughout the core suggest an algal source of organic matter, however bulk $\delta^{13}C$ values, when considered independently, suggest a terrestrial source of OM. From ~2400 cal yr BP, OM content of the core becomes extremely low, therefore low TOC/TN values could be due to the small amount of sample.

Figure 38. TOC/TN vs. $\delta^{13}C$ diagram for Pantano de Martos.

Figure 39. Bulk $\delta^{13}C$ values and TOC/TN against age for the Pantano de Martos core. Throughout the core both parameters track each other. Bulk $\delta^{13}C$ values remain within terrestrial C_3 vegetation throughout the core. TOC/TN values suggest a terrestrial source of OM throughout the core, except between 12-18,000 cal yr BP where TOC/TN fall slightly below the boundary of terrestrial material.

Figure 40. Combined figure displaying the P_{aq} and ACL_{23-33} values for the Pantano de Martos core.

Figure 41. Norm31 vs. P_{aq} for the Pantano de Martos core.

Figure 42. Norm31 vs. P_{aq} for a) Aguajal Agua Blanca and b) Aguajal del Loretillo.

Figure 43. Bird et al. (2011) $\delta^{18}O_{calcite}$ record from Lake Pumacocha, Peru.

Figure 44. Reuter et al. (2009) $\delta^{18}O$ stalagmite (speleothem) record obtained Cascayunga Cave, Peru.

Figure 45. Summary pollen diagram of the four ecological groups found in the Aguajal Agua Blanca core. For a more detailed diagram of the most frequent taxa identified in the core, including the percentage pollen abundance see appendix. Palynological data obtained from Berrio, unpublished data.

Figure 46. Martinson Stack record converted into δD to provide an easier comparison to the Pantano de Martos core. Data obtained from Martinson et al (1987).

Figure 47. The normalised (raw) deuterium data and the ice volume corrected deuterium data for the Pantano de Martos core.

Figure 48. The normalised and ice corrected δD record for Pantano de Martos, highlighting some of the key events occurring within the record.

Figure 49. The paleorecords used as a comparison against the Pantano de Martos core. From top to bottom: Van Breukelen et al. (2008) stalagmite record from Cueva del Tigre Perdido, Peru. Thompson et al. (1995) $\delta^{18}O$ record from Huascarán ice core, Peru. Kanner et al. (2012) Stalagmite record from Pacupahuain Cave, Peru. Mosblech et al. speleothem record from Santiago Cave, Ecuador. Fornace et al. (2014). Leaf wax n-alkane δD record from Lake Titicaca, Bolivia.

Figure 50. The Average position of the ITCZ over South America in austral winter (July) and summer (January). Taken from Tedesco et al. (2007).

Figure A1a & A1b. Bacon-derived age depth model for Aguajal Agua Blanca using; a) all the radiocarbon data and b) selected radiocarbon dates (removed suspected outlier).

Figure A2. Bacon-derived age-depth model for Aguajal del Loretillo using all the conventional radiocarbon ages obtained.

Figures A3a and A3b. Bacon-derived age-depth model using a) all conventional radiocarbon ages and b) selected radiocarbon ages where the outliers have been removed for the Pantano de Martos core.

Figure A4. Age-depth model from Parnell et al's (2008) study on Northern European Holocene pollen records (from Blaauw and Christen, 2011). In this example, the dates shown in red were classed as outliers and were rejected from the study.

Figure B1. Percentage pollen diagram for Aguajal Agua Blanca displaying 28 of the most frequent taxa identified from the Aguajal Agua Blanca core. Source: Berrio, unpublished data.

Figure B2. The ecological groups obtained from pollen data for the Pantano de Martos core.

Source: Berrio, unpublished data.

List of Tables

Table 1: the isotopic abundance of the five most commonly applied stable isotopes: carbon, hydrogen, nitrogen, oxygen and sulphur. Taken from fry, (2006).

Table 2. The relative volume and typical δD and $\delta^{18}O$ values for the hydrospheric reservoirs. Taken from Criss (1999).

Table 3. The correlation coefficients for the δD_{wax} values of the C_{27} vs. C_{29} , C_{27} vs. C_{31} and C_{29} vs. C_{31} for Aguajal Agua Blanca.

Table 4. The correlation coefficients for the δD_{wax} values of the C_{27} vs. C_{29} , C_{27} vs. C_{31} and C_{29} vs. C_{31} for Aguajal del Loretillo.

Table 5. The correlation coefficients for the δD_{wax} values of the C_{27} vs. C_{29} , C_{27} vs. C_{31} and C_{29} vs. C_{31} for Pantano de Martos.

Table 6. The highest, lowest and average δD_{wax} values for Aguajal Agua Blanca, Aguajal del Loretillo and Pantano de Martos cores.

Table 7. Hydrogen isotope fractionation within water. Taken from Mook (2001).

Table A1. Radiocarbon ages and calibrated ages for Aguajal Agua Blanca. Calibration was conducted using Calib v.7.1 using the Intcal13 calibration curve. The radiocarbon date at 120cm is highlighted in red due to the age being ~1000 years older than the age below. As a result, it was decided to remove this date from the age-depth model.

Table A2. Radiocarbon ages produced for the Aguajal del Loretillo core

Table A3. The conventional radiocarbon ages associated with the age-depth model for the Pantano de Martos core. Highlighted in red are the suspected problematic ages that deviate from the trend shown by the rest of the radiocarbon ages.

Table B1. Pollen groups (%) for the Tipisca core Aguajal Agua Blanca. Source: Berrio, unpublished data.

List of Abbreviations

AAO – Antarctic Oscillation

ACL – Average Chain Length

AISA - Absolute International Standard Activity

Al₂O₃ – Aluminium Oxide

AMOC - Atlantic Meridional Overturning Circulation

asl – Above sea level

Cal yr BP – Calibrated age in years before present

CH₄ – Methane

CO₂ – Carbon dioxide

CPI – Carbon Preference Index

DCM - Dichloromethane

D/O – Dansgaard-Oeschger Events

ENSO – El-Niño Southern Oscillation

GC-MS – Gas Chromatography-Mass Spectrometry

GMWL – Global Meteoric Water Line

GNIP – Global Network of Isotopes in Precipitation

H₂O – Water (vapour)

IAEA - International Atomic Energy Agency

IPCC - Intergovernmental Panel on Climate Change

IRMS – Isotope Ratio Mass Spectrometry

ITCZ – Intertropical Convergence Zone

LGM – Last Glacial Maximum

LIA – Little Ice Age

m – Metre(s)

mm – Millimetre(s)

MCA – Medieval Climate Anomaly

MeOH - Methanol

NAO – North Atlantic Oscillation

P_{aq} – P-aqueous ratio

PDO – Pacific Decadal Oscillation

SASM – South American Summer Monsoon

SST – Sea surface temperatures

TOC – Total Organic Carbon

TN – Total Nitrogen

VSMOW – Vienna Standard Mean Ocean Water

YD – Younger Dryas

List of definitions

δD_p – The δD values of precipitation

δD_{wax} – The δD values obtained from leaf-wax *n*-alkanes

Apparent Fractionation (ϵ_{app}) – the relationship to describe the difference in δD values between δD_{wax} and δD_p .

Average Chain Length – the average number of carbon atoms per molecule in higher plants (Poynter and Eglington, 1990).

Carbon Preference Index – Captures the degree to which odd carbon number alkanes dominate over even carbon numbers and is used as an indication of the alkane source (Marzi et al, 1993).

Dansgaard-Oeschger (D/O) events - abrupt warmings, known as interstadials, followed by more gradual cooling to stadial conditions (Kanner et al, 2012).

Heinrich events - cold intervals lasting $\sim 500 \pm 250$ years that are primarily characterised by the presence of massive layers of ice-rafted debris (IRD) in the North Atlantic (Heinrich, 1988; Bond et al, 1992).

Isotopologue – A molecular entity that differs only in isotopic composition.

Meteoric – relating to or denoting water derived from the atmosphere by precipitation or condensation.

Norm31 - the ratio between the longer C_{29} and the C_{31} alkanes and is thought to be an environmentally sensitive parameter (Carr et al, 2015)

Páramo – a diverse vegetation zone occurring in high-altitudes. In South America specifically, areas of páramo vegetation are located in the humid tropical Andes Mountains and occur as an altitudinal belt between the uppermost forests and perennial snow (Cleef, 1981)

P_{aq} – characterises the relative proportion of mid-chain length (C_{23} - C_{25}) versus the long-chain length (C_{27} , C_{29}) homologues, which expresses the relative input of submerged /floating aquatic macrophytes versus terrestrial plant input (Damsté et al, 2011).

TOC/TN – the ratio of total organic carbon to total nitrogen within a sample

Chapter 1: Introduction

Climate patterns have changed throughout the earth's history, therefore to understand the present change in climate it is imperative to look at climate and its changes in the past. Since the 1800s most of these changes have been attributed to anthropogenic influences (Hoyos et al, 2013). Over the last century alone, the global average temperature has risen by 0.74°C (Arguez, 2007), with expected increases in temperature of up to 7°C by the end of the century (Stocker, 2013). Globally, these changes in climate are affecting the economy, ecosystems and human populations. One of the major influences of these climatic changes is due to the role atmospheric water plays in the generation of sources and sinks of heat, and how it modulates the exchange of both solar and terrestrial radiation (Labraga et al, 2000). Although still uncertain, changes to the hydrological cycle will occur with a changing climate. It has been predicted that annual snowmelt will occur much earlier on in the season and snowfall will become rainfall, both of which will cause substantial changes in the volume and timing of spring floods (IPCC, 2001). These changes will then have a strong influence on ecosystem functioning.

Of significant importance is the Amazon Basin. The Amazon Basin is a major centre of atmospheric precipitation and convection, providing the main source of heat and water that regulates the global climate system (Garcin et al, 2012). It is the world's largest drainage basin, with approximately 17% of the annual global discharge into the oceans originating from the Amazon River (Brienen et al, 2012). The Amazon Basin is also one of the most species rich areas on earth (Foley et al, 2002), containing ~50% of the world's undisturbed tropical forest (Mellio et al, 1996) and supporting 60% of all plant and animal species (Dirzo and Raven, 2003). As a result, the hydrological cycle is tightly coupled to the carbon cycle of the Amazon rainforest which further reinforces its importance when taking into consideration the fact that ~30% of global vegetation carbon stocks are stored in Amazonian forests (Viera et al, 2004).

Changes in the hydrological cycle of the Amazon therefore have a direct impact on atmospheric dynamics through altering atmospheric CO_2 concentrations (Brienen et al, 2012). Over the last decade alone, the Amazon has suffered two severe droughts (Marengo et al, 2011; Zeng et al, 2008), suggesting that the hydrological cycle is already undergoing changes. Whether this is due to anthropogenic influences or whether this can be attributed to longer-term natural climate variability is still under debate. Understanding these feedbacks is also imperative when

thinking about the effects on a global scale. Life and vegetation are dependent on the availability of water. As the tropics are the global centre of moisture transport, supplying low-latitude continental regions with water, understanding tropical hydrological changes is vital (Schefuss et al, 2005).

One way of understanding these feedbacks is through understanding the characteristics and forcing's of past climatic changes. Across South America, meteorological data taken from weather stations are available for current precipitation records, however these tend to be only reliable for the past 60 years (Costa et al, 2009 in Brienen et al, 2012). This has therefore created demand for long-term proxy records of climatic change. One of the most interesting methods of understanding such changes is through the analyses of stable isotopes. Multiple studies have applied stable isotopes across South America to reconstruct past climate changes through ice cores (Hoffman et al, 2003; Jouzel et al, 1987; Petit et al, 1999), tree rings (Brienen et al, 2012), speleothem records (Kanner et al, 2012; Reuter et al, 2009) and lacustrine sediments (Baker et al, 2001; Bird et al, 2011).

Most recently, compound-specific δD analysis of sedimentary lipids, in particular leaf-wax *n*-alkanes, have created a new opportunity in palaeohydrological research. *n*-alkanes derive from the epicuticular layer of terrestrial higher plants and are used in paleoclimate reconstruction as they have been found to record the hydrogen isotopic composition of precipitation (Feakins et al, 2016b; Schefuss et al, 2005). They are ubiquitous in the environment and can survive within the geological record for millions of years (Tierney et al, 2013), making their application in palaeohydrological research flexible globally. Even so, calibration studies for sedimentary *n*-alkane δD tend to only be available for mid-to-high latitudes (Aichner et al, 2010; Xia et al, 2008), and originate from marine records (marine cores). Recent developments in the use of the δD values of *n*-alkanes have begun in the tropics, however this is mainly in tropical Africa (Schefuss et al, 2005) and regions of southern South America (Fornace et al, 2014, 2016). Within northern South America, climate records remain scarce (Brienen et al, 2012; Polissar et al, 2006).

Consequently, this thesis aims to apply compound specific δD analysis of leaf-wax *n*-alkanes in northern South America, an area lacking in paleoenvironmental archives. Palaeohydrological analysis will focus on two locations within Colombia – the Amazon Basin and the high-altitude Páramo region of the Colombian Andes. As climate proxies within these areas are scarce, it is hoped that these records will produce novel insight into long-term palaeohydrological changes within two regions of both climatic and biodiversity importance.

Chapter 2: Literature Review.

2.1 The Importance of Stable Isotopes

2.1.1. Stable Isotopes – An Overview

Stable isotopes are naturally occurring forms of elements that contain different nuclear masses and therefore exhibit some different physical properties (Rubenstein and Hobson, 2004). In environmental research, the most widely applied stable isotopes are carbon (^{13}C), hydrogen (^2H), nitrogen (^{15}N), oxygen (^{18}O), and sulphur (^{34}S). Isotopes of elements have almost identical properties, but due to mass differences, they behave differently during some physical, chemical and biological processes. The resulting changes in isotope ratios therefore impart a specific environmental signal (McCarroll and Loader, 2004). Isotopes of a molecular entity are known as isotopologues (IUPAC, 1997). As they do not undergo radioactive decay, stable isotopes provide a way to trace aspects of element cycling, and can function as natural tracers in the environment (West et al, 2006).

Table 3: The isotopic abundance of the five most commonly applied stable isotopes: carbon, hydrogen, nitrogen, oxygen and sulphur. Taken from Fry (2006).

| Element | Relative Isotope Abundance (%) | |
|--|--------------------------------|-----------|
| | Low Mass | High Mass |
| Carbon ($^{12}\text{C}/^{13}\text{C}$) | 98.89 | 1.11 |
| Hydrogen ($^1\text{H}/^2\text{H}$) | 99.894 | 0.016 |
| Nitrogen ($^{14}\text{N}/^{15}\text{N}$) | 99.64 | 0.36 |
| Oxygen ($^{16}\text{O}/^{18}\text{O}$) | 99.76 | 0.20 |
| Sulphur ($^{32}\text{S}/^{34}\text{S}$) | 95.02 | 4.21 |

All isotopes are measured using mass spectrometry with the measured ratios quoted relative to those of international standards (Rubenstein and Hobson, 2004). These are expressed using delta notation (δ) in parts per thousand (‰) using the equation:

$$\delta = \left[\frac{R_{\text{Sample}}}{R_{\text{Standard}}} - 1 \right] \times 1000$$

Where R is the ratio of the heavy to light isotope (for example D/H, $^{18}\text{O}/^{16}\text{O}$ or $^{13}\text{C}/^{12}\text{C}$) (Flanagan et al, 1991). In the case of carbon this is expressed relative to the $^{12}\text{C}/^{13}\text{C}$ ratio of the Pee Dee Belemnite formation (ibid). Positive δ values signify an enrichment of the heavy isotope relative to that of the standard, while a negative value indicates depletion relative to the standard (Gat, 1996). Most δ values range between -100 and $+50\text{‰}$ for natural samples (the natural abundance range). The only exception is hydrogen, where δ measurements span a much broader range due to the high mass difference between isotopes. For atmospheric water, δD varies between -200 and $+100\text{‰}$ (Fry, 2006), with natural variation typically 250‰ (Mook, 2001).

2.1.2. Fractionation

The difference between the isotopic ratio of a substrate and a product is called isotopic fractionation. Fractionation occurs in all reactions and is expressed as Δ (Fry, 2006). In all elements, the strength of the chemical bonds involving different isotopes vary, with the lighter isotope having bonds that are weaker (Fry, 1996). A difference in the rate at which the bond is broken dictates how an isotope will behave in environmental processes, with the heavy isotopes favouring the part of the system where they are more strongly bound (Gat, 1996). There are two types of fractionation: kinetic and equilibrium.

Kinetic fractionation results from irreversible, physical or chemical unidirectional processes such as the evaporation of water. The effects of kinetic fractionation are dependent on the binding energy of the original compound (Mook, 2001), with the rate at which the bond is broken producing a (kinetic) isotope effect (Melander, 1960). During the evaporation of water, kinetic fractionation occurs at the same time as the withdrawal of the water vapour, preventing further contact with the water (Mook, 2001). Heavier isotopologues have a lower mobility and therefore a lower diffusion velocity. Additionally, their higher bonding energies mean that in kinetic reactions it is the lighter isotopes that usually react faster (Fry, 2006), tending to become concentrated in the product. As a result, the residual water molecules become isotopically enriched.

On the other hand, equilibrium fractionation occurs due to an isotope exchange mechanism (Mook, 2001). Equilibrium fractionations occur in closed, well-mixed systems at chemical equilibrium, where the potential energy is as low as possible. At a particular temperature, the ratios of the different isotopes are constant and therefore are in isotopic equilibrium (Kendall

and McDonnell, 1998). Within the environment, equilibrium reactions occur in processes such as the condensation of water vapour within rain clouds. During condensation the heavier isotopes become enriched in the liquid phase, whilst in the vapour phase, the lighter isotopes remain (*ibid*).

Raleigh fractionation is used to explain the fractional distillation of mixed liquids and describes the separation of isotopes between two reservoirs as one decreases in size (Sharp, 2007). Much of the variability within the isotopic values of precipitation and atmospheric vapour can be explained through Raleigh-type processes during condensation and evaporation. The Raleigh equation is used if material is continuously removed from a well-mixed system containing molecules of two or more isotopic species ($^2\text{H}/^1\text{H}$ or $^{16}\text{O}/^{18}\text{O}$) in chemical and isotopic equilibrium with one another. The fractionation accompanying the removal of a molecule is described by the fractionation factor (α) which remains unchanged during the removal process (Kendall and McDonnell, 1998). Raleigh fractionation is expressed:

$$(R/R^0) = (X/X^0)^{\alpha-1}$$

Where R is the ratio of the isotopes in the reactant, R^0 is the initial isotope ratio, X is the concentration of the more abundant (lighter) isotope (for example ^{16}O), X^0 is the initial concentration of such isotope and α is the fractionation factor (Gat, 1996; Kendall and McDonnell, 1998). Ideally, Raleigh fractionation should only be used for chemically open systems where the reactant reservoir is finite and well-mixed and does not re-react with the product (Clark and Fritz, 1997). However, ‘closed-system’ Raleigh fractionations occur, such as in the condensation of vapour to droplets within a cloud. During this process, the material removed from one reservoir accumulates in a second reservoir and isotopic equilibrium is maintained throughout the process (Gat and Gonfiantini, 1981).

2.1.3. The Stable Isotopes of Water

The isotopic composition of water can provide key insights into the strength and functioning of the hydrological cycle (Brienen et al, 2012). Isotopes of oxygen and hydrogen are applied extensively in hydrological studies. Their isotopic signatures vary along geographic gradients in a manner that is well understood in terms of the underlying fractionation processes (Ehleringer et al, 2008). Oxygen has three stable isotopes, with masses of 16, 17 and 18. In the case of hydrogen, there are two stable isotopes, protium (^1H or H) and deuterium (^2H or

δD), with deuterium having approximately twice the mass of protium (2.014102 to 1.007825 respectively (Criss, 1999)). Both isotopes are expressed in reference to the Vienna Standard Mean Ocean Water (VSMOW) when referring to water, ice and plant material (McCarroll and Loader, 2004).

Over the oceans, δD and $\delta^{18}O$ in atmospheric water vapour are fairly uniform, with almost all samples having $\delta^{18}O = 0 \pm 1\text{‰}$ and $\delta D = 0 \pm 5\text{‰}$ VSMOW (Craig and Gordon, 1965). Additionally, the δD and $\delta^{18}O$ concentrations differ in absolute value, but are usually comparable in ocean water (Friedman, 1953). However, it has been shown that the physical processes influencing the production, transportation and condensation of atmospheric water vapour cause large variations in the isotopic composition of meteoric water (Criss, 1999). Variations of δD and $\delta^{18}O$ in meteoric waters are strongly correlated but differ in magnitude (Gat, 1980). For δD , the natural range is approximately $+40\text{‰}$ to -500‰ (Dansgaard, 1964), and for $\delta^{18}O$, the total range is $\sim +4$ to -62‰ (Criss, 1999). In modern precipitation, these values closely conform to an empirical relationship known as the “meteoric water line” (Craig, 1961), expressed through the equation:

$$\delta(D) = 8\delta(^{18}O) + d$$

This describes the linear relationship between the isotopic compositions of precipitation across the globe (Kendall and McDonnell, 1998). This relationship originates from the oceans, which are the initial source of moisture and thus isotopic composition. Subsequent variation is adequately described through Rayleigh evaporation. As an air mass moves across a continent, the heavier isotope is preferentially lost through rainout, creating an air mass increasingly enriched in the lighter isotope (for further information see Craig, 1961; Craig and Gordon, 1965). The Global Meteoric Water Line (GMWL) slope of 8 is fixed by the equilibrium condensation of rain at $\sim 100\%$ humidity according to the Rayleigh paradigm (Kendall and McDonnell, 1998). The y intercept in the equation, d , is defined as the ‘deuterium excess’ parameter (Dansgaard, 1964), with the most common d -excess of 10‰ used in the GMWL, defined by the equation:

$$\delta(D) = 8\delta(^{18}O) + 10\text{‰}$$

(Craig, 1961). In vapour, the d -excess value is recognised as a tracer, as it is thought to reflect environmental conditions such as the relative humidity, wind speed and sea surface temperature where evaporation initially took place (Merliat and Jouzel, 1979). The precise value of the d -excess varies geographically, creating GMWLs with different slopes and intercepts in different

regions. For example, in the eastern Mediterranean, Gat and Carmi (1970) found that a d-excess value of +18 better reflected the precipitation of the region than the initial d-excess proposed by Craig (1961). Feakins et al (2016b) obtained a mean value of +7 from biweekly precipitation samples that across an elevation range in the eastern flanks of the Andes, Peru, with the local meteoric water line better characterised as $\delta D = 7.62 \delta^{18}O + 4.30\%$.

Table 4. The relative volume and typical δD and $\delta^{18}O$ values for the hydrospheric reservoirs. Taken from Criss (1999).

| Reservoir | Volume (%) | δD (‰) | $\delta^{18}O$ (‰) |
|-------------------------------------|-------------------|----------------------------------|--------------------------------------|
| Ocean | 97.2 | 0±5 | 0±1 |
| Ice caps and Glaciers | 2.15 | -230±120 | -30±15 |
| Freshwater Lakes | 0.017 | -50±60 | -8±7 |
| Saline lakes and inland seas | | -40±60 | -2±5 |
| River and stream channels | | -50±60 | -8±7 |
| Atmospheric water | 0.001 | -150±80 | -20±10 |

Both $\delta^{18}O$ and δD vary between different locations and environments at global and local scales (Gat, 1996; McCarroll and Loader, 2004). Slight differences in the mass of each isotope of water lead to differences in the saturation vapour pressure of the molecule (Moore et al, 2014). These changes lead to the heavier isotopologue to collect in the condensed phases whereas the lighter isotopologue accumulates in the vapour phase (*ibid*). These variations have served as invaluable guides in determining the source regions of meteoric waters, enabling the identification of different water masses and the tracing of their interrelationships (Bowen, 2008; Dansgaard, 1964; Gat, 1996; West et al, 2006).

Changes in $\delta^{18}O$ and δD have also allowed studies to deduce the relationships between isotopic variation and temperature, altitude, latitude, proximity to the ocean and amount of precipitation (Dansgaard, 1964). All precipitation originates from the tropical marine belt, and forms when a cooling process causes the initial precipitation (*ibid*). Due to fractionations during evaporation, D and ^{18}O in the resulting water vapour are depleted relative to the tropical marine belt source. As temperatures decrease, the atmosphere can store less water, which causes condensation to exceed evaporation (Hendricks et al, 2000). This results in greater effective

rainfall, causing the preferential release of the lighter isotopes and thus depleted isotopic values of precipitation (Dansgaard, 1964). This is known as the ‘temperature effect’, with the greatest influence found in the mid-to-high latitudes (Dansgaard, 1964; Rozanski et al, 1993). $\delta^{18}\text{O}$ rainfall studies show a decrease of $\sim 11\text{‰}$ ($0.50\text{‰}/^{\circ}\text{C}$) coinciding with warm-front cooling from 12°C to -8°C , therefore highlighting the influence of temperature on isotopic values (Dansgaard, 1953).

The ‘latitude effect’ describes the decrease in $\delta^{18}\text{O}$ and δD in precipitation with increasing latitude. This ‘latitude effect’ is attributed to the preferential removal of the heavier isotope during condensation, as precipitation is transported poleward and temperatures decrease (Dansgaard, 1964). Thus, in general, $\delta^{18}\text{O}$ and δD of precipitation are high near the equator and very low near the poles (Hendricks et al, 2000). In polar regions $\delta^{18}\text{O}$ can be as low as -50‰ (Mook, 2001).

The ‘altitude’ effect is also greatly influenced by temperature and describes the relative depletion in the heavier isotope as a cloud mass increases in altitude (Poage and Chamberlain, 2001). As described by the temperature effect, as a cloud increases in altitude, fractionation occurs alongside increased precipitation, therefore producing lower $\delta^{18}\text{O}/\delta\text{D}$ values in rainfall. This occurs in areas of orographic uplift (Dansgaard, 1964; Rozanski et al, 1993). For example, in the Sierra Nevada, Rose et al (1996) found that $\delta^{18}\text{O}$ values decreased by $\sim 2.3\text{‰}$ for every vertical kilometre increase.

Decreasing $\delta^{18}\text{O}$ and δD caused by air masses moving over land away from their oceanic source is caused by the preferential removal of isotopically enriched precipitation during rainout and is known as the ‘continental effect’ (Rozanski et al, 1993; Worden et al, 2007; Liu et al, 2010). Although this effect has been found to be more variable than the others described by Dansgaard (1964) (Criss, 1999), studies have found varying isotopic values with increasing distance away from the oceans. For example, across Eurasia, Ferronsky and Polyakov (1982) found $\delta^{18}\text{O}$ decreased by $\sim 0.3\text{‰}$ per 100 km of lateral distance from the source. Additionally, in a study of European precipitation, Rozanski et al. (1982) found that the inland gradient of δD values amounted to $-3.3\text{‰}/100$ km in winter and $\sim -1.3\text{‰}/100$ km in summer.

Finally, the ‘amount effect’ describes the decrease in δD and $\delta^{18}\text{O}$ of precipitation with increasing rainfall amount or rainfall intensity (Collins et al, 2013; Dansgaard, 1964; Risi et al, 2008; Moore et al, 2014). The amount effect is thought to be caused by the preferential removal of heavy isotopologues by rainout as clouds cool (Moore et al, 2014). As convection increases,

precipitation rate, average drop size and relative humidity in the downdrafts increase. As relative humidity increases, evaporation decreases. Typically, evaporation after raindrop formation enriches rainfall by preferentially removing the lighter isotopes. When evaporation decreases, rainfall is isotopically lighter, leading to the occurrence of the ‘amount effect’. This is especially apparent in heavy rainfall as large drops do not evaporate as significantly as smaller drops (Stewart, 1975). The amount effect is most pronounced during the rainy season in the tropics and mid-latitudes (Dansgaard, 1964; Worden et al, 2007) and appears clearly over tropical ocean locations (Collins et al, 2013; Kurita et al, 2009). Additionally, a strong amount effect is seen in regions where there is a seasonal transition to a rainy season (Kurita et al, 2009) and has been found to be increasingly pronounced during heavy storm events (Mook, 2001).

2.1.4. Isotopes in Tropical South America.

In the tropics, where the climate is seasonally moist, the amount effect has been found to be the most influential control on rainfall $\delta^{18}\text{O}$ and δD (Dansgaard, 1964). Using atmospheric general circulation models, Vuille et al (2003) found that in tropical South America, the amount effect influences $\delta^{18}\text{O}$ by approximately $-0.4\text{--}0.8\text{‰}$ per 100 mm increase in mean annual precipitation. In contrast, the temperature effect is negligible in South America (Vuille et al, 2003; Kurita et al, 2009; Bird et al, 2011). This is due to mean annual temperatures remaining consistent throughout the year, typically averaging $\sim 26^\circ\text{C}$ (Gat and Matsui, 1991). In an analysis of $\delta^{18}\text{O}$ data collected from multiple sources globally between 1960 to 2006, Bowen (2008) found that the transition from temperature to precipitation controlled isotopic content occurs at $\sim 30^\circ\text{N/S}$, suggesting that temperature in the tropics is not a dominant control on isotopic variation.

Across South America, the continental effect should have some influence on isotopic values, with the $\delta^{18}\text{O}$ and δD of vapour and precipitation becoming lower than their oceanic source (Dansgaard, 1964; Gat, 2000). However, Worden et al (2007) found continental vapour observations having higher isotopic values than their Atlantic Ocean source. In tropical South America, Gat and Matsui (1991) found that water recycling as a result of forest transpiration enriched precipitation relative to the ocean. However, Salati et al. (1979) found that the continental effect could be found within the Amazon Basin, but the inland gradient value was minimal at $\sim -0.6\text{‰}/100\text{ km}$. It is suspected that in environments such as the Amazon Basin,

where between 50% and 88% of total rainfall is due to vegetation-recycled precipitation (Lettau et al, 1979; Salati et al, 1979), evapotranspiration exerts the dominant control on rainfall isotopic composition (Victoria et al, 1991). Evapotranspiration is considered a non-fractionating process once a steady state in the leaf has been reached (Flanagan et al, 1991), and returns water back to the atmosphere that is of a similar isotopic composition to its source (rainwater) (Victoria et al, 1991). The isotopic composition of the rainwater is 'heavier' than the isotopic composition of the surrounding water vapour from which the rain came, meaning that as an air mass moves inland it will receive a constant input of isotopically heavier water from the rainforest as a result of evapotranspiration (*ibid*). This explains the contradictory findings of Salati et al. (1979) and Gat and Matsui. (1991).

However, it is also important to note that water evaporation from the forest canopy can also complicate this signal. Studies have found as much as 25% of the precipitation trapped on leaves is returned to the atmosphere through evaporation (Leopoldo et al. cited in Victoria et al, 1991). As fractionation occurs during evaporation, it is expected that isotopic values of precipitation will become lower than their source, returning isotopically lighter vapour back into the atmosphere. During years of high precipitation, the atmosphere will have an isotopic signal composed of the 'lighter' isotope (higher $\delta^{18}\text{O}/\delta\text{D}$), with precipitation having lower $\delta^{18}\text{O}/\delta\text{D}$ due to the combined effects of evaporation, transpiration and the amount effect (Lee and Fung, 2008). Because of this increased precipitation recycling over the Amazon basin, it is suggested that isotopic signatures will reflect multiple amount effects.

However, in the Andean Region isotopic values decrease with increasing altitude. Vimeux et al. (2011) studied a year-long based isotopic time series along the Zongo Valley in Bolivia ($16^{\circ}20'\text{S}$; $67^{\circ}47'\text{W}$), located on the north-eastern side of the Bolivian Cordillera Real. A common isotopic signature from the base to the top of the valley led to the conclusion that it is the same air masses that precipitate along the Andean slope, however isotopic values were found to decrease by approximately $-1.5\text{‰}/100\text{ m}$. Vimeux et al. (2005) also found a similar trend in the same area, with seasonal isotopic values between 1999-2004 producing an isotopic depletion of $-1.7\text{‰}/100\text{ m}$. Vimeux et al. (2011) study showed that individual precipitation events have no control on the average $\delta^{18}\text{O}/\delta\text{D}$ values of precipitation, leading to the conclusion that mean annual isotope precipitation values are an integrated signal of seasonal precipitation events.

2.1.5 Conclusions

Isotopic analyses are a key proxy for understanding the hydrological processes. Isotopes from modern samples can track the pathway the precipitation travels and provide information regarding the precipitation source. Globally, both $\delta^{18}\text{O}$ and δD are influenced by temperature, altitude, latitude, distance from the ocean and precipitation amount. However, the degree to which each factor influences $\delta^{18}\text{O}$ and δD varies between specific locations. In the tropics, although all isotopic variation is somewhat a function of temperature it is mainly the amount effect that exerts a dominant control on variations in both $\delta^{18}\text{O}$ and δD .

Extensive isotope research has allowed for greater understanding in how the isotopes of water behave in the hydrological cycle on a continental scale across South America. Here, vegetation feedbacks influence the isotopic values within heavily forested areas such as the Amazon Basin. Processes such as evapotranspiration return isotopically similar precipitation back to the atmosphere limiting the impact of the continental effect. Additionally, within the low latitude regions of the continent evaporation from the vegetation to the atmosphere complicates the isotopic signal, returning moisture that is depleted relative to the source and therefore causing lower isotopic values of subsequent rainfall. In contrast, at higher latitudes of South America, the controls on isotopic composition within precipitation are easier to understand and are mainly a function of altitude and most importantly, temperature.

2.2. Isotopes in South American Paleoclimate Studies

Across South America, the use of isotopes are widely applied in the study of palaeohydrological change notably in studies of speleothems (Apaestegui et al, 2018; Cheng et al, 2013; Cruz et al, 2005; Kanner et al, 2012; Mosblech et al, 2012; Reuter et al 2009; Van Breukelen et al, 2008), lacustrine carbonates (Baker et al, 2001; Bird et al, 2011; Polissar et al, 2013; Seltzer, 2000; Zhang et al, 2017) and ice cores (Hoffman et al, 2003; Thompson et al, 2000). This has facilitated a deeper understanding of past hydroclimatic variation, which is especially useful given the number of long-term meteorological stations at low latitudes is small (Hoffman et al, 2003).

Speleothems commonly contain water-filled cavities that are filled with cave drip-water from the time of formation (Van Breukelen et al, 2008). It has been established that the cave-drip water is isotopically identical to local rainwater for both δD and $\delta^{18}\text{O}$ (McDermott et al, 2006),

and due to the fact that rainfall amount and $\delta^{18}\text{O}$ have been observed to be inversely correlated in areas of deep convection (Gat, 1996), speleothem records are widely accepted as a proxy for past rainfall amount. Due to the high resolution (decadal or centennial timescales) records that can be obtained using high precision Uranium-series dating (Apaestegui et al, 2018), speleothem records have provided detailed insights into palaeohydrological change during the last glacial period and Holocene.

Similarly, ice cores provide long-term records of climatic variations (Thompson et al, 1995). It is widely accepted that the $\delta^{18}\text{O}$ within polar ice can be used successfully as a temperature proxy (Thompson and Davis, 2007) and some studies have found that over intra-annual timescales, temperature is the dominant feature within South American ice cores (Thompson et al, 2003). However, other studies have concluded that the $\delta^{18}\text{O}$ of tropical ice reflects the $\delta^{18}\text{O}$ of precipitation (Rozanski et al, 1993; Baker et al, 2001). Even so, ice core records provide paleoclimatic insights extending back to ~25,000 yr BP.

This section aims to understand the paleoclimate of South America, using information obtained from $\delta^{18}\text{O}$ and δD isotope records. The discussion focusses particularly on the Last Glacial Maximum, Younger Dryas, the Holocene, the Medieval Climate Anomaly and Little Ice Age. Additionally, an overview about what is known regarding the impact of Dansgaard-Oeschger and Heinrich events will also be presented.

2.2.1 The Last Glacial Maximum (LGM)

The Last Glacial Maximum (LGM) is defined as the most recent interval in the Earth's history where global ice sheets reached their maximum integrated volume (Mix et al, 2001), and is thought to have occurred between 26.5 – 19 ka (Clark et al, 2009). During the LGM, South American temperatures were ~5°C cooler, and as a result influenced precipitation across the continent (Cross et al, 2001). Using two speleothem records collected from the eastern flanks of the Andes in northern Peru (5°56'S, 77°18'W; 5°44'S, 77°30'W), Cheng et al (2013) argued that the LGM was relatively wetter than the Holocene, with LGM $\delta^{18}\text{O}_{\text{calcite}} \sim 2\text{‰}$ lower than Holocene $\delta^{18}\text{O}_{\text{calcite}}$. This is supported by several other studies that infer wetter conditions in the high Andes during the LGM (Baker et al, 2001; Kanner et al, 2012). In slight contrast, Mosblech et al. (2012) found the LGM to be a time of no considerable change to either arid or humid conditions. The speleothem $\delta^{18}\text{O}$ record obtained from Santiago Cave in the lowland wet forests of Ecuador in Western Amazonia (2°42'S, 78°18'W), although exhibiting lower

$\delta^{18}\text{O}_{\text{calcite}}$ than the Holocene, showed subtle changes around the LGM, as opposed to the abrupt shifts of $\sim 1\text{-}2\text{‰}$ during both Heinrich and D/O events (see 2.2.3). This suggested that conditions were relatively stable during the LGM.

Not all the paleoclimate records of South America show increased LGM precipitation. In Rio Grande do Norte, a semi-arid region in north-eastern Brazil currently known for its severe and current droughts ($05^{\circ}36'\text{S}$, $37^{\circ}44'\text{W}$), the opposite conditions were found (Cruz et al, 2009). During the LGM, higher $\delta^{18}\text{O}_{\text{calcite}}$ from a speleothem record indicated predominantly dry conditions at the study site, with a decrease in $\delta^{18}\text{O}$ of $5\text{-}6\text{‰}$ occurring during the transition from the LGM into the early-mid Holocene ($\sim 10\text{-}5$ ka BP). This suggests that in northern Brazil, the LGM was characterised by drier conditions whereas the early to mid-Holocene exhibited wetter conditions (*ibid*). This contradicts the findings in the Central Andes (Seltzer et al, 2000), south-eastern Brazil (Cruz et al, 2005; Cruz et al, 2006) and western Amazonia (Van Breukelen et al, 2008). However, Sifeddine et al (2003) also found dry conditions during the LGM in a sedimentary record obtained from Caçó Lake, located in the Maranhão State of northern Brazil ($2^{\circ}58'\text{S}$, $43^{\circ}25'\text{W}$).

2.2.2 Younger Dryas (YD)

The Younger Dryas (YD) describes the abrupt return to glacial conditions in the Northern Hemisphere between 12,900 to 11,700 yr BP (Rasmussen et al, 2006), which temporarily reversed post-glacial warming trends. During the YD, Greenland ice cores show a depletion in $\delta^{18}\text{O}$ of $\sim 3\text{‰}$, thought to represent a temperature decrease of up to 9°C (Alley, 2000). In parts of South America, the YD is shown to be a time of increased precipitation. Cheng et al (2013) inferred an abrupt increase in precipitation, as reflected in a reduction in speleothem $\delta^{18}\text{O}$ of 1.5‰ . On the border between Peru and Bolivia, lake levels at Lake Titicaca were found to overflow, coinciding with the YD (Baker et al, 2001). Additionally, the stalagmite record from Cueva del Tigre Perdido, Peruvian Amazon shows the YD to be a period of increased convective rainfall, as shown by a decrease in $\delta^{18}\text{O}$ of $\sim 2\text{‰}$ (Van Breukelen et al 2008). However, although convective rainfall was increased compared to the LGM, the increased rainfall amounts were moderate compared to those inferred throughout the Holocene (*ibid*). In fact, isotope values from the YD in the study were found to be comparable to modern values from the site, suggesting that rainfall amounts of ~ 1500 mm/yr. The opposite trend can be found in northern areas of the continent. For example, Mosblech et al. (2012) Ecuadorian data

show a rapid increase in $\delta^{18}\text{O}$ at the onset of the YD, interpreted as representing a decrease in precipitation amount. Similarly, in the Cariaco Basin multiple studies have inferred cool and arid conditions during the YD from Titanium and iron concentration data (Haug et al, 2001) and $\delta^{18}\text{O}$ records of foraminifera, which show increased salinity due to increased net evaporation and lower sea level (Lin et al, 1997). More recently, Makou et al. (2007) utilised the δD values for the C_{16} – C_{32} fatty acids to understand paleoclimatic changes within the Cariaco Basin. δD values were higher during the YD, whereas values from the late Glacial and the Holocene appeared much lower.

2.2.3 Dansgaard-Oeschger (D/O) and Heinrich Events

In some high-resolution records of obtained from some tropical speleothem records, it is possible to consider the manifestation of abrupt Northern Hemisphere climate perturbations. Correlations with both Dansgaard-Oeschger (D/O) interstadials and Heinrich Events (Heinrich, 1988; Bond et al, 1992) have been identified in several records (Kanner et al, 2012; Mosblech et al, 2012). Both Heinrich and D/O stadials are influenced/influenced by the Atlantic Meridional Overturning Circulation (AMOC). An increase in AMOC (warmer Greenland temperatures), increased SSTs in the northern subtropical Atlantic, causing a northward displacement of the ITCZ, reduced Atlantic moisture contributions to the Amazon Basin and wetter conditions in the northern Neotropics (Peterson et al, 2001). Conversely, a slowdown in the AMOC (Greenland cold events) coincides with warmer SSTs in the southern Neotropics (cooler north Atlantic SSTs), which cause a southward displacement of the ITCZ and therefore increased moisture advection into the Amazon and a strengthening of the SASM (Mosblech et al, 2012).

The Pacupahuain Cave speleothem record from the central Peruvian Andes (11.24°S, 75.82°W), shows higher $\delta^{18}\text{O}$ values during D/O events, reflecting a transition to drier conditions in the high Andes (Kanner et al. 2012). The record also shows a weaker SASM during D/O interstadials, which they attributed to latitudinal shifts of the ITCZ driven by northern hemisphere temperature changes. Similarly, Mosblech et al (2012) Ecuadorian study found D/O events in the North Atlantic to be concurrent with the weakest SASM strengths and therefore driest conditions in the Amazon Basin. This is also supported by Cheng et al (2013) who found an abrupt increase in $\delta^{18}\text{O}$ of $\sim 1.5\text{‰}$, corresponding to D/O events.

In contrast to the drier conditions seen during D/O events, Kanner et al (2012) found Heinrich events to be periods of increased precipitation (HS 1-5). This finding was also supported by Mosblech et al (2012) who also found Heinrich events to appear as abrupt, sustained wet events. In the Nordeste region of Brazil, Cruz et al (2009) also found dry conditions during the late Pleistocene to be interrupted by abrupt shifts to $\delta^{18}\text{O}$ values as low as -5.5‰ from 25.9 to 25.0 kyr BP and -6.5‰ from 17.3 to 15.1 kyr BP which correspond to Heinrich events 2 (HS2) and 1 (HS1) respectively. Their record showed HS1 to be characterised by high amplitude $\delta^{18}\text{O}$ variations showing extreme changes from dry to wet conditions (Cruz et al, 2009).

2.2.4 The Holocene

The Holocene began at $\sim 11,650$ cal yr BP, after the Younger Dryas cold period (Walker et al, 2009). $\delta^{18}\text{O}$ records from Greenland ice cores show an increase in $\delta^{18}\text{O}$ values of $\sim 3.5\text{‰}$, corresponding to a temperature increase of $\sim 11^\circ\text{C}$ into the Holocene (Alley, 2000). Enhanced Northern Hemisphere summer insolation and reduced sea ice extent caused a northward shift of the ITCZ (Haug et al, 2001), establishing humid conditions on land in the northern subtropics (Baker et al, 2001). Van Breukelen et al. (2008) inferred that convective rainfall increased by a further 15-30% throughout the Holocene in Northern Peru, while temperatures remained stable. This is supported by $\delta^{18}\text{O}_{\text{calcite}}$ data from Lake Junin (10.9975°S , 76.1088°W), which decline to as low as -11‰ during the Holocene (Seltzer, 2000). Additionally, from 10 ka, a lacustrine calcite record also obtained from Lake Junin shows a decrease in $\delta^{18}\text{O}$ of $\sim 6\text{‰}$ throughout the remainder of the Holocene, suggesting that the climate became progressively wetter and cooler. In slight contrast to these findings, Cruz et al (2005) found an increase in $\delta^{18}\text{O}$ of $\sim 3\text{‰}$ into the Holocene from their record sampled from Boutevera Cave, subtropical Brazil. However, the isotopic record becomes progressively more negative over the course of the Holocene suggesting increased precipitation. This finding is supported by palynological evidence indicating an expansion of the Atlantic Rainforest into coastal regions of Southern Brazil (Behling, 2002) and also a southward expansion of the Amazon rainforest along Brazil's southwestern border (Baker et al, 2001). Both findings indicate increased moisture availability over the course of the Holocene, most probably sourced from the Amazon Basin. Additionally, the Holocene has also been recorded as a time of population and agricultural expansion in Amazonia (Bush et al, 2007), therefore suggesting that there was increased water availability throughout the continent.

However, in the southern parts of South America, the opposite can be found. $\delta^{18}\text{O}$ records from the Sajama ice core in Bolivia ($18^{\circ}06'\text{S}$; $68^{\circ}58'\text{W}$) show increased warming and consequently drying well into the Holocene, with lakes becoming desiccated (Thompson et al, 2000). This is seen in the record of insoluble dust concentration which reaches eight times that of the LGM. Thompson et al (2000) attributed this to increased volcanic activity and elevated Holocene snow lines. Baker et al (2001) also found the onset of the Holocene (between 11,500 to 10,000 cal yr BP) to be a time of aridity, with $\delta^{13}\text{C}_{\text{organic}}$ increasing above -23‰ (lake levels falling below their outlet) and salinity increasing. This was shown through an increase in the presence of CaCO_3 in the sediments during this interval. Mg/Ca ratios and $\delta^{18}\text{O}$ measurements of surface-dwelling foraminifers also showed salinity to increase in the Atlantic Ocean, suggesting that conditions were slightly drier than before (Arbuszewski et al, 2013).

2.2.5 The Medieval Climate Anomaly (MCA) and the Little Ice Age (LIA)

The Medieval Climate Anomaly (MCA) and the Little Ice Age (LIA) represent two of the most recent palaeohydrological transitions identifiable in the paleoenvironmental record of South America. The MCA occurred between 1000 and 1300 A.D. (Chen et al, 2015), and is seen in Northern Hemisphere records as the most recent pre-industrial warm interval (Trouet et al, 2009). $\delta^{18}\text{O}_{\text{calcite}}$ from speleothems collected from the Umajalanta-Chiflonkhakha cave system in the Bolivian Andes show the MCA was characterised by more negative values, indicating increased SASM activity in the Andes, therefore wetter conditions (Apaestegui et al, 2018). However, this finding contradicts those of Bird et al (2011), whose lacustrine calcite record from Laguna Pumacocha, located in the Central Peruvian Andes (10.70°S , 76.06°W ; 4800 m asl), shows a period of marked aridity, with $\delta^{18}\text{O}$ values increasing from ~A.D. 900 to A.D. 1100. Comparing the Pumacocha record to the Quelccaya ice core approximately 500 km southwest of Pumacocha ($13^{\circ}56'\text{S}$, $70^{\circ}50'\text{W}$), it can be seen that the timing and mean changes of the two records are in agreement with each other, with $\delta^{18}\text{O}$ in the ice core increasing at A.D. 1100 (Thompson et al, 1986). These findings could therefore imply that the results from Apaestegui et al (2018) during the MCA could be a regional anomaly.

The Little Ice Age (LIA) is thought to have occurred from approximately A.D. 1450 to 1850 (Apaestegui et al, 2018), and corresponds to pronounced cooling over the Northern Hemisphere (Mann et al, 2009). In tropical South America, the LIA has been shown to be a period of enhanced precipitation, indicating increased South American Summer Monsoon (SASM)

activity due to the southward displacement of the ITCZ (Apaestegui et al, 2018; Bird et al, 2011; Haug et al, 2001; Polissar et al, 2006; Reuter et al, 2009). During the LIA, Bird et al (2011) identified a prolonged decrease in $\delta^{18}\text{O}$, starting as early as A.D. 1300, with the most negative $\delta^{18}\text{O}$ values found between A.D. 1400 and 1820. Across the 2300-year-old record, the LIA showed the most dramatic decrease in $\delta^{18}\text{O}$, indicating a strong increase in the SASM. Reuter et al. (2009) study of a speleothem record from Cascayunga Cave in Northeast Peru ($6^{\circ}05'30''\text{S}$, $77^{\circ}13'30''\text{W}$) also shows a precipitation increase. When comparing the record to 20th century precipitation of the site, it was found that $\delta^{18}\text{O}$ values were 1‰ lower than the 20th century, implying precipitation was ~10-20% higher during the LIA than in the 20th century.

In the sub-modern sections of the Pumacocho record, Bird et al (2011) found a general increase in $\delta^{18}\text{O}$ from ~A.D. 1820 to present day. Between A.D. 1908 and 2007 $\delta^{18}\text{O}$ increased by ~2‰ per year from -15.0‰ to -12.9‰, indicating a rapid transition into dry conditions in the Peruvian Andes. The results suggest a long-term reduction in the intensity of the SASM, which leads to drier conditions.

2.2.6 Limitations and Conclusions

Overall, significant variability Late Pleistocene and Holocene hydrological conditions are observed across the South America, Throughout the LGM and the Holocene, the presently available isotope proxy data suggests that wetter conditions in the northern parts of the continent coincide with drier conditions in southern South America. Additionally, the records have shown that even when temperatures have increased drastically, such as in the transition from the Younger Dryas into the Holocene (Alley, 2000), precipitation amount was still the dominant control of variations in $\delta^{18}\text{O}$. Both Cruz et al. (2005) and Van Breukelen et al. (2008) conclude that temperature did not affect isotopic values in either Southern Brazil or Peru respectively. Instead, precipitation amount is inferred to be the dominant control on $\delta^{18}\text{O}$. Similarly, Mosblech et al (2012) attributed variations in $\delta^{18}\text{O}$ to reflect changes in the source and amount of precipitation rather than changes in temperature, even when ice core records have been interpreted as showing relatively large temperature increases (Alley, 2000; Thompson et al, 2000).

However, it must be noted that there are limitations to the use of speleothem, lacustrine and ice core records. One of the major limitations is their restricted geographical location. Ice core records are restricted to high mountains in the Andes (Thompson and Davis, 2007) and

speleothem records can only be obtained from areas where caves exist. Lacustrine records depend on suitable carbonate or silica producers such as diatoms, which are not ubiquitous (Sachse et al, 2012). Another limitation in these records is the timespan they encompass. Despite a growing body of paleoclimate data from South America, patterns of hydroclimate variation in Amazonia are poorly documented prior to the Holocene (Cheng et al, 2013). In the case of lacustrine records, very few span the last glacial-interglacial transition (Seltzer et al, 2000). This is mainly due to the fact that most lakes in the Andes were formed during deglaciation and are therefore <14,000 years old (Seltzer, 1990). Additionally, lacustrine records are constrained as most tropical lowland lakes are ephemeral (last for a short amount of time) or lack a continuous/high temporal resolution record due to a slow sedimentation rate (Ledru et al, 1996). This has resulted in contradictory paleoclimate inferences (Ledru et al, 1998; Sifeddine et al, 2003).

Present-day climatic changes are also influencing the reliability of these proxies. Since the 1980s mean warming has been recorded $\sim 0.1^{\circ}\text{C}$ per decade, with an estimated increase of between $1\text{-}4^{\circ}\text{C}$ by the end of the 21st century (Magrin et al, 2014). Consequently, the ice cores situated in the tropical Andes have been influenced by this temperature change. The retreat of Andean glaciers began after the Little Ice Age, but the rate of retreat (area reduction between 20% and 50%) has intensified since the 1970s (Magrin et al, 2014). The Qori Kalis outlet glacier from the Quelccaya ice cap has retreated 14 m/yr from 1983 to 1991 and from 2000/2001 the rate increased to 203 m/yr (Thompson and Davis, 2007). Davis et al (1995) found that percolating meltwater in lower-elevation glaciers in the Cordillera Blanca (Peru) caused the previously distinctive seasonal $\delta^{18}\text{O}$ signal from the top of the Huascarán ice cap to be completely obliterated. Similarly, in the Pucahirca ice core (Peru), the seasonal signals of $\delta^{18}\text{O}$ from 1984 were completely smoothed by 1990 (Thompson and Davis, 2007) due to climatic warming. These examples show that as the climate changes, our ability to understand past climatic variations through ice core proxies will be severely affected and may become impossible if ice retreat becomes extensive.

Additionally, even though some speleothem studies have concluded temperature does not influence $\delta^{18}\text{O}$ values, Thompson et al (2000) argue that temperature change will always exert some influence on ice core, speleothem and lacustrine calcite records. As a result, other more robust proxies are needed to understand the palaeohydrology in South America. One of the most promising and widely applied proxies, although not yet extensively used in South America, is the use of hydrogen isotopes within leaf wax *n*-alkanes.

2.3. Leaf Wax *n*-Alkanes as a Paleoclimatic Proxy

Most of these aforementioned studies utilised the ^{18}O composition of speleothem calcite as a hydrological proxy. However, since the 1930s, quantitative analyses of the relative abundances of both protium and deuterium focusing on the hydrogen isotopes within environmental water have been applied in research. In 1967, the focus of such research became the hydrogen isotope composition of organic matter (Sessions, 2016). Studies such as Shiegl and Vogel (1970) and Smith and Epstein (1970) considered the hydrogen isotope composition of fresh plant material, noting that relative to the surrounding environmental water they were relatively D-depleted. Further studies of hydrogen isotope composition progressed but were constrained by the fact that many organic compounds contain hydrogen within functional groups that exchange readily with both mineral H and water (Schimmelmann et al, 2006). Analytical developments in the late 1990s created the ability to measure compound-specific hydrogen isotopes within organic matter, which provided an exciting and vital new technique for studying palaeohydrological changes via targeted analysis of organic compounds known to be preserved in the geological record and to be less affected by hydrogen exchange (Sessions, 2016; Summons et al, 2008). In recent years, the use of organic biomarkers has made substantial contributions in the understanding and interpretation of paleoclimatic changes across the globe (Fornace et al, 2014, 2016; Schefuss et al, 2005). One of the most important class of biomarker used in the reconstruction of both climate and vegetation change is leaf waxes – in particular leaf wax *n*-alkanes (Tierney et al, 2010; Sinninghe-Damsté et al, 2011), which are also amenable to compound-specific isotope analysis (Sessions, 2016).

2.3.1. Leaf Wax Structure and Use

Leaf surface waxes comprise complex mixtures of long chain aldehydes, alkenes, alcohols, ketones, esters and alkanes (Jenks and Ashworth, 1999), which are also largely hydrophobic in character. Leaf waxes have been studied across the fields of chemistry, botany, physics and biochemistry (Jenks and Ashworth, 1999). It is widely known that terrestrial plants are covered with epicuticular waxes that form a hydrophobic outer surface of the plant, covering the cuticle. This cuticle is present on the surface of the leaves, roots and stems of a plant (Harwood, 1997) and is composed of an insoluble lipid polymer, cutin. This epicuticular layer acts as a protective barrier to the plant for both biotic stresses, such as fungal pathogens, and abiotic stresses such as extreme temperatures and solar radiation (Jenks and Ashworth, 1999). In the case of solar

radiation, epicuticular wax crystals have been found to protect plant species through the absorption, scattering and reflection of light (Riederer, 2006).

Due to the hydrophobic nature of these leaf waxes, one of the most common and important functions is water retention and repellence of excess external water (Shepherd and Griffiths, 2006). This is especially useful during times of water stress. As a result, leaf wax compositions and concentrations have been found to be environmentally sensitive. For example, thick waxy cuticles tend to be found on plants in desert environments (Maffei et al, 1997), and the epicuticular wax load of a species has been found to increase during drought conditions, for example in species of wheat (Merah et al, 2000).

Epicuticular waxes are also widely distributed in the environment. Wind and dust ablate the waxes, causing them to become present in atmospheric aerosols (Conte and Weber, 2002). This leads to their widespread presence in amounts in soils and ultimately, preservation in the sedimentary record (Schimmelmann et al, 2006). One of the most valuable use of waxes therefore is their role in paleoenvironmental reconstructions. This is mainly possible due to their high preservation potential, allowing the leaf waxes to survive in the geological record for millions of years (Bush and McInerney, 2013).

2.3.2. *n*-alkanes

One of the most important components of leaf waxes are *n*-alkanes, which contribute to the hydrophobic properties of a plant by reducing non-stomatal water loss (Jetter et al, 2008). Long chain *n*-alkanes (nC_{21} - nC_{35}) are the most widely utilised terrestrial plant biomarkers (Bush and McInerney, 2013). As straight chain hydrocarbons lacking functional groups, *n*-alkanes can remain in the sedimentary record for many millions of years (Sessions, 2016). Even though decomposition of *n*-alkanes in soil is possible, the time it takes for this to occur is substantial (Cranwell, 1981; Diefendorf et al, 2011; Eglinton and Hamilton, 1967). After the decay of a plant, *n*-alkanes are deposited in sediment, typically within the area they were produced. However, they can also be transported through winds and rivers, and deposited in lake or ocean sediment in the surrounding areas (Schreuder et al, 2008). As a result, *n*-alkanes can provide an integrated signal of the wax composition of regional-scale vegetation and environmental conditions (e.g. Rommerskirchen et al. 2003). If the deposition of *n*-alkanes is continuous and there is minimal disturbance and degradation, chronological records of the *n*-alkanes can be developed, creating records spanning of tens of millions of years (Johnson et al, 2016). As

many studies support the hypothesis that the *n*-alkanes present in soils and sedimentary records were originally derived from the surrounding vegetation (Carr et al. 2014; Schefuss et al, 2005; Schreuder et al, 2008), *n*-alkane records are an important proxy for past and current vegetation (Schwark et al, 2002).

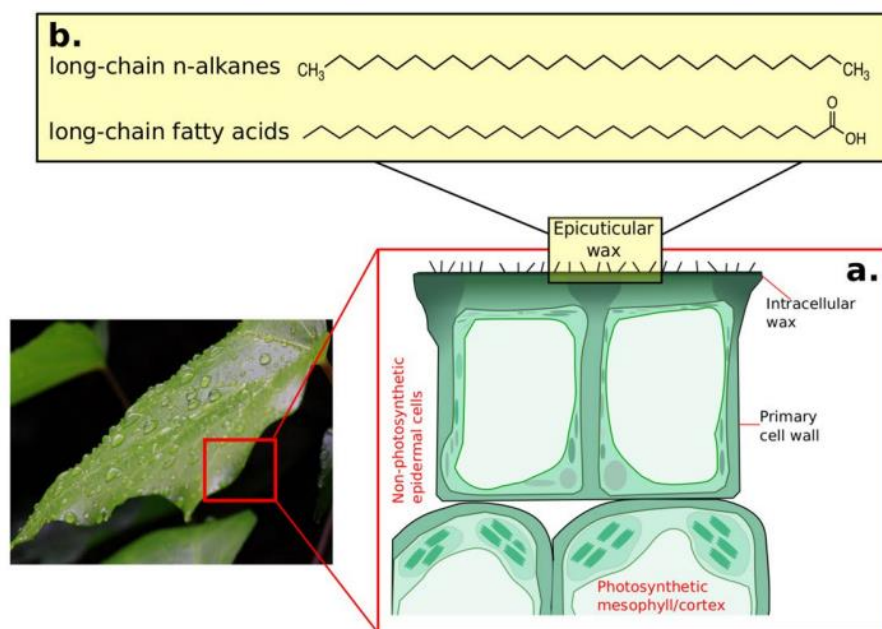


Figure 1. The morphology and chemistry of leaf epicuticular waxes through a) a diagram of the epidermal cells of intracellular and epicuticular wax and b) the structure of long-chain *n*-alkanes and fatty acids which are typical compounds found within terrestrial higher plants. Taken from Eley and Hren (2018).

2.3.2.1. Using *n*-alkanes in scientific study – taxonomic indicators or environmental biomarkers?

There is wide debate as to how successful *n*-alkanes are in describing vegetation change and composition (Halinski et al, 2011). This stems from the fact that some argue that *n*-alkane composition is species specific and therefore certain *n*-alkane distributions are representative of specific species, genera, family or plant functional type. Alternatively, others believe that environmental conditions prevailing at specific locations influence plant *n*-alkane composition, hindering their reliability as chemotaxonomic indicators (Bush and McInerney, 2013).

Multiple studies have utilised the assumption that a predominance of certain homologues is indicative of specific species' or plant types (Halinski et al, 2011; Li et al, 2012; Maffei et al, 1997; Sonibarea et al, 2005). Mimura et al. (1998) considered *Huberia*, a small genus of Melastomataceae, comprising dicotyledonous flowering plants typically found in the tropics.

In *H. Ovalifolia*, $n\text{-C}_{31}$ was found to be the dominant homologue with high levels of $n\text{-C}_{33}$ present. This allowed for separation of this species from others. When comparing their samples to others across the study area of ~1700km, from Bahia to Sao Paula, Mimura et al. (1998) also found little intraspecific variation between samples, concluding that n -alkanes for the *Huberia* species are specific to the plant and not influenced by environmental conditions. In support of this, Halinski et al (2011) discovered that in species of eggplant from Asia and Africa, that even throughout the growth period, the alkane fraction of leaf wax remained almost constant. In slight contrast, Tipple et al (2013) found that n -alkane distributions during the initial growth period of a plant vary. However, as the leaf matures, the distributions remain constant until senescence and finally deposition into soils.

In other studies, clear difficulties also arise when trying to distinguish species using alkanes as a taxonomic indicator. For example, for South African flora, Carr et al (2014) found considerable overlap between herbaceous and woody vegetation n -alkane distributions in the Fynbos and Succulent Karoo biomes, as well as considerable site to site variation for some species, and very little for others, concluding that using n -alkanes to distinguish between the two is unlikely to be successful. Similarly, it has been found that in warmer tropical and subtropical climates, plants synthesise longer chain wax components than species found in temperate regions (Gagosian and Peltzer, 1986). As a result, Bush and McInerney (2013) suggest that it is reasonable to hypothesize that n -alkane distribution is to some extent influenced by environmental adaptation. Consequently, the application of n -alkanes in the systematic classification of individual species has come into question especially in paleoenvironmental research where the n -alkane signal in sediment or marine samples represents an integrated signal of vegetation across the surrounding geographic area (Schwark et al, 2002). In general, vascular plants such as grasses, sedges, trees and shrubs tend to be dominated by long chain n -alkanes ($\text{C}_{29}\text{-C}_{31}$), typically with C_{29} dominant in woody plants and C_{31} tending to be more dominant in Graminoid (grasses) species (Bush and McInerney, 2013). This more cautious approach can be refined somewhat on a site-specific basis via analysis of modern plants and soils (e.g. Carr et al 2015). Stronger and more consistent patterns tend to emerge when considering aquatic plants and algae. In this instance, $\text{C}_{17}\text{-C}_{19}$ are thought to originate from species of algae (Ficken et al, 2000), and submerged or floating plants such as sphagnum are characterised by medium chain length n -alkanes ($\text{C}_{23}\text{-C}_{25}$) (Nott et al, 2000).

2.3.2.2. Characterising distributions within *n*-alkanes

The average chain length (ACL) and carbon preference index (CPI) are used to numerically characterise *n*-alkane distributions. CPI values capture the degree to which odd carbon number alkanes dominate over even carbon numbers (Marzi et al, 1993) and are expressed by the equation:

$$\text{CPI} = \frac{\Sigma_{\text{odd}}(C_{21-33}) + \Sigma_{\text{odd}}(C_{23-35})}{(2\Sigma_{\text{even}}(C_{22-34}))}$$

A CPI greater than 1 indicates a predominance of odd over even chain lengths. The carbon preference index is used as an indication of the alkane source (Jeng, 2006), and has been used in paleoenvironmental studies to deduce whether alkanes present in the sample material originated from terrestrial or aquatic plant species. Variations in CPI are thought to represent different plant types. CPIs greater than three are typically associated with modern higher land plants (Bianchi and Canuel, 2011; Bush and McInerney, 2013), and CPI values close to one are thought to indicate greater input from marine microorganisms and/or recycled organic matter (Kennicutt et al, 1997). In sediment, a CPI value ≥ 5 is used to indicate a terrestrial plant source and implies that there is no petrochemical contamination within the sample (Rao et al, 2009).

It has been proposed that variation within CPI values is somewhat controlled by climate. Considering marine sediments from Japan, Ishiwatari et al (1994) showed that CPI values reflected transitions between glacial-interglacial cycles, with higher CPI values being recorded in cold, dry glacial periods. Xie et al (2004) found high CPI values corresponding to cold and arid climatic conditions within loess. Rao et al (2009) also found that latitude influenced CPI values in surface soils from eastern China. In this study, CPI values at 18°N ranged from between 4 and 6, however at 50°N CPI values had increased to 13. All studies therefore indicate that CPI values are a product of the climatic conditions in which the plant is found, therefore might be a useful indicator in the study of paleoclimate. However, other studies (e.g. Carr et al. 2014) have found no strong relationship between CPI and climate/vegetation, other than a weak tendency for samples with the longest and narrowest distributions to also have high CPIs.

Average Chain Length is the abundance-weighted mean chain length (Poynter and Eglington, 1990) for a specified chain length range, and is defined by the equation:

$$\text{ACL} = \frac{\Sigma(C_n \times n)}{\Sigma(C_n)}$$

Where C_n is the concentration of each n -alkane with n carbon atoms (Bush and McInerney, 2013). Variation in ACL is observed within and between different plant types. For example, leaf lipids derived from grasslands generally have longer chain lengths than those from plants in forests (Cranwell, 1973; Sachse et al, 2006; Sinninghe-Damste et al, 2011; Schwark et al., 2002). In modern plants, ACL has been shown to vary with climatic conditions and it has been suggested that in warmer climates, plants produce lipids with longer chain lengths (Castaneda et al, 2009; Poynter et al, 1989). Simoneit et al (1991) found that in warmer climates of Southern China, higher molecular weight n -alkanes predominate. Changes in precipitation have also been found to influence ACL values. This is attributed to plants synthesising longer chain n -alkanes in order to provide a more efficient waxy coating to cope with the effects of water stress (Calvo et al, 2004; Carr et al. 2014). In the case of plant lipids preserved in sediment, there is a fundamental assumption that leaf lipids derived from grasslands may have, on average, longer chain lengths than lipids originating from forests (Sinninghe-Damste et al, 2011). If this is correct then ACL values would reflect transitions between forest and grassland, and thus show changes between environment and climate (Wang et al, 2015). However, recent studies comparing the ACL values from both fresh plant material and soils across transects from Australia suggest that distinguishing forest and grassland is not that simple. For example, Howard et al (2018) found average ACL values of trees of 28.9 ± 1.4 , whereas ACLs for forbs, grasses and shrubs were 31.0 ± 1.2 , 31.2 ± 0.9 and 30.3 ± 1.2 respectively. However, the ACL of soils ranged from 27.4 to 30.9 and averaged 28.8 ± 0.9 , exhibiting an offset from the observed n -alkane characteristics of the measured plant material. The study therefore concluded that ACL can help to reconstruct a regional, time-averaged signal of vegetation rather than short term variability in vegetation changes.

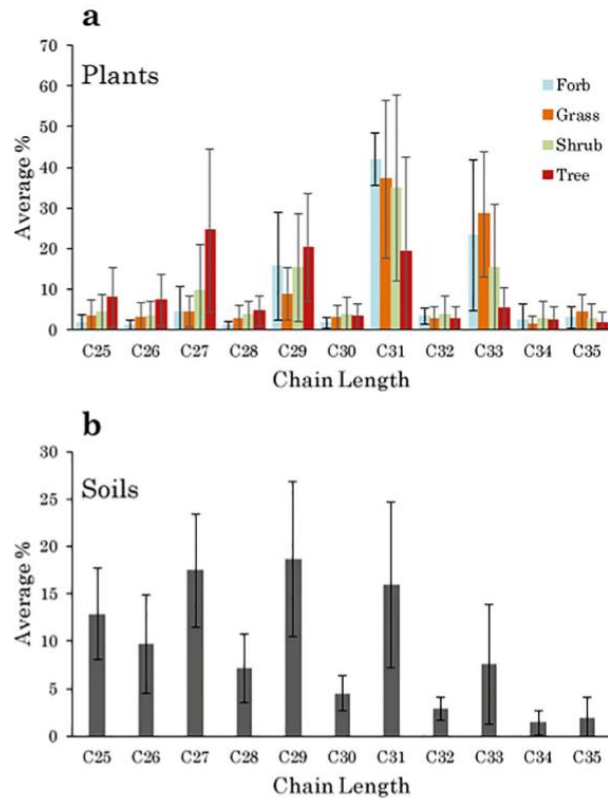


Figure 2. The relative abundance of *n*-alkanes from a) fresh plants and b) soils taken from Howard et al. (2018). The results are displayed as an average percentage for each chain length, with the error bars representing standard deviation.

Another way of expressing the typical chain length distribution for terrestrial plants is through the Norm31 parameter. Norm31 expresses the ratio between the longer C₂₉ and the C₃₁ *n*-alkanes, is thought to be an environmentally sensitive parameter (Rommerskirchen et al, 2003) and is expressed through the equation:

$$\text{Norm31} = C_{31} / (C_{31} + C_{29})$$

Taylor et al (2018) suggested that Norm31 can be used to identify the changes within the terrestrial community and demonstrate temporal variability in long-chain *n*-alkane production related to the landscape-scale terrestrial vegetation composition. Others have also suggested that changes within Norm31 values could represent changes in climate. For example, Norm31 values closer to 1 indicate a greater predominance of the C₃₁ *n*-alkane which has been linked to grassier ecosystems such as savanna (Hermann et al, 2016).

One fairly consistent observation from leaf waxes have been that aquatic and riparian plants tend to produce significantly shorter chain length waxes (Sachse et al, 2004; Ficken et al, 2000; Gao et al, 2011) As a result, the P_{aq} proxy was proposed as a means quantifying the relative

contribution of terrestrial/riparian/aquatic plants to sedimentary *n*-alkane distributions. The P_{aq} proxy was first established by Ficken et al (2000) and is expressed by the equation:

$$P_{aq} = (C_{23} + C_{25}) / (C_{23} + C_{25} + C_{29} + C_{31})$$

The ratio characterises the relative proportion of mid-chain length (C_{23} - C_{25}) versus the long-chain length (C_{27} , C_{29}) homologues, and is interpreted in terms of the relative inputs of submerged/floating aquatic macrophytes and terrestrial plants (Sinnighe-Damsté et al, 2011). Through sampling the plants found in the Lakes in the Mount Kenya National Park, Ficken et al (2000) discovered that, typically P_{aq} values between 0.1-0.23 were typical of terrestrial vegetation, 0.25 (0.07-0.61) was typical of emergent species and 0.69 (0.48-0.94) was typical of submerged or floating species. This index has since been used extensively in paleoclimatic studies utilising aquatic sediment. In paleoclimate studies, P_{aq} has been used to infer changes in the dominant *n*-alkane origin. For example, Carr et al (2015) found an increased in P_{aq} values in sediment aged ~8000 cal yr BP corresponded to a greater input of the short to mid chained *n*-alkanes and therefore more submerged/floating macrophytes. Similarly, Taylor et al (2018) also used the P_{aq} index to broadly characterise the environment within different samples of their study. They found P_{aq} values close to zero indicated a “dry” environment, whereas P_{aq} values closer to one were indicative of “humid” conditions.

Although the use of *n*-alkane distributions to provide insights into plant community changes and therefore paleoclimate has proven successful in some studies, there is still ongoing debate as to whether specific *n*-alkanes represent large plant groups. Using distribution analyses as singular indicators of climatic changes is therefore not advised. However, such data are very valuable when combined with other climate and vegetation proxies such as pollen or isotope records (Bush and McInerney, 2013) and as in this study, the analysis of hydrogen isotopes from the leaf wax *n*-alkanes themselves.

2.4 Hydrogen Isotopes in Leaf Wax

The hydrogen isotopic composition of leaf waxes is increasingly utilised in paleoenvironmental reconstructions, most importantly in the reconstruction of past hydrological conditions (Schefuss et al, 2005; Collins et al, 2013; Yao and Liu, 2014). Since environmental water is the primary source of hydrogen for leaf wax (Sessions, 2016), leaf wax δD values (δD_{wax}) are thought to represent environmental water from the time at which they were synthesised (Sachse et al, 2012). Initial studies revealed that both aquatic and terrestrial lipid biomarkers have δD values that are offset, but highly correlated with the organism's water source (Sauer et al, 2001; Sessions et al, 1999). Multiple studies have supported this hypothesis, showing that in soil and lake surface sediment studies, δD_{wax} and the δD values of local precipitation (δD_p) are correlated (Rao et al, 2009, Luo et al, 2011, Garcin et al, 2012; Herrmann et al., 2017).

As the primary factor controlling δD_{wax} is the hydrogen isotope composition of precipitation, this analysis provides a direct link to palaeo-hydrological reconstructions. It is widely accepted that isotopic variation within precipitation is driven directly by fractionations associated with the conversion of water from the solid, liquid and vapour phases (Sessions, 2016), with the effects proposed by Dansgaard (1964) significantly influencing the signal. As meteoric precipitation is then incorporated into the leaf wax, further fractionations occur during plant biosynthesis, which as a result, alter the δD signal. This is referred to as apparent fractionation (ϵ_{app}). Multiple studies have tested the reliability of using *n*-alkanes as a palaeohydrological proxy, taking into consideration the apparent fractionations that occur between lipids and precipitation. Apparent fractionation describes the difference in δD values between the hydrogen source, which in the case of plants is precipitation, and the δD values found in leaf waxes, and is expressed through the equation:

$$\epsilon_{\text{app}} = \left(\frac{1000 + \delta D_{\text{wax}}}{1000 + \delta D_p} - 1 \right) \times 1000$$

(Hou et al, 2018). Rearranging, Hou et al. (2018) show that δD_{wax} can be expressed as a function of both δD_p and ϵ_a as:

$$\delta D_{\text{wax}} = \epsilon_{\text{app}} + \frac{1000 + \epsilon_a}{1000} \times \delta D_p$$

A fundamental assumption when using δD_{wax} as a proxy for δD_p is that the apparent fractionation between leaf-wax components and precipitation remained constant (Hou et al, 2018). However, studies have concluded that apparent fractionations varied in different regions (Hou et al, 2008; Liu et al, 2006). Sachse et al (2012) suggested that there are three potential

sources of apparent fractionation – soil-water evaporation, leaf-water transpiration and biosynthetic fractionation. Additionally, studies have also found that δD_{wax} is affected by secondary factors such as plant growth form, vegetation type and evapotranspiration (Liu et al, 2006; Smith and Freeman, 2006; Feakins and Sessions, 2010; Kahmen et al., 2013).

In general, hydrogen atoms are introduced into the plant biomass during photosynthesis and are derived from plant water (Vogts et al, 2016). Plant water is, in turn, controlled by soil water, which is the only water source for most plants, originating from the local precipitation (Sachse et al, 2012). The isotopic signature of both the local precipitation and soil water are incorporated into the plant through uptake via stem water (Flanagan and Ehleringer, 1991). It is widely accepted that no isotope effects are associated with the uptake of soil water by the plant (Ehleringer and Dawson, 1992). However, when water reaches the leaf, evaporation (transpiration) at the site causes a preferential loss of the lighter isotopes creating enriched leaf water δD (McCarroll and Loader, 2004; Sachse et al, 2009). As leaf-wax lipids are then synthesised within the plant leaves (Sachse et al, 2012), it is thought that these fractionations will affect the isotopic composition of synthesised tissues, and as a result will be correlated, but not identical. For example, it is known that sucrose formed in the leaf reflects the isotopic composition of leaf water, but with a 27‰ enrichment (Sternberg et al, 1986 in McCarroll and Loader, 2004). Similarly, Hou et al (2008) demonstrated the δD_{wax} values of the C_{28} *n*-alkanoic acid to show a significant correlation with the δD_p with an apparent isotopic enrichment of $\sim 99 \pm 8\%$.

Net apparent fractionation differences from source water to lipids have been associated with the biosynthetic pathways of different vegetation types, such as C_3 vs C_4 plants (Sachse et al, 2012; Wang et al, 2013) or different water-use strategies (Hou et al, 2007). Smith and Freeman (2006) found the δD_{wax} values of C_4 grasses are generally more positive ($\sim 21\%$) than those of C_3 grasses, when grown side by side under greenhouse experiment conditions and in their natural environment. Similarly, Sachse et al (2012) found that apparent fractionation differed between C_3 graminoid species which are monocotyledonous and C_3 species such as shrubs, trees and forbs which are dicotyledonous. In the case of the C_3 monocots, apparent fractionation averaged $-149\% \pm 28\%$, whereas for C_3 dicots apparent fractionation averaged $-113\% \pm 31\%$. Additionally, average fractionation for C_4 monocots were typically 15‰ more than C_3 monocots and averaging $-134\% \pm 27\%$.

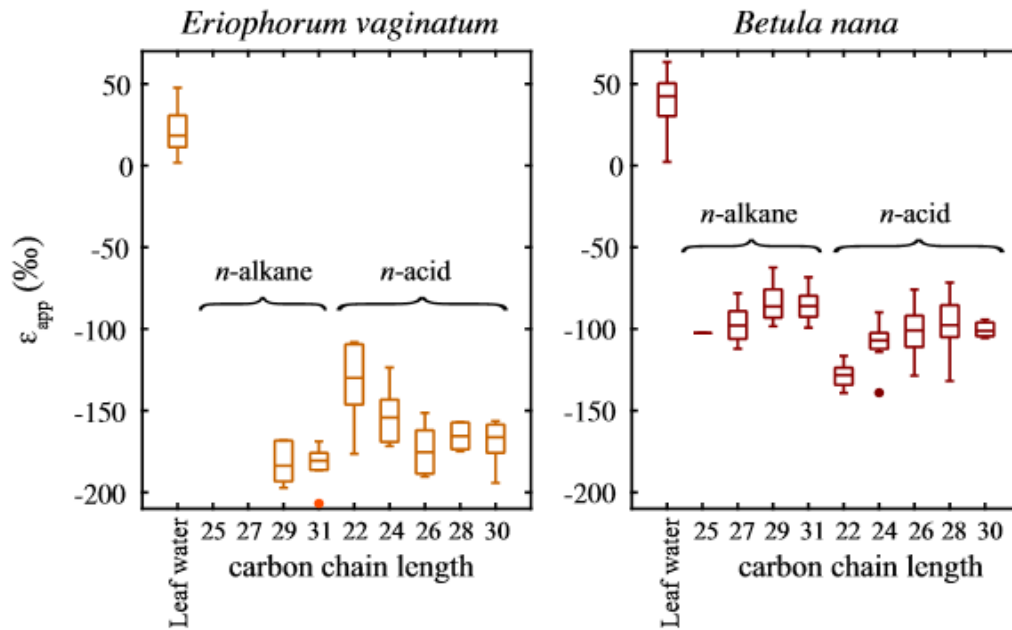


Figure 3. The net apparent fractionation for a) *Eriophorum vaginatum*, a C₃ monocot and b) *Betula nana* a C₃ shrub. Taken from Daniels et al. (2017).

To assess the impact of varying apparent fractionations from different plant photosynthetic pathways on δD_{wax} (and thus proxy reliability) Garcin et al (2012) and Wang et al (2013) tested individual sedimentary *n*-alkanes across geographic transitions between C₃ and C₄ vegetation. Both studies analysed multiple *n*-alkanes to ascertain which *n*-alkanes were more sensitive to change as vegetation and water availability changed. Both found the C₂₉ *n*-alkane to show the least change during abrupt transitions between C₄ grasses and C₃ dicots. This led to the conclusion that when large shifts in the vegetation are known, the C₂₉ *n*-alkane is the most reliable homologue to use in palaeohydrological reconstruction, as the δD signal remains least biased, whereas both the C₃₁ and C₃₃ *n*-alkane δD values were sensitive to changes between C₃ and C₄ vegetation.

Another constraint in using the δD values from plant leaf waxes is the seasonal variability generating large differences in isotopic values. In modern plant species, Pendentchouk et al (2008) found that δD_{wax} values of angiosperm species varied by as much as 20‰ across the growing season, even when the isotopic composition of irrigation water remained relatively constant. Similarly, Sachse et al (2009) found significant variation of up to 40‰ in the individual isotopic values of the deciduous trees in their study (*Fagus sylvatica* and *Acer pseudoplatanus*) during the growing season. However, near identical values δD values from leaves during senescence and those of leaf litter, lead Sachse et al (2009) to conclude that the

isotopic signal of the leaves produced late in the season is the signal that is preserved in the soils, and it is the location and timing of wax synthesis that causes the variable δD_{wax} values. This finding is also in agreement with an earlier study by Sachse et al (2006), who discovered that although the δD_{wax} of plants show a correlation with the δD values of precipitation along a climatic gradient in Europe, the variability of these values is much larger than the δD_{wax} values taken from lake sediments along the same gradient. This suggests that sediment integrates the δD_{wax} values over larger space and timescales, which removes short-term variability.

Furthermore, apparent fractionation has also been found to vary due to climatic influences and their effect on plant type. Feakins et al (2016b) found that the transition into a grassland environment created an apparent fractionation as large as -150‰, whereas in dry woody environments the apparent fractionation tended to be small, at $\sim 90\%$ (Feakins and Sessions, 2010) due to leaf water enrichment. To test the variability of fractionation factors across environmental gradients, Feakins et al (2016a) studied forest canopy trees across a highly biodiverse 3 km elevation range on the eastern flanks of the Andes, Peru. The study compared the C_{29} *n*-alkane from 176 plant samples from 32 species. Across the elevation range, δD_{wax} values ranged over 100‰, from -102‰ to -278‰, with the apparent fractionation $-129 \pm 2\%$ in all samples. This fractionation factor was consistent with the value reported for a humid, temperate forest in Massachusetts ($-130 \pm 4\%$; Hou et al, 2007). Additionally, Sachse et al (2012) reported an average apparent fractionation of -121‰ for humid environments globally, suggesting that apparent fractionation within humid environments produces similar values. All findings supported previous studies who concluded that apparent fractionation shows minimal change as a function of relative humidity (McInerney et al, 2011; Feakins and Sessions, 2010). This is an important issue for the tropics, as humidity is the prominent feature of tropical climate. Additionally, Feakins et al (2016b) concluded that high biodiversity did not affect isotopic variability within leaf waxes, therefore leading to the conclusion that δD_{wax} combines the signal of all plant communities within the study region.

Overall, multiple factors influence apparent fractionation within leaf wax, and thereby the δD_{wax} signal. However, these factors are now relatively well documented and as a result can be taken into consideration when applying δD_{wax} values as a paleohydrological proxy. Large differences in the δD values of species and individuals have been found, but the greatest variations largely came from fresh plant material (Pendentchouk et al, 2008; Sachse et al, 2009) and the averaging effects within soils and sediment mean that δD variation is much less varied

in the sedimentary record (Sachse et al, 2009). Additionally, studies taking into consideration areas of high biodiversity have found that increased species diversity did not affect the δD_{wax} signal (Feakins et al, 2016b). In tropical climates, of interest to this study, apparent fractionation has been estimated to be $\sim -129 \pm 2\text{‰}$ (Feakins et al, 2016b), which agrees with both global estimates (Sachse et al, 2012) and also findings from regions with a similar climate (Hou et al, 2007). This indicates that within humid tropical environments, apparent fractionation remains relatively similar throughout across a wider study region, even though the species composition of the vegetation is changing. A relatively consistent difference of apparent fractionation concerns monocots vs. dicots, but this can be taken into account when pollen and isotope data are available (Wang et al, 2013). Taking all of these factors into consideration and understanding that the δD values of leaf-wax must be interpreted by incorporating factors such as biosynthetic fractionation and evapotranspiration it can be concluded that in most instances δD_{wax} of *n*-alkanes is a reliable palaeohydrological proxy. Therefore, it is correct to assume that the hydrogen isotopic composition of δD_{wax} reflects the signal of source water after modification by both evaporation and biosynthetic fractionation (Hou et al, 2008; Kahmen et al, 2013a; Tipple and Pagani, 2013; Wang et al, 2013) and can therefore be used to reconstruct changes in precipitation. Examples of coherent paleoenvironmental reconstructions using this method outlined in the next section support this argument.

2.5. The use of n-alkanes in Palaeohydrological Research

Multiple studies have concluded that the hydrogen isotope of plant leaf wax successfully records the isotopic composition of precipitation (Balascio et al, 2018; Garcin et al, 2012; Hermann et al, 2017; Luo et al, 2011; Rao et al, 2009; Sachse et al, 2012; Sauer et al 2001; Sessions et al 1999; Wang et al, 2013; Yao and Liu, 2014). Currently, most leaf wax palaeohydrological records available originate from tropical Africa. However, other records from Europe and China are increasingly available. δD_{wax} records have been obtained from climatic gradients (Garcin et al, 2012; Herrmann et al. 2017; Sachse et al, 2006), marine sediment cores (Schefuss et al, 2005; Niedermeyer et al, 2010) and local surface sediments (Yao and Liu, 2014) and have become increasingly popular as a proxy for hydrological, vegetation and climatic changes. However, across South America, the application of this proxy, and as a result the availability of these records, remains scarce.

Throughout the literature, δD_{wax} has been used to understand the main controls on the δD_{wax} values of precipitation. In tropical Africa, Niedermeyer et al (2010) inferred that the amount effect had the most significant influence on their study area, with the lowest δD_{wax} values corresponding to increased precipitation. Niedermeyer et al (2010) measured the stable hydrogen isotope composition of terrestrial leaf waxes using the C_{31} *n*-alkane from a marine sediment core obtained from the continental slope off the coast of Senegal. The study found that lower isotopic values and therefore wet periods in the record coincided with local maximum summer insolation at 15°N . Similarly, drier periods in the record corresponded to times of local minimum insolation, and also with North Atlantic Heinrich Stadials.

Yao and Liu (2014) measured δD_{wax} across the Qinghai-Tibetan Plateau in China to understand changes in the δD_{wax} . Again, values increased during dry periods and decreased during times of increased rainfall, which the study attributed to a combined effect of evapotranspiration and humidity. However, the study also showed that changes in δD_{wax} mainly reflected a shift to different vegetation types which Yao and Liu (2014) then attributed to the availability of water. This illustrates the need to couple δD_{wax} records with $\delta^{13}\text{C}$ measurements to ascertain whether large changes in δD_{wax} values are due to changes in vegetation composition or due to differences in rainfall amount. Schefuss et al (2005) reconstructed hydrological change in the Congo Basin over the past 20,000 years and found that δD_{wax} ranged from -131‰ to -165‰ after correcting the values against ocean water. To understand whether the large δD_{wax} range was a function of vegetation change, the study compared the values to $\delta^{13}\text{C}$. Minimum variation was found within the $\delta^{13}\text{C}$ record leading to the conclusion, that within the Congo Basin, it is predominantly precipitation δD that controls the δD_{wax} signal. This enabled their record to be interpreted as hydrological variability over time, rather than changes in vegetation.

The necessity of combining δD_{wax} with $\delta^{13}\text{C}$ measurements was also illustrated in a study from Laguna La Gaiba (17.75°S , 57.58°W) in the Bolivian margin of the Pantanal wetlands. Fornace et al (2016) documented significant changes in C_3 - and C_4 -dominated vegetation communities since the last glacial period. The record showed an increase in *n*-alkane chain length was correlated with a decrease in δD_{wax} values, suggesting a vegetation effect on δD_{wax} via apparent fractionation changes. Without taking this into consideration, it would be assumed that the decrease in δD_{wax} represented wetter conditions. The study found an increase in $\delta^{13}\text{C}$ values coincided with low δD_{wax} , which was interpreted as an increase in C_4 vegetation during a time of water stress. In contrast to other paleoclimate studies from South America, the record showed the LGM to be a time of drought or decreased seasonality, where an open landscape of

C₄ grass and C₃ herb communities dominated. Additionally, Fornace et al (2016) found a pronounced vegetation shift to C₃ forest after the LGM, coinciding with deglacial warming, followed by a dramatic shift to a mixed C₃/C₄ community from ~12.7 to 11.6 ka, which was also thought to be caused by hydrology driven changes and an increased leaf wax contribution from the wetland regions. Overall, the study concluded that it is imperative to understand landscape cover throughout the record as the shift from C₃ to C₄ vegetation created an isotopic signal that overwhelmed changes in δD_p . Combining the record with $\delta^{13}C$ values allowed the hydrological signal to be distinguished, but the study suggested that pollen records are needed in areas where strong climate-induced vegetation changes are found to fully understand the isotopic variation within the samples.

Hydrological variability from δD_{wax} was also documented in Lake Titicaca (15.8533°S; 69.1404°W), a freshwater lake situated on the borders of Bolivia and Peru. The record used lacustrine sediment from the Lago Grande Basin on the Bolivian border, to reconstruct hydrological variability over the last 60,000 years (Fornace et al, 2014). Throughout the core, δD_{wax} values ranged from -236‰ to -114‰, with glacial values typically more depleted than those sampled from the Holocene. During the glacial period δD_{wax} values averaged -207‰ whereas during the Holocene δD_{wax} values were more positive averaging -152‰. These findings of wetter glacial and a drier Holocene conditions largely agree with ice cores records obtained from Bolivia (Thompson et al, 2000) and previously published $\delta^{13}C$ records also obtained from Lake Titicaca (Baker et al, 2001). Higher δD_{wax} was thought to represent the Bølling–Allerød (~15.5-13.8 ka), suggesting drier conditions, followed by lower values coinciding with the Younger Dryas stadial. Again, this finding supports the previous climatic inferences from Lake Titicaca. During the Bølling–Allerød, Baker et al (2001) suggested a dry/warm climate over Lake Titicaca due to an increase in benthic diatoms and a decrease in freshwater planktonic diatoms within the lake sediment. Similarly, records from the Sajama ice core in Bolivia suggest an abrupt warming creating a drier climate, as reflected through an increase in nitrate concentrations by a factor of 3 to 5 (Thompson et al, 2000). These findings therefore show that the δD_{wax} values from Lake Titicaca correlate with already published climate data and therefore successfully record hydrological changes.

In addition, Fornace et al (2014) also compared their findings with the δD record of the Illimani ice core published by Ramirez et al (2003) to ascertain how reliably the δD_{wax} record from Lake Titicaca records the isotopic variability of precipitation. Although the range of δD_{wax} values was larger in the Titicaca record than in the ice core record, the values were largely

correlated. However, although the study provides a greater insight into the hydrological variability within the Bolivia/Peru region, it is important to note that the record explains hydrological change within an already well documented area of South America. Additionally, although the study did provide insight into hydrological changes, the causes of such change were not fully explained. Therefore, it is important to develop the use of the proxy within poorly studied areas of South America with the aim of understanding regional-scale changes in hydrological regime.

2.5.1 Conclusions

Although there are records available which allow further understanding of palaeohydrological variability in South America, there are few continuous records that extend into the last glacial period (Fornace et al, 2016). As mentioned previously, Andean ice core records tend to only extend back to the LGM (Rameirez et al, 2003; Thompson et al, 1995, 1998), and other isotopic records obtained from lake sediment (e.g. Bird et al, 2011) confined to the Holocene. This has increased the need for proxies that have the ability to provide insights into hydrological change across greater timescales. δD values from leaf-wax *n*-alkanes is a promising way of reconstructing these changes, especially in areas of South America where other climate proxies are limited. Multiple studies have concluded that δD_{wax} successfully reflects changes within precipitation and, owing to the abundance of *n*-alkanes within the environment, can be applied to studies anywhere across South America where organic sediment is well-preserved.

However, even though multiple studies globally have used δD_{wax} values to reconstruct changes in both vegetation and hydrological regime, records within South America remain scarce. Where δD_{wax} records are available, they tend to focus on study areas that are already well documented (e.g. Fornace et al. 2014). As a result, additional information regarding hydrological change is needed across South America. This thesis, therefore, aims to utilise δD_{wax} data in order to reconstruct necessary palaeohydrological changes from within two poorly-documented areas in Colombia – the Amazon Basin and the Pantanó region to the east of Bogotá.

Chapter 3: Materials and Methods.

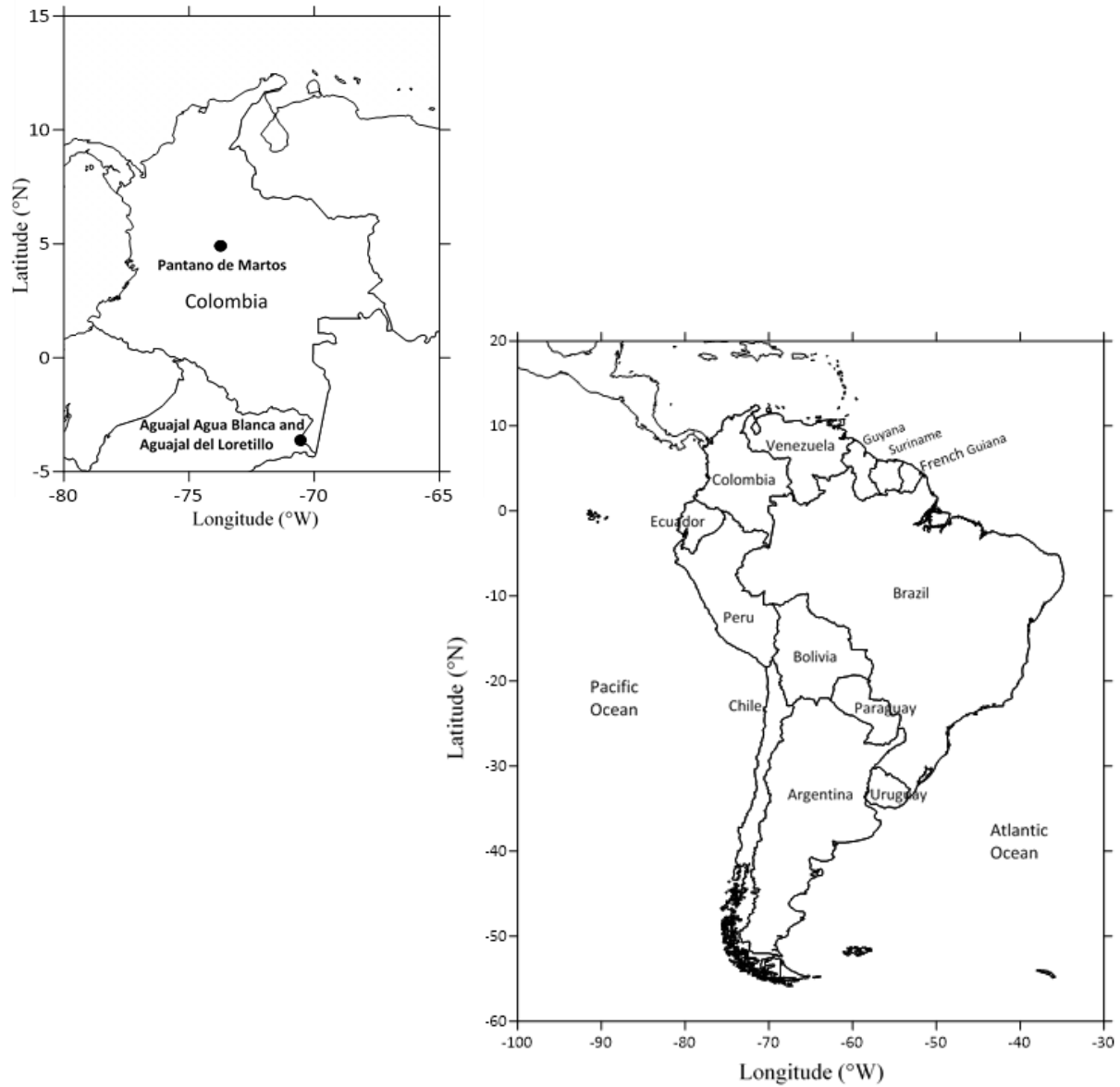


Figure 4. Map showing South America and also the locations of Pantano de Martos, Aguajal Agua Blanca and Aguajal del Loretillo – the three records used in this study within Colombia.

3.1. San Pedro de Tipisca – Aguajal Agua Blanca and Aguajal del Loretillo

3.1.1. Background

The Amazon Basin predates the separation of South America from Africa ~110 million years ago (Junk et al, 2010) and generally is found below 200 m asl, covering an area of 8 million km² (Hoorn and Wesselingh, 2010). Up to 6 m of rain falls on the Amazon Basin, most of which is returned to the atmosphere via evaporation after plant interception (26.6%) and transpiration after plant uptake (45.5%) (Salati, 1985). The high rainfall amounts lead to low soil fertility through runoff, which results in the majority of nutrients being stored within plant biomass (Myster, 2017). Nutrient cycling within the Amazon Basin is said to be fast and efficient within a closed system (*ibid*). However, it is thought that the western part of the Amazon is composed of relatively young and fertile soil, which leads to greater forest turnover and speciation, thus higher biodiversity than found in Eastern Amazonia (Myster, 2017). The Western Amazon rainforest, in particular, sections within the Colombian Rainforest are one of the most diverse areas on earth (Myers et al, 2000), due to the fact that the majority is unaffected by human activity and therefore has suffered the smallest loss of biodiversity and forest fragmentation (Bierregaard et al, 2001). More specifically, the Colombian Amazon covers 42% of the country's area (483,119 km²) and is a humid tropical forest, known for its many palms (Balslav et al, 2017).

3.1.2. Site Description

Two cores named Aguajal Agua Blanca and Aguajal del Loretillo were obtained from a palm swamp near to the village of San Pedro de Tipisca located in the Puerto Nariño area of the Amazonas state, Colombia (co-ordinates S 03°38'56.2" W 070°37'0.00"; S 03°38'34.9" W 070°36'23.5"). Situated ~78 m asl, the climate at the site is tropical, with average temperatures between 26°C and 27°C throughout the year (Schongart et al, 2002). Rainfall is significant throughout the year, due to the tropical climate, however the rainy season, by definition, extends from November to May, with the highest rainfall occurring in April (Galeano et al, 2015). The dry season extends from June to October, with the driest month typically being August (*ibid*). Monthly averages in the area are ~266 mm (Dominguez, 1985), with mean annual rainfall averaging 2846 mm yr⁻¹ (Climate-data.org, 2019).

The cores were collected from the edge of the Amazon floodplain, on the Loretoyacu floodplain. Both cores are situated close to the Loretoyacu River (~1.6 km and ~0.59 km for Aguajal Agua Blanca and Aguajal del Loretillo respectively), and the smaller Loretillo River. Both rivers are slow moving and have high suspended sediment loads, which could possibly originate from material recycled from the river bed. The site was chosen due to the minimal influence of human activity in the form of forest cut-back, a reflection of the difficulty in accessing the area. The water table at the site was also high, with water input predominantly originating from the Loretoyacu River. The two cores were collected to maximise the chances of obtaining a good record of palaeohydrological change within the area.

The main species found in the palm swamp is *Mauritia flexuosa* (Arecaceae), a straight stemmed dioecious palm species that has between 8-25 large (up to 6 m long) costapalmate leaves on its exterior (Rull and Montoya, 2014). *Mauritia flexuosa* is abundant and widely distributed throughout South America, at both sides of the equator from 12°N to 20°S. It is, however restricted to the lowlands (below 1000 m elevation), where an optimal warm and wet climate for its growth is found (Rull, 1998; Rull and Montoya, 2014; Ter Steege et al, 2013; Virapongse et al, 2017). *Mauritia flexuosa* is particularly abundant in permanently flooded, poorly drained soils of flood plains, but also the lower terraces in the Amazonian alluvial valleys (Henderson, 1995). Due to the abundance of water throughout the year, the soils on which the species are found, in both Igapo and Varzea forests, are notably acidic (pH ~ 4.0-5.0) organic soils (Histosols) (Galeano et al, 2015). *Mauritia flexuosa* can grow up to 30-40 m in height (Virapongse et al, 2017), and typically form a closed canopy, significantly reducing light penetration (Rull and Montoya, 2014). The rooting system of the species grow to 60 cm in depth, but also develop horizontally, reaching as deep as 40 m (Koolen et al, 2018). Aerial roots named pneumatophores are also present, which allow for growth and respiration in anaerobic conditions (Delgado et al, 2007). It is also estimated that stands of *Mauritia flexuosa* represent a very important carbon sink (Galeano et al, 2015). *Mauritia flexuosa* store carbon in thick layers of decaying organic matter, which are regarded as important sources of carbon exchange and sequestration (Draper et al, 2014), and are typically found on partially decomposed soils of high organic content (Silva et al, 2014). As this species is the most dominant vegetation found in the site area, it is hypothesised that *Mauritia flexuosa* will contribute the primary source of organic matter to the sediment.

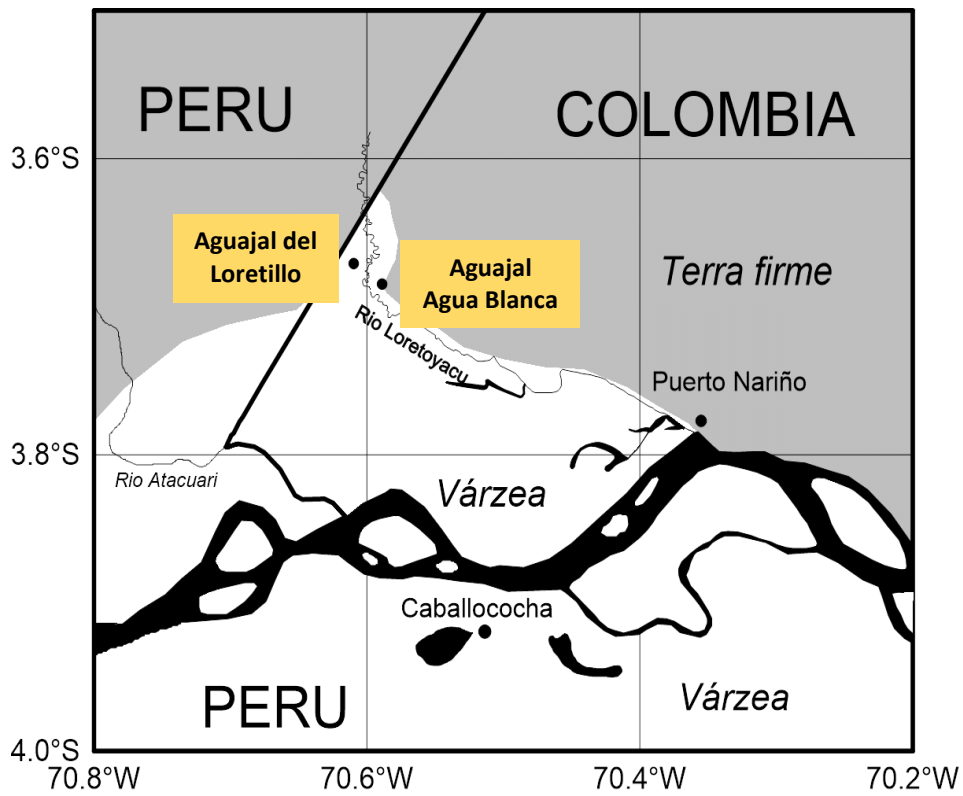


Figure 5. The location of the Tipisca cores Aguajal Agua Blanca and Aguajal del Loretillo. Map includes information regarding the proximity to the Rio Loretoyacu and the forest types found close to the palm swamp.



Figure 6. The Loretoyacu River close to where both Aguajal Agua Blanca and Aguajal del Loretillo were sampled.



Figure 7. The closed canopy environment of where the cores were sampled.

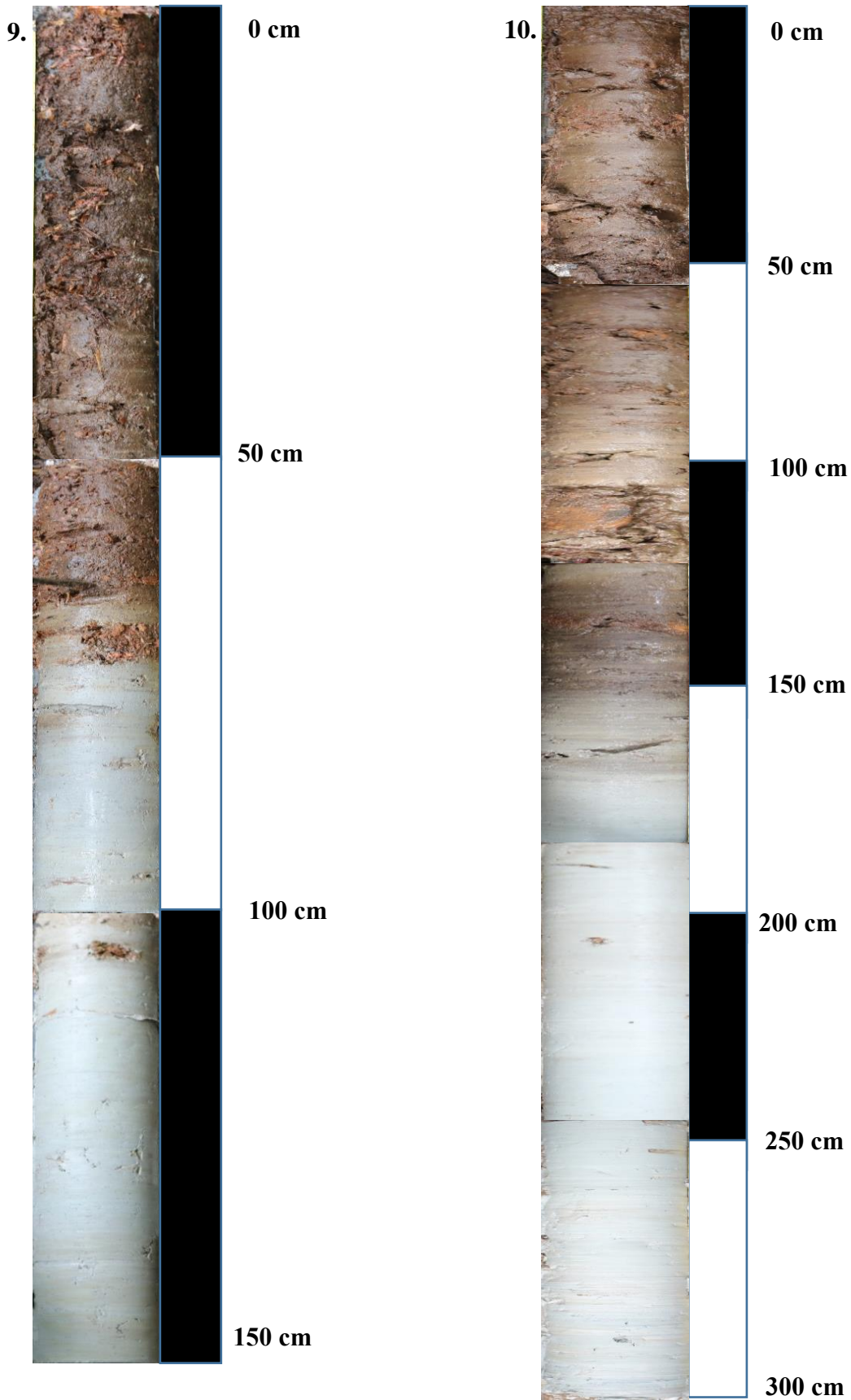


Figure 8. The environment where the cores were obtained. Note the large amounts of organic matter on the ground, originating from the surrounding vegetation.

3.1.3. Core Description

Aguajal Agua Blanca (S 03°38'56.2" W 070°37'0.00") measured 1.5 m in length and is composed of predominantly tropical organic peat. In the youngest part of the sediment, the peat is formed by roots and tree trunks, this can be seen in the core as the subsamples contained an abundance of macroremains from the vegetation. At ~0.8 m, there is a transition from the tropical organic peat to clay material. Small fragments of peat material can be seen between 0.8 m and ~1 m, however after this point the core is mainly composed of clay. The sediment remains a grey/white colour from ~1 m until the end of the core. After 1.5 m it became impossible to core any deeper due to the high-water content of the core.

Aguajal del Loretillo (S 03°38'34.9" W 070°36'23.5") measured 3 m in length. The first ~1.75 m of the core is composed of peat, but there is also a distinct transition into clay material at ~1.8 m. Similar to Aguajal Agua Blanca, the organic peat layers of the sediment contained an abundance of macroremains from the surrounding vegetation. The clay sediment is found until 3 m and is predominantly white/grey in colour. After this point, no further coring could take place due to hitting the bedrock.



Figures 9 and 10. Combined image displaying the Aguajal Agua Blanca (fig 9; aged ~1200 cal yr BP) and the Aguajal del Loretillo cores (fig 10; aged 4800 cal yr BP).

3.2. Guatavita – Pantano de Martos

3.2.1. Background

Since ~3-5 Ma, the Eastern Cordillera has risen by between 1500-2000 m as a result of crustal shortening (Mora-Perez et al, 2016). As a result, vegetation communities show a strong altitudinal zonation reflecting the strong up-slope variations in temperature and precipitation (*ibid*). These transition from montane forest (between 1000 to ~3200 m asl) to upper montane forest and subpáramo (between 3200 and 3800 m asl) and finally to Páramo vegetation at the highest altitudes (up to 4200 m asl) (Cleef and Hooghiemstra, 1984).

Of great importance are the páramo regions in the high-altitude areas of the Eastern Cordillera. Areas of páramo vegetation are located in the humid tropical Andes Mountains and occur as an altitudinal belt between the uppermost forests and perennial snow (Cleef, 1981). Due to the complex evolutionary processes within the last 3-5 Ma, vegetation within páramo ecosystems are diverse (Chacon et al, 2006), consisting of ~2,385 species from ~487 genera (Luteyn et al, 1992). Several studies have recognised páramo ecosystems as one of the world's hyper-hot biodiversity mini-hotspots (Myers et al, 2000). Additionally, within Colombia, the Páramo region is recognised as a highly efficient water regulation system, due to the high frequency of precipitation events and the low natural water consumption creating a large surplus of water which feeds the rivers descending to both the coastal areas and the Amazon Basin (Buytaert et al, 2006). This has not only allowed for the establishment of diverse plant communities (Berdugo-Lattke et al, 2016; Madriñán et al, 2013), but has also sustained human activities including water use and agriculture (Hofstede and Witte, 1993). In recent years Colombian Páramo areas has been over-exposed to fire, grazing and harvesting, which has led to a decrease in biodiversity and therefore a reduction in water retention capacity (Buytaert et al, 2006).

3.2.2. Site Description

Pantano de Martos is an ombrotrophic peat bog at ~3000 m asl within the Páramo of Monquentiva, in the municipality of Guatavita, approximately 40 km north east of Bogota. The Páramo of Monquentiva encompasses a total area of 14,142 ha at an altitude of 2900-3400 m asl and is home to high Andean forests, bushes, meadows and peat bogs (Avella et al, 2014). Work is currently underway to declare the area a Regional National Park due to its biological and cultural importance (Cleef, 2012). However, the land has undergone significant human

alterations. The limited available literature on the Martos site suggest that before the 17th century, Pantano de Martos contained an extensive lagoon which was surrounded by both forest and Páramo vegetation and was fed by numerous gorges. The establishment of drainage channels in the 1630s drained the lagoon, transforming the site into a wetland ecosystem (Gomez and Rubio, 2003). During the 1950s and the 1970s additional channels were dug in the marshes and swamps of the area to dry the area and adapt it for livestock. An extensive network of ditches were made to divert the waters of the south slope out of the swamp to further dry the area (Avella et al, 2014). However, since the 1990s efforts have been made to conserve the environment, with the local government initiating a natural recovery process to maintain the current marsh environment found today (*ibid*).

Rainfall in the area is of unimodal-bimodal type, with heavy rain falling between the months of March and August. The dry season occurs between December and February, with average annual precipitation being ~2000 mm (CAR, 2000). The Martos site is part of the water recharge zone of the Lagunero River, which is itself part of the great basin of the Orinoco River (Avella et al, 2014). Seasonal precipitation at the site is primarily controlled by the seasonal migration of the ITCZ (Poveda and Mesa, 1997) and it is mainly the tropical Trade winds that influence the site (Saylor et al, 2009). Given its altitude, Pantano de Martos characterised by low annual mean temperatures, of between 12°C and 14°C (Londono et al, 2014; Van Wesenbeek et al, 2003), although diurnal temperature variation can be substantial (Cleef, 1981).

Typically, páramo includes open vegetation types that occur above the upper forest line in the mountains of the humid tropics of Latin America (Bosman et al, 1993). Within the Pantano de Martos peat bog, vegetation is distributed in a mosaic mode and is predominantly composed of the peat-forming plant *Sphagnum megellanicum*. Surrounding the peat bog are species such as *Puya goudotiana*, a genus of Bromeliaceae typically found in South America (Horning-Leoni and Sosa, 2008) and species of *Espeletia* (*grandiflora* and *argénte*a), *Espeletiopsis corymbosa*, *Paepalanthus* and also *Calamagrostis effusa* (Avella et al, 2014).

3.2.3. Pantano de Martos Core

The Pantano de Martos core measured 3.75 m and was composed predominantly of peat. Fresh *Sphagnum* moss material made up the first ~0.1 m of the core, followed by approximately 0.7 m of black fine textured degraded peat. From ~1 m, the core is composed of a much more clay rich sediment, however is still peat material. This clay rich sediment can be seen throughout the remainder of the core, to the deepest part at ~3.75 m. Total organic content is high throughout the core and throughout macroremains in the form of degraded plant material remained are present. It is also important to note the white band of clay sediment found at ~1.3 m. Organic content throughout this material was low and was distinctly different to the peat material found in other parts of the core.

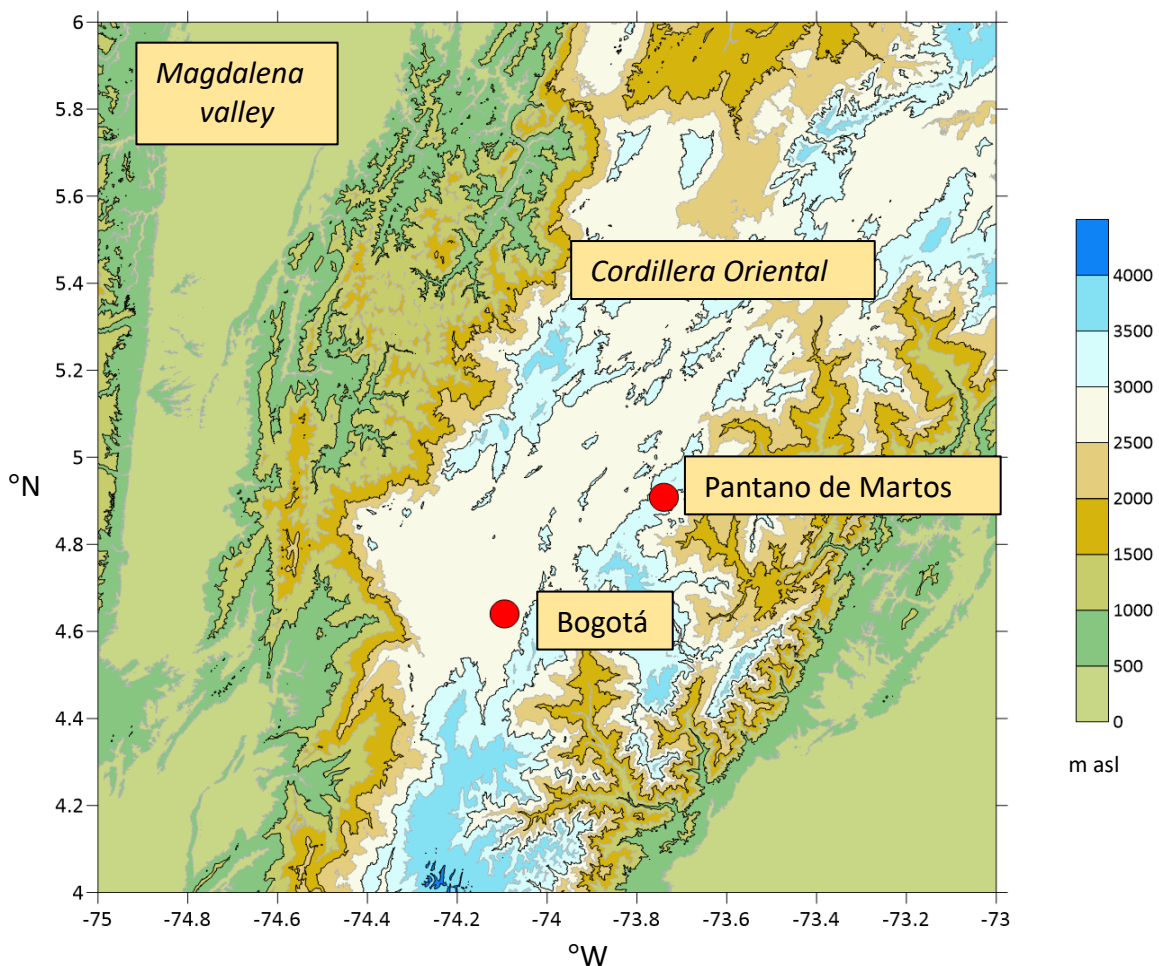


Figure 11. The Location of the Pantano de Martos core, with reference to Bogota and the Cordillera Oriental



Figure 12. The location of the Pantano de Martos core.



Figure 13. Local vegetation where the core was sampled. Note, the top of the core was obtained from a blanket of *Sphagnum* moss.

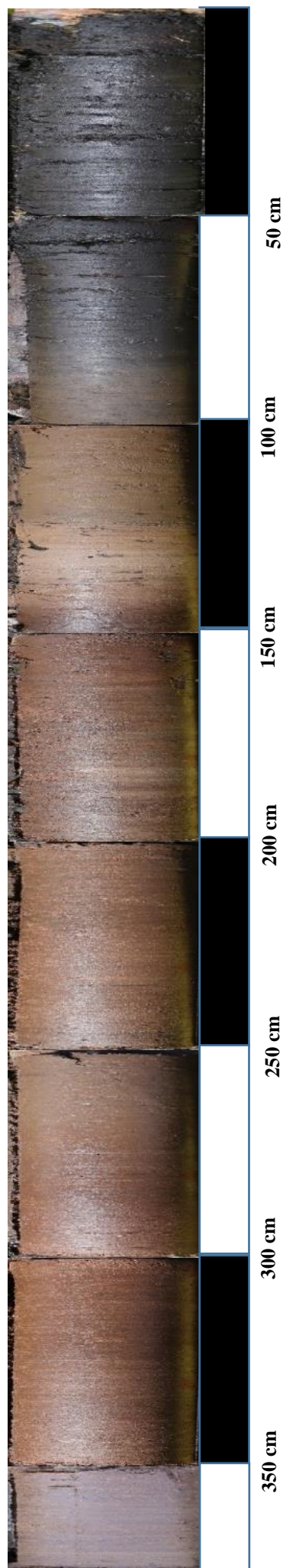


Figure 14. Combined image of the Pantano de Martos core, taken in 50 cm increments. The approximate age of the core is ~80,000 cal yr BP.

3.3. Sample Preparation

Cores were obtained with a Russian corer 50 cm in length. The cores were subsampled in the field in 2 cm increments and placed into individual zip-lock bags to minimise disturbance in the record. All samples were freeze dried for 24 hours using a Mini Lyotrap freeze drier. Subsamples of the freeze-dried material was ball milled and stored in Eppendorf tubes. The remainder of the sample was kept in the original sample bag for future analysis.

3.3.1 Radiocarbon Analysis

Information regarding the samples chosen for radiocarbon dating and the associated age-depth models for the Tipisca cores and Guatavita core can be found in Appendix A. For each core, samples from the top of the core, near the transition between differing sediment and towards the end of the core were chosen, with the aim creating a full representation of the cores age. The fine fraction of each sample was sampled for dating and efforts were made to ensure the samples did not come into contact with any contaminants. Additionally, macroremains were removed from the sample to avoid contamination and ensure that the ages generated were as accurate as possible. All samples were individually wrapped in foil, placed in a zip-lock bag and sent to the UCI Keck-Carbon Cycle AMS (Keck-CCAMS) laboratory in the Earth System Science Department at the University of California, for conventional radiocarbon analysis.

3.4. Total Organic Carbon and Total Nitrogen Analysis

Between 3-5mg of material (3mg for Aguajal Agua Blanca and Pantano de Martos; 5mg for Aguajal Agua Blanca and Aguajal del Loretillo) was encapsulated in tin cups for analysis of the total organic carbon (TOC), total nitrogen (TN) and $\delta^{13}\text{C}$ and $\delta^{15}\text{N}$ compositions. Samples were analysed using a SerCon ANCA Gas Solid Sample (GSL) elemental analyser coupled to a SerCon Hydra 20-20 continuous flow Isotope Ratio Mass Spectrometer (IRMS). Each sample run included a blank, a dummy and reference material. All samples were compared to the Pedro Palo C+N standard where nitrogen = 1.11%, $\delta^{15}\text{N}$ = 4.42‰, carbon = 13.96% and $\delta^{13}\text{C}$ = -21.69‰.

3.5. Lipid Extraction

3.5.1. Obtaining the lipid content of the sample

Lipid analysis was carried out on all three cores of the study. A portion of the unmilled 2cm sub-sample for each core was weighed out, 10 μ l of standard (49.068 mg squalane in 50 ml toluene) added to each sample. The samples were placed in a 10 ml Thermo-Scientific extraction cell and the lipids extracted using a Dionex Accelerated Solvent Extractor (ASE) machine with 9:1 dichloromethane (DCM) and methanol (MeOH) at 100°C and 1000psi.

The amount of sample was scaled to the suspected organic content. For example, in the case of Aguajal Agua Blanca, where there was a clear transition into clay-like material towards the bottom of the core, between 0.5g and 3g of sample was extracted in the upper half of the core and 7g of sample was used for the lower half.

The resulting total lipid extract was concentrated using a Techne Sample Concentrator linked to N₂ gas and a Stuart SB162 heater block set to 75°C. A chromatographic column comprising aluminium oxide (Al₂O₃) and Silica glass wool was used to purify and separate the lipid fraction into apolar and polar lipids using a 9:1 ratio of hexane and dichloromethane (DCM) for the apolar fraction and DCM for the polar fraction. A third fraction from methanol was collected to ensure all lipids were collected into their respective fractions. Approximately 2 ml of each fraction was collected.

3.5.2. Gas Chromatography Mass Spectrometry

The apolar fraction in the 9:1 ratio (Hexane:DCM) containing the *n*-alkanes of interest to the study was then evaporated and 1 ml of hexane added prior to analysis using Gas Chromatography-Mass Spectrometry (GC-MS). Samples were analysed using a Perkin Elmer Clarus 500 mass spectrometer, equipped with a CP-Sil 5CB-MS (30 m x 0.25 mm x 0.25 μ m) column. The oven programme of the GC-MS was set to 60°C increasing to 120°C at 20°C/min (following Carr et al, 2014).

Results were analysed using Turbomass 6.1, with compounds identified on the basis of their mass spectra and retention time. The absolute concentrations were determined based on the area of peaks relative to the squalane standard added before solvent extraction. The C₂₇, C₂₉

and C₃₁ *n*-alkanes were consistently the most abundant compounds present and were selected for deuterium analyses.

3.5.3. Deuterium Analyses

Compound-specific δD analyses of the C₂₇, C₂₉ and C₃₁ leaf wax *n*-alkanes were carried out using a ThermoFisher Scientific Trace GC equipped with HP-5 ms column (30 m, 0.25 mm, 1 μ m) coupled via a pyrolysis reactor operated at 1420°C. An SSL split/splitless injector was used to inject the samples at 280°C. The GC temperature was increased from 120°C (held 3 min) to 200°C at a rate of 30°C/min and then to 320°C at 4°C/min (held 24 min). Samples were measured in triplicate, with a typical replicate precision of better than $\pm 5\%$. The H₃⁺ factor for the mass spectrometer was determined daily by observing changes in the (mass-3)/(mass-2) ion-current ratio as the pressure of H₂ in the ion source varied (Luo et al, 2011). The instrument was tuned so that the H₃⁺ factor was always around 4.3 and varied minimally over the course of the analyses. δ values become less accurate as sample/standard pairs become more widely separated as a result of instrumental drift (Sessions, 2006). As a result, normalisation of the isotopic values is essential to ensure that data from all laboratories are comparable. A normalisation line is constructed by analysing a suite of standards of known isotopic composition, which vary over the range of expected δ values (Sessions, 2006). This corrects all measurements in case of instrumental error. As a result, all data was normalised according to Sessions et al (1999), and all δD values produced were given in permil (‰) relative to Vienna Mean Standard Ocean Water (VSMOW) (Hermann et al, 2017). All results are presented against the ages obtained through radiocarbon dating and subsequent age-depth modelling. For more information see Appendix A.

Chapter 4: Results.

4.1. Aguajal Agua Blanca

4.1.1. Total Organic Carbon (TOC), Total Nitrogen (TN) and the TOC/TN Ratio

Total organic carbon (TOC), total nitrogen (TN) and the TOC/TN ratio are displayed in figure 15. TOC ranged from 0.41% to 44.8%. Between 400 and 600 cal yr BP TOC declines rapidly from ~44% to <1%. Between 600 to 1200 cal yr BP, TOC declines further to ~0.5%. TN ranges from 0.04 to 3.03% and largely tracks TOC; however, the amount of nitrogen is significantly lower. Again, a significant reduction of TN is found from the 0 to 600 cal yr BP. From 600 cal yr BP to ~1200 cal yr BP TN declines to ~0.05%. TOC/TN ranges from 7.3 to 27.7. TOC/TN is relatively high (between ~14 to 27) between 0 to ~560 cal yr BP before dropping to ~9.9 at the bottom of the core (1200 cal yr BP). The most significant drop in the TOC/TN occurs between 540 and 620 cal yr BP. During this period, TOC/TN declines from 27.7 to 7.3.

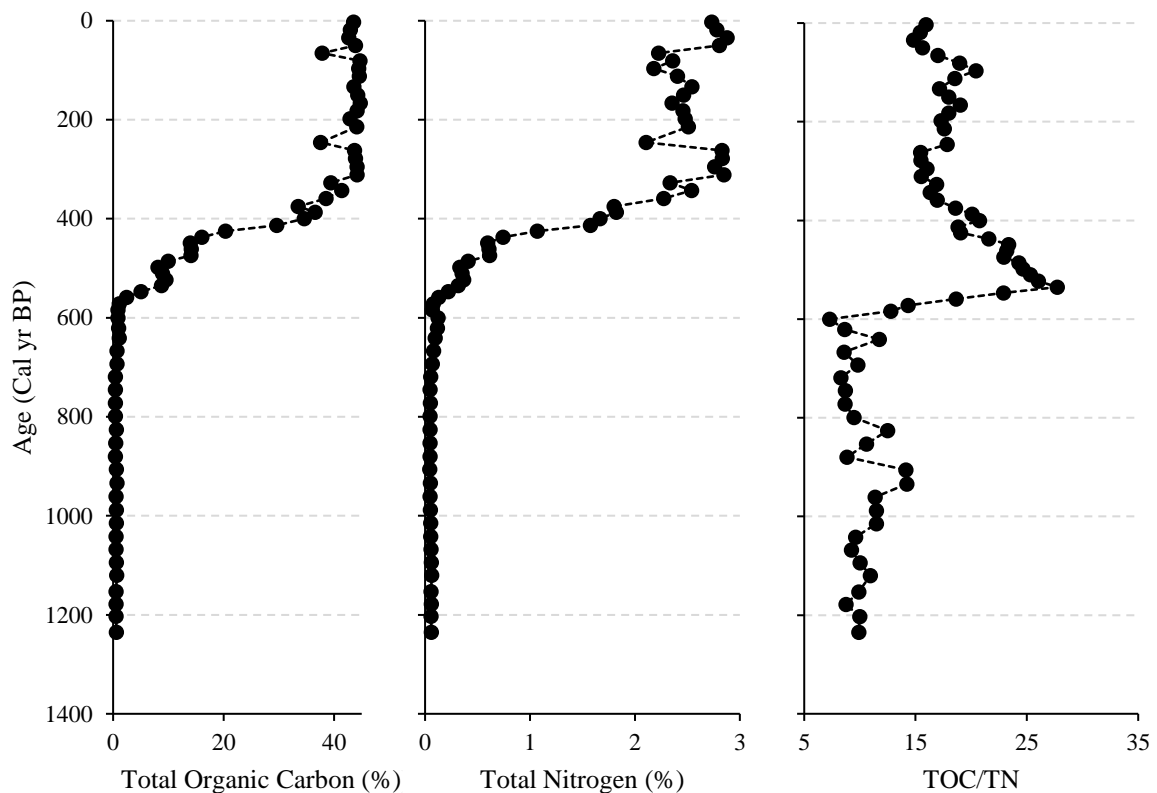


Figure 15. Down-core trends in total organic carbon (TOC), nitrogen (TN) and the TOC/TN ratio for Aguajal Agua Blanca.

4.1.2. Bulk Isotope Data - $\delta^{13}\text{C}$ and $\delta^{15}\text{N}$

The $\delta^{13}\text{C}$ and $\delta^{15}\text{N}$ values for Aguajal Agua Blanca are displayed in figure 16. $\delta^{13}\text{C}$ ranges from -32.1‰ to -14.7‰, averaging -27‰. Between 0 and 900 cal yr BP, a progressive trend to higher $\delta^{13}\text{C}$ is observed, increasing from -30.5‰ to -14.7‰. From this point until the end of the core (~1200 cal yr BP) $\delta^{13}\text{C}$ values decline to -21.2‰.

In contrast $\delta^{13}\text{C}$, the $\delta^{15}\text{N}$ values for Aguajal Agua Blanca show a marked difference. Between 0 and 500 cal yr BP, $\delta^{15}\text{N}$ values remain constant at ~4‰. However, after 500 cal yr BP, $\delta^{15}\text{N}$ values become highly scattered, most probably due to measurement imprecision because of extremely low N concentration (Figure 15).

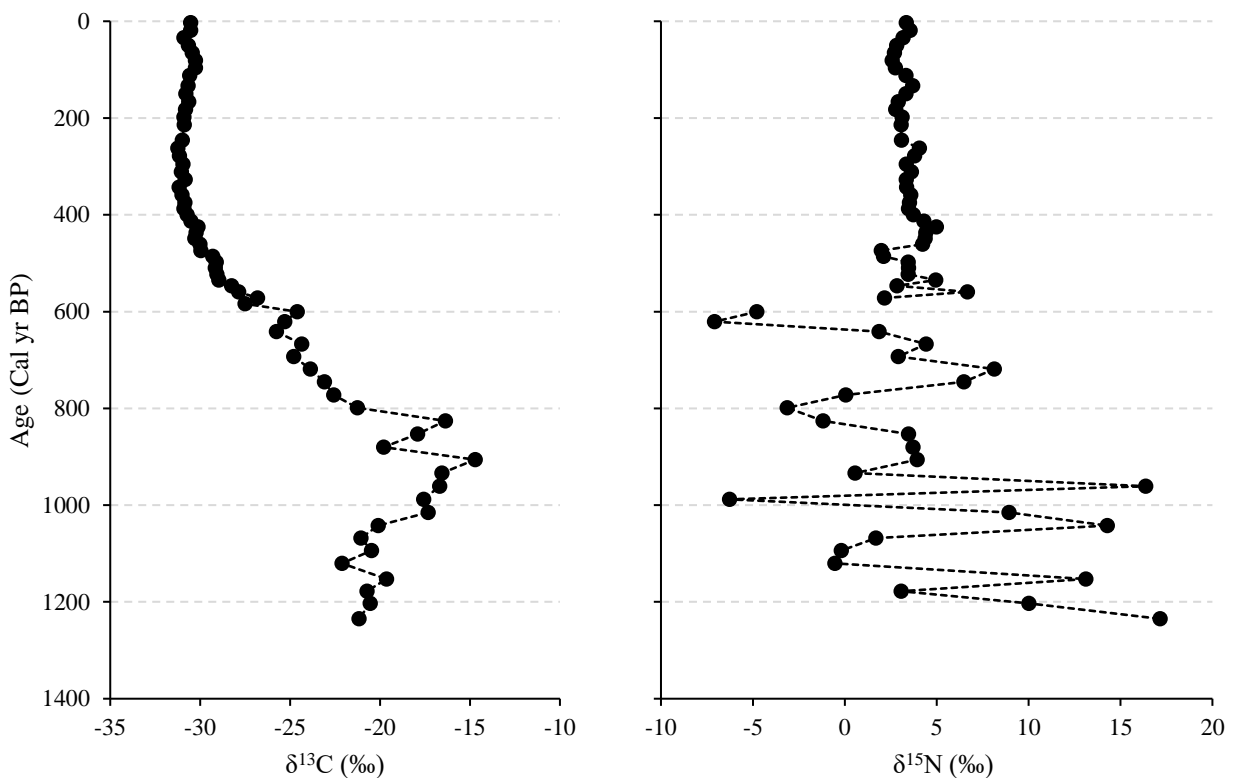


Figure 16. Down-core trends in $\delta^{13}\text{C}$ and $\delta^{15}\text{N}$ for Aguajal Agua Blanca obtained by elemental analysis.

4.1.3. Leaf wax *n*-alkane distributions

Long chain *n*-alkanes were identified throughout the Aguajal Agua Blanca core, with the most consistently identifiable *n*-alkanes spanning the range C₁₇ to C₃₃. The most abundant *n*-alkane at all depths is C₂₉, making up on average ~31% of the total *n*-alkane abundance. Short to mid-chain *n*-alkanes (C₁₇–C₂₆) were present in all samples, except for the C₂₄ alkane, which was only present in small amounts after 81 cal yr BP (below 28 cm). Overall, even though the short to mid chain *n*-alkanes are present, their relative abundance is significantly lower than the long chain *n*-alkanes (C₂₇–C₃₃). Typically, the mid-chained (C₂₁–C₂₅) *n*-alkanes contributed a combined abundance of between 1.6 and 6.4% across the whole of the core, with the highest abundances in specific samples typically averaging around between 8-13%.

For the majority of the core, the C₂₉ and C₃₁ alkanes were consistently the most abundant, making up a combined average abundance of ~52%. However, at 540 cal yr BP (90 cm), the abundance of the C₂₉ and C₃₁ *n*-alkanes decreases and the C₂₅ alkane increases, increasing in relative abundance from 9.2% to 40.3% (fig. 17). After 540 cal yr BP the abundance of all alkanes decreases significantly, to an almost undetectable level. Alkanes were not preserved in sediment older than 550 cal yr BP.

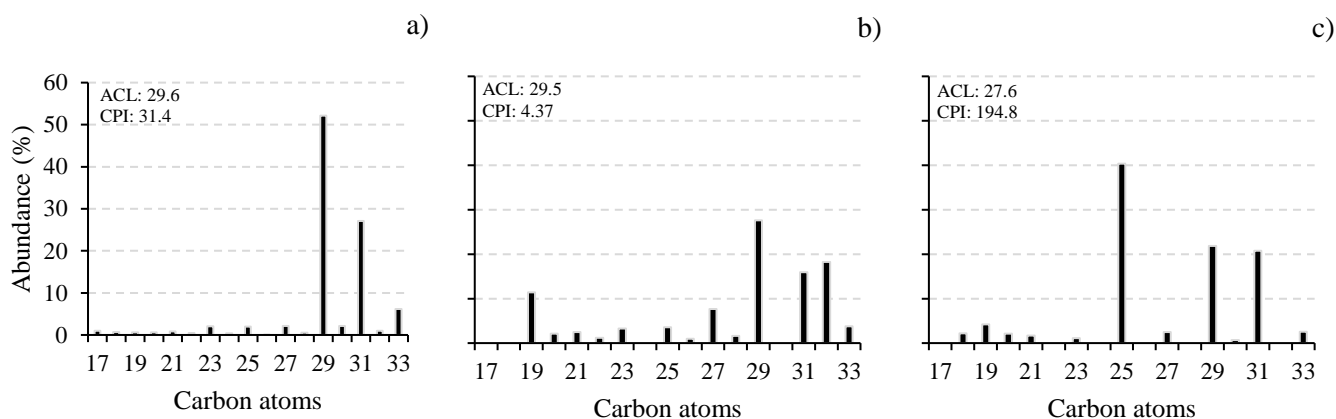


Figure 17. *n*-alkane distributions for a) -68 cal yr BP (0 cm), b) 246 cal yr BP (48 cm) and c) 535 cal yr BP (90 cm) of the Aguajal Agua Blanca core.

The average chain length (ACL₂₃₋₃₃) and the carbon preference index (CPI₂₃₋₃₃) are displayed in figure 18. ACL₂₃₋₃₃ values range from 26.6 to 30.5 (averaging 29.2). There is an apparent cyclical pattern of increasing and decreasing average chain lengths over a ~200-year period (figure 18). Between 0 and 200 cal yr BP, ACL₂₃₋₃₃ values decrease from 29.86 to 28.74. This

is followed by an apparent increase from ~200 to 400 cal yr BP where ACL_{23-33} increases again towards 29.76. After 400 cal yr BP, ACL_{23-33} values begin to decrease again, reaching a value of 27.7 at 540 cal yr BP.

The CPI_{23-33} values for the Aguajal Agua Blanca core indicate an odd over even predominance and range from 2.4 to 194.8. Across the total length of the core CPI_{23-33} values averaged 23.1. In contrast to the ACL data, there are no down-core trends in CPI_{23-33} ; instead the values are scattered and show no relationship with age. It must also be noted that CPI values from between 520 and 540 cal yr BP (140.56 and 194.83) were excluded from the figure, so that the distribution of the other samples and their respective CPI values could be seen more clearly. The large CPI values are expected to be due to the extremely low amounts of the even-chained *n*-alkanes.

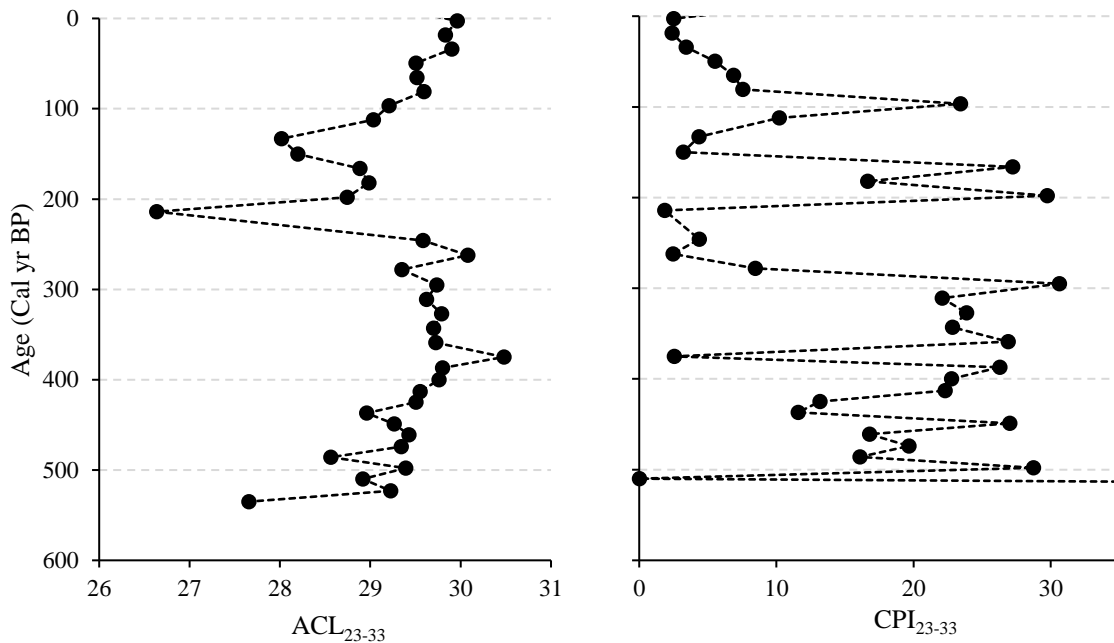


Figure 18. The average chain length (ACL_{23-33}) and the carbon preference index (CPI_{23-33}) for Aguajal Agua Blanca.

The P_{aq} ratio (Ficken et al, 2000) and Norm31 ($C_{31} / (C_{31} + C_{29})$) are shown in figure 19. Both P_{aq} and Norm31 values show subtle variation throughout the core. Across the core, P_{aq} values range from 0.03 to 0.49, with average P_{aq} typically of 0.12. It is only in the modern section of the core (~0 cal yr BP) where more pronounced variation is found. In this section, P_{aq} values range from 0.04 up to 0.38. The most pronounced change in P_{aq} can be seen between 0 and 100

cal yr BP. During this time, P_{aq} decreased from 0.15 to 0.03. Towards the older parts of the core, P_{aq} values show minimal change, only varying between the values of 0.1-0.2.

Norm31 values range from 0.02 to 0.54 across with core, with an average value of ~ 0.41 . In general, between the top of the core to ~ 200 cal yr BP a trend of decreasing Norm31 values with increasing age is seen. During this time Norm31 values decrease from 0.54 to 0.29. Between 200 and 300 cal yr BP, Norm31 values increase and become substantially less varied.

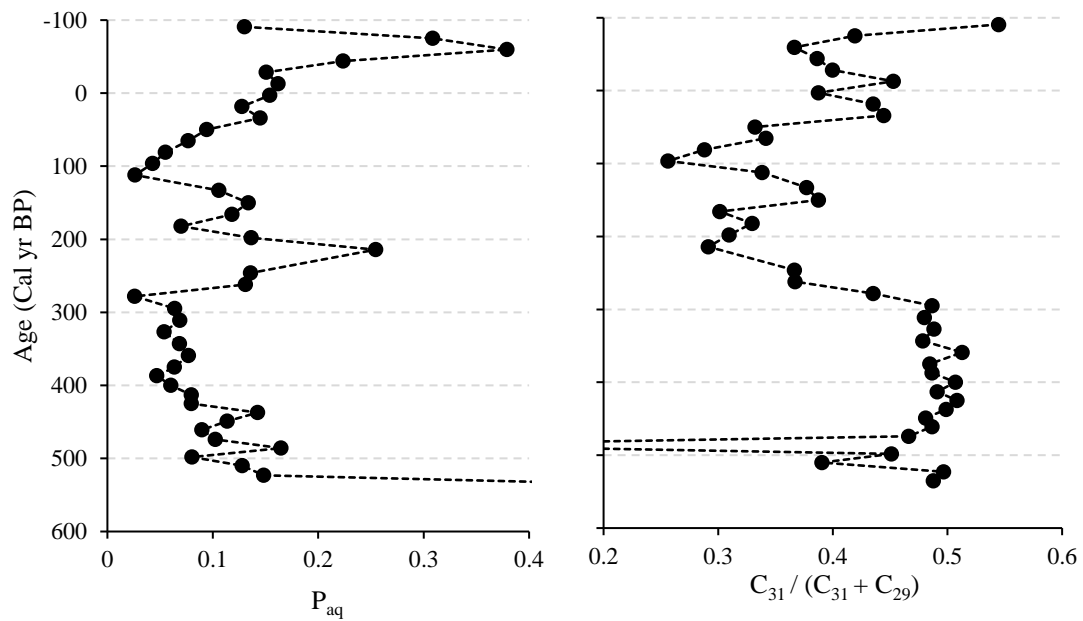


Figure 19. The P-aqueous (P_{aq}) ratio and Norm31 values for Aguajal Agua Blanca.

4.1.4. Leaf wax *n*-alkane δD

δD_{wax} results for the C_{27} , C_{29} and C_{31} *n*-alkanes are shown in figure 20. δD_{wax} values of the C_{27} *n*-alkane ranged from -106‰ to -180‰ throughout the core. Across the modern section (~0 to 65 cal yr BP), a transition towards more positive δD_{wax} values can be seen with δD_{wax} values increasing from -153‰ to -128‰. Excluding the sudden increase in δD_{wax} at 260 cal yr BP (-157‰), a trend towards more negative δD_{wax} values is seen between 64 cal yr BP and 290 cal yr BP, reaching -180‰ – the most negative value found across the core. After this point, δD_{wax} values start to increase towards -156‰. Variation in the δD_{wax} values of the C_{29} *n*-alkane are less pronounced than those of C_{27} . Across the core, δD_{wax} values of the C_{29} *n*-alkane range from -141‰ to -174‰. As seen for C_{27} , a transition towards more positive δD_{wax} can be seen in the youngest 200 years of the core. After this a shift towards more negative δD_{wax} values is observed between 100-130 cal yr BP, with δD_{wax} remaining relatively stable, fluctuating between -155‰ and -164‰. δD_{wax} values of the C_{31} *n*-alkane range between -137‰ and -173‰ through the core, with the majority of the δD_{wax} values approximately -150‰. As is the case of the C_{27} and C_{29} *n*-alkanes, δD_{wax} values show a transition to more positive values between the modern fractions of the core down to 200 cal yr BP. A transition to more negative δD_{wax} values is also found between 350 and 450 cal yr BP. A correlation coefficient was calculated for the δD_{wax} values and is shown in table 3. It is only the δD_{wax} values of the C_{27} vs. C_{29} *n*-alkanes that show a similar trend, giving a coefficient value of 0.71. The δD_{wax} values for the C_{29} vs. C_{31} show the weakest correlation throughout the record. This is probably due to the larger range in δD_{wax} for the C_{29} *n*-alkane.

Table 3. The correlation coefficients for the δD_{wax} values of the C_{27} vs. C_{29} , C_{27} vs. C_{31} and C_{29} vs. C_{31} for Aguajal Agua Blanca.

| C ₂₇ vs. C ₂₉ | | C ₂₇ vs. C ₃₁ | | C ₂₉ vs. C ₃₁ | |
|-------------------------------------|----------|-------------------------------------|---------|-------------------------------------|---------|
| Correlation coefficient | P-value | Correlation coefficient | P-value | Correlation coefficient | P-value |
| 0.71 | 1.15E-07 | 0.40 | 0.32 | 0.16 | 0.0087 |

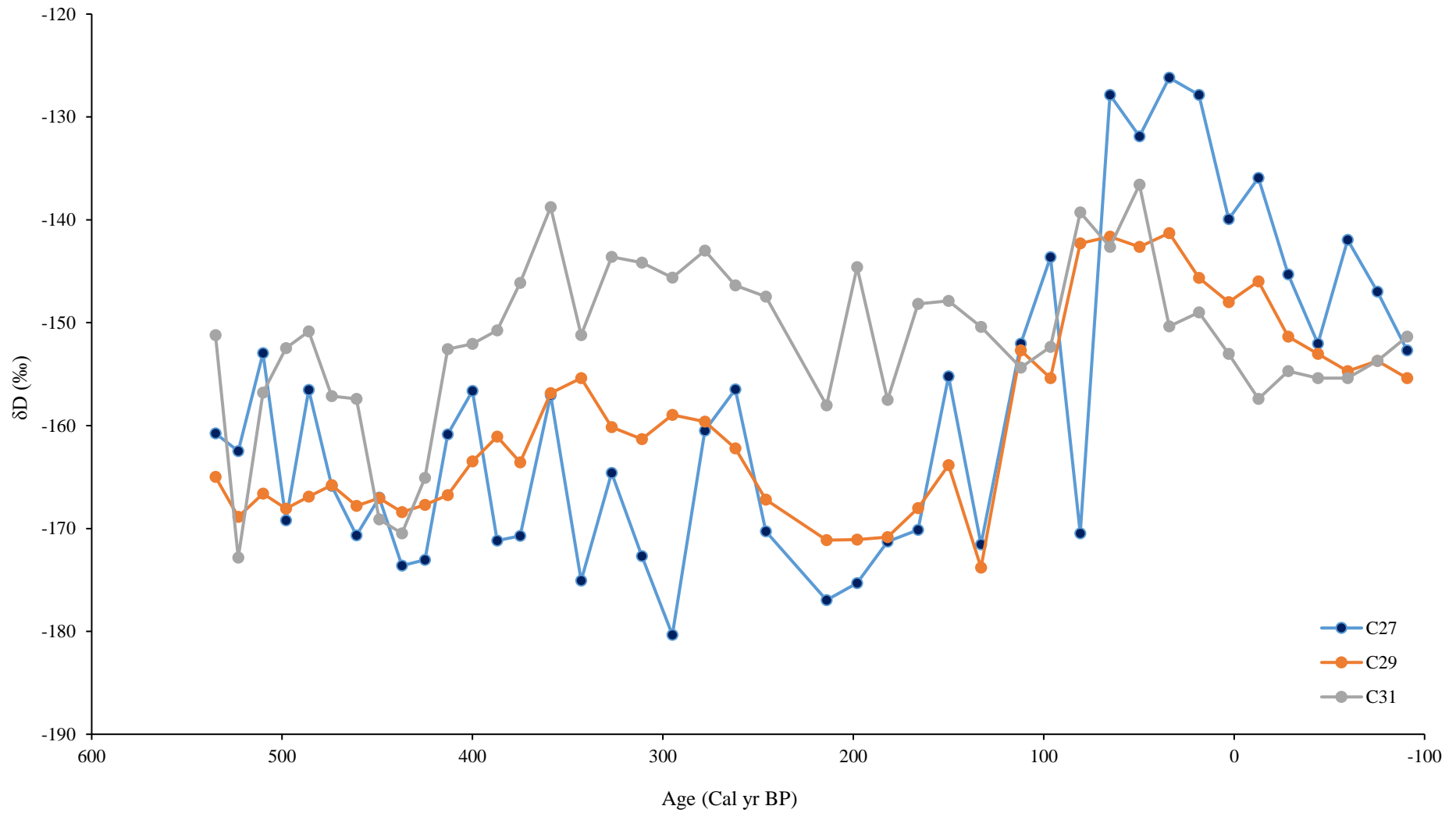


Figure 20. δD_{wax} values for the C₂₇, C₂₉ and C₃₁ *n*-alkanes for the Aguajal Agua Blanca core.

4.2. Aguajal del Loretillo

4.2.1. Total Organic Carbon (TOC), Total Nitrogen (TN) and the TOC/TN Ratio

Total organic carbon (TOC), total nitrogen (TN) and the TOC/TN ratio are shown in figure 21. TOC ranged from 0.26% to 44.4%. As at Aguajal Agua Blanca, TOC declines markedly down the core. Between ~0 cal yr BP to ~2000 cal yr BP, TOC declines from ~44% to ~6%. From 2000 cal yr BP to the oldest section of the core (~4600 cal yr BP) TOC declines further, to 0.3%. TN largely tracks TOC, however the amount of nitrogen in the core is significantly lower. TN ranges from 0.05% to 2.3%. Like TOC, the greatest decline in TN is found between ~0 and 2000 cal yr BP. During this time, TN decreases by 1.9%. From 2000 cal yr BP until the oldest parts of the core (~4600 cal yr BP), TN values decrease further to 0.05%. TOC/TN values again show a similar trend to those seen in TOC and TN. TOC/TN ranges from 0.1 to 16.2. During the first ~1000 years of the core, TOC/TN increases slightly, with TOC/TN values averaging ~11. Between 1000 and 2000 cal yr BP TOC/TN shows no marked trend. From 2000 cal yr BP to ~4600 cal yr BP TOC/TN values remain below 2.0, with the majority of values falling below 0.58.

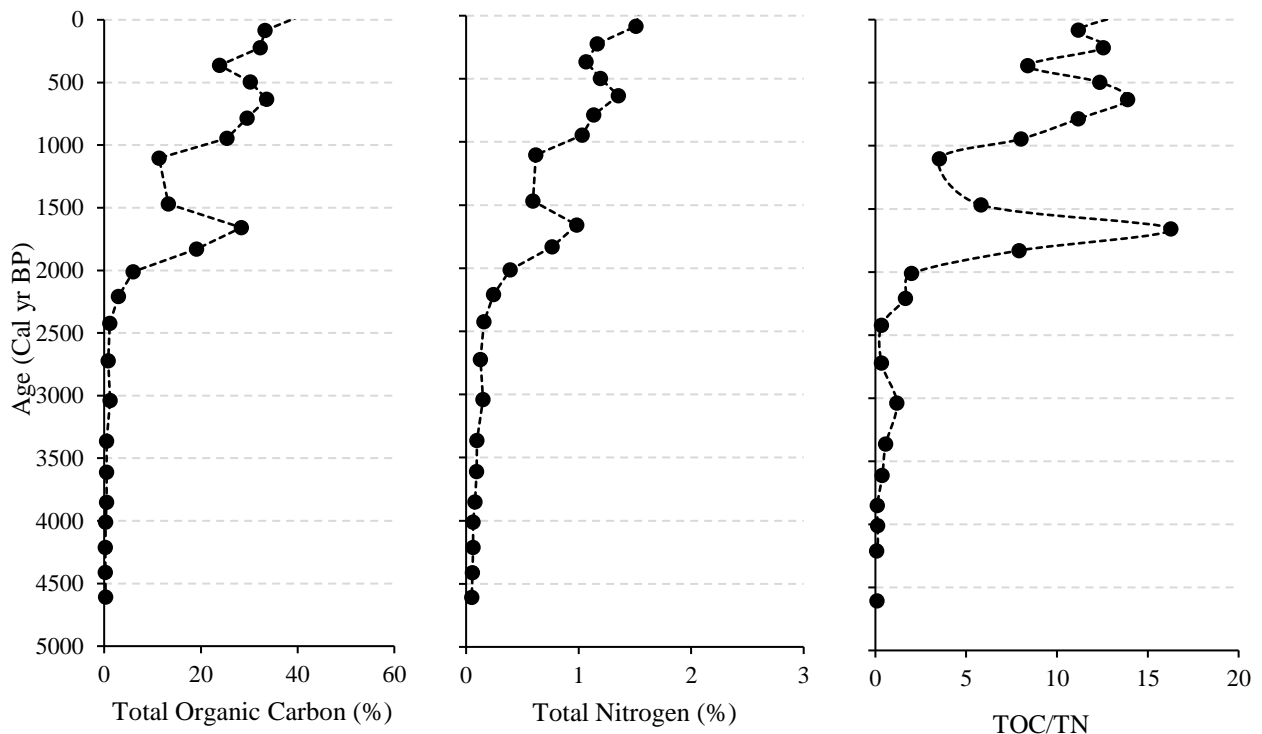


Figure 21. Down-core trends in total organic carbon, nitrogen and the TOC/TN ratio for Aguajal del Loretillo.

4.2.2. Bulk Isotope Data - $\delta^{13}\text{C}$ and $\delta^{15}\text{N}$

The $\delta^{13}\text{C}$ and $\delta^{15}\text{N}$ for Aguajal del Loretillo are shown in figure 22. $\delta^{13}\text{C}$ values range from -25.5‰ to -32.5‰, averaging -28.7‰. A transition to lower $\delta^{13}\text{C}$ occurs between the modern sample to ~2000 cal yr BP. During this period $\delta^{13}\text{C}$ decreases from ~27.0‰ to -32.0‰. A transition towards more positive $\delta^{13}\text{C}$ is observed between 2000 cal yr BP and 4600 cal yr BP. During this time $\delta^{13}\text{C}$ increases by ~4‰, producing a value of -28.4‰ at 4600 cal yr BP. Generally, $\delta^{15}\text{N}$ values gradually decline through the core, with $\delta^{15}\text{N}$ decreasing by ~3.7‰ between ~0 and 3400 cal yr BP. Between 3400 and 4600 cal yr BP a slight increase in $\delta^{15}\text{N}$ is found, with $\delta^{15}\text{N}$ values averaging at ~3.0‰.

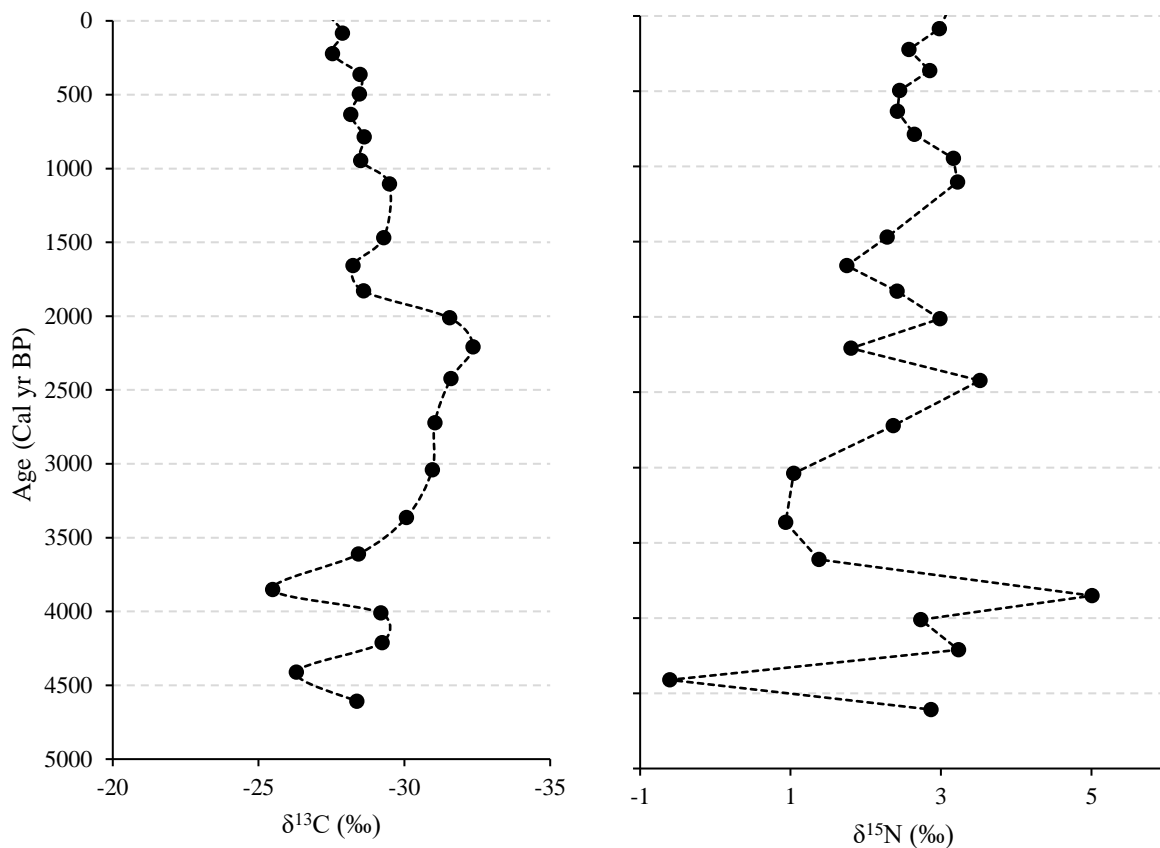


Figure 22. Down-core trends in $\delta^{13}\text{C}$ and $\delta^{15}\text{N}$ for Aguajal del Loretillo obtained by elemental analysis.

4.2.3. Leaf wax *n*-alkane distributions

Throughout the Aguajal del Loretillo core long chain *n*-alkanes were identified spanning the range C₁₁ to C₃₃. Due to this broad distribution, the relative concentrations of individual *n*-alkanes are relatively small, with the most abundant peak in any sample typically making less than 50% of the total *n*-alkane abundance. For the majority of samples, the C₂₉ and C₃₁ alkanes were consistently the most abundant (fig. 23). Typically, these *n*-alkanes made up ~ 24% and 15% of the total *n*-alkane abundance respectively. Shorter chain-length *n*-alkanes (C₁₁-C₁₉) were present in all samples, but their relative abundance typically was ~4% of the total *n*-alkane abundance. Mid-chain *n*-alkanes (C₂₀-C₂₆), were also relatively low in concentration (<7%), especially in the younger parts of the core (<1800 cal yr BP; 170cm depth)

At 2400 cal yr BP (200cm depth), the C₃₃ alkane disappears and is not distinguishable in the *n*-alkane distribution (fig. 23). Interestingly, at this time the relative abundance of the other longer chain *n*-alkanes decrease, while the relative abundance of the shorter chain *n*-alkanes (C₁₉-C₂₂) greatly increases. In this instance the shorter chain *n*-alkanes each make up ~20% of the total *n*-alkane abundance and show an even over odd predominance, whereas the abundance of the C₂₉ and C₃₁ alkanes decreases to between 4-7%. Overall, after 2400 cal yr BP the presence of all *n*-alkanes significantly diminishes. Where there are *n*-alkanes present, their abundance is minimal, creating difficulties in the interpretation of the data. From ~3000 cal yr BP (220cm depth), *n*-alkanes are no longer detected.

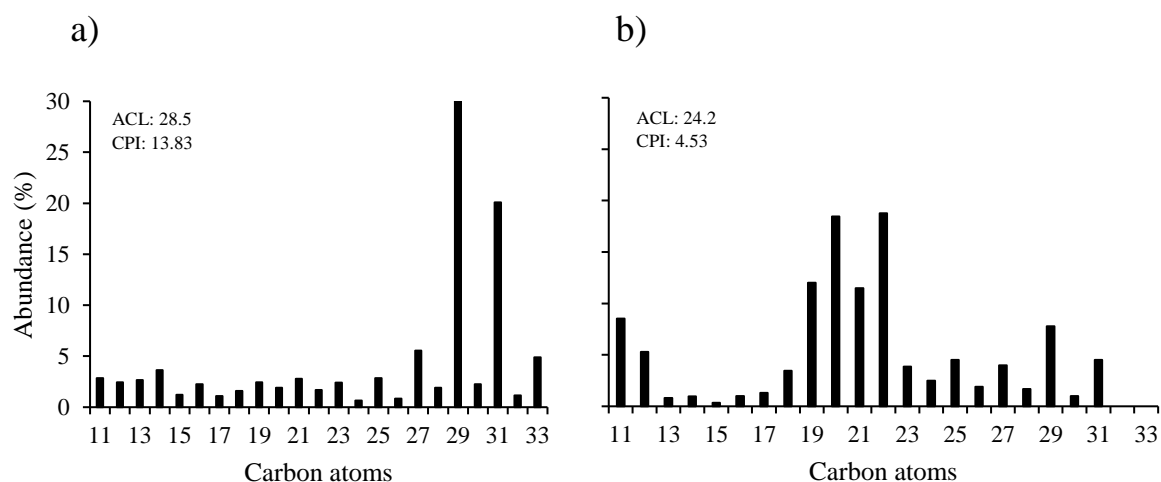


Figure 23. *n*-alkane distribution graphs for samples at a) 84 cal yr BP and b) 2400 cal yr BP.

The average chain length (ACL_{23-33}) and the carbon preference index (CPI_{23-33}) are displayed in figure 24. ACL_{23-33} ranges from 27.1 to 29.6 through the core, with ACL_{23-33} values averaging 28.7. A trend for decreasing ACL_{23-33} values with increasing age is seen between 0 and ~1800 cal yr BP. During this time ACL_{23-33} values decrease from 29.3 to 28.1. At 2000 cal yr BP ACL_{23-33} values increase to 29.3, followed by another sudden decrease of ACL_{23-33} values at 2423 cal yr BP (27.14). At ~3 ka cal yr BP, ACL_{23-33} values increase again to 29.0, followed by another subtle decrease in chain length.

Due to the reduced presence of long chain *n*-alkanes with age, CPI_{23-33} values could only be calculated until ~2500 cal yr BP. CPI_{23-33} values for the Aguajal del Loretillo core all show an odd over even chain length preference with CPI_{23-33} values ranging from 4.5 to 21.7. Throughout the core, the average CPI_{23-33} was 11.2. Although very subtle, a trend towards lower CPI values with increasing age can be seen across the core from ~1600 to 2500 cal yr BP. In the earlier sections of the core, CPI_{23-33} values are more scattered, but on average range from 15-20, compared to 5-10 in the lower half of the core.

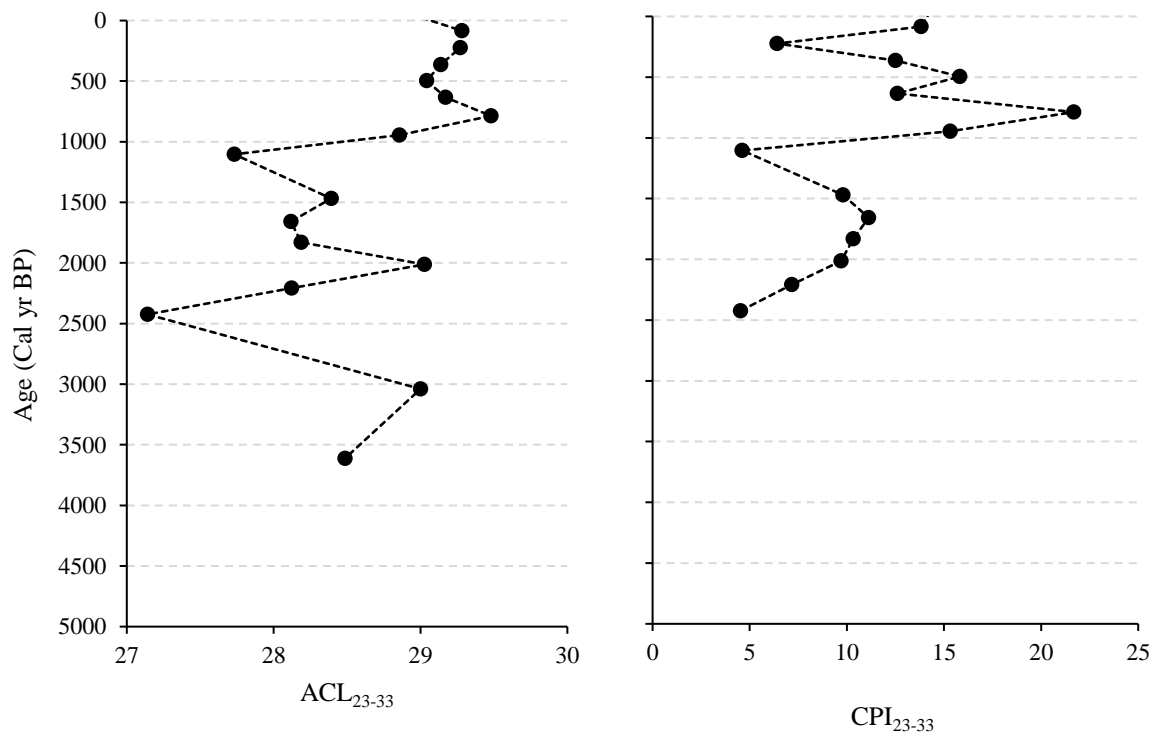


Figure 24. The average chain length (ACL_{23-33}) and the carbon preference index (CPI_{23-33}) for Aguajal del Loretillo.

The P_{aq} ratio and Norm31 values are shown in figure 25. Throughout the core, P_{aq} values range from 0.03 to 0.40, although the majority of values lie between 0.1-0.2. A gradual decline in P_{aq} from the top of the core to ~1000 cal yr BP can be seen. From 1000 to 2000 years P_{aq} increases to 0.3. The highest P_{aq} value is found at 3000 cal yr BP (0.40). This is then followed by a drop in P_{aq} to the lowest value found across the core (0.01).

In contrast to the more noticeable changes in P_{aq} , the Norm31 data show more subtle change. Across the core Norm31 values range from 0.31 to 0.51, with the average Norm31 being 0.38. Like P_{aq} , Norm31 declines between the top of the core to 1000 cal yr BP, from 0.51 to 0.31. An increase in Norm31 is followed after this time up to 2200 cal yr BP, where values reach 0.43. As seen in the P_{aq} values, Norm31 then declines again into the older sections of the core.

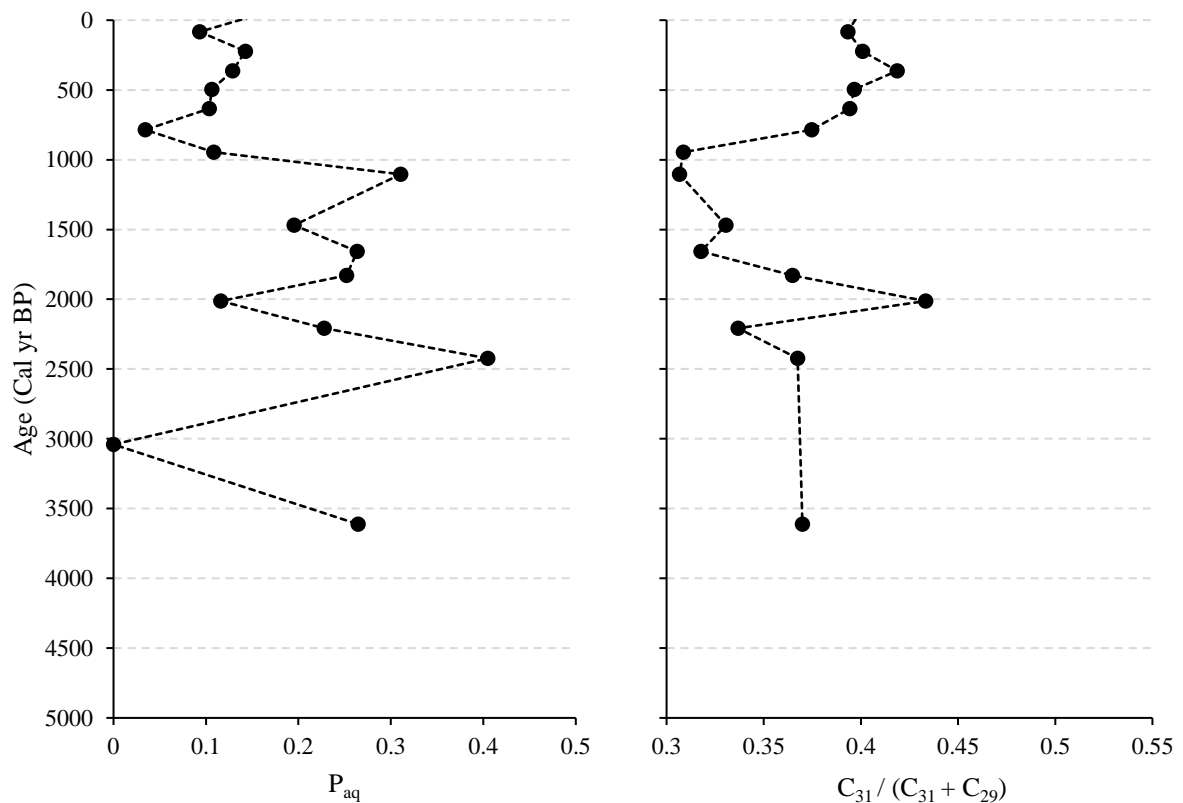


Figure 25. The P-aqueous (P_{aq}) ratio and Norm31 values for Aguajal del Loretillo.

4.2.4. Leaf wax *n*-alkane δD

The δD_{wax} values for the C_{27} , C_{29} and C_{31} *n*-alkanes obtained for the Aguajal del Loretillo core are shown in figure 26. δD_{wax} values of the C_{27} *n*-alkane range from -129‰ to -180‰, although typically δD_{wax} values fall around -150‰. Higher δD_{wax} values are found at -180, 300, 1100, 1500 and 1900 cal yr BP, all of which are followed by a transition to more negative δD_{wax} values. The lowest δD_{wax} can be seen at 1700 cal yr BP, where values reach -176‰. Variation in the δD_{wax} values of the C_{29} *n*-alkane is much less pronounced during the youngest parts of the core. Between ~0 cal yr BP (the modern section of the core) until 800 ka cal yr BP δD_{wax} values only vary by ~10‰. In contrast, the older sections of the core show a more marked variability in δD_{wax} , especially between 1400 and 2200 cal yr BP. During this time δD_{wax} values change by ~70‰. Overall, δD_{wax} values across the length of the core range between -135‰ to -209‰. Throughout the majority of the core, the δD_{wax} values for the C_{31} *n*-alkane show a similar pattern as found in the C_{27} and the C_{29} *n*-alkanes. The main noticeable variation occurs at ~1500 cal yr BP where δD_{wax} values become significantly more negative (-202‰). A correlation coefficient was calculated to ascertain the correlation between the δD_{wax} values. All correlations are weak, with the C_{29} vs. C_{31} showing the highest correlation. Even so, this is still low at 0.46.

Table 4. The correlation coefficients for the δD_{wax} values of the C_{27} vs. C_{29} , C_{27} vs. C_{31} and C_{29} vs. C_{31} for Aguajal del Loretillo.

| C_{27} vs. C_{29} | | C_{27} vs. C_{31} | | C_{29} vs. C_{31} | |
|--|---------|--|---------|--|---------|
| Correlation coefficient | P-value | Correlation coefficient | P-value | Correlation coefficient | P-value |
| 0.44 | 0.0051 | 0.32 | 0.045 | 0.46 | 0.0023 |

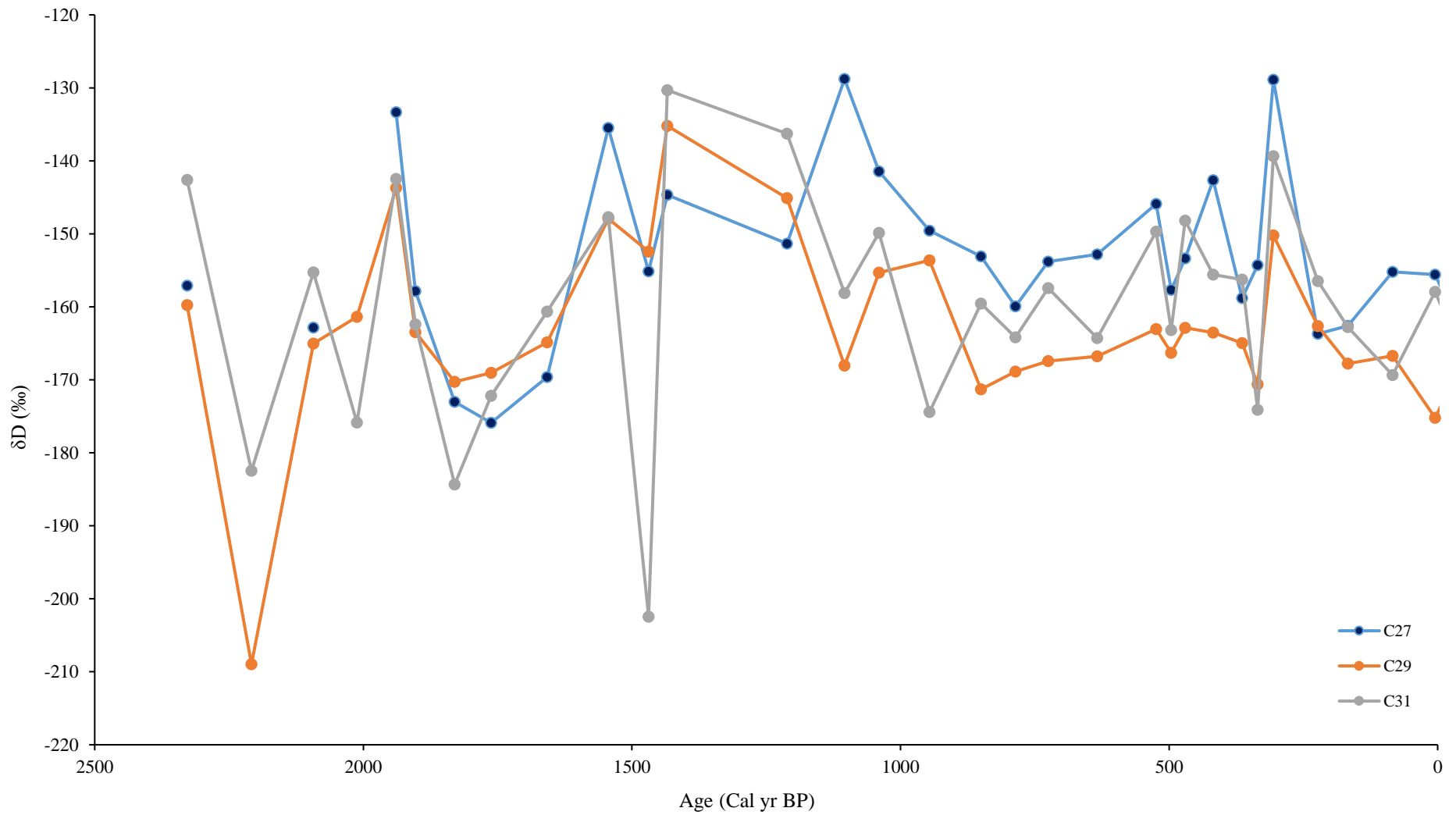


Figure 26. The δD_{wax} values for the C₂₇, C₂₉ and C₃₁ *n*-alkanes obtained from the Aguajal del Loretillo core.

4.3. Pantano de Martos

4.3.1 Total Organic Carbon (TOC), Total Nitrogen (TN) and the TOC/TN Ratio

Total organic carbon (TOC), total nitrogen (TN) and the TOC/TN ratio for the Pantano de Martos core are displayed in figure 27. TOC ranged from 6.4% to 58.5%, with an average across the whole core of 39.1%. TOC declines from the top of the core, reaching a minimum of 6-8% between 13,000-30,000 cal yr BP. TOC then increases to a maximum of 58.5% at ~41,000 cal yr BP before fluctuating between 35.5% and 57.8% to the base of the core. One of the most noticeable findings is that even towards the base of the core at ~340 cm (~74,000 cal yr BP), TOC remains high, reaching up to 58%. TN largely follows the same trends as TOC, but the amount of nitrogen is significantly lower. Total nitrogen values range from 0.3% up to 2.3%, with an average of 1.3%. Again, a significant reduction of TN is seen from the top of the core down to 13,000 cal yr BP, reaching a minimum of 0.3%. Total nitrogen increases slowly into the deeper parts of the core, but does not exceed values seen at the top of the core fluctuating between 0.9 and 1.8%. Throughout the core, the TOC/TN ratio ranges from 15.7 to 43.5, with an average of 30.7. When comparing the TOC/TN ratio to the total carbon and nitrogen data (fig.27), some of the lowest TOC/TN values - between 19 and 23 – occur between 13,000 to 30,000 cal yr BP. Throughout there is significant variability in TOC/TN, seemingly over tens of thousands of year timescales. However, the lowest values are found in the youngest 5,000 years (between 0 and 4400 cal yr BP). As depth increases, the values of the TOC/TN tend to increase on average, but with clear fluctuations over ~10,000 periodicities.

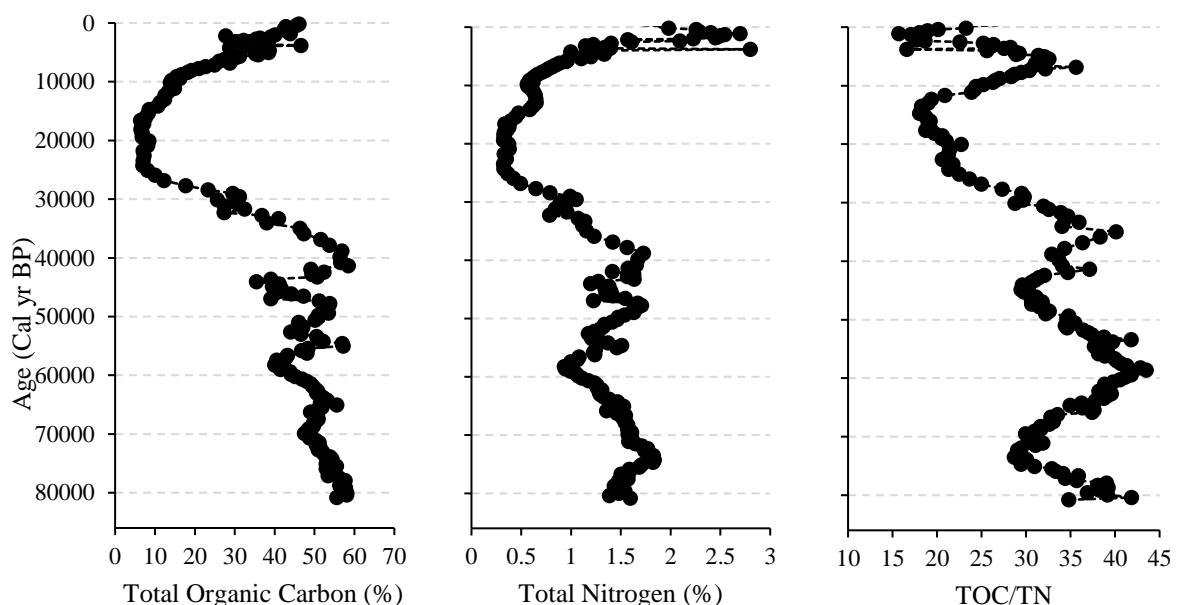


Figure 27. Total organic carbon (TOC), total nitrogen (TN) and the TOC/CN ratio for the Pantano de Martos core.

4.3.2. Bulk Isotope Data - $\delta^{13}\text{C}$ and $\delta^{15}\text{N}$

The $\delta^{13}\text{C}$ and $\delta^{15}\text{N}$ for the Pantano de Martos core are shown in figure 28. $\delta^{13}\text{C}$ throughout the core varies from -23.4‰ to -29.1‰. From the top of the core down to between 13,000 and 30,000 cal yr BP there is a trend towards lower $\delta^{13}\text{C}$, increasing to -24‰ at 35,800 cal yr BP. Excluding the brief transition to lower values between ~54,000 and 64,000 cal yr BP, where $\delta^{13}\text{C}$ reaches -26.1‰, $\delta^{13}\text{C}$ values stay mainly between -23 to -24‰ from 36,000 to 73,000 cal yr BP.

Throughout the core, $\delta^{15}\text{N}$ values show marked variation, ranging from 0.92‰ (22,000 cal yr BP) up to 7.6‰ (19,000 cal yr BP), with average $\delta^{15}\text{N}$ of 3.1‰. Although not as pronounced as for $\delta^{13}\text{C}$, there is a transition to lower $\delta^{15}\text{N}$ values from the top of the core to ~30,000 cal yr BP ($\delta^{15}\text{N}$ average around 1-2‰). After this point, the $\delta^{15}\text{N}$ increases, reaching a maximum of 4‰ at 55,000 cal yr BP. Unlike $\delta^{13}\text{C}$, $\delta^{15}\text{N}$ decreases towards the base of the core, to ~1.6‰ at 80,000 cal yr BP.

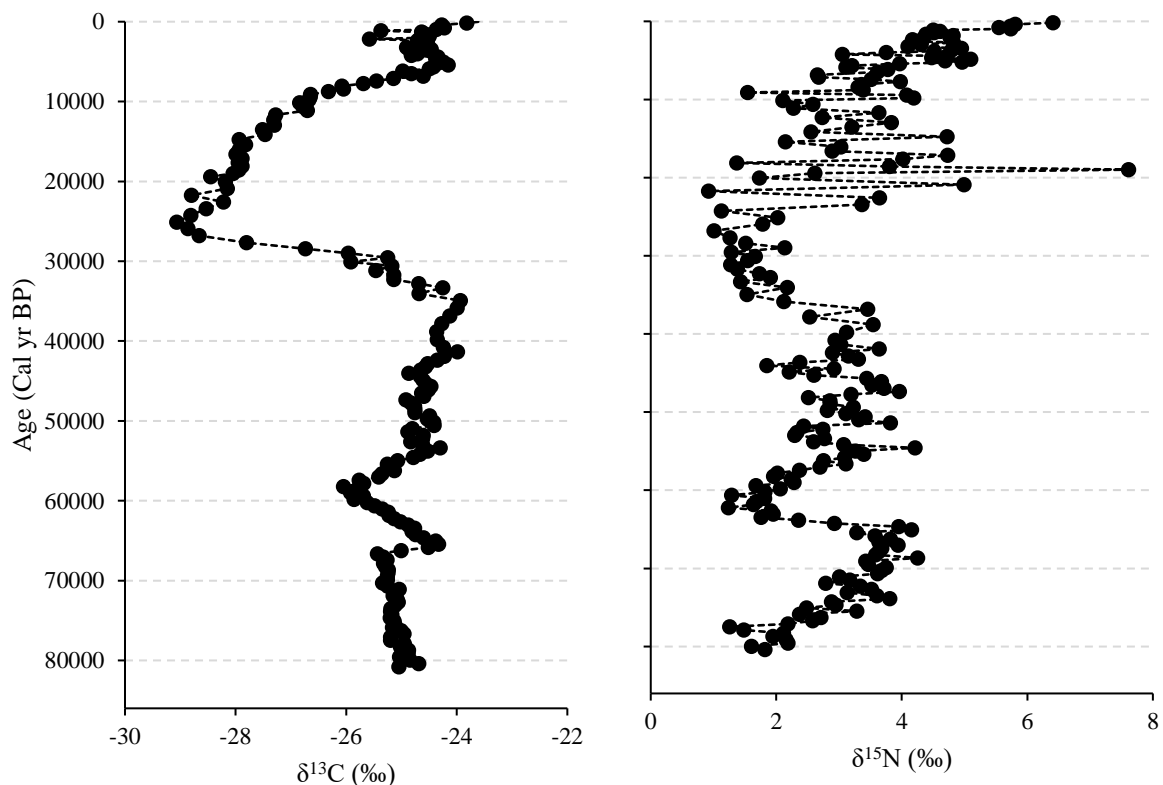


Figure 28. Down-core trends in the $\delta^{13}\text{C}$ and $\delta^{15}\text{N}$ for the Pantano de Martos core

4.3.3. Leaf wax *n*-alkane distributions

Throughout the Pantano de Martos core, long chain *n*-alkanes were identified in all samples and span the range from C₁₁ to C₃₁. Given this broad distribution, individual relative abundances were generally small, with the most abundant *n*-alkanes typically making up less than 50% of the total. This can be seen in figure 29e, where the dominant homologue in the distribution makes up ~50% of the total *n*-alkanes present. Throughout the core, the longer chain *n*-alkanes, C₂₇ and C₂₉, are typically the most abundant. For samples older than 22,000 cal yr BP (below 130 cm), the *n*-alkane distribution reaches the C₃₅ alkane, although the abundance of this homologue was typically low (<5% of total alkanes). Exceptions to this are the samples between 26-30,000 cal yr BP (140-154 cm) where the C₃₅ alkane reaches between 6-16% of total alkanes present. Shorter chain-length *n*-alkanes (C₁₁-C₁₉) were present in all samples and typically made up less than 4% of total lipid concentration. At the top of the core at 0 cm, where fresh plant material composed of *Sphagnum* was extracted and analysed, the C₂₃ alkane was the dominant homologue, making up 33% of the total *n*-alkane content (figure 29a). Of note however is the abundance of the C₁₉ *n*-alkane. In the younger material (from 0 to 31,000 cal yr BP) the C₁₉ *n*-alkane makes up ~1% of the total alkane abundance. However, this increases to 27% at 41,200 cal yr BP and 45,000 cal yr BP (~50% of total alkanes present).

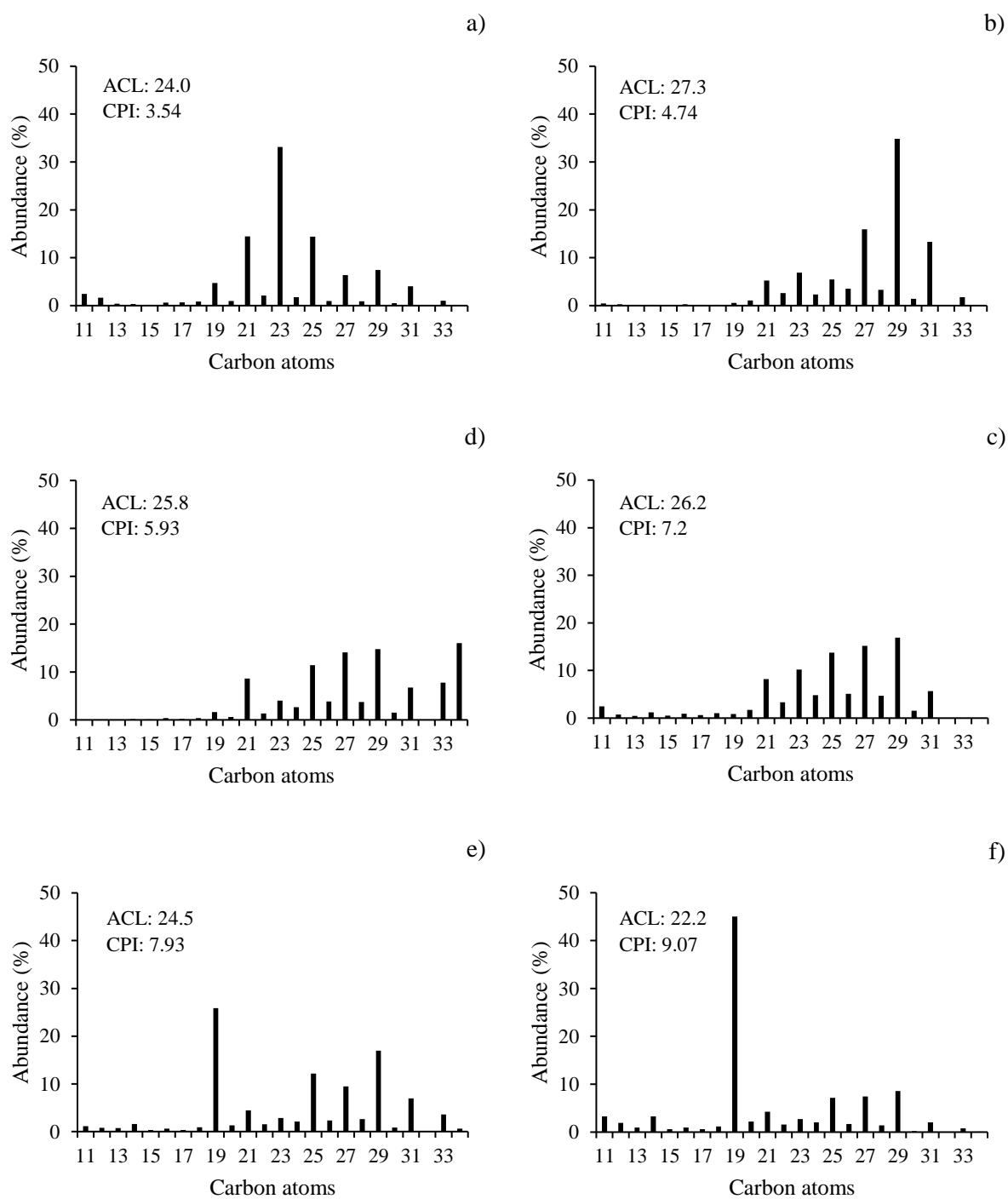


Figure 29. *n*-alkane distributions for samples a) 0cm, b) 50cm, c) 100cm, d) 150cm, e) 178cm and f) 198cm (-348, 440, 13,000, 29,500, 39,800 and 44,800 cal yr BP).

The average chain length (ACL_{23-33}) and the carbon preference index (CPI_{23-33}) for the Pantano de Martos core are shown in figure 30. ACL_{23-33} values ranged from 25.2 to 28.9, averaging 27.2. From ~ 3000 to 15,000 cal yr BP ACL_{23-33} values gradually decline to ~ 26.2 , before increasing to 28.1 at 37,000 cal yr BP. This increase in chain length coincides with the emergence of the longer chain lengths (C_{33} and C_{35}) that were not present in the upper parts of the core. A slight decrease in chain length is then seen from 40,000 cal yr BP towards the oldest parts of the core ($\sim 70,000$ cal yr BP).

The CPI_{23-33} for the Pantano de Martos core demonstrates that all samples showed an odd over even chain length predominance, with CPI_{23-33} values ranging from 4.0 to 23. Lowest CPI values were correlated with the broadest dispersion in *n*-alkane distribution (figure 31). For example, at $\sim 21,000$ cal yr BP (130 cm), where the lowest CPI value was found, all alkanes are present, however their abundances are less than 15% with the most dominant homologue, C_{27} , making up 14.7% of the total *n*-alkanes. In contrast to this, the sample at ~ 7000 cal yr BP (72 cm) produced the highest CPI value of 23.2, and here the C_{29} alkane is dominant, making up 65.5% of the total *n*-alkane concentration (Fig.31a and 31b).

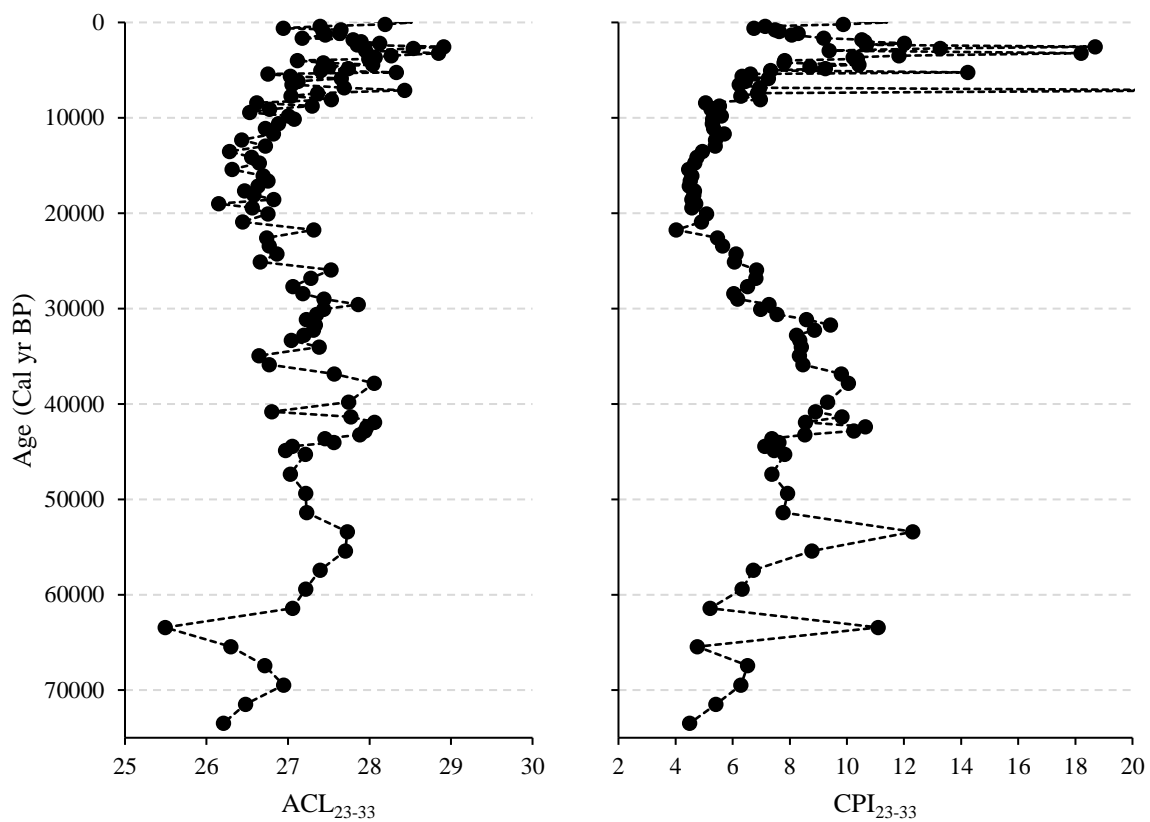


Figure 30. Down core trends in the average chain length (ACL_{23-33}) and the carbon preference index (CPI_{23-33}) of the Pantano de Martos core.

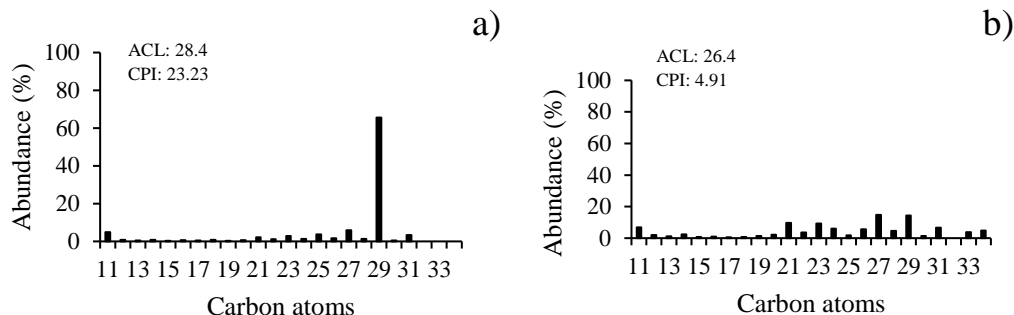


Figure 31. *n*-alkane distributions for the samples with the highest (a) and lowest (b) CPI_{23-33} values at 7000 cal yr BP and 21,000 cal yr BP respectively.

The P_{aq} ratio and Norm31 ($C_{31} / (C_{31} + C_{29})$) are displayed in figure 32. P_{aq} ranges from 0.07 to 0.81 across the whole of the core, with average values typically being 0.4. The youngest 20,000 years of the core (0-20,062 cal yr BP) are associated with higher P_{aq} , increasing from 0.17 to 0.53 between 0 and ~19,400 cal yr BP. P_{aq} tends to decrease between 20,000 and 55,000 cal yr BP. During the oldest 15,000 years of the core, P_{aq} values are more varied, but is typically between 0.5 and 0.8. Norm31 values range from 0.05 to 0.40. The majority of the core (between 0 and 47,000 cal yr BP) exhibits a relatively stable Norm31. Between 47-57,000 cal yr BP Norm31 increases, followed by an abrupt transition to the lowest values found throughout the whole of the core between 60-70,000 cal yr BP.

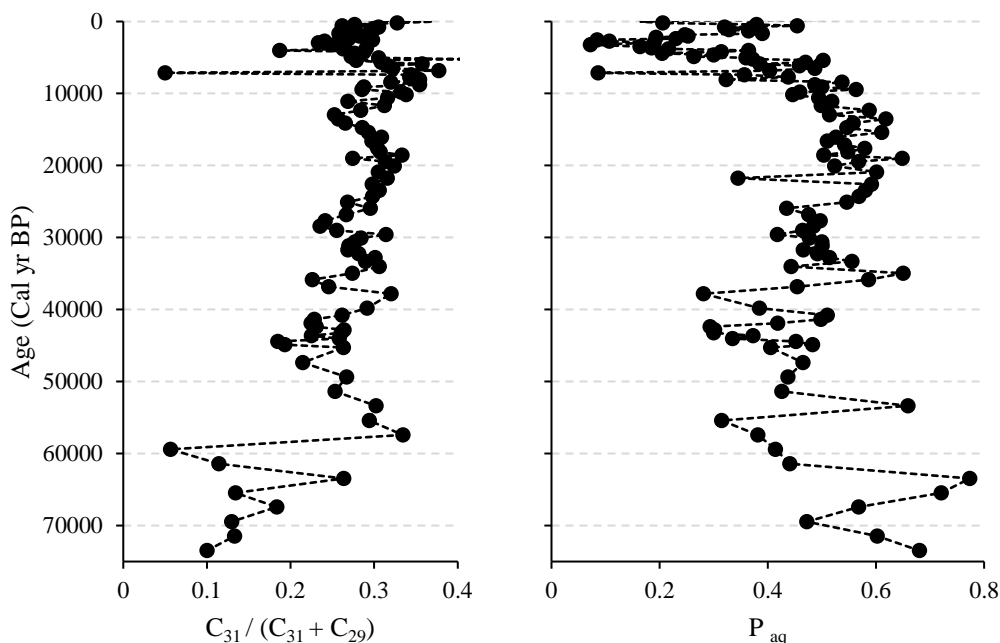


Figure 32. The P-aqueous (P_{aq}) ratio and Norm31 ($C_{31} / (C_{31} + C_{29})$) for the Pantano de Martos core.

4.3.4. Leaf wax *n*-alkane δD

Leaf wax *n*-alkane δD results for the C_{27} , C_{29} and C_{31} are shown in figure 33. The δD_{wax} values of all three homologues exhibit similar patterns throughout the course of the core. This is supported by the correlation coefficient, which exhibited high correlation between the *n*-alkanes (between 0.6 and 0.76) and extremely low P-values further increased their significance.

A gradual transition towards more negative δD_{wax} values can be seen between 20 and 45,000 cal yr BP. Between 44 to 69,500 cal yr BP δD_{wax} values increase from -219‰ to -188‰ for the C_{27} *n*-alkane, and -212‰ to between -177‰ and -179‰ for the C_{29} and C_{31} *n*-alkanes respectively. For all *n*-alkanes this shift towards more positive δD_{wax} is the most dramatic change throughout the core and does not appear to be associated with any major change in *n*-alkane distribution. Overall, δD_{wax} values range from -185‰ to -219‰ for the C_{27} alkane, -173‰ to -215‰ for the C_{29} and -175‰ to -219‰ for the C_{31} *n*-alkane.

Table 5. The correlation coefficients for the δD_{wax} values of the C_{27} vs. C_{29} , C_{27} vs. C_{31} and C_{29} vs. C_{31} for Pantano de Martos.

| C_{27} vs. C_{29} | | C_{27} vs. C_{31} | | C_{29} vs. C_{31} | |
|--|----------|--|----------|--|----------|
| Correlation coefficient | P-value | Correlation coefficient | P-value | Correlation coefficient | P-value |
| 0.76 | 1.50E-17 | 0.6 | 6.53E-10 | 0.76 | 1.48E-17 |

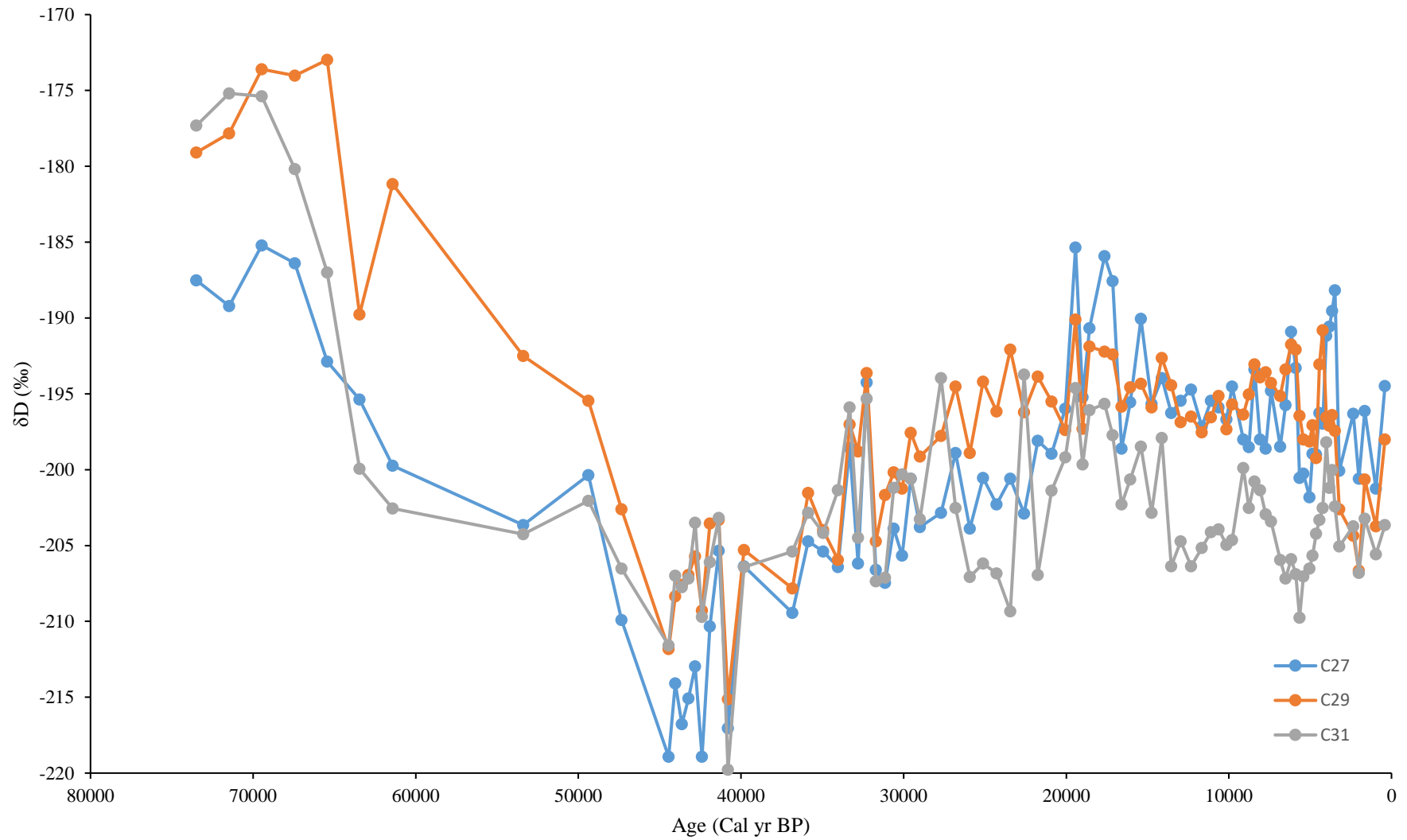


Figure 33. δD_{wax} measurements for the C₂₇, C₂₉ and C₃₁ *n*-alkanes in Pantano de Martos core.

Chapter 5: Discussion.

5.1. TOC, TN, TOC/TN and the isotopic values of bulk organic matter ($\delta^{13}\text{C}$)

5.1.1 TOC

In all three cores, TOC values were high in the uppermost parts of the core. In the case of the Tipisca cores (Aguajal Agua Blanca and Aguajal del Loretillo), the highest TOC values were ~44%, whereas in the Pantano de Martos Core, TOC values were ~59% in the most recently deposited layers of peat. TOC values gradually decline in both of the Tipisca cores, becoming as low as 0.3% in the oldest parts of the cores. By contrast, TOC in the Pantano de Martos core remains around 50%, even in samples dated in excess of ~80,000 cal yr BP.

The environments of the sites could help explain the contrasting organic matter content of the sedimentary cores. Gallego-Sala et al (2018) suggest that in lower-latitude tropical peatlands, higher temperatures drive microbial activity and as a result enhance decomposition within the peat record. As a result, carbon accumulation rates are lower than in peatlands from higher latitudes (lower temperatures). This could be a contributing factor in the depletion of TOC within the Amazonian cores. At Tipisca, current temperatures remain ~ 26°C throughout the year (Schongart et al, 2002), compared to the annual mean temperatures of 12°C found at the Pantano de Martos site (Londono et al, 2014). These higher temperatures therefore could lead to higher amounts of organic matter processing/degradation through microbial activity.

It is important to note the significant reduction in TOC values in the Pantano de Martos core from ~13,000 cal yr BP until ~26,000 cal yr BP. During this period, TOC decreases substantially to a low of 6% at ~21,000 cal yr BP. After this point, TOC values return to between 50% and 60%. The lowest TOC values correspond to the LGM where temperatures are estimated to have been between 4-8°C cooler than the current Colombian climate (Heine, 2000) and atmospheric CO₂ concentrations were at their lowest (200 ppmv) (Barnola et al, 1987). The reduction in organic matter could therefore imply a reduction in peat productivity due to the cooler temperatures and, as a result, changes in climatic water balance. It is generally accepted that peatlands can be identified by the carbon content of the soil, and this value is typically around 50% (Wellock et al, 2011). Low TOC values during the LGM therefore suggest that peat is no longer present. This is also supported by the appearance of the sediment during this time. When looking at the core images (fig. 14) there is a clear band of different

sediment, coincident with the LGM and the low carbon content (depth: ~130-140 cm). Therefore, it is suspected that during the LGM the current peatland did not exist.

5.1.2. TN

Nitrogen in tropical forests has been found to be more available than in temperate forests, and functions as an excess nutrient in most tropical forests as a result of a much more open N cycle (Martinelli et al, 1999). However, this is not the case for any of the cores of this study. TN values for all core are below 3%, and in the case of the Amazonian cores, TN values decrease with increasing age of sediment. In the youngest sediment, TN is ~3% for Aguajal Agua Blanca and ~2.4% for Aguajal del Loretillo. TN values reach ~0.05% in Aguajal Agua Blanca by 600 cal yr BP and by 3000 cal yr BP in Aguajal del Loretillo, which could also be a result of degradation of organic matter within the core.

TN values in the Pantano de Martos core are below 3% throughout the core. Like TOC, TN reaches a minimum during the LGM, implying that the cooler temperatures may have influenced the vegetation composition and thus the nitrogen availability and organic N input. The highest TN values are found in the earliest sections of the core where *Sphagnum* dominates. It is widely accepted that in ombrotrophic peatlands, the main source of N is atmospheric deposition (Andersson et al, 2012). Where these peatlands are dominated by *Sphagnum*, the species responds quickly to N loading and retains much of the deposited N (Vitt et al, 2003). This could explain the relatively high levels of TN throughout the core, and further suggests that the peat bog was not present during the LGM.

5.1.3. TOC/TN

The TOC/TN ratio is a fundamental indicator of biogeochemical cycles within ecosystems, with shifts in the ratio influencing ecosystem structure, composition and ecosystem functions (Liu et al, 2016). The TOC/TN ratio can also provide information regarding the source and preservation of soil organic matter within peat sediment (Andersson et al, 2012), as bacteria and algae have C/N values that are distinct from terrestrial vegetation (Lamb et al, 2006). In general, TOC/TN values from 3 to 9 suggest a protein rich aquatic or algal source, values between 10 to 20 indicate a mixture of aquatic and terrestrial sources, and high TOC/TN values above 20 are indicative of organic matter terrestrial sources (Brodie et al, 2011).

The TOC/TN ratios from the Amazonian cores suggest a much more varied source of organic matter than the Andean core. In the case of Aguajal Agua Blanca, the TOC/TN ratios range from 7.3 to 27.7 throughout the core, suggesting a combined input of both aquatic and terrestrial sources. Between ~450 cal yr BP to ~560 cal yr BP TOC/TN values increase to 27.7, suggesting increased contributions from terrestrial sources of organic matter. However, after ~560 cal yr BP there is a significant drop in TOC/TN values to ~7, suggesting an increased contribution from an algal/aquatic source. For the remainder of the core TOC/TN values fluctuate on the boundary of algal or mixed aquatic/terrestrial source (Fig. 15). TOC/TN values for Aguajal del Loretillo are much lower than Aguajal Agua Blanca, ranging between 0 and 16. Between 0 and 2000 cal yr BP, TOC/TN values fluctuate between 2.0 and 16.3, implying an algal and mixed aquatic/terrestrial origin. Prior to 2000 cal yr BP, TOC/TN remains close to zero, implying a strong algal input in the sediment core. In deeper layers of sediment, TOC/TN values have previously been reported to decrease significantly due to progressive decomposition removing a greater amount of carbon than nitrogen (Kuhry and Vitt, 1996). This finding can account for low TOC/TN ratios deeper in these cores, reflecting preferential decomposition of N-containing organic matter, rather than increased algal input. Taking into consideration the depletion of all bulk proxies in the older sections of the sediment, this could be a possibility.

In contrast to the Amazonian cores, TOC/TN values in the Pantano de Martos core are predominantly above 20 throughout, implying a strong terrestrial source of sediment. Lower TOC/TN values, indicating a mix of aquatic and terrestrial vegetation, occur in the earliest stages of the core (0 to ~2500 cal yr BP) where it is known that *Sphagnum* is dominant and also between ~13,000 to 18,000 cal yr BP. Andersson et al. (2012) found high TOC/TN values (between 20 and 60) to occur in *Sphagnum* dominated peat, which supports the findings of this study. They also suggest that high TOC/TN probably reflects a better preservation of organic matter as a result of wetter and/or anoxic conditions. Additionally, the cyclic nature of the TOC/TN Martos record could be a result of biogeochemical processes relating to the cycling of C and N between mosses and vascular plants (*ibid*). Generally, ombrotrophic peatlands are nitrogen-limited ecosystems, whose sole nitrogen source is atmospheric deposition (Jonasson and Shaver, 1999). As a result, TOC/TN ratios should remain high throughout the record, influenced mainly by the availability of carbon rather than nitrogen. However, in contrast to most vascular plants, *Sphagnum* can rely on different sources of nitrogen (Asada et al, 2005), and are able to utilize the organic form of nitrogen, and also fix atmospheric nitrogen through

the symbiotic associations with cyanobacteria (Basilier, 1980). Additionally, *Sphagnum* species can retain the majority of atmospherically-deposited nitrogen, which has been found in some instances to be as great as 90% of the total deposition (Li and Vitt, 1997). This is due to their thin-walled outer cortical stem cells and their unistratose leaves, both of which allow the plant to absorb nutrients effectively (Asada et al, 2005a). As a result, in times where species of *Sphagnum* are present, it can be hypothesised that TOC/TN ratios will be lower as a result of their higher productivity during times of increased nitrogen supply (Li and Glime, 1990). This finding could therefore explain the variability in TOC/TN throughout the Martos record.

5.1.4. Bulk $\delta^{13}\text{C}$

The $\delta^{13}\text{C}$ values of organic matter is a sensitive palaeoenvironmental indicator, which can be used to provide insight into changes within biogeochemical processes (Hayes, 1993). Within organic sediment, various processes control the stable isotope ratios of both carbon and nitrogen (Andersson et al, 2012). These include sedimentation processes, microorganisms and the contributions of different classes of organisms, such as mosses, fungi and vascular plants (*ibid*). The isotopic source of organic matter is preserved in sediment for potentially millions of years, which can help reconstruct long-term environmental changes within a sedimentary record (Meyers, 1994), predominantly through information regarding whether C_3 or C_4 vegetation dominated over different time periods.

Although compound-specific measurements of $\delta^{13}\text{C}$ allow for a more precise reconstruction of vegetation type (Taylor et al, 2018), it is generally accepted that bulk $\delta^{13}\text{C}$ values reflect the average isotopic composition of the species found within a particular environment (Andersson et al, 2012). The $\delta^{13}\text{C}$ values of sedimentary organic matter generally range from -6‰ to -37‰. C_3 and C_4 plant contributions can be inferred from differences in the isotopic values of plant tissues derived from these two photosynthetic pathways (Brodie et al, 2011). Typically, bulk C_4 plant $\delta^{13}\text{C}$ values range from -6‰ to -15‰, averaging -12.5‰ whereas C_3 $\delta^{13}\text{C}$ values range from -22‰ to -37‰ and average -27‰ (Brodie et al, 2011; Farquhar et al, 1989; O’Leary, 1988; Sinninghe-Damse et al, 2011). The large difference in $\delta^{13}\text{C}$ between C_3 and C_4 vegetation, can allow the varying contribution of plant material from these photosynthetic pathways to be distinguished in the sedimentary record.

In the context of this study, it is assumed that the $\delta^{13}\text{C}$ values within peat sediment remain well preserved and reflect the isotopic composition of original peat-forming debris as opposed to

post-depositional processes that occur within the sediment (Skrzypek et al, 2010). Therefore, the bulk $\delta^{13}\text{C}$ values for all three cores should provide insight into the vegetation prevailing on the wetland at the time, and as a result it is possible to interpret these changes as a function of environmental influences.

Average bulk $\delta^{13}\text{C}$ values were -27.0‰, -28.7‰ and -25.4‰ for Aguajal Agua Blanca, Aguajal del Loretillo and Pantano de Martos respectively, suggesting a terrestrial input of predominantly C_3 vegetation. Average bulk $\delta^{13}\text{C}$ values for the Amazonian cores were closer to the most common C_3 $\delta^{13}\text{C}$ signal of -27‰ (Farquhar et al, 1989), and, in the case of Aguajal del Loretillo remained within the range of C_3 vegetation throughout the core, with $\delta^{13}\text{C}$ ranging from -32.4‰ to -25.5‰. However, in the Aguajal Agua Blanca core, $\delta^{13}\text{C}$ values progressively increase from ~-30‰ to -17‰ from 0 to ~800 cal yr BP. Between 826 to 1015 cal yr BP $\delta^{13}\text{C}$ values range from -19.8‰ to -14.7‰ and average -17.1‰. The highest $\delta^{13}\text{C}$ value, although only occurring once at 906 cal yr BP, falls within the estimated $\delta^{13}\text{C}$ range for bulk C_4 plants (O’Leary, 1988), which could suggest a shift in the vegetation from C_3 to C_4 species. However, due to environmental context of the cores location, and the available palynological dataset (see appendix) it is possible but highly unlikely to be C_4 vegetation. Vascular terrestrial plants can adapt to increasing aridity by closing the stomata to counteract water loss (Beerling and Royer, 2002), resulting in a ^{13}C enrichment of photosynthetic products in fresh plant material (Farquhar et al, 1989). Consequently, the increasing $\delta^{13}\text{C}$ with age could also possibly relate to a decrease in available water. However, this seems unlikely due to how high the bulk $\delta^{13}\text{C}$ values are, especially when considering that $\delta^{13}\text{C}$ values from South African desert C_3 plants range between -25 to -29‰ (Carr et al, 2014). As a result, it is suspected that the $\delta^{13}\text{C}$ values at depth in the Aguajal Agua Blanca core are not plant-derived.

Andersson et al. (2012) also found bulk $\delta^{13}\text{C}$ values of a *Sphagnum* dominated peat bog to range from -28.4‰ to -25.3‰, which also agrees with the range of bulk $\delta^{13}\text{C}$ values found in the Martos core. Additionally, because *Sphagnum* lack stomata, they are unable to regulate their carbon intake (Rice, 2000). As a result, the $\delta^{13}\text{C}$ values of *Sphagnum* species are influenced by environmental variables such as temperature, light intensity and moisture (Loisel et al, 2010), which could mean that variations in bulk $\delta^{13}\text{C}$ are a signal of environmental response of vegetation rather than changes in species. During wetter conditions discrimination against ^{13}C has been found to decline as water increases the resistance to CO_2 uptake by creating a barrier to CO_2 diffusion (Farquhar et al, 1989). This leads to more positive $\delta^{13}\text{C}$ values in *Sphagnum* tissues. When drier conditions prevail, increased discrimination against

^{13}C occurs which leads to more negative $\delta^{13}\text{C}$ values (Rice, 2000). Under this assumption, the bulk $\delta^{13}\text{C}$ record for the Martos core shows relatively wet conditions for the majority of the core, except for the period between ~18,000 to 26,000 cal yr BP where low $\delta^{13}\text{C}$ could be interpreted as drier conditions. However, this interpretation is complicated due to the behaviour of *Sphagnum* mosses within ombrotrophic peatlands. Nicholls et al. (2009) suggest that $\delta^{13}\text{C}$ values of *Sphagnum* species in ombrotrophic peatlands are also influenced by the CH_4 fluxes associated with methanotrophic bacteria living symbiotically with *Sphagnum* mosses. In these peatlands specifically, methane has a very negative $\delta^{13}\text{C}$ value of between -85‰ and -55‰ (Hornibrook, 2009). The oxidation of methane as it diffuses through the oxic-anoxic interface of the acrotelm - the upper aerobic (living) peat layer (Flores, 2014) – creates an additional source of carbon through CO_2 (oxidised CH_4) which is ^{13}C depleted. Under wetter conditions this diffusion of CH_4 may cause a shift to lower (more negative) bulk $\delta^{13}\text{C}$ values (Andersson et al, 2012). This finding therefore suggests that other proxies are needed to understand bulk as a function of environmental change.

However, analysis of the isotopic values of bulk sediment has proven difficult to interpret as they only provide general information regarding an environment (Siffeddine et al, 2004). This is mainly because the bulk sediment is composed of several components such as sedges, mosses and fungi that contribute to the carbon pool (Pancost et al, 2003). Additionally, bulk sediment $\delta^{13}\text{C}$ values have been found to be biased towards the plant components preferentially preserved in the sediment (Arens and Jahren, 2000). This is mainly due to microbial alteration within sediment causing the preferential loss and degradation of some organic compounds (Gröcke, 2002). For example, lipids are known to be most depleted in $\delta^{13}\text{C}$ compared to lignins, carbohydrates and proteins (Galimov, 1985) and are known to be one of the most long-lived components within sediment (Schimmelmann et al, 2006). Therefore, a strong C_3 signal within the sediment could actually be the result of selective decomposition of specific compounds within the initial mix of organic matter, therefore altering the $\delta^{13}\text{C}$ signal of the remaining material. Other studies have reported that in soil organic matter that is composed of predominantly vascular plants, an assimilation of polysaccharides caused by bacteria produce a lignin-rich residue within the sediment that has more negative $\delta^{13}\text{C}$ values due to the fact that lignins are more ^{13}C depleted than cellulose (Benner et al, 1987). Additionally, alteration of sedimentary $\delta^{13}\text{C}$ as a result of ^{13}C fractionation through interactions between roots, soil organic matter and microorganisms also complicate the bulk $\delta^{13}\text{C}$ signal as an indicator of plant composition (Werth and Kuzyakov, 2010). This is due to bacteria preferentially metabolising

the ^{12}C -rich fraction of soil organic matter, also creating an enrichment in $\delta^{13}\text{C}$ (Skrzypek et al, 2007).

Combining the bulk $\delta^{13}\text{C}$ values with the TOC/TN ratio is a potentially useful tool for inferring the potential origin of bulk organic matter (Sifeddine et al, 2004). Figure 34 depicts how the different sources can be differentiated within bulk samples according to Sifeddine et al. (2004). In the case of the Pantano de Martos core, combining the proxies in this manner suggests that nearly all of the organic matter within the core is derived from C_3 vegetation. However, this combination of the proxies proved insufficient in explaining some of the variability in the Amazonian cores. In the case of Aguajal Agua Blanca, the samples lie within the algae and C_3 vegetation ranges, and over half the samples from Aguajal del Loretillo lay within the algae group. However, multiple samples from all three cores lay outside of the end-member source groups proposed by Sifeddine et al. (2004), indicating that this proxy is not as useful in this study as in previous studies (Meyers, 1994; Sifeddine et al, 2004) and other information is needed to ascertain organic matter origin.

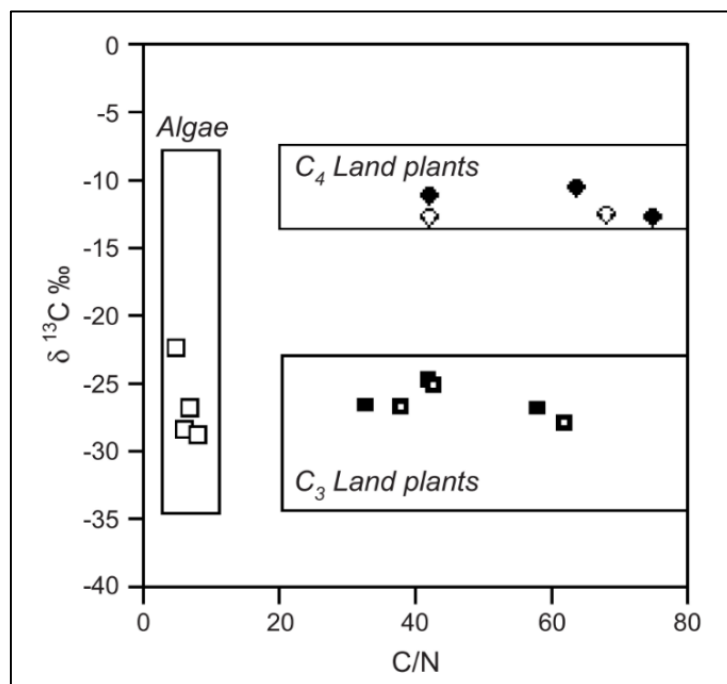


Figure 34. TOC/TN vs. $\delta^{13}\text{C}$ diagram, taken from Sifeddine et al (2004).

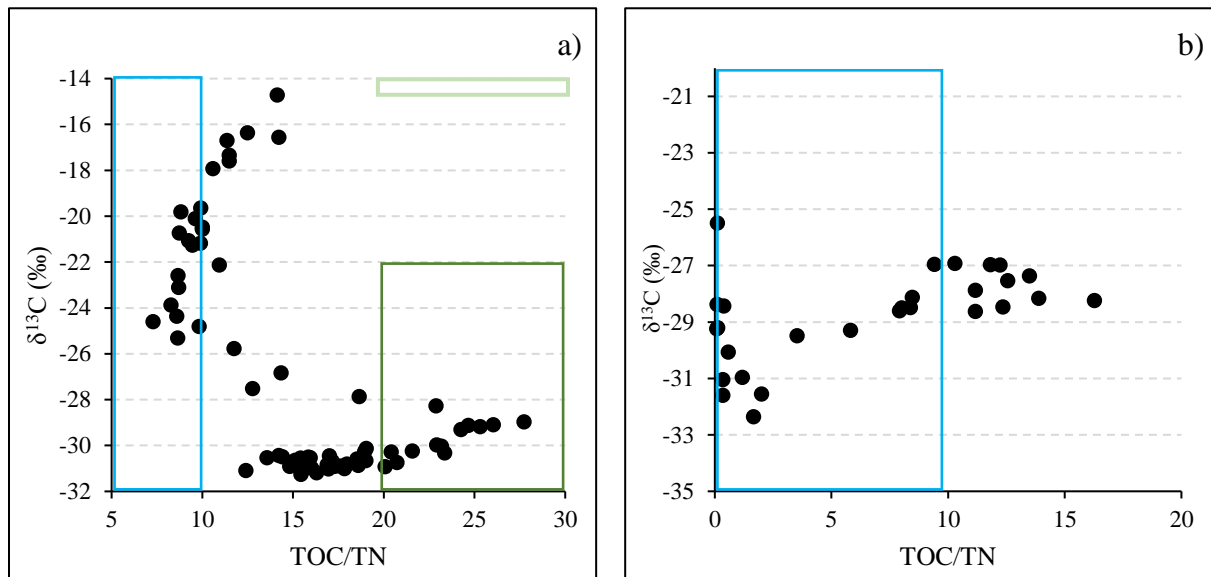


Figure 35. TOC/TN vs. $\delta^{13}\text{C}$ diagram for a) Aguajal Agua Blanca and, b) Aguajal del Loretillo. Clusters of samples are grouped into algae, C_3 land plants and C_4 land plants.

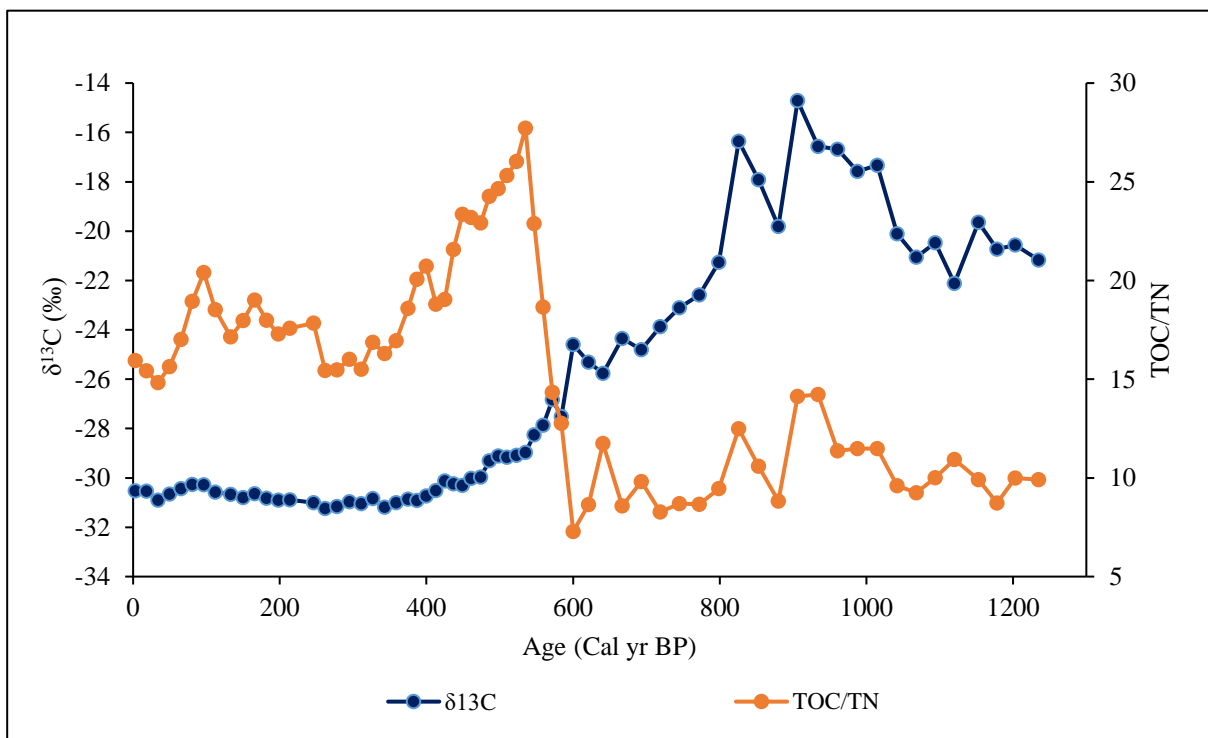


Figure 36. Bulk $\delta^{13}\text{C}$ values and TOC/TN against age for the Aguajal Agua Blanca core. Figure 34a depicts the clusters of samples within the Aguajal Agua Blanca core. Combining the parameters with the age of the core shows that the samples that fall into the algae cluster of samples occur at ~600 cal yr BP until the end of the core. Therefore, it is suspected that from this point, the source of organic matter within the sediment is not of C_3 , or even possible terrestrial origin.

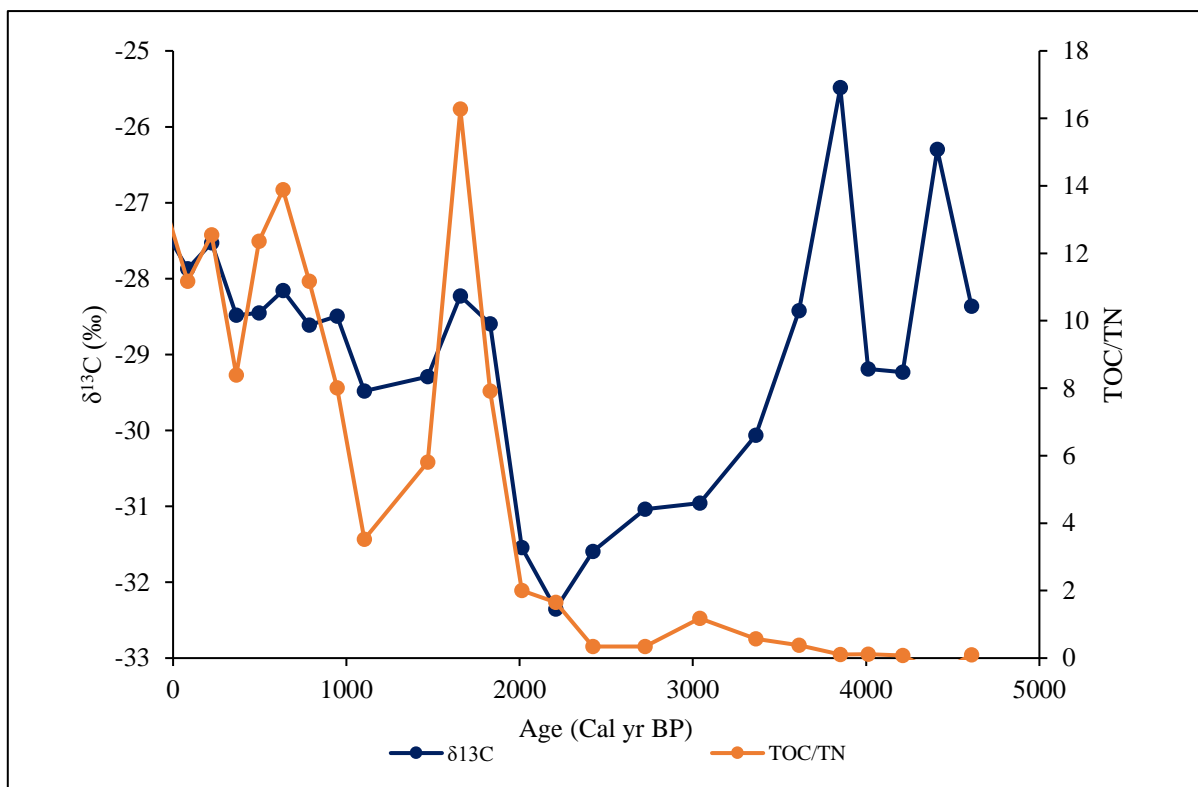


Figure 37. Bulk $\delta^{13}\text{C}$ values and TOC/TN against age for the Aguajal del Loretillo core. TOC/TN values throughout the core suggest an algal source of organic matter, however bulk $\delta^{13}\text{C}$ values, when considered independently, suggest a terrestrial source of OM. From ~ 2400 cal yr BP, OM content of the core becomes extremely low, therefore low TOC/TN values could be due to the small amount of sample.

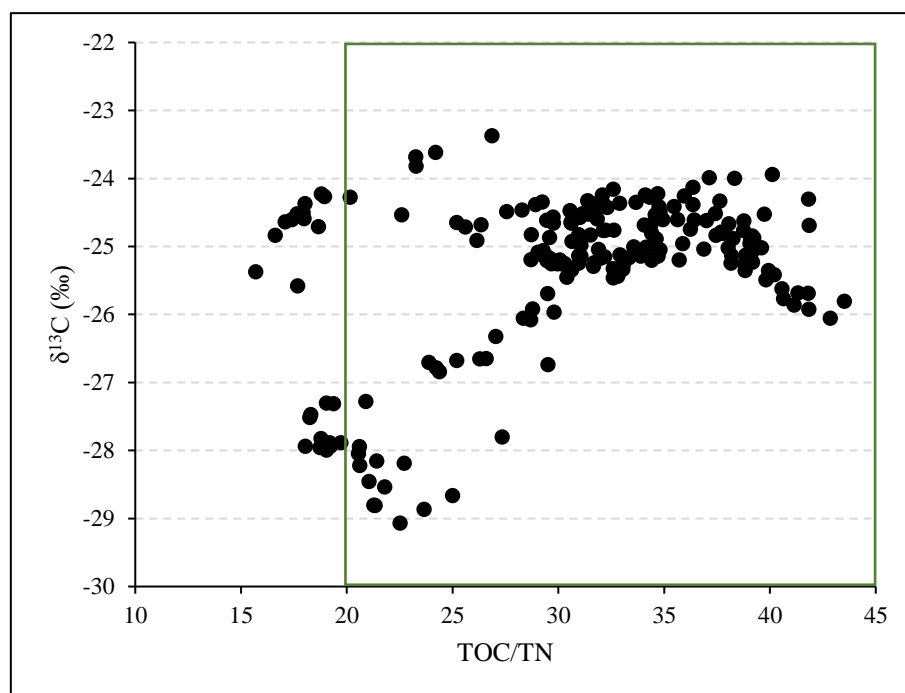


Figure 38. TOC/TN vs. $\delta^{13}\text{C}$ diagram for Pantano de Martos.

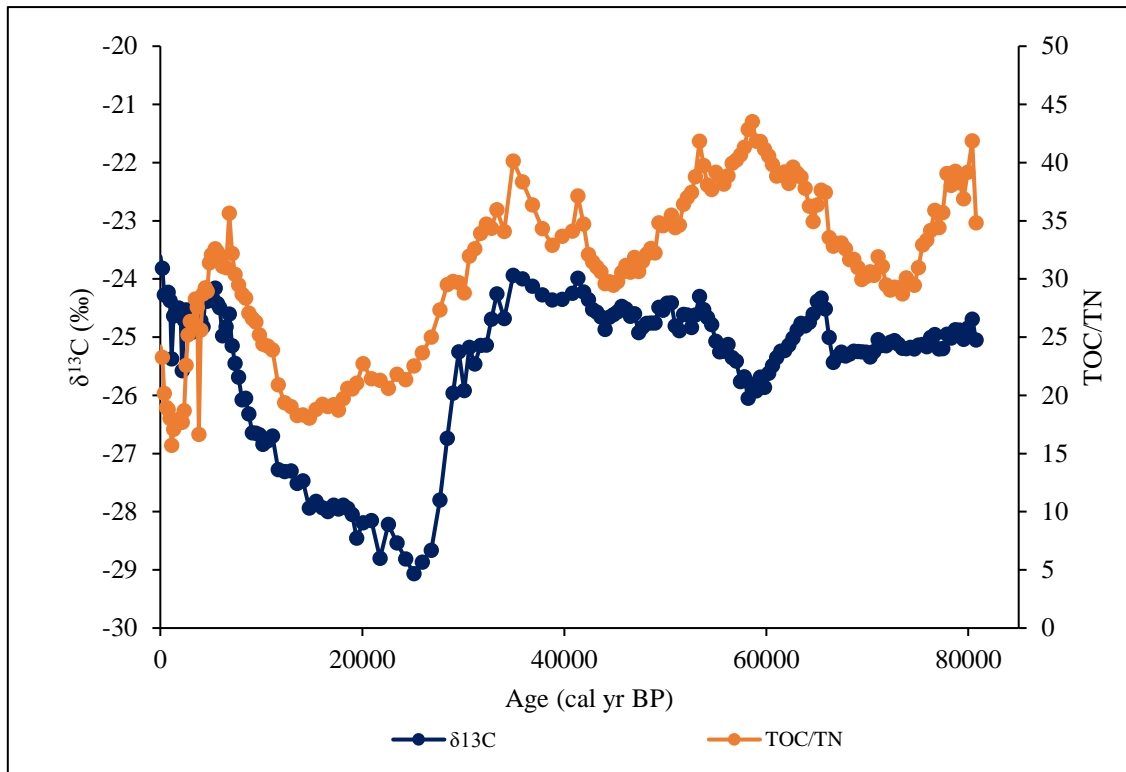


Figure 39. Bulk $\delta^{13}\text{C}$ values and TOC/TN against age for the Pantano de Martos core. Throughout the core both parameters track each other. Bulk $\delta^{13}\text{C}$ values remain within terrestrial C_3 vegetation throughout the core. TOC/TN values suggest a terrestrial source of OM throughout the core, except between 12-18,000 cal yr BP where TOC/TN fall slightly below the boundary of terrestrial material.

5.2. Leaf wax *n*-alkane distributions

5.2.1. Leaf wax *n*-alkane distributions

A wide range of *n*-alkanes were present in the three cores of this study. In the Aguajal Agua Blanca core, *n*-alkanes spanned the range C₁₇- C₃₃ whereas in both Aguajal del Loretillo and Pantano de Martos, *n*-alkanes spanned the range C₁₁- C₃₁. In all cores, the C₂₉ *n*-alkane was the most abundant, but with high relative abundances of C₃₁ and C₂₇ *n*-alkanes in the Amazonian and Andean cores respectively. Alkanes were not detected at depth in the Amazonian cores, corresponding to ages of ~540 and ~2400 cal yr BP for Aguajal Agua Blanca and Aguajal del Loretillo respectively. This loss of *n*-alkanes coincided with a significant depletion of TOC, with values decreasing to ~0.5% for both cores. By contrast, *n*-alkanes were present in all samples of the Pantano de Martos core, even those estimated to be ≥80,000 years old.

Leaf wax *n*-alkanes contribute to the protective properties of the epicuticular wax layer. The synthesised waxes isolate the leaf tissue from the atmosphere and are largely thought to prevent non-stomatal water loss (Koch and Ensikat, 2008), although other functions have also been suggested (Stevenson, 1966). Studies have shown that leaf wax *n*-alkanes accumulate rapidly during leaf flush, with the distribution and abundance remaining largely constant throughout the growing season (Tipple et al, 2013). As a result, leaf waxes in the sediment can reliably be thought of as a combined signal of the vegetation during a particular time and can be applied as an indicator of a broad ecosystem changes (Bush and McInerney, 2013). Typically, terrestrial plants synthesise a characteristic range of long chain *n*-alkanes, particularly C₂₇, C₂₉ and C₃₁ (Eglinton and Hamilton, 1967). Therefore *n*-alkanes in sedimentary samples can be utilised as an indicator of terrestrial plant-derived organic matter. Both ACL and CPI are examples of parameters that can be used to characterise the leaf wax *n*-alkane distributions within sedimentary material (Bendle et al, 2007; Carr et al, 2015). In this study both parameters were calculated from the *n*-alkane range C₂₃-C₃₃ as it encompassed the *n*-alkane range in all cores, and it was suspected that this would provide an insight into any changes between terrestrial or submerged vegetation.

5.2.1.1. Carbon Preference Index (CPI)

For all three cores, CPI values were greater than zero, indicating a predominance of odd over even chain lengths, and suggesting terrestrial vegetation as the source of the *n*-alkanes (Bray and Evans, 1961). In both Aguajal del Loretillo and Pantano de Martos, CPI values were similar, ranging from 4.5 to 21.7 and 4.0 to 23.3 for Aguajal del Loretillo and Pantano de

Martos respectively. However, in the Aguajal Agua Blanca core, CPI values span a much larger range of 2.4 to 194.8. The large range of CPI values in the Aguajal Agua Blanca core is mainly due to the high abundance of the odd chained *n*-alkanes compared to the even numbered *n*-alkanes. In some of the subsamples, even numbered *n*-alkanes were not found at all, which led to the highest CPI values of the core.

Schemmel et al. (2017) attribute changes in CPI to relate to changes in in situ vegetation, however given the broader distribution of CPI values in the Aguajal Agua Blanca core this seems unlikely. Additionally, within peat sediment, decreasing CPI has been associated with greater microbial degradation of organic matter due to changes in water table depth (Xie et al, 2004; Zhou et al, 2010). However, no such trend can be seen in any of the cores of this study, as CPI values are either random as in the Aguajal Agua Blanca core, or remain relatively constant into the deepest parts of the Pantano de Martos sediment. Therefore, in this instance CPI is thought to predominantly characterise the vegetation within the environments, showing that all cores contain vegetation of terrestrial origin.

It must be noted, however, that although slight, there is a decrease in CPI in the Pantano de Martos core coinciding with the LGM. During the LGM, CPI values decrease to ~4 and remain relatively constant until the onset of the Holocene where CPI values start to increase again. Although high CPI values (>1) are widely accepted as an indicator of terrestrial sources of organic matter, multiple studies note that CPI values of terrestrial higher plants show distinct odd-even predominance due to the abundance of C₂₇, C₂₉ and C₃₁ and therefore exhibit CPI values always greater than 5 (Eglinton and Hamilton, 1967; Ling et al, 2017; Rieley et al, 1991; Rao et al, 2009). The lower CPI values during the LGM therefore suggest that the vegetation may contain an abundance of shorter chain lengths. A decrease in CPI also coincides with a reduction of both TOC and TN (6% and 0.3% respectively). As tropical peatlands are, by definition, carbon rich ecosystems composed of ~56% carbon on a dry mass basis (Könönen et al, 2015), the combined results suggest that during the LGM, the Pantano de Martos site was not a peatland. Instead, it is hypothesised that the lowering temperatures by ~5°C and the subsequent reduction of atmospheric CO₂ of 50% as a result of increased abundance of Northern Hemisphere ice sheets (Berman et al, 2016) created an environment in the Pantano de Martos region that was of lower plant species diversity than present, which most probably contained monospecific vegetation composed of a dominant shorter-chained length vegetation species. Prior to the onset of the LGM (60-30,000 cal yr BP) and after the end of the LGM

into the Holocene (~10,000- 0 cal yr BP), CPI values are more varied, therefore suggesting a return to a more diverse vegetation composition containing a wider *n*-alkane distribution.

5.2.1.2. Average Chain Length (ACL)

Average ACL values for the three cores are 29.2, 28.7 and 27.2 for Aguajal Agua Blanca, Aguajal del Loretillo and Pantano de Martos respectively. These values suggest that the dominant vegetation source in the sediment is woody plants such as trees/shrubs (Bush and McInerney, 2013), and also support the findings of Ecuadorian *n*-alkane studies which show a predominance of the C₂₉ *n*-alkane in a tropical setting (Jansen et al, 2006). Variations in ACL have been linked to climatic conditions, notably aridity, with longer *n*-alkane chain lengths and thus higher ACL values being found in warmer/drier environments (Carr et al., 2014; Eley and Hren, 2018; Sachse et al, 2006; Vogts et al, 2012). Although subtle, this trend can be seen through the average ACL values, with the Pantano de Martos core producing a lower ACL than the Amazonian cores. This finding also supports Feakins et al. (2016a) tropical forest elevation study from Peru. They found that across all sites, C₂₉ and C₃₁ were prominent, however at higher latitudes the C₂₇ *n*-alkane was also abundant, and therefore caused average ACL values to decrease. Additionally, Feakins et al. (2016a) found ACL to be highly variable, ranging from 27.2 to 32.6 across the elevation transect. Their results also support the findings of this study, as all ACL values fall within the elevation transects range.

In the Aguajal Agua Blanca core, ACL values largely remain between 28 and 30, but decrease to 26.63 and 27.66 at 214 cal yr BP and 535 cal yr BP ACL respectively. Even so, all values within the core relate to the typical values for trees and shrubs. ACL values in Aguajal del Loretillo also range between 27 and 29, again indicating a terrestrial input. A drop in ACL at ~2400 cal yr BP corresponds to an increase in the shorter chained C₁₉ and C₂₁ *n*-alkanes. This is interesting as C₁₉ is thought to originate from species of algae (Ficken et al, 2000) and that the *n*-alkane abundance of all chain lengths diminishes after this point. This could suggest, that some sort of degradation is occurring in the core as a result of the presence bacteria or algae, which reduces the amount of *n*-alkanes in each sample and therefore effects the ability in calculating distribution parameters.

In contrast to Aguajal del Loretillo, ACL could be calculated throughout the whole of the Pantano de Martos core, with values ranging from 25.2 to 28.9 and averaging 27.2. ACL is lowest during the LGM, where TOC, TN and CPI values also decrease. The highest ACL

values occur at around 37,000 cal yr BP, which also coincides with higher CPI values. Given the fact that *Sphagnum*, which produces largely C₂₃ and C₂₅, dominates in the upper parts of the core, a lower average ACL in the Pantano de Martos core was expected in the youngest samples (Nott et al, 2000). In these *Sphagnum* dominated samples, ACL values average 25.2. Additionally, ACL values also decrease into the LGM, where the CPI values suggest a monospecific vegetation environment composed predominantly of an abundant shorter chained *n*-alkanes. As a result, it is therefore feasible to assume changes in the ACL are mostly driven by the contribution of the shorter chained *n*-alkanes throughout the core.

5.2.1.3. P_{aq} and Norm31

The P_{aq} parameter was used to understand the importance of the mid-chained C₂₃ and C₂₅ *n*-alkanes within the three cores. An increase in P_{aq} values is thought to indicate a greater contribution of the shorter (C₂₃-C₂₅) *n*-alkanes, which has been interpreted as reflecting more of the relative abundance of submerged plants (Ficken et al. 2000; Gao et al, 2011; Taylor et al, 2018). For much of the record, P_{aq} values for Aguajal Agua Blanca remain below 0.2, indicating a largely terrestrial plant wax source, as is the case for Aguajal del Loretillo which remains below 0.3 throughout the record. A slight increase in P_{aq} is found at ~2400 cal yr BP, where values increase to ~0.5. This suggests that the relative input of the mid-chain *n*-alkanes increased, which could reflect a wetter environment and a greater input from aquatic plants. However, P_{aq} between ~2500 to 3500 cal yr BP is <0.2 suggesting that this increase in mid-chained *n*-alkanes is short-lived.

In contrast to the Amazonian cores, P_{aq} values in Pantano de Martos span a larger range, with the highest P_{aq} ~0.8. In *Sphagnum* dominated peatlands specifically, Nicholls et al. (2006) suggest that that P_{aq} can be used as a palaeohydrological indicator due to the hydrological control on *Sphagnum* extent and that *Sphagnum* species produce predominantly C₂₃ and C₂₅. At ~0 cal yr BP, where it is known that *Sphagnum* is abundant, P_{aq} values are at their highest (0.8) indicating a large input of C₂₃/C₂₅ but also wet conditions, due to the waterlogged conditions *Sphagnum* requires (Nicholls et al, 2010). Between ~2-3,000 cal yr BP, there is a sharp decrease in P_{aq}, implying a significant reduction in the shorter chained *n*-alkanes and therefore drier conditions. However, from ~4400 to 20,000 cal yr BP, P_{aq} values increase, to ~0.65 implying a transition into wetter conditions during the LGM. Finally, between 45,000 to 75,000 cal yr BP, P_{aq} values fluctuate between 0.3 and 0.8, with the highest P_{aq} values occurring at ~63,000 cal yr BP. The results suggest that mid-chained *n*-alkanes are dominant throughout

the core and as a result, suggests that conditions have always been relatively wet at the Pantano de Martos site. Additionally, Taylor et al (2018) suggest that a large range in P_{aq} can indicate a highly variable vegetation composition. In the Pantano de Martos core, P_{aq} values have a range of 0.74, which compared to the P_{aq} range in the Amazonian cores, 0.46 and 0.33 for Aguajal Agua Blanca and Aguajal del Loretillo respectively, is significant. It is most likely that the highly variable vegetation composition occurred in the oldest sections of the core (50 to 75,000 cal yr BP) where CPI values also show a large range.

Combining ACL with P_{aq} can also help in understanding *n*-alkane contributions and therefore infer suspected changes within the environment. Low P_{aq} and high ACL values imply relatively dry surface conditions and a predominance of vascular plants (Carr et al, 2015; Schemmel et al, 2017). In contrast high P_{aq} and low ACL indicates a wider spread of *n*-alkane chain lengths, with lower CPI values also occurring alongside this finding (Carr et al, 2015). Interestingly, the high P_{aq} and low ACL is especially apparent during the LGM, suggesting a wetter environment in the Pantano de Martos site. In contrast, the Holocene, from 11,650 cal yr BP to present shows an increase in ACL and a decrease in P_{aq} , therefore reflecting a change to drier surface conditions and a greater input of terrestrial plants.

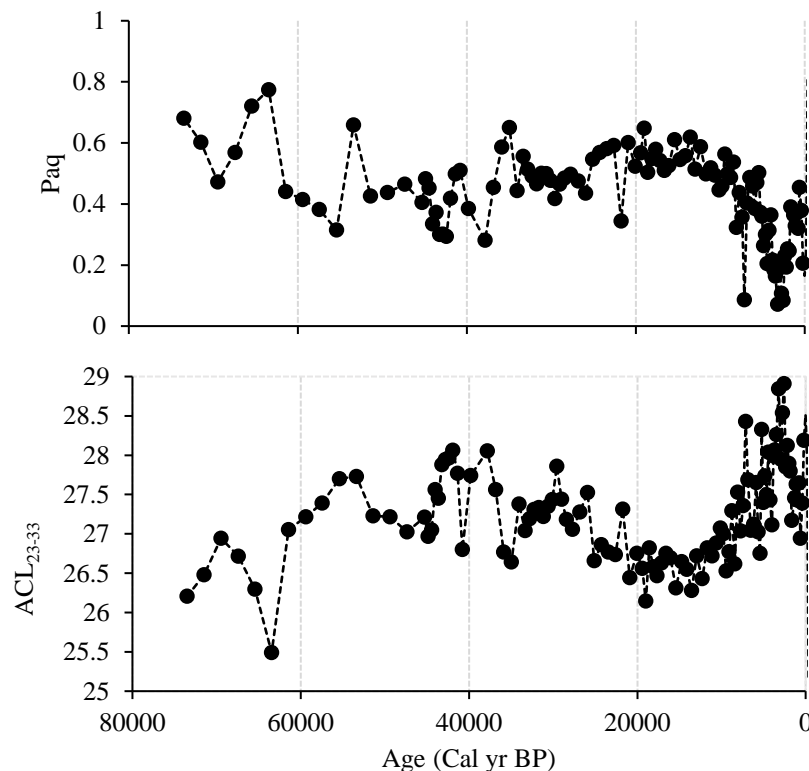


Figure 40. Combined figure displaying the P_{aq} and ACL_{23-33} values for the Pantano de Martos core.

Finally, Norm31 can be used to infer the changes within the terrestrial vegetation community and can demonstrate temporal variability in long-chain *n*-alkane production (Taylor et al, 2018). This is because the parameter uses the long chained C₂₉ and C₃₁ *n*-alkanes, which typically occur in trees and grasses (Bush and McInerney, 2013). In all three cores, changes in Norm31 are subtle, owing to the low abundance of the C₃₁ *n*-alkane. Consequently, across the records, Norm31 remained below 0.5, reflecting an affinity to the C₂₉ *n*-alkane across all records. In the case of the Martos core, comparing Norm31 with P_{aq} reinforces the fact that changes in the distribution parameters are mostly driven by the short-chained *n*-alkanes (fig. 40). Throughout the core, Norm31 remains relatively constant at ~0.3, whereas P_{aq} is more varied. Similarly, Norm31 also remains relatively constant in the Amazonian cores. In contrast to the Martos core, although P_{aq} shows subtle variation, values remain below 0.4 suggesting that the sites did not contain large proportions of the C₂₃ *n*-alkane, and therefore were possibly drier than the Martos site.

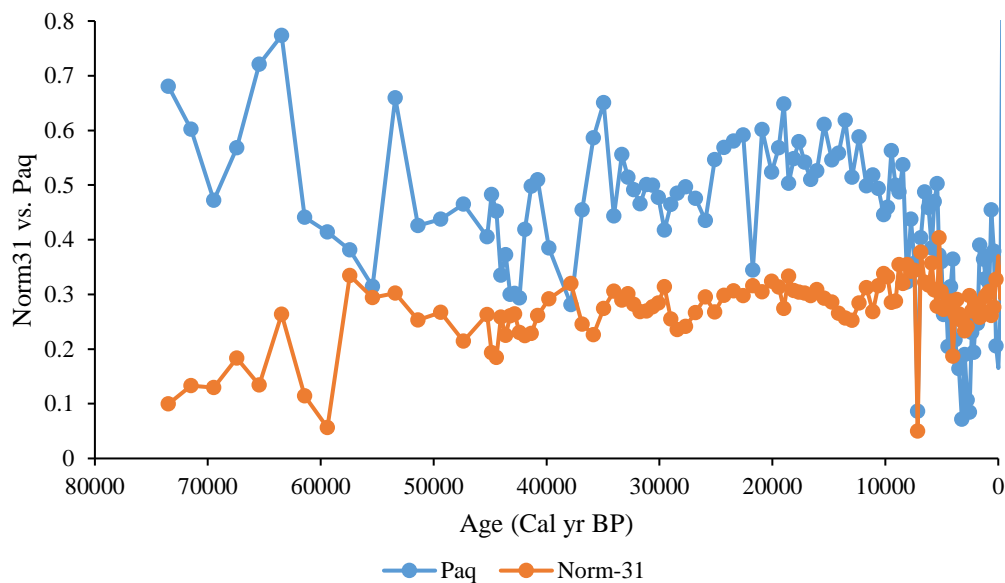


Figure 41. Norm31 vs. P_{aq} for the Pantano de Martos core.

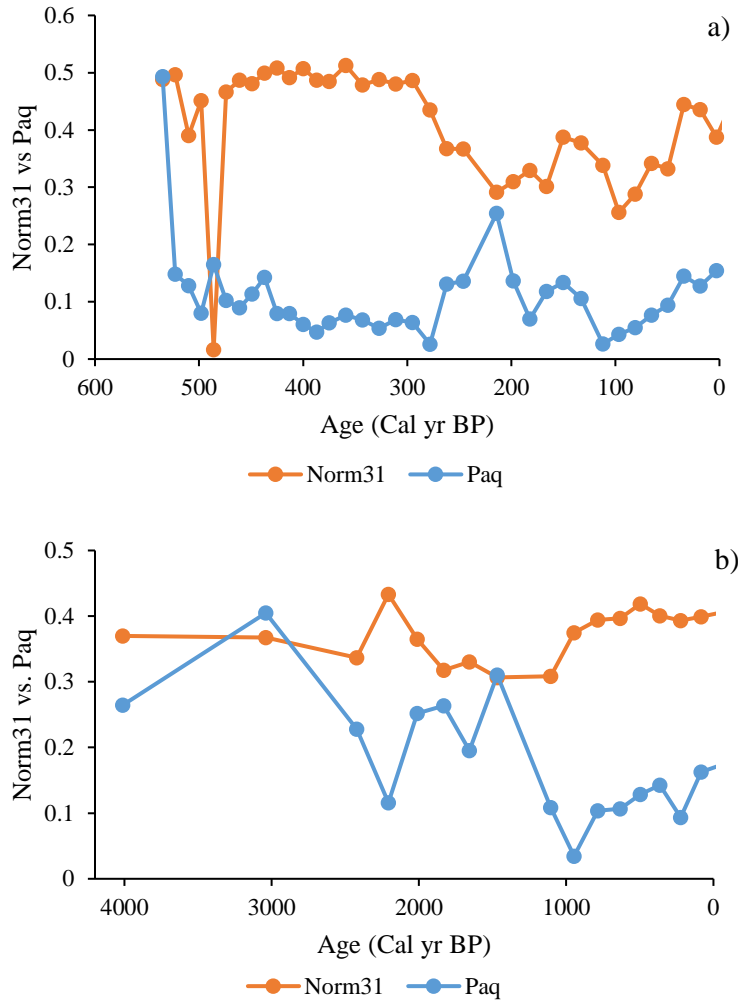


Figure 42. Norm31 vs. P_{aq} for a) Aguajal Agua Blanca and b) Aguajal del Loretillo.

5.3. Leaf wax *n*-alkane δD

The discussion will focus on the C_{29} *n*-alkane values to interpret the palaeohydrology of each core. The low concentrations of C_{31} in the Pantano de Martos core hinder the precision of the δD measurements and thus the potential reconstruct palaeohydrology successfully. Other studies have also chosen to focus their discussion on single *n*-alkane. For example, Collins et al. (2013) used the C_{31} *n*-alkane in the discussion of the palaeohydrology over Western Africa due to the fact that it was the most cleanly separated homologue.

5.3.1 Leaf wax origin and reliability in palaeohydrological reconstruction

Leaf wax *n*-alkanes can be transported by eolian or fluvial transport, meaning that they may be transported over long distance (Conte and Weber, 2002). As a result, the δD_{wax} signal found in the cores may be of a regional rather than a local terrestrial source. Even though marine sediment cores are valuable in palaeohydrological reconstruction, due to their relatively large source areas, they integrate a leaf-wax signal from large continental areas (Schefuss et al. 2011; Collins et al, 2013). However, in the case of the three cores, it is likely that the leaf wax source is ultimately the local vegetation (e.g. Carr et al. 2015). Due to the steep Andean topography in the case of the Martos core, it is unlikely that there would have been a significant contribution of leaf waxes via long-range transport (Conte and Weber, 2002). Similarly, in the Tipisca cores, the densely vegetated forest surrounding the site, which is predominantly composed of the palm *Mauritia flexuosa* (Arecaceae), suggests that a signal from wider areas into the Amazonian cores is unlikely to be significant. This is supported by palynological data from both the Martos and Tipisca sites, which show that the pollen-derived vegetation composition is very similar to the species composition at the sites today (Berrio, unpublished data. See appendix). As a result, the δD_{wax} signal can be assumed to reflect the local vegetation at both sites, and therefore the precipitation both sites experienced.

Both Smith and Freeman (2006) and Sachse et al (2012) warn that interpreting δD_{wax} is complicated by the metabolic pathways of a plant and relative humidity both influencing the δD_{wax} values. As a result, the studies concluded that before palaeohydrological change can be reconstructed accurately, it is important to determine the influence that changes in vegetation and consequently changes in plant functional groups would have had on δD (McInerney et al, 2011). However within South America, this is mainly a cause for concern in locations such as savanna, where C_4 grasses and C_3 shrubs/trees are found in close proximity to one another

therefore complicating the δD_{wax} signal (Fornace et al, 2016). As the Pantano de Martos site is a *Sphagnum* dominated peat bog, which are known to be characterised by low vascular plant biodiversity (Nicholls et al, 2010), the effects of a dramatic shifts in vegetation, and therefore a vegetation effect on δD_{wax} values can be ruled out. Similarly, it is unlikely that drastic vegetation changes occurred within the Amazonian environment. Such an assumption is supported by the minor changes in ACL in these cores, as well as palynological data from both the Amazonian and Andean sites (Berrio, unpublished data). As it is suspected that vegetation composition did not change dramatically, δD_{wax} values are assumed to reflect a local environmental signal of precipitation.

5.3.2. Water source

The tropical Atlantic Ocean is the primary source of moisture for both sites throughout the year (Thompson, 2000). The meridional Atlantic sea surface temperature (SST) gradient influences the amount of rainfall experienced over South America, with lower SSTs in the Northern Equatorial Atlantic causing increased rainfall over the Amazon Basin (Baker et al, 2001). The easterly trade winds then transport air and moisture, from the Atlantic Ocean over tropical South America into the Amazon Basin (Trenberth, 1999). Within the Amazon Basin, ~40-50% of annual precipitation is lost as runoff, with the remaining precipitation returned to the atmosphere via evaporation and transpiration. Most of the recycled water vapour is via transpiration, therefore linking the hydrologic balance of lowland South America to its vegetation (Gat and Matsui, 1991). The isotopic composition of precipitation over the Amazon Basin is therefore thought to reflect the isotopic composition of moisture recycling and the atmospheric water balance (Gat, 2000). Atmospheric flow, from east to west transports water vapour from the lowland Amazon Basin to the high Andes, in particular, up the eastern Cordillera, which is of importance to this study (Fornace et al, 2014; Polissar et al, 2006). Circulation patterns and steep topography combine to form an east to west precipitation gradient (Stansell et al, 2007), which integrates the isotopic effects of oceanic evaporation, lowland moisture recycling and orographic uplift (Polissar et al, 2006). All processes are ultimately controlled by the position and intensity of the ITCZ, which is linked to the seasonal cycle of solar declination (Stansell et al, 2007). As a result, the isotopic values of the Martos site are expected to relate to those found in the Amazonian records, but with differences in the overall average δD_{wax} values as a result of altitude and temperature effects.

Table 6. The highest, lowest and average δD_{wax} values for Aguajal Agua Blanca, Aguajal del Loretillo and Pantano de Martos cores.

| δD_{wax} (‰) | Aguajal Agua Blanca | Aguajal del Loretillo | Pantano de Martos |
|-------------------------|--------------------------------|----------------------------------|------------------------------|
| High | -141.3 | -135.2 | -173.0 |
| Low | -173.8 | -209.0 | -215.1 |
| Average | -159.7 | -163.5 | -196.7 |

Comparing the isotopic records from both the Amazonian and Andean sites indicate the influence of the transport path of precipitation on δD_{wax} values. Average δD_{wax} values from the Pantano de Martos core are $\sim 30\%$ lower than in the Amazonian cores (table 6), reflecting the influence of both orography, prior lowland moisture recycling and temperature on δD_{wax} values of the low latitude Amazonian sites relative to the high-altitude Andean site. The difference in altitude between the sites is expected to exert the most noticeable effect on δD_{wax} differences. The altitude effect is predominantly a function of temperature and describes the relative depletion in the ‘heavier’ isotope as a cloud mass increases in altitude (Poage and Chamberlain, 2001). Between the Amazonian (~ 78 m asl) and the Andean (~ 3000 m asl) sites, there is a ~ 2900 m difference in altitude, and consequently, a $\sim 12^\circ\text{C}$ difference in temperature. Average temperatures in the Amazonian site are $\sim 26^\circ\text{C}$ (Schongart et al, 2002), whereas at Pantano de Martos, average temperature is $\sim 14^\circ\text{C}$ (Londono et al, 2014). An estimate of the expected temperature effect on δD_{wax} values can be calculated using the equation:

$$^2\varepsilon_{v/l} = -85\ 626/T + 213.4\text{‰}$$

Where $^2\varepsilon_{v/l}$ represents the fractionation of liquid water to water vapour and is approximately equal to $^2\delta(y) - ^2\delta(x)$ (Mook, 2001). Using this formula, a 12°C difference in temperature will cause a 12% difference in apparent fractionation. Although this difference is substantial, there remains an 18% difference between the sites, which must be due to other influences, such as moisture recycling in the Amazon Basin (evaporation and transpiration effects), the amount of rainfall and additional altitude related effects. Water vapour that is derived from evaporation is known to be isotopically more negative than initial precipitation (Polissar et al, 2006), and as water balance calculations suggest that between 40 to 50% of annual precipitation is lost as either runoff or recycled through evaporation and transpiration before returning to the atmosphere in tropical forests (Costa and Foley, 1999; Polissar et al, 2006), this would explain

the difference in the average isotopic values between cores. However, although the balance between precipitation and evaporation can be estimated through climate models and is a critical climate parameter (Nicholls et al, 2010), the degree of moisture recycling is difficult to quantify and is beyond the scope of the thesis.

5.4. Interpreting the δD_{wax} record - Aguajal Agua Blanca and Aguajal del Loretillo

Although the Amazonian records were obtained within close proximity of one another, their δD_{wax} records cannot be easily compared due to the differing timescale and temporal resolutions of the records. δD_{wax} values for Aguajal Agua Blanca are available for ~540 cal yr BP, whereas although still only providing insight into the late Holocene, δD_{wax} values for Aguajal del Loretillo span a larger timespan of ~2400 cal yr BP. On a broad scale both records exhibit low δD_{wax} values during to the time corresponding to the Little Ice Age, and in the case of Aguajal del Loretillo, the Medieval Climate Anomaly (Figure 26). In contrast to studies such as Hoffman et al. (2003) who suggest that intense water recycling smoothes temporal variation in the isotopic signature within the Amazon Basin, δD_{wax} values for the Amazonian cores show clear variation that can provide insights into late Holocene climate variability.

5.4.1. Aguajal Agua Blanca

Between ~540 and 130 cal yr BP, the time corresponding to the Little Ice Age (LIA; 500-100 BP), δD_{wax} varies only slightly, suggesting a relatively constant amount of rainfall. Additionally, δD_{wax} values are lowest during this time (-165‰), implying that rainfall during the LIA was higher than at present. This supports the findings of $\delta^{18}O_{calcite}$ (Bird et al, 2011) and $\delta^{18}O$ speleothem records obtained from northern Peru (Reuter et al, 2009) and Bolivia (Apaestégui et al, 2018), which find low $\delta^{18}O$ values during the LIA. Both records also show an increase in $\delta^{18}O$ in the most recent ~100 years of the records, leading to the conclusion that precipitation levels over the northern parts of the continent are currently lower than those of the recent past. Polissar et al. (2006) also reported an advance in glacier position in the high Venezuelan Andes during the LIA; however, instead of interpreting this as a change in temperature, the study concluded that advancement of the glaciers was evidence of higher precipitation because of a steeper tropical lapse rate.

From ~120 cal yr BP to 81 cal yr BP, δD_{wax} increases by ~30‰, implying a significant decrease in precipitation in the latest Holocene. Similarly Bird et al. (2011) reported an increase in $\delta^{18}O$ during the late Holocene. From 80 to 34 cal yr BP, δD_{wax} values remain around ~ -140‰,

suggesting that current precipitation levels are lower than those of the past. However, there is a subtle decline in δD_{wax} values between 34 and 0 cal yr BP of $\sim 6\%$, suggesting that in the last ~ 50 years rainfall within the Amazon Basin has slightly increased. This contradicts data obtained from fluviometric stations within the Basin that estimate a decrease in rainfall of $-0.23\% \text{ yr}^{-1}$ (Villar et al, 2009), therefore further information is required to ascertain modern changes in precipitation.

5.4.2. Aguajal del Loretillo

δD_{wax} from the Aguajal del Loretillo record is more variable between ~ 2400 - 1200 cal yr BP than for the most recent 1000 years. Between 1830 to 1434 cal yr BP, δD_{wax} increases by 35%, suggesting that the climate became significantly drier. Interestingly, the same increase in isotopic values is not seen in other northern South American records. For example, records from Lake Valencia, Venezuela show an increase in $\delta^{18}\text{O}$ from 1900-1800 yr BP, however values after 1800 yr BP decrease suggesting increased rainfall at that site (Curtis et al, 1999). δD_{wax} values decrease after this point, suggesting a return to wetter conditions.

A transition to lower δD_{wax} values were found at the onset of the Medieval Climate Anomaly (MCA; 950-650 BP) suggesting increased precipitation during this time. Interestingly, these findings correlate with the findings of Apaéstequi et al. (2018) who found lower $\delta^{18}\text{O}$ values in their speleothem record from the Umajalanta–Chiflonkhakha cave system in Bolivia. Additionally, δD_{wax} values from the LIA are slightly higher than the MCA, which contradicts the findings of other northern tropical records. In the northern tropics, the climate during the MCA has been found to coincide with a drought due to a weakened SASM as a result of warming in the Northern Hemisphere and North Atlantic (Bird et al, 2011; Vuille et al, 2012). However, the lower δD_{wax} values found during the MCA suggest that a drought was not experienced within the palm swamp.

There is a sharp transition to more positive δD_{wax} values during the LIA suggesting a sudden change to drier conditions. However, as this event is only represented by one datapoint, the significance is difficult to ascertain. Excluding the sample at 306 cal yr BP (-150.2%), δD_{wax} values during the LIA remain between -162% and -170% , indicating that precipitation levels remained low from the end of the MCA into the LIA. In the youngest samples in the record, from 84 to 5 cal yr BP, δD_{wax} values decrease by 9% to the lowest value of the core (-175%). This record therefore also suggests that within the Amazonian site, precipitation levels have slightly increased.

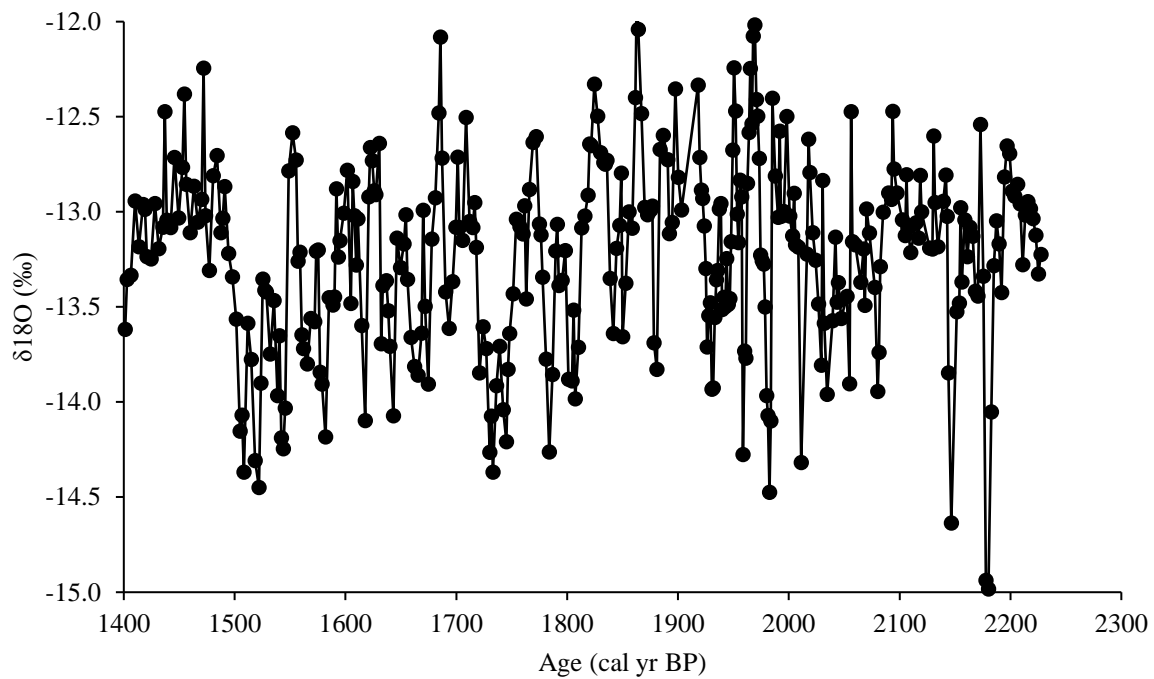


Figure 43. Bird et al. (2011) $\delta^{18}\text{O}_{\text{calcite}}$ record from Lake Pumacocha, Peru.

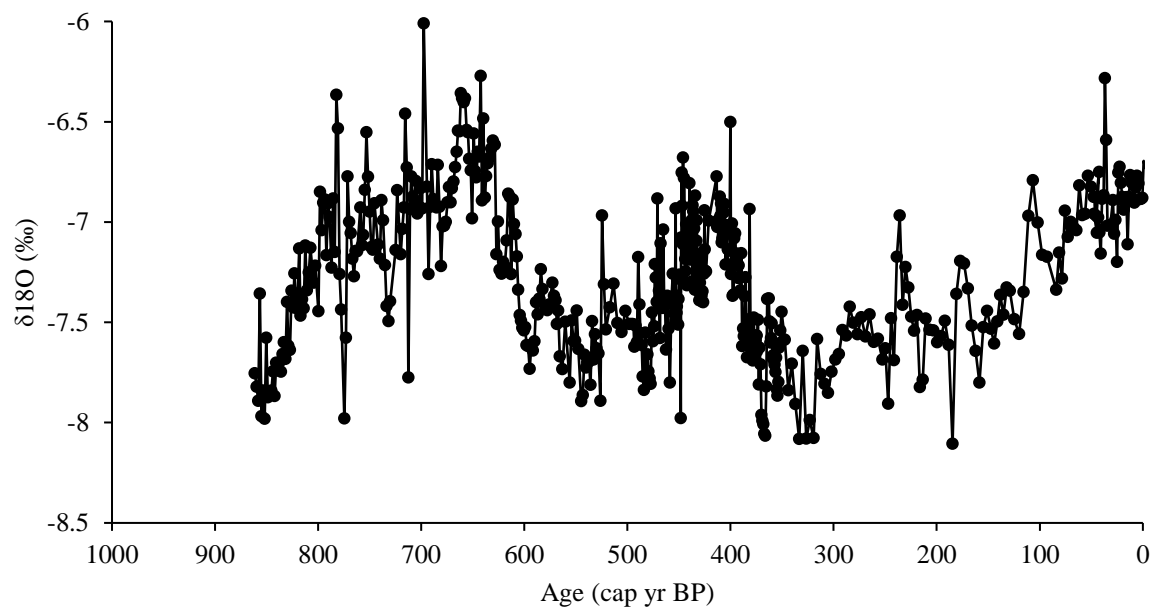


Figure 44. Reuter et al. (2009) $\delta^{18}\text{O}$ stalagmite (speleothem) record from Cascayunga Cave, Peru.

5.3.2 Longevity of the records

Polissar et al (2006) previously noted that there are no long proxy records of the isotopic composition of precipitation from lowland South America. Through the isotopic analyses of this study, it has been shown that when using a biomarker known to be resistant to degradation (Schimmelmann et al, 2006), a long-term climate record is still difficult to obtain. Lipid extraction was carried out on all sub-samples of the Aguajal Agua Blanca core. However, after ~600 cal yr BP, *n*-alkanes disappeared. A similar trend can be seen in Aguajal del Loretillo. Even though the age-depth model produced an estimate core age of ~5000 cal yr BP, *n*-alkanes were only be obtained from the earliest ~2000 years of the record. The loss of the records with depth may reflect two hypotheses:

1. The palm swamp environment did not exist past ~3000 years ago. Or,
2. There are underlying processes causing the complete degradation of *n*-alkanes within the sediment.

Although palynological data is available for Aguajal Agua Blanca, due to the shorter length of the core, insights into the vegetation at the site are only available to ~2200 cal yr BP (fig. 45). However, up until this point there is a strong abundance of palm vegetation, suggesting that the swamp environment was maintained over the last ~2500 years, implying the explanation lies in hypothesis 2.

To test the effect of degradation on the Amazonian cores, a few samples of the polar extracts from each core were treated with methanol with a TMS (trimethylsilane) derivative. Using this treatment transformed the polar lipids into apolar lipids so that they can be analysed in the same way as the apolar *n*-alkanes. The results showed that fatty acids such as stearic acid and plant resins such as friedelan-3-one, a triterpenoid found in many plants (Ludwiczuk et al, 2017) were present in the sub-samples, which could possibly be used as an alternative to *n*-alkanes for paleoenvironmental reconstruction. However, the TMS derivatising agent adds three extra carbon atoms into the sample which can influence the isotopic values produced, and the process of TMS derivatization is labour-intensive and time-consuming (Tao et al, 2008). As a result, no further isotopic analyses were performed on the polar extracts and the rest of the discussion focusses on the Pantano de Martos record to understand long-term palaeohydrological change in Colombia.

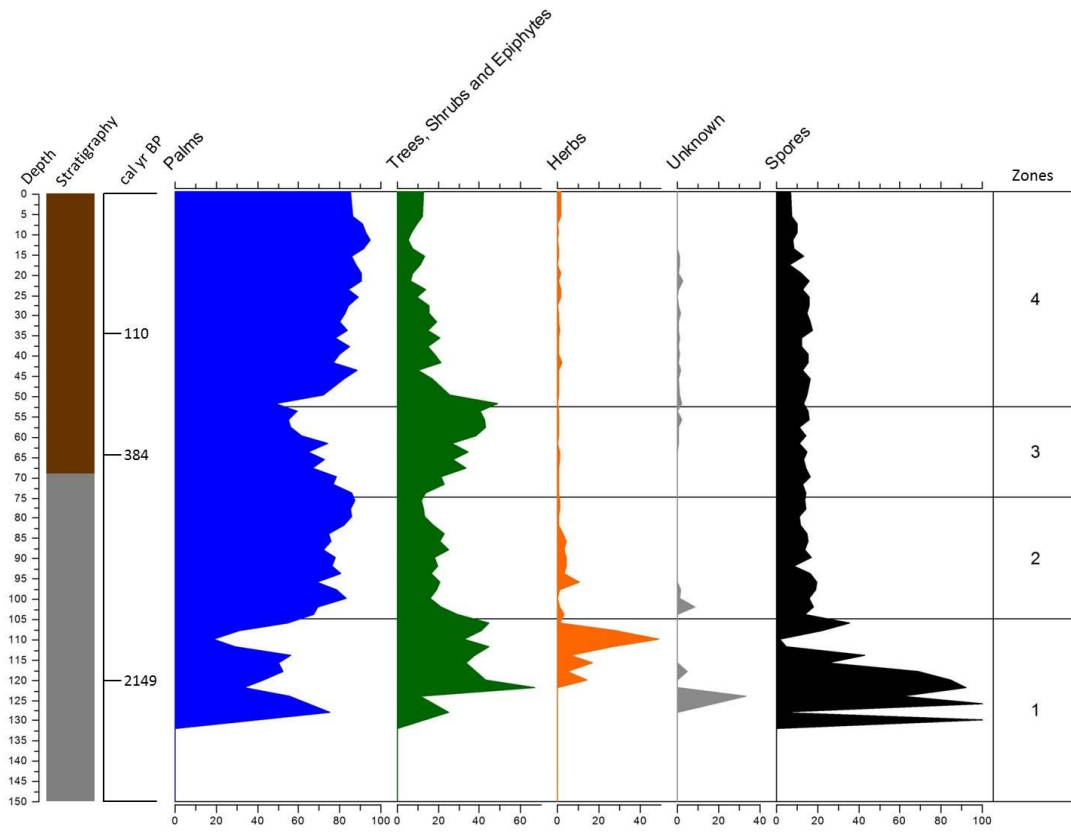


Figure 45. Summary pollen diagram of the four ecological groups found in the Aguajal Agua Blanca core. For a more detailed diagram of the most frequent taxa identified in the core, including the percentage pollen abundance see appendix. Palynological data obtained from Berrio, unpublished data.

5.5. Interpreting the δD_{wax} record - Pantano de Martos

5.5.1. Ice volume correction on the Pantano de Martos record

Given the age of the Pantano de Martos core (<85,000 years), ice volume correction is needed to account for variations in the $\delta^{18}\text{O}$ value of ocean water. Currently, marine proxies provide a relatively stable comparison point as ocean water is well mixed and typically has a $\delta^{18}\text{O}$ value of $\sim 0\text{‰}$ (Sessions, 2016). However, an increase in global ice volume increases the $\delta^{18}\text{O}$ value of the ocean. During the LGM, the global ice volume was $\sim 52 \times 10^6 \text{ km}^3$ greater than today (Lambeck et al, 2014). This difference in ice volume produced a $\sim 1.5 \text{‰}$ increase in sea water $\delta^{18}\text{O}$ and therefore changed the reference point for isotopic measurements that are concerned with the hydrological cycle, such as leaf wax δD . The $\delta^{18}\text{O}$ values from the Martinson Benthic Stack record (Martinson et al, 1987) were used to ascertain the isotopic value of the ocean for the timespan of the Martos record. Based on the benthic $\delta^{18}\text{O}$ values, the likely impact on the value of seawater δD was estimated using the slope of Global Meteoric Water Line (GMWL) equation:

$$\delta D = 8 * \delta^{18}\text{O} + 10\text{‰}$$

(Craig, 1961). The converted δD values obtained from the Benthic Stack record are displayed in figure 46.

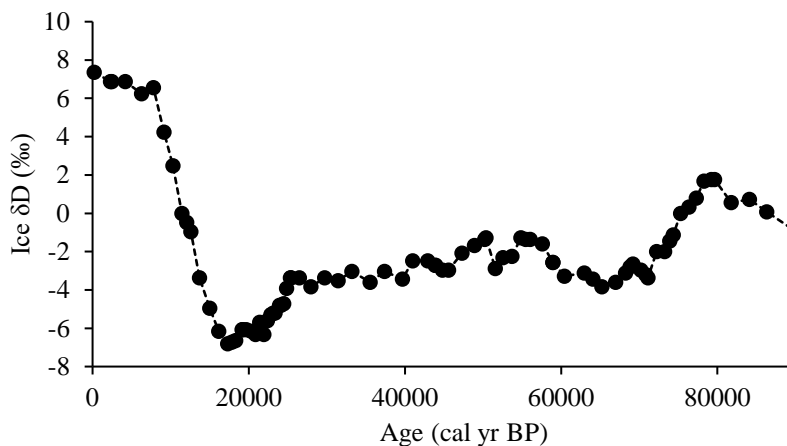


Figure 46. Martinson Stack record converted into δD to provide an easier comparison to the Pantano de Martos core. Data obtained from Martinson et al (1987).

To correct the Martos record in light of the differences in sample age, the correction of the Martos record was achieved by a linear fit between ages in the Martinson Stack record that encompassed dates in the Martos record, using the formula:

$$y = mx + c$$

The values produced were added to the uncorrected δD values obtained from the Martos core and are displayed in figure 47. These ice-corrected δD_{wax} values will be used to infer paleohydrological changes for the Pantano de Martos site from this point, as they remove any variation related to changes in the δD of ocean water.

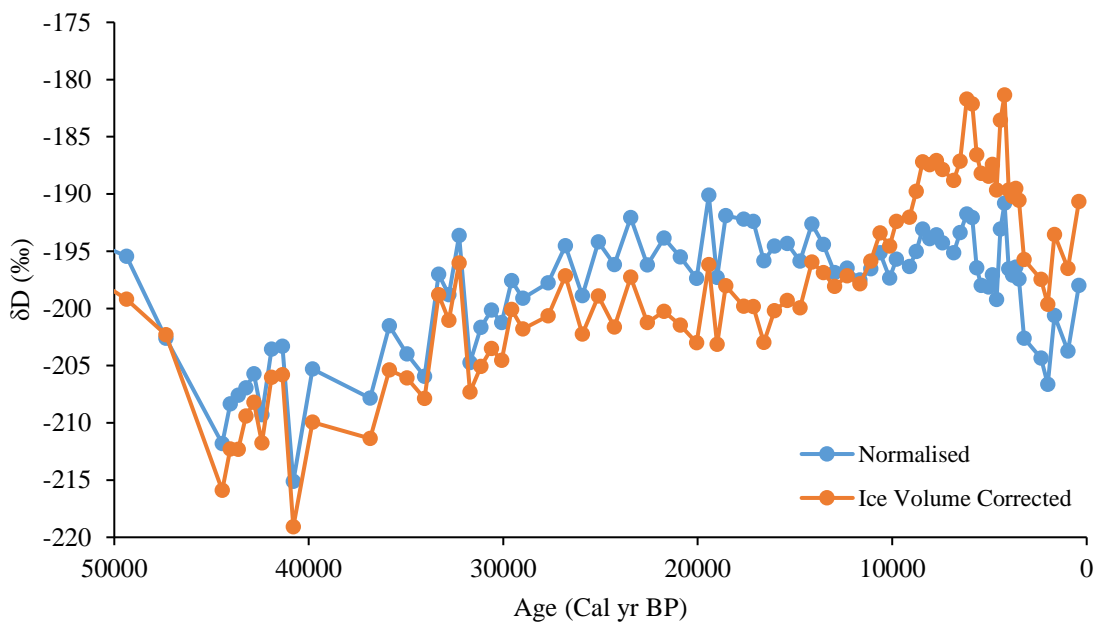


Figure 47. The normalised (raw) deuterium data and the ice volume corrected deuterium data for the Pantano de Martos core.

Prior to interpretation of the δD_{wax} record, it is imperative to understand the causes of δD_{wax} differences between the normalised and ice-corrected Martos records. The most pronounced differences occur the Late Holocene (between ~4000 to 9000 cal yr BP), where the δD record shows higher δD values, and during the LGM (~19,000 to 23,000 cal yr BP) where δD values are ~6‰ lower than initially suspected. These differences indicate that larger fractionations occurred during the LGM as compared to the Late Holocene. An average δD_{wax} value was taken for the Late Holocene and the LGM to understand changes in fractionation. The values produced were -189‰ and -201‰ for the Late Holocene and LGM respectively, indicating a fractionation increase of ~12‰ during the LGM.

Changes in fractionation within the δD_{wax} record in the Pantano de Martos core are thought to be due to three things; vegetation changes, temperature differences and the amount effect. The extent to which each factor influences the record can be calculated and has been accounted for using simple observations. It is known from pollen records obtained from the Pantano de Martos sample area that vegetation remained relatively stable throughout the record, being predominantly composed of Páramo vegetation (Berrio, see appendix). As a result, it is accepted that vegetation changes will not have had an influence on the fractionation and therefore changes in δD_{wax} . Consequently, this suggests that both temperature and the amount of rainfall were the cause of changes in the δD_{wax} values of the Martos record. Previous estimates on LGM temperature show that the climate was anywhere between 3-5°C cooler than present day (Farreira et al, 1999). Taking the most extreme scenario of a 5°C decrease in temperature, the estimated hydrogen isotope fractionation was calculated using the equation;

$$^2\varepsilon_{v/l} = -85\ 626/T + 213.4\text{‰}$$

Where $^2\varepsilon_{v/l}$ represents the fractionation of compound y relative to compound x and $T = t\ (^{\circ}\text{C}) + 273.15\ \text{K}$ (Mook, 2001). The resulting fractionation values for hydrogen within water are displayed in table 7.

Table 7. Hydrogen isotope fractionation within water. Taken from Mook (2001).

| t (°C) | t (K) | $^2\varepsilon_{v/l}$ (‰) |
|---------------|--------------|---|
| 0 | 273 | -101 |
| 5 | 278 | -94.8 |
| 10 | 283 | -89 |
| 15 | 288 | -83.5 |
| 20 | 293 | -78.4 |
| 25 | 298 | -73.5 |
| 30 | 303 | -68.9 |
| 35 | 308 | -64.6 |
| 40 | 313 | -60.6 |

The equation showed that a 5°C temperature difference at the Martos site would have caused a fractionation difference and therefore would have influenced the deuterium values by 5‰. Accounting for a temperature effect of 5‰ leaves 7‰ of the 12‰ fractionation difference to be accounted for from the Holocene into the LGM. However, a machine error of 5‰, leaves 2‰ remaining to be explained. Therefore, during the LGM it is estimated that the amount effect influenced the deuterium values in the Martos record by 2‰. As a result, although subtle, the results suggest that at 3000 m asl within the Pantano de Martos site, the Last Glacial Maximum conditions were slightly wetter than present day conditions.

Although δD_{wax} values for the Pantano de Martos core were obtained up to an age of ~73,000 cal yr BP, the discussion focusses on the first ~50,000 years of the core. This is due to the abrupt change in the observed variability in δD_{wax} , from relatively subtle variability from 0-40,000 cal yr BP, to increases in δD_{wax} values of ~10‰ between each sample after 50,000 cal yr BP from -211‰ to -174‰. This is most likely a result of lower temporal resolution as δD_{wax} values were only produced for samples every 10 cm after 50,000 years rather than every 2 cm, leading to age differences between 2 and 7000 years between each data point. Additionally, age estimates for sediments older than 50,000 years are subject to significant error (see appendix A). Therefore, to ensure an accurate representation of Andean paleohydrology was presented, it was decided to omit the oldest ~30,000 years from the discussion.

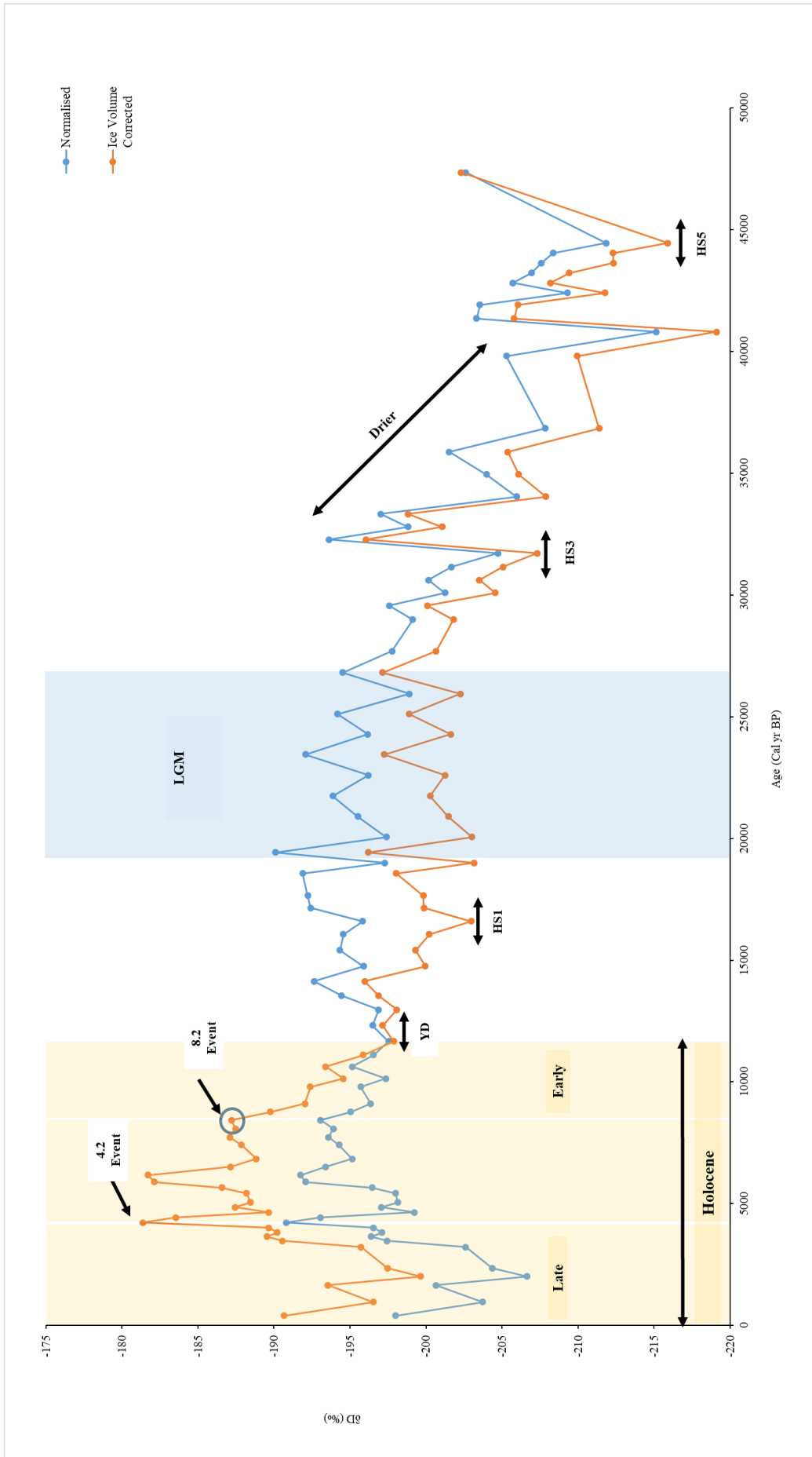


Figure 48. The normalised and ice corrected δD record for Pantano de Martos, highlighting some of the key events occurring within the record. It is important to note that these are highlighted to show where they should be found within the peat record, as opposed to the events actually showing a strong signal in the Pantano de Martos site.

5.5.2 Glacial climate variability

Between ~40-27,000 cal yr BP, δD_{wax} values increase from -219‰ to -197‰ suggesting that the climate became progressively drier during this time. This contradicts the findings from a speleothem record obtained from the Pacupahuain cave in the Central Peruvian Andes, which show the climate was becoming progressively wetter from ~38-28,000 yr BP (Kanner et al, 2012). However, speleothem records from Ecuador also show an increase in $\delta^{18}O$ from 40,000 to ~24,000 yr BP (Mosblech et al, 2012), suggesting that in the north of the continent rainfall decreased. The trend of increasing δD_{wax} values is interrupted at 45,000 and 30,000 cal yr BP, where δD_{wax} values decrease by ~12‰ for ~500 years. This decrease in δD_{wax} values approximately coincides with Heinrich events 5 and 3 respectively (HS1, HS3) (Bond et al, 1992) and suggests that Heinrich events, when identifiable in the record are associated with wet events. This is supported by both Kanner et al. (2012) and Mosblech et al. (2012) who found Heinrich events to appear in their records as abrupt, sustained wet events.

At the onset of the LGM (~26,500 cal yr BP), δD_{wax} values decrease by ~4‰, suggesting that precipitation increased slightly. Throughout the LGM, δD_{wax} values range between -197‰ and -203‰, suggesting that rainfall fluctuated slightly. At the termination of the LGM into the late glacial transition δD_{wax} values increase by ~5‰, indicating that rainfall decreased at the site. In Mosblech et al. (2012) Ecuadorian speleothem record, the LGM does not stand out as a time of extreme aridity or humidity. This finding is thus similar to the Pantano de Martos record, where only subtle changes in δD_{wax} are seen at the onset and termination of the LGM. Similarly, although Kanner et al. (2012) record shows a strong transition to wetter conditions prior to the onset of the LGM, only subtle changes are found during the LGM. However, both studies show that, when compared to present day, the LGM was wetter than current precipitation levels. This is also true for the Martos core, with Late Holocene δD_{wax} values ~12‰ higher than during the LGM.

In contrast, δD_{wax} studies from Bolivia show a more dramatic decrease in δD_{wax} during the LGM. Lake Titcaca records indicate a decrease in δD_{wax} of ~36‰ during the LGM, suggesting that conditions were significantly wetter in the southern parts of the continent (Fornace et al, 2014). An increase in δD_{wax} of 12‰ at the end of the LGM also suggests that conditions became drier, therefore reinforcing the LGM as a wet period in Bolivia. As seen in HS5 and HS3, a decrease in δD_{wax} occurs at the time corresponding to HS1. Immediately after, δD_{wax} values

increase by 5‰ during the Bolling-Allerod warm interval where precipitation has been found to decrease in northern South America (Kanner et al, 2012).

In southern parts of the continent, the YD has been found to be a time of increased precipitation (Baker et al, 2001; Cheng et al, 2013; Van Breukelen et al, 2008) as a result of the abrupt return to glacial conditions in the Northern Hemisphere (Rasmussen et al, 2006). However, the opposite is true for the Martos record. Although detailed changes in δD_{wax} cannot be obtained due to the resolution of the core, δD_{wax} values of the YD are 4‰ higher than those found during HS1, implying that conditions during the YD were slightly drier than in the widely-known wet events of Heinrich stadials. These findings support previously published research showing the YD interval as a time of decreased precipitation in northern South America (Mosblech et al, 2012). This is also inferred from numerous studies of the Cariaco Basin (Haug et al, 2001; Makou et al, 2007) and from ice core records from the Peruvian Andes (Nevado Huascarán, 9°S), which show higher $\delta^{18}O_{ice}$ (~6‰) during the interval identified as the YD and the early Holocene (Thompson et al, 1995). However, as $\delta^{18}O_{ice}$ is used as a proxy for temperature it is difficult to ascertain whether this enrichment is due to a decrease in precipitation or an increase in temperature.

5.5.3 Holocene climate variability

The Holocene refers to the most recent unit within the geological record covering the time interval from 11,700 yr BP to present and it represents the warm episode after the termination of the last glacial (Walker et al, 2012). Recent research has suggested a formal separation of the Holocene Epoch into three subdivisions, namely the Greenlandian (11,700-8326 yr BP), the Northgrippian (8326-4250 yr BP) and the Meghalayan stages (4250 yr BP - present) (*ibid*). This discussion therefore will frame the δD_{wax} variability of the Holocene in these three stages.

The early-to-middle Holocene boundary is characterised by the 8.2 event (8.2 ka BP), which is recorded in Greenland ice as a shift to lower $^{16}O/^{18}O$ and D/H values as a result of abrupt cooling in the Northern Hemisphere (Alley et al, 1997). Although records from South America have shown the 8.2 event to be a time of increased precipitation as a result of the strengthening of the South American Summer Monsoon (SASM) (Cheng et al, 2009), this event is not identifiable within the Pantano de Martos record, mainly due to the temporal resolution of the record. Instead, a trend of progressively higher δD_{wax} values is found in the Martos record,

beginning at Heinrich Stadial 1 (~16,000 cal yr BP) and continuing until ~6000 cal yr BP. Similarly, Van Breukelen et al. (2008) reported an isotope maximum at ~9000 cal yr BP in their speleothem record from Peruvian Amazonia, which coincided with an insolation minimum south of the equator. Thompson et al. (2000) found that during times of increased solar insolation, surface temperatures increased, but also were converted to latent heat, which caused increased convective rainfall. Therefore, during times of low solar insolation, the climate was most probably cooler and/or drier.

The mid-to-late Holocene boundary describing the transition from the Northgrippian to the Megahalayan stage contains the 4.2 event (4.2 ka BP), which represents the widespread climatic phenomenon of mid-to-low latitude aridification (Walker et al, 2012). Mayewski et al. (2004) suggest that the southward migration of the ITCZ in combination with the increased strength of the westerlies over the North Atlantic led to the low-latitude aridity. In the Martos record, δD_{wax} values increase by 8‰ between 4847 and 4221 cal yr BP, to -181.4‰, which is the highest δD_{wax} value of the record. This strongly suggests that precipitation decreased close to the 4.2 event at the Martos site and therefore supports the low-latitude aridification found in other climate proxies. Immediately after the high δD_{wax} value at 4221 cal yr BP, δD_{wax} decreases substantially to -199.6‰ at ~2000 cal yr BP. This supports palynological records from Colombia, which record a shift between 4000-3500 yr BP to relatively moist environmental conditions (Marchant et al, 2001) and records from Lake Titicaca, which show an increase in lake levels of 100 m at 3800 yr BP (Cross et al, 2000). Interestingly, this contradicts other palynological records from Colombia, which imply a drier climate between 3800 and 3200 yr BP due to a reduced discharge of the Caqueta River (Behling et al, 1999), and also Ti records from the Cariaco Basin (Haug et al, 2001). Haug et al. (2001) concluded that Ti accumulation closely followed the precessional changes in direct solar forcing, with a northward shift in summer season solar forcing causing increased rainfall in northern South America. Therefore, they interpreted the early to mid-Holocene to be wetter than the late Holocene. However, the results obtained from Pantano de Martos show the opposite trend. During the mid-Holocene, δD_{wax} values are between -188-181‰, whereas the late Holocene shows the largest decrease in δD_{wax} of 18‰, suggesting that the site became wetter. Additionally, ice core records obtained from the Sajama ice cap in Bolivia also suggest a drier climate during the Late Holocene, due to a peak in dust concentration appearing in the record at 3500 yr BP (Thompson et al, 1995), which further suggests that wetter conditions at the Martos site do not follow the same patterns as other published climatic information.

In contrast to studies such as Abbott et al. (2000) who found a progressively wetter climate from ~3900 yr BP to present day, and Seltzer (2000) who found $\delta^{18}\text{O}_{\text{calcite}}$ values to decrease by 6‰ from 10,000 yr BP to present, the Martos core shows the opposite. $\delta\text{D}_{\text{wax}}$ values in the Martos record begin to increase from 2000 cal yr BP to present by ~9‰, implying that the climate of the Páramo site has become drier since ~2000 cal yr BP. However, due to the lower resolution of the record, recent changes in precipitation levels are difficult to quantify. Therefore, for the interpretation of precipitation from ~2000 cal yr BP to present it is better to interpret changes from the Amazonian cores.

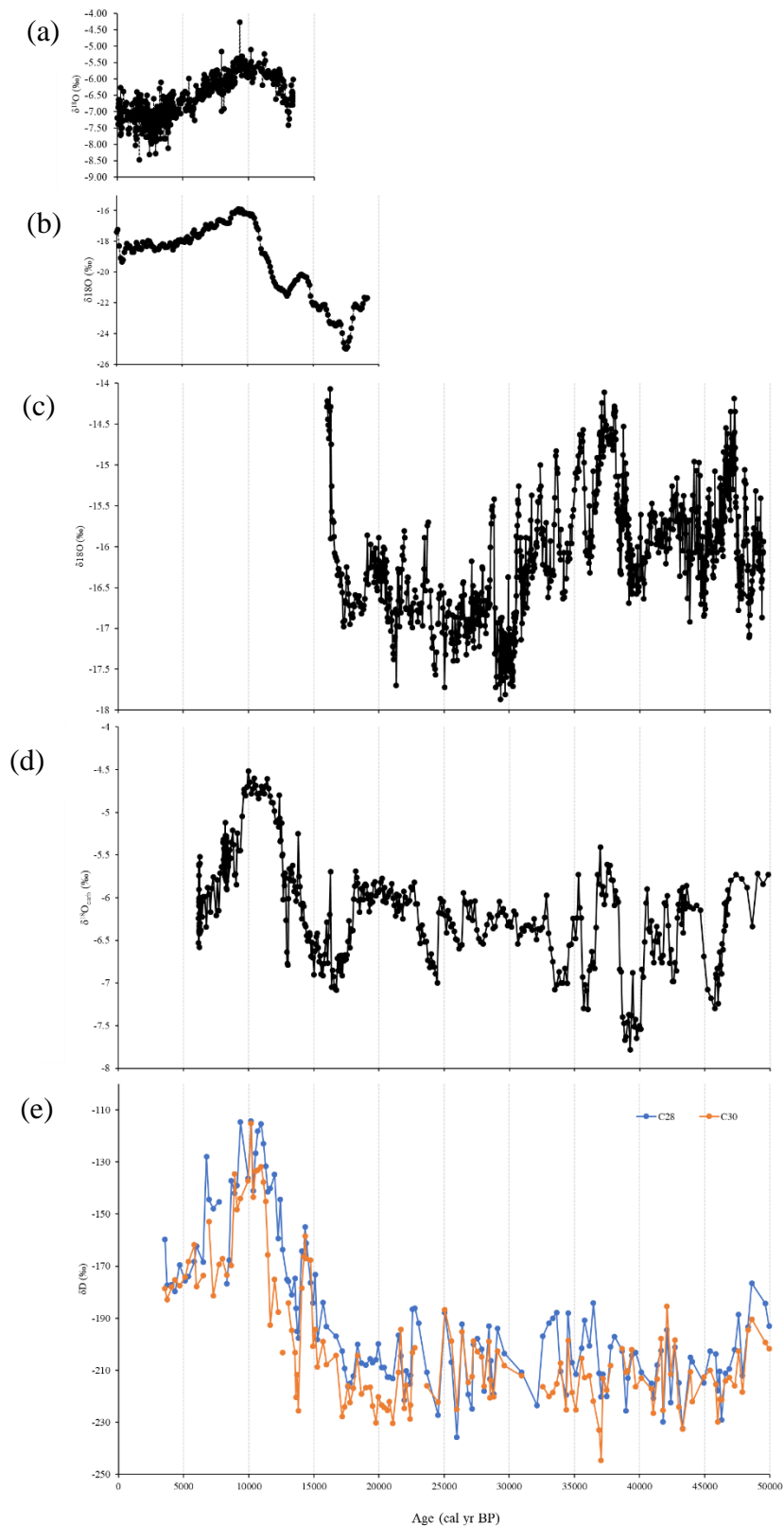


Figure 49. The paleorecords used as a comparison against the Pantano de Martos core. From top to bottom (a-e): (a) Van Breukelen et al. (2008) stalagmite record from Cueva del Tigre Perdido, Peru. (b) Thompson et al. (1995) $\delta^{18}\text{O}$ record from Huascarán ice core, Peru. (c) Kanner et al. (2012) Stalagmite record from Pacupahuain Cave, Peru. (d) Mosblech et al. speleothem record from Santiago Cave, Ecuador. (e) Fornace et al. (2014). Leaf wax n-alkane δD record from Lake Titicaca, Bolivia.

5.6 Factors controlling the changes in precipitation

Over northern South America, changes in SST gradients regulate the latitudinal position of the ITCZ and therefore control amount of moisture reaching tropical South America (Haug et al, 2001). Currently, the ITCZ is situated at 5°N over the modern Atlantic Ocean (Arbuszewski et al, 2013) (fig. 50), however, throughout the Holocene and the last glacial, the average position of the ITCZ is thought to have been displaced southward (Arbuszewski et al, 2013; Fornace et al, 2014). This occurred as a result of high-latitude cooling, increased North Atlantic sea ice cover and a reduction in thermohaline circulation (Chiang and Bitz, 2005). Typically, a southward displacement increases precipitation in southern South America (Kanner et al, 2012; Van Breukelen et al, 2008; Yoon and Zeng, 2010), but causes precipitation to decrease in the northern parts of the continent due to changes in Hadley circulation increasing subsidence (dry conditions) over the northern branch of the ITCZ (Kanner et al, 2012).

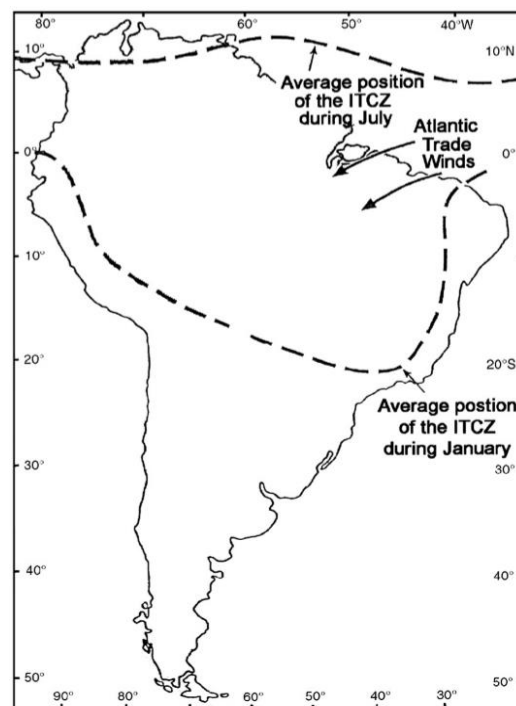


Figure 50. The Average position of the ITCZ over South America in austral winter (July) and summer (January). Taken from Tedesco et al. (2007).

The expanded Northern Hemisphere ice sheets during the LGM are suggested to be the cause of a southward shift of the ITCZ (Chiang and Bitz, 2005) at this time, with studies from Lake Titicaca (Bolivia) showing increased rainfall (Fornace et al, 2016). Fornace et al. (2014) attribute lower δD_{wax} during the glacial period (60-20 ka) compared to the Holocene (11.5 ka-

present) to higher precipitation along the SASM trajectory. However, if this is true, an increase in Martos δD_{wax} during the LGM should be expected, reflecting drier conditions. Although δD_{wax} values do increase by $\sim 20\%$ from the last glacial into the Holocene, this change is subtle when comparing to the difference in δD_{wax} of $\sim 121\%$ in the Lake Titicaca record. Similarly, Mosblech et al. (2012) found an increase in $\delta^{18}\text{O}$ into the Holocene but values only increase by $\sim 3\%$, also indicating a subtle change in precipitation in the north of the continent.

A northward shift of the ITCZ during the early Holocene reflects the retreat of Boreal ice sheets and the establishment of orbital precession, enhanced summer insolation and warming (Arbuszewski et al, 2013). During this time, humid conditions were experienced in the northern subtropics and dry continental conditions were experienced in areas such as lowland Brazilian caves as inferred through a slowdown in speleothem growth (Baker et al, 2001; Wang et al, 2004). δD_{wax} values from the Martos core, however, show the opposite to the findings of other northern South America climate proxy records. δD_{wax} values steadily increase during the early Holocene suggesting that conditions were becoming progressively drier. However, from Laguna Blanca in the Venezuelan Andes, Polissar et al. (2013) found increasingly humid conditions throughout the early Holocene, with an extremely arid interval at 4,000-2,000 yr BP, when the most abrupt transition to wetter conditions is seen in the Martos record. However, the high δD_{wax} values in the Martos record could be a result of high evaporation and lower effective moisture reaching the highest elevations of the tropical Andes as inferred by other Andean climate proxies (Seltzer et al, 2000).

On a more recent timescale, evidence disputing the antiphase relationship between northern and southern South America is provided by the Amazonian cores. Bird et al. (2011) interpret the Peruvian Pumacocha stalagmite record to show wetter conditions during the LIA as a result of a southward displacement of the ITCZ. However, the Amazonian cores exhibit lower δD_{wax} at this time implying increased precipitation when lower precipitation levels were expected. Such observations also led Polissar et al. (2006) to conclude that orbital forcing of the ITCZ cannot explain precipitation variability across South America alone as the anti-phase relationship between the two hemispheres of the continent would mean that opposite responses should consistently occur. This is supported through the increase in δD_{wax} in the Pantano de Martos record corresponding to increases in $\delta^{18}\text{O}$ in Cruz et al. (2009) stalagmite record from the Nordeste, Brazil. Therefore, it is wise to assume that although the migrations of the ITCZ would have influenced δD_{wax} to some extent, perhaps over glacial-interglacial scales; it cannot solely explain the trends of the record.

In the case of the Amazonian cores, ENSO events may account for some of the δD_{wax} variations. El Niño events disrupt atmospheric convection through the formation of anomalous Hadley cells (Reuter et al, 2009). The Hadley cells have descending atmospheric motion over northern South America which prevents deep convection and water-vapour advection into the area (Poveda et al, 2001). As a result, below normal precipitation levels are experienced over the northern parts of South America during El Niño episodes (Gareaud et al, 2009). Although the resolutions of the Amazonian records are not detailed enough to interpret δD_{wax} on the annual scale that is required for insights into ENSO related activity (Bouma et al, 1997), some insights can be made. A general trend to more positive δD_{wax} in the most recent samples of the Aguajal Agua Blanca record occurs at a time when there is evidence of strong El Niño occurrences in the late 20th and early 21st century (Bouma et al, 1997; Yoon and Zeng, 2010). As it is known that Colombia is sensitive to ENSO activity (Mantilla et al, 2009), it is probable that ENSO events may have influenced the δD_{wax} values of the core, especially in the youngest sections.

Chapter 6: Conclusions.

Changes in the hydrological cycle are predicted to occur alongside climatic changes. One of the most important regions thought to experience such changes is South America, in particular the Amazon Basin. Therefore, to understand possible future climatic changes, it is imperative to understand climatic changes of the past. The hydrogen isotopes of leaf-wax *n*-alkanes have become a popular tool in palaeohydrological reconstruction across the tropics, as the isotopic composition of *n*-alkanes has been found to successfully record the isotopic composition of precipitation. However, within northern South America climate records are scarce. To provide insight into northern South American palaeohydrological change, three sediment cores were obtained from Colombia – two from the Amazon Basin and one from the Páramo region of the Andes to the north-east of Bogotá.

6.1. Aguajal Agua Blanca and Aguajal del Loretillo

For both cores, *n*-alkanes spanned a large range (C₁₇-C₃₃), with the C₂₉ and C₃₁ *n*-alkanes being consistently the most abundant. *n*-alkane distribution parameters showed that the samples were of terrestrial origin (CPI ≥ 1) and predominantly reflected vegetation likely to be woody plants/trees (ACL = 28-30). Additionally, application of the P_{aq} proxy suggested that submerged/aquatic plants were not readily found at the site (P_{aq} ~ ≤ 0.3). Bulk isotope analysis further supported the findings of the distribution parameters suggesting a terrestrial source of vegetation. Average bulk δ¹³C values were -27.0‰ for Aguajal Agua Blanca and -28.7‰ for Aguajal del Loretillo, falling within the range for C₃ vegetation. Additionally, in the youngest sections of the records, TOC values were high at ~44% which were expected due to the organic rich environment of the palm swamp in which the cores were obtained.

However, degradation processes occurring within the Tipisca sites hindered the ability to produce long-term palaeohydrological records. This was shown through a reduction in TOC, TN and TOC/TN values at depth in both cores and increasing bulk δ¹³C suggestive of an algal input of organic matter. Additionally, at depth (~540 cal yr BP for Aguajal Agua Blanca and ~2400 cal yr BP for Aguajal del Loretillo) *n*-alkanes were not detectable, limiting isotopic analysis. However, some key findings were discovered. In Aguajal Agua Blanca, the lowest δD_{wax} values of the record were found during the LIA (-165‰), indicating increased rainfall, and supporting already published palaeohydrological data from Peru and Bolivia. Interestingly,

the MCA was also found to be a time of increased precipitation in Aguajal del Loretillo, correlating with paleoclimate archives found in southern South America. Both increases in precipitation coincided with a southward displacement of the ITCZ, which is typically known to cause decreased precipitation in northern South America. Finally, both records, showed a decrease in δD_{wax} values in the youngest sections of the core suggesting that rainfall in recent years has increased.

6.2. Pantano de Martos

In contrast to the Amazonian site, it is suspected that the lower temperatures of the Martos site enabled the higher preservation of organic matter. This allowed for all analyses to be carried out on the sub-samples within the core. Throughout the majority of the core, bulk isotope analyses, TOC, TN and *n*-alkane distribution data implied a strong terrestrial source of sediment (TOC = 59%; TOC/TN = ≥ 20 ; CPI ≥ 5 ; ACL = 25-28), composed of predominantly C₂₇, C₂₉ and C₃₁ *n*-alkanes. This was further supported by the bulk $\delta^{13}C$ values (-23.4‰ to -29.1‰). However, between 13-26,000 cal yr BP, the time corresponding to the LGM, a decrease in all values was found. During the LGM, TOC levels decline to 6%, suggesting that, as peat, by definition must have a carbon content of ~50%, the Martos site was not a peat bog. Lower CPI and ACL values also coincided with this finding, leading to the conclusion that during the LGM the environment changed from a peatland into an environment of mono-specific vegetation composed of the shorter chained *n*-alkanes. This was reinforced by an increase in P_{aq} during this time, suggesting an increase in the proportion of aquatic/algae species and also palynological data from the site. All analyses therefore suggested that as the proportion of aquatic species increased and parameters such as ACL decreased, the Martos site was wetter during the LGM.

Although subtle, a decrease in δD_{wax} of ~4‰ suggests that precipitation increased during the LGM at the Martos site, supporting the findings of the other results in this study. Additionally, Heinrich events appeared in the record as sustained wet events of ~500 years which have also been found in studies from Ecuador. Rainfall during the YD was also found to be slightly higher than HS1 (~4‰), supporting findings from the Cariaco Basin and the Peruvian Andes. Throughout the Holocene, δD_{wax} became progressively higher, suggesting that rainfall decreased substantially at the Martos site. The highest δD_{wax} occurred at ~4200 cal yr BP, supporting the low-latitude aridification suggested as the '4.2 event'. Finally, a large decrease in δD_{wax} was found in the Late Holocene, suggesting that conditions at the Martos site became

progressively wetter. However, the earliest 2000 cal yr BP of the record showed an increase in δD_{wax} of 9‰, therefore suggesting that rainfall over the Martos site decreased over the last 2000 years.

6.3. Overall Conclusions

For all three records, the source of *n*-alkanes within samples was concluded to reflect predominantly local vegetation. This was attributed to the locations of the sites limiting the possibility of large-scale *n*-alkane transport, and evidence from palynological records showing that C₄ vegetation was not present. For both locations, the tropical Atlantic Ocean is the primary source of moisture throughout the year. A comparison of the average δD_{wax} for each core show that δD_{wax} values for the Pantano de Martos core are ~30‰ lower than those at the Tipisca site. This therefore supports the findings of multiple studies which note the effects of factors such as altitude, temperature and moisture recycling on δD_{wax} . The suspected influences on δD_{wax} were taken into consideration when interpreting each record, and as a result enabled δD_{wax} to be a reliable proxy for precipitation. Palaeohydrological insights into the last ~50,000 years were shown through the Pantano de Martos core, whereas a much shorter record was obtained for the Amazonian cores. Even so, the cores provided information regarding events such as the LGM, YD, MCA and LIA as well as both Heinrich and D/O events.

Interpreting the causes of palaeohydrological change in the cores however was more difficult to understand. A southward shift of the ITCZ, in theory should cause rainfall to decrease at the Martos site, however the record shows that rainfall, although subtle increased during a southward displacement. Similarly, increased precipitation during the LIA in the Amazonian cores occurred during a southward displacement of the ITCZ. Consequently, the records suggest that ITCZ variation cannot solely explain δD_{wax} variations in northern South America. In the Amazonian cores, ENSO events may contribute to some of the δD_{wax} variation, however due to the resolution of the record, the extent of such effect is difficult to ascertain. Therefore, further research is needed to understand the causes of such change. Even so, all three records have provided novel insight into palaeohydrological change within Colombia, and suggest wetter conditions in times where decreased rainfall was expected.

Appendix A – Age-depth modelling.

1.1. Radiocarbon Dating Results

Radiocarbon dating is a geochronological method, typically used to date organic material younger than 50,000 years (Blauuw and Christen, 2011). The radiometric age of a sample is calculated assuming a time-independent atmospheric ^{14}C level in all past times (Stuiver and Polach, 1977). Conventional radiocarbon ages (years BP) are calculated in reference to the absolute international standard activity (AISA), which is accepted to be 95% of the activity in AD.1950 of the NBS oxalic acid, normalised to $\delta^{13}\text{C} = -19\text{‰}$ PDB (Olsson, 1970). As a result, any results obtained from this dating technique that are younger than AD.1950 are equal to 0yrs BP. Ages are also corrected to account for isotope fractionation, which is achieved by normalising to -25‰ for ^{13}C - the postulated mean value for terrestrial wood (Stuiver and Polach, 1977). After the corrections, an approximate mean radiocarbon age is obtained alongside a standard measuring error, typically described as $y \pm \sigma$ (Blauuw and Christen, 2011).

The conventional radiocarbon ages for all three cores in this study are displayed below. AMS analyses were performed at the KECK Carbon Cycle AMS Facility in the Earth Science department at the University of California. Prior to combustion, peat samples (Pantano de Martos core) were treated with acid-base-acid (1N HCl and 1N NaOH, 75°C). In the case of the Amazonian cores which were predominantly clay, samples were treated with acid-only (1N HCl at 75°C) prior to combustion. All results have been corrected for isotope fractionation and are presented as fractions of the modern standard $\delta^{14}\text{C}$, and conventional radiocarbon age according to the conventions of Stuiver and Polach (1977), with $\delta^{13}\text{C}$ values measured on prepared graphite using the AMS spectrometer. Sample preparation backgrounds have been subtracted, based on measurements of ^{14}C -free wood and coal. For additional information regarding the pre-treatment and methods of the dating technique see Santos et al (2007).

Samples labelled as “modern” contained an excess of ^{14}C , most likely due to the mid-20th century atmospheric thermonuclear weapons tests. As the assumption of an invariant atmospheric ^{14}C content is not valid, these ages were calibrated to calendar years (Blauuw and Christen, 2011; Reimer et al, 2013), as is typical in the application of this method (Klein et al, 1982; Hogg et al, 2013). Calibration was performed using the Calib 7.1 software (Stuiver et al,

2018) with the Intcal13 calibration dataset, which pertains to the last 50,000 years for the Northern Hemisphere (Reimer et al, 2013).

1.1.1. Aguajal Agua Blanca

Table A1 shows the radiocarbon dating results for Aguajal Agua Blanca. Initially, three samples were sent for radiocarbon dating in March 2018. In August 2018 another two samples were analysed. The organic content of the sediment declines towards the bottom of the core and this was reflected in the radiocarbon dating. The organic content in the deepest sample sent for dating (140cm) was so low that the sample required different treatment. The clay in the sample was acid treated, washed and then burned off to get an approximate radiocarbon age (see Santos et al, 2007). Problems arise when looking at the final two samples, taken from the bottom of the core. Sample 200551 is highlighted in red below as its radiocarbon age is significantly older than the date obtained for sample 207569 (~1000 years in difference). Overall, the ages obtained show the core spans ~1200 years.

Table A1. Radiocarbon ages and calibrated ages for Aguajal Agua Blanca. Calibration was conducted using Calib v.7.1 using the Intcal13 calibration curve. The radiocarbon date at 120cm is highlighted in red due to the age being ~1000 years older than the age below. As a result, it was decided to remove this date from the age-depth model.

| Sample | Depth (cm) | Radiocarbon age (14C year BP) | 1 σ Error (year) | Calibration Data | 95.4% (2 σ) Cal age ranges (cal year BP) | Relative area | Median probability (cal year BP) |
|--------|------------|-------------------------------|-------------------------|------------------|--|---------------|----------------------------------|
| 200549 | 34 | 115 | 15 | Intcal13 | 58-142 | 0.61 | 110 |
| 200550 | 64 | 325 | 15 | Intcal13 | 349-456 | 0.8 | 384 |
| 207568 | 98 | 480 | 15 | Intcal13 | 506-531 | 1 | 519 |
| 200551 | 120 | 2155 | 20 | Intcal13 | 2100-2162 | 0.56 | 2149 |
| 207569 | 140 | 1180 | 15 | Intcal13 | 1061-1174 | 1 | 1117 |

1.1.2. Aguajal del Loretillo

Table A2 shows the radiocarbon ages for the Aguajal del Loretillo core. In contrast to Aguajal Agua Blanca, Aguajal del Loretillo shows a consistent increase with age down core, without any conflicting ages in the deeper sections. Sample 200556 has a higher 1 sigma uncertainty than the rest of the samples which can be attributed to small sample size. Additionally, 207571 contained very little carbon. As a result, the sample was treated with acid only. Overall, the core is shown to span the last ~4000 years.

Table A2. Radiocarbon ages produced for the Aguajal del Loretillo core.

| Sample | Depth (cm) | Radiocarbon age (14C year BP) | 1 σ Error (year) | Calibration Data | 95.4% (2σ) Cal age ranges (cal year BP) | Relative area | Median probability (cal year BP) |
|---------------|-------------------|--------------------------------------|---|-------------------------|--|----------------------|---|
| 200555 | 98 | 555 | 20 | Intcal13 | 527-560 | 0.59 | 554 |
| 207570 | 130 | 1125 | 15 | Intcal13 | 979-1061 | 1 | 1019 |
| 200556 | 194 | 2225 | 30 | Intcal13 | 2153-2278 | 0.8 | 2228 |
| 207571 | 230 | 3135 | 15 | Intcal13 | 3339-3391 | 0.95 | 3367 |
| 200557 | 296 | 4145 | 20 | Intcal13 | 4581-4729 | 0.69 | 4689 |

1.1.3. Pantano de Martos

Table A3 shows the radiocarbon ages from the Andean core Pantano de Martos. Compared to the Amazonian cores, Pantano de Martos is substantially older. The lower-most date exceeds 50 ka in age. However, there are also some uncertainties regarding the dating of this core, which are highlighted in red in the table. The main outliers in the core are found in dates before 160cm. These produce an age reversal in the core, especially at sample 150cm, where there is a 10 ka difference in age between that sample and the one before at 144cm. The final four samples also indicate uncertainty, with samples 190cm, 240cm and 260cm fluctuating in age.

Table A3. The conventional radiocarbon ages associated with the age-depth model for the Pantano de Martos core. Highlighted in red are the suspected problematic ages that deviate from the trend shown by the rest of the radiocarbon ages.

| Sample | Depth (cm) | Radiocarbon age (^{14}C year BP) | 1 σ Error (year) | Calibration Data | 95.4% (2σ) Cal age ranges (cal year BP) | Relative area | Median probability (cal year BP) |
|--------|------------|--|-------------------------|------------------|--|---------------|----------------------------------|
| 200558 | 40 | 2575 | 20 | Intcal13 | 2717-2751 | 1 | 2738 |
| 207572 | 62 | 4940 | 20 | Intcal13 | 5607-5715 | 1 | 5654 |
| 200559 | 90 | 9095 | 45 | Intcal13 | 10189-10301 | 0.89 | 10244 |
| 207573 | 110 | 13475 | 30 | Intcal13 | 16048-16378 | 1 | 16216 |
| 207574 | 124 | 16235 | 35 | Intcal13 | 19456-19777 | 1 | 19597 |
| 200560 | 140 | 14090 | 50 | Intcal13 | 16932-17387 | 1 | 17136 |
| 207575 | 144 | 23930 | 210 | Intcal13 | 27647-28464 | 1 | 28002 |
| 207576 | 150 | 13620 | 30 | Intcal13 | 16237-16610 | 1 | 16409 |
| 207577 | 158 | 21350 | 80 | Intcal13 | 25497-25877 | 1 | 25694 |
| 207578 | 164 | 29420 | 170 | Intcal13 | 25497-25877 | 1 | 25694 |
| 207579 | 178 | 34680 | 320 | Intcal13 | 38528-39919 | 1 | 39193 |
| 200561 | 180 | 37860 | 660 | Intcal13 | 41120-43042 | 1 | 42119 |
| 207580 | 190 | 35290 | 350 | Intcal13 | 38984-40694 | 1 | 39857 |
| 207581 | 240 | 40780 | 680 | Intcal13 | 43118-45450 | 1 | 44297 |
| 200562 | 260 | 37630 | 640 | Intcal13 | 40926-42866 | 1 | 41961 |
| 200563 | 364 | >52800 | - | Intcal13 | - | - | - |

1.2. Age-Depth Modelling

Obtaining the age of sediment (and associated proxy data) throughout a core is vital and requires the establishment of a reliable relationship between sample depth and age. Typically, for sediments containing organic matter, and with ages younger than c.50,000 years, radiocarbon dating is used to create such an age-depth model (Blaauw and Christen, 2005; Blaauw and Christen, 2011; Piotrowska et al, 2011). These are usually subsampled with depth along a sediment core, and assuming that there is a monotonic relationship between depth and time (age should always increase with depth), a curve can be fitted to the data and the age of the dated and the non-dated samples inferred (Blaauw and Christen, 2005). Uncertainties in the ^{14}C dates are dealt with in many ways both prior to and during analysis. For example, examining the stratigraphy of the core before radiocarbon dating allows for the identification of mixed or reversed sediments and, as a result, enables such cores to be ruled out from further analysis (Blaauw and Christen, 2011).

In this study, age-depth models for all three cores were created using Bacon (Blaauw and Christen, 2011), which is ran through the R programming environment. Age-depth modelling in the Bacon software uses Bayesian statistics which fundamentally assumes that sediments accumulate in a chronological order and that deeper sediments should be older than samples higher up in the core (i.e. “prior” information). Unlike other methods used in age-depth modelling, which produce age estimates by fitting a curve based only on the dated points (Blaauw, 2010), Bacon produces much more environmentally realistic ages by taking into consideration the underlying processes that affect the age of a core.

Before creating an age-depth model, it is possible to add in prior knowledge (“priors”) for sections of the model where the behaviour of the model may be uncertain. This could be due to factors such as limited data or age reversals (Crann et al, 2015). This allows the model to treat this section of the core as a separate entity to the rest. To calibrate the ^{14}C ages and reduce the need for detecting and removing outliers within the radiocarbon dates the software also uses Student-t model distributions with wide tails (Christen and Perez, 2009). The wide tails of this model allow a more cautious approach to dating and ensure that all information provided by possible extreme values is properly included. This leads to a wider, smoother distribution of ages, and makes the model less prone to mistaken ages and observations (Christen and Perez, 2009). Using the student-t distributions is also a much more reliable way of interpreting age models when they contain outliers. Outliers may also be removed using this approach, however increased precision is not guaranteed.

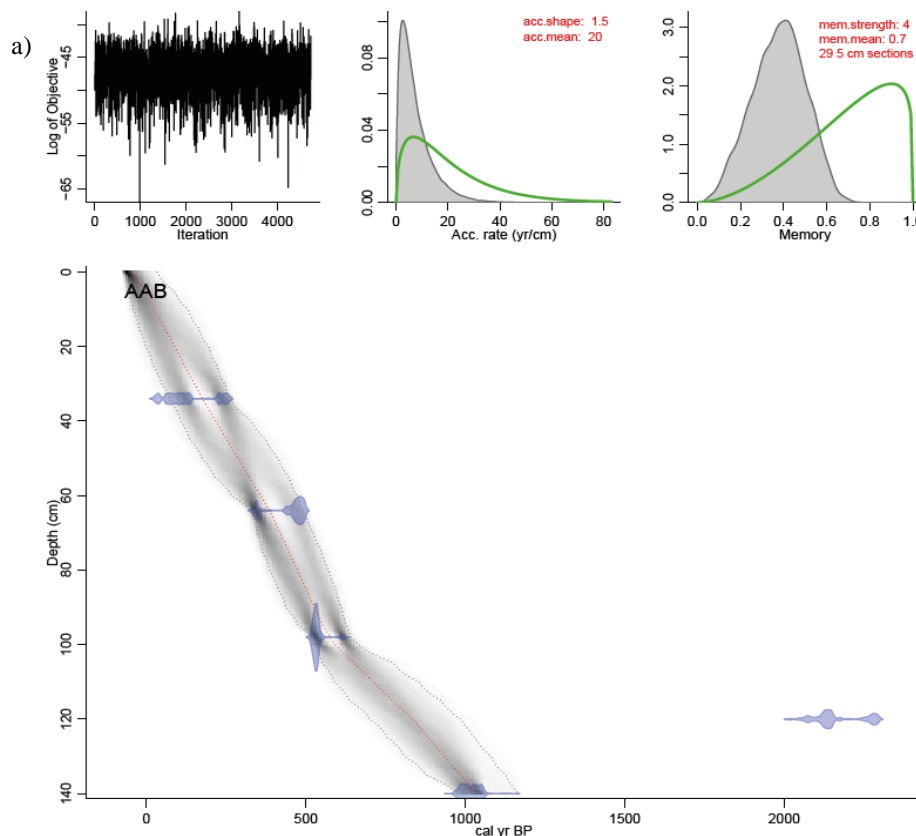
The two graphs produced alongside the age-depth model represent the accumulation rate prior (figures A1-3, left panel) and the memory (figure A1-3, right panel). The accumulation rate prior is similar to a normal/Gaussian distribution and has two parameters; acc.shape and acc.mean. The default for acc.mean is typically 20 yr/cm. However, if the age estimates indicate an accumulation rate that is substantially different to the default value, this will automatically be changed before the model runs. For all cores, the acc.shape value was kept as the default. It is also important to note that the values for the accumulation rate are always positive due to the safe assumption that deposits did not accumulate backwards in time. The memory defines the extent to which the accumulation rate in a particular part of the core is dependent on the accumulation rate of the depth above it. Memory values range from 0 (no assumed memory) to 1 (100% memory). In the case of the Martos core (fig. A3), both mem.strength and mem.mean were kept as the default values as they allow for a wider range of memory values to be generated during the model run. Also depicted on the memory graph

are the thickness and section settings of the model. The software defines the section thickness as 5cm and was used to model the cores. This is due to multiple thin sections creating a smoother model and reducing the likelihood of abrupt changes in accumulation rate (Blauuw and Christen, 2011).

1.3. Amazonian Cores

1.3.1. Aguajal Agua Blanca

Figures A1a and A1b show the age depth model produced for Aguajal Agua Blanca. It was decided to remove the suspected outlier seen in figure A1a at 207569 (~2000 cal yr BP) as it was assumed that the date would skew the age information produced from the software. Looking at figures A1a and A1b it can be seen that removing the date does not change the estimated age range of the model. Using all radiocarbon dates, the hypothesised basal age of the core lies at ~1200 cal yr BP, with the same age estimate also being found when the radiocarbon date at 120cm is removed from the model. Removing this sample however, did result in all dates lying within the 95% probability range of the model. Sediment accumulation is also shown in the model and is estimated to be ~5cm yr⁻¹.



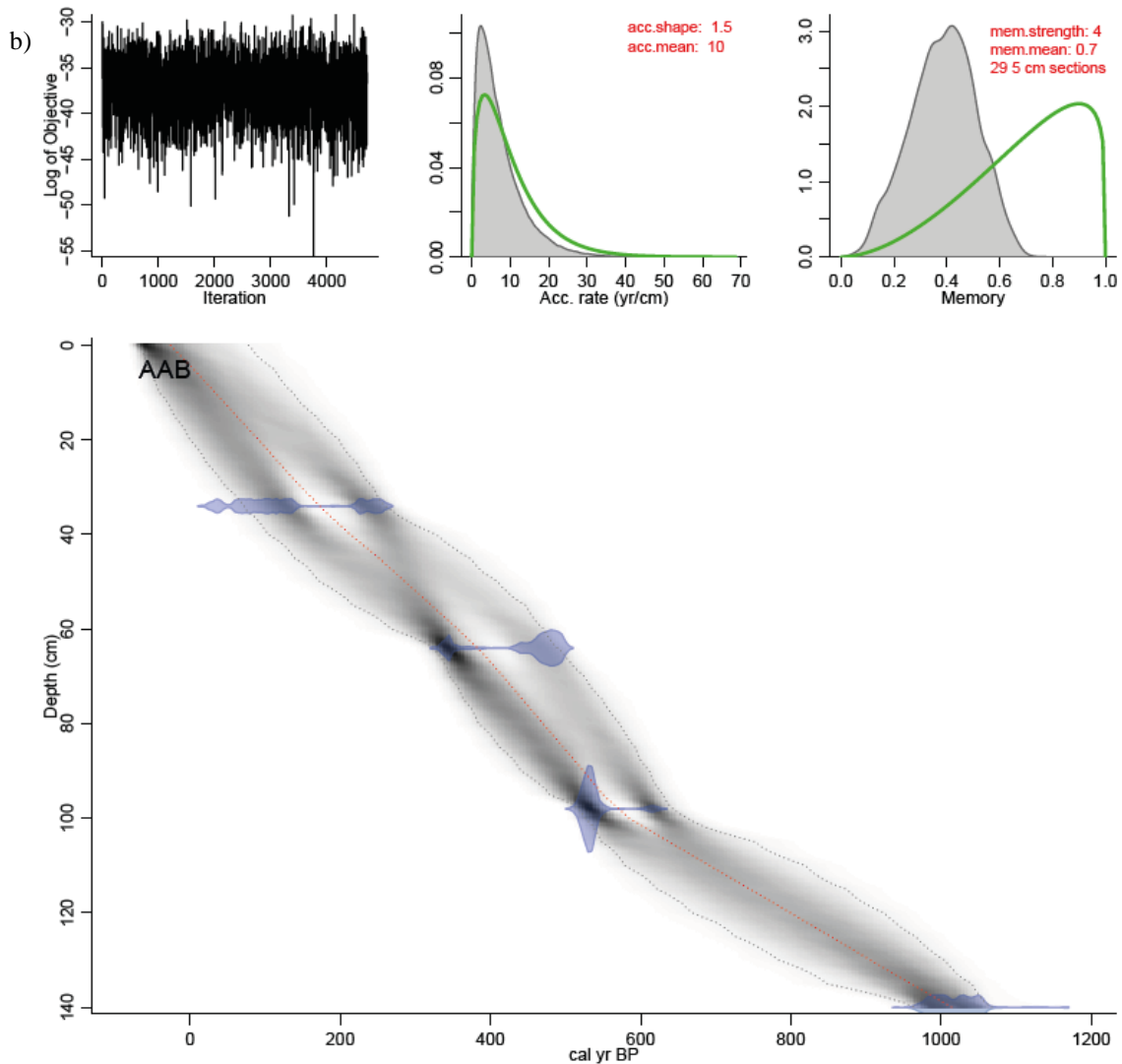


Figure A1a & A1b. Bacon-derived age depth model for Aguajal Agua Blanca using; a) all the radiocarbon data and b) selected radiocarbon dates (removed suspected outlier).

1.3.2. Aguajal del Loretillo

Figure A2 shows the age-depth model for Aguajal del Loretillo. Unlike Aguajal Agua Blanca, which contained suspect dates lying outside Bacon’s 95% confidence range, all dates obtained for Aguajal del Loretillo lie within the range and there is a linear relationship between depth and age. The basal age of the core is ~5200 cal yr BP. As the first radiocarbon date was situated at 98cm, an estimated age of the upper metre of the core was obtained by extrapolating the age of the core in Excel. Using the same formulas used in the age depth model shows that approximately the first 50cm of the core is younger than 1950 and therefore ‘modern’. Sediment accumulation in the core is estimated to be 20 cm yr⁻¹.

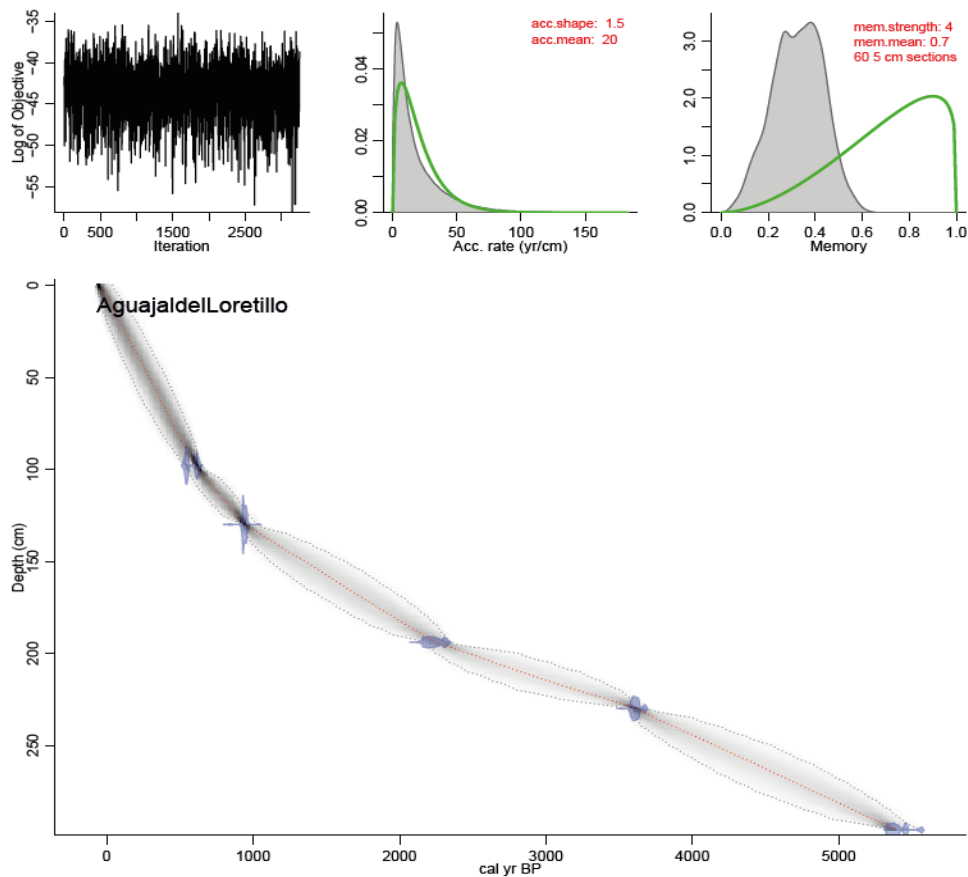
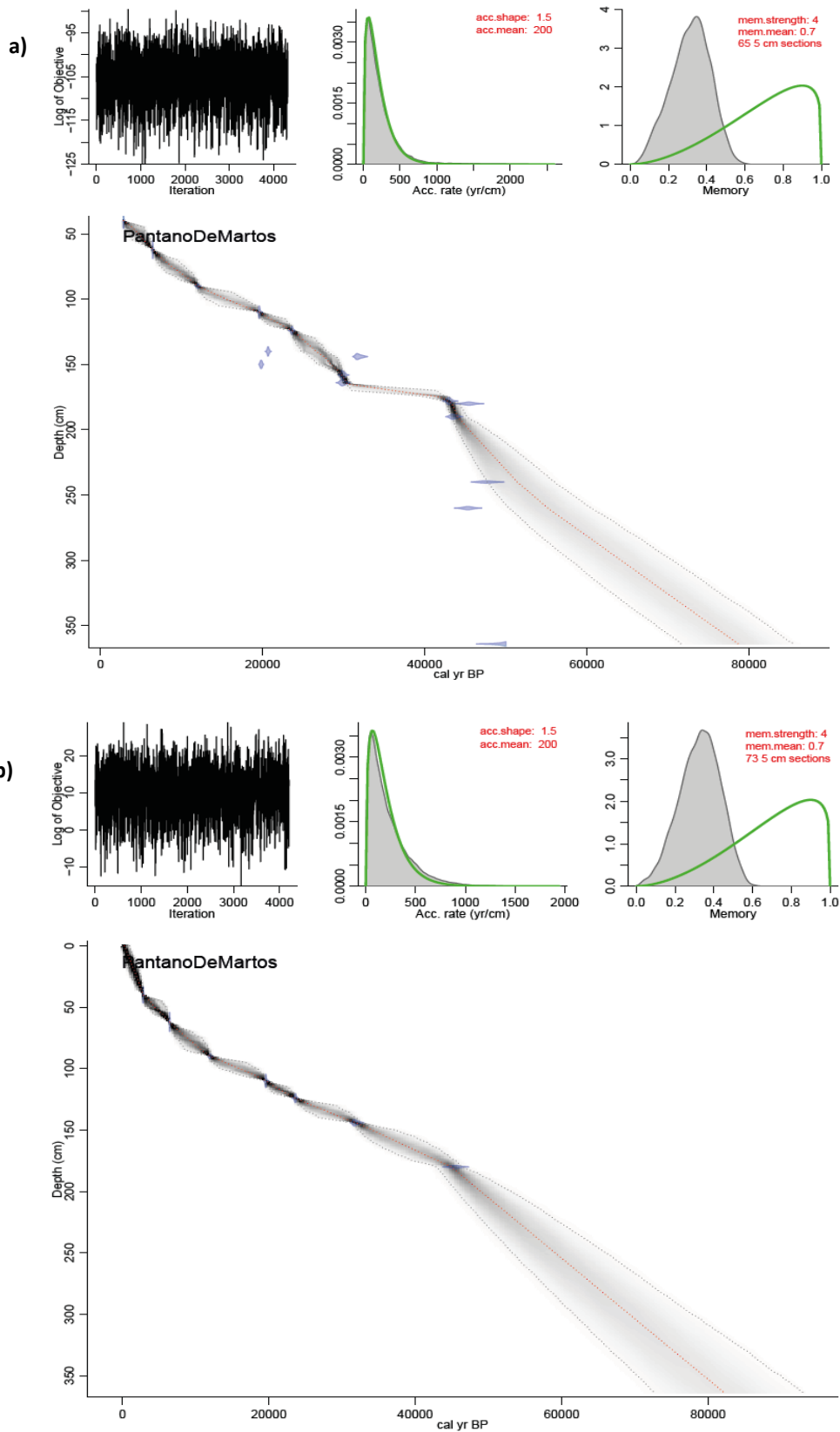


Figure A2. Bacon-derived age-depth model for Aguajal del Loretillo using all the conventional radiocarbon ages obtained.

1.4. Andean Core – Pantano de Martos

Figures A3a and A3b show the age-depth models for the Pantano de Martos. Using all dates, it can be seen that there are multiple outliers (circled in black in figure A3a). After approximately 200cm, the radiocarbon dates systematically deviate from the accumulation rate trend in the first two metres of the core. The lowest radiocarbon sample (200563) deviates significantly from this trend and lies outside the modelled age range of the core, as calculated by the Bacon software. Additionally, only 53% of the conventional radiocarbon ages lie within the 95% probability range generated alongside the running of the Bacon model. Removing the suspected outliers produces an age-depth model that is much more linear (i.e. the accumulation rate is less invariant). Here, the estimated (extrapolated) age of the bottom of the core ranges between ~75-100,000 years (mean age 85000 cal yr BP), whereas with all radiocarbon dates the age of the core had a maximum estimated age of 85,000 cal yr BP.



Figures A3a and A3b. Bacon-derived age-depth model using a) all conventional radiocarbon ages and b) selected radiocarbon ages where the outliers have been removed for the Pantano de Martos core.

1.5. Outliers

As noted by Blaauw et al (2005), the presence of outliers is a constant factor in the analysis of ^{14}C data. Even though outliers were present in the Amazonian cores, due to the fact that largely they were found outside the confidence range of the model, they did not influence the overall estimated age of the core. In contrast to this, the Martos core shows a substantial difference in age when all dates are included in the model where suspected outliers have been removed.

Several studies encountered this issue and have removed specific radiocarbon dates on the assumption that they are outliers. Some of the most common causes of ‘noise’ in an age-depth the model arise from factors such as disturbance in the record and contamination during sample collection (Parnell et al, 2008). Problems during sample collection may explain the suspected outliers for samples 13620 and 207577 in the Pantano de Martos core. The Pantano de Martos core was sampled in 50 cm increments, therefore the sample at 150 cm represents the end of one subsection and the start of another. The sample being ~10,000 years younger than the sample above it can be explained by a contamination with younger material from the surrounding area during sample collection. It is also possible to explain the sample at 158cm through this conclusion also, due to its close proximity to the transition.

Typically, in the Bacon software, efforts are made to counteract the problem of mixing and backwards dating in peat sediment. This is extremely useful in high resolution dating, where many core slices are dated, but also in studies where the core is not too long (usually up to 2 m). However, for longer cores the method can become too restrictive (Blaauw and Christen, 2005). This can be seen in the Martos record where there are multiple reversals. Additionally, it would seem that even though multiple samples were dated, due to its length, the dates did not create a high enough resolution to counteract the effects of some of the outliers. As a result, it was decided to remove the suspected dates following Blaauw and Christen (2011), who state that in cases where younger ages are found further down in the core, it is wise to exclude these samples from the analysis. This selective removal of dates based on the lack of resolution follows Crann et al’s (2015) study on sediment accumulation from lakes in the Northwest Territories of Canada. Suspected outliers were removed on an ad hoc basis in parts of the core where dating resolution was low (less than one radiocarbon date per one thousand years). In this study, the dates removed were ones that created either an age reversal or a shift in the accumulation rate that was unexplained by sedimentological evidence.

Previous studies have also noted that because the chronologies of the model are developed by the overall information and statistics provided by the software data, some of the age estimates that do not fall into the probability range can immediately be seen as outliers and can be ruled out of the study (Parnell et al, 2008). An example is shown in figure A4. This justification was applied in the Amazonian core Aguajal Agua Blanca. Although removing these dates did not greatly affect the estimated age of the core, it helped to minimise the age range associated with the core.

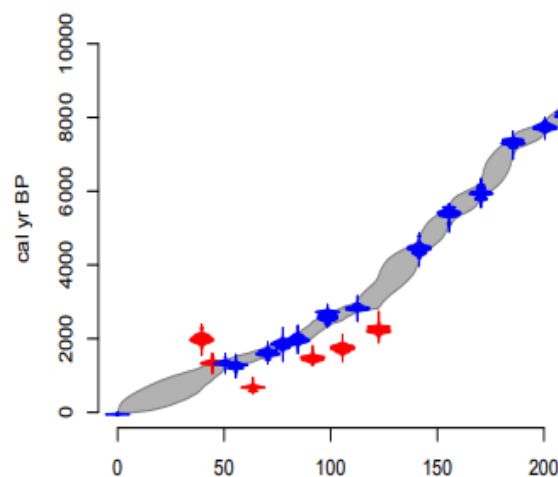


Figure A4. Age-depth model from Parnell et al’s (2008) study on Northern European Holocene pollen records (from Blaauw and Christen, 2011). In this example, the dates shown in red were classed as outliers and were rejected from the study.

Overall, contamination when sampling is the most probable explanation in the suspected outliers in the Martos core. With this in mind, it is wise to treat sample 200563 with caution. Additionally, samples with low amounts of ^{14}C remaining are most prone to contamination, therefore the ages obtained in the Martos core after 2 m were removed from the age-depth model. Although all samples are pre-treated during radiocarbon dating, usually by treating the sample with alkaline solution (acid-base-acid (ABA) pre-treatment) (Turney et al, 2001), the reliability of this pre-treatment in removing all contaminants in older sediment is questionable. As a result, this has led to studies concluding that the pre-treatments alone are insufficient in removing the secondary contamination in older sediment (Bird et al, 1999; Gillespie, 1997; Hatte et al, 2001), with some laboratories even concluding that quoting ^{14}C ages over 40,000 years BP are ‘infinite’ or, in other words, indistinguishable from procedural error (Bird et al, 1999). This therefore supports the decision to remove these dates from the age-depth model.

Briant and Bateman (2009) tested the extent to which modern contamination affected their ^{14}C age-depth models in a study of luminescence dated Devensian fluvial sediments in lowland Britain. A 0.5% contamination of modern carbon in a sample with an age of 20 ka led to a negligible age underestimation. However, the same contamination in samples aged 30 and 40 ka produced age underestimations in excess of 2 to 7 ka respectively. When increasing the contamination to 2%, the underestimation of the sample age increased again to 10 ka. At even older ages of between 40 and 60 ka, a 2% contamination yields ^{14}C ages that are near identical to those found at 30 ka. These examples show, that although ages for deeper parts of the core can be obtained, they must be treated with caution. This probably explains some of the age reversals found towards the end of the core, and reinforces the idea that although the final sample of the core is dated >52 ka BP, the actual age of the sediment could be much greater.

Appendix B – Supplementary Pollen Data

Table B1. Pollen groups (%) for the Tipisca core Aguajal Agua Blanca. Source: Berrio, unpublished data.

| Depth (cm) | Palm (%) | Trees, Shrubs and Epiphytes (%) | Herbs (%) | Unknown % | Spores (%) | Total (%) |
|------------|----------|---------------------------------|-----------|-----------|------------|-----------|
| 0 | 85.3 | 12.7 | 1.7 | 0 | 7.1 | 100 |
| 6 | 86.3 | 12 | 1.3 | 0 | 7.4 | 100 |
| 8 | 91 | 9.3 | 0 | 0 | 10 | 100 |
| 10 | 92.7 | 7 | 0.3 | 0 | 9.9 | 100 |
| 12 | 94.5 | 5.5 | 0 | 0 | 8.1 | 100 |
| 14 | 91.7 | 7.7 | 0.3 | 0 | 8.4 | 100 |
| 16 | 85.7 | 13 | 0.3 | 1 | 13 | 100 |
| 18 | 87.7 | 11.3 | 0 | 1 | 6.4 | 100 |
| 20 | 90.4 | 7.6 | 1.3 | 0.7 | 11.9 | 100 |
| 22 | 90.4 | 6.3 | 0.7 | 2.7 | 15.8 | 100 |
| 24 | 83.9 | 13.8 | 1.6 | 0.7 | 12.9 | 100 |
| 26 | 88.9 | 9.5 | 1.6 | 0.3 | 15.7 | 100 |
| 28 | 84.1 | 15.3 | 0 | 0.6 | 15.9 | 100 |
| 30 | 82.8 | 15.6 | 0.3 | 1.3 | 14.9 | 100 |
| 32 | 79.7 | 19 | 0.7 | 0.3 | 16.2 | 100 |
| 34 | 83.7 | 15 | 1 | 0.3 | 17.3 | 100 |
| 36 | 77.7 | 20.6 | 0.7 | 1 | 11.9 | 100 |
| 38 | 84.7 | 15 | 0.3 | 0.3 | 12.2 | 100 |
| 40 | 79.9 | 18.2 | 0.7 | 1.3 | 15.5 | 100 |
| 42 | 76.7 | 21 | 2.3 | 0.3 | 15.2 | 100 |
| 44 | 88.1 | 10 | 0.3 | 1.6 | 12.9 | 100 |
| 46 | 82.2 | 17.2 | 0.7 | 0.3 | 16.2 | 100 |
| 50 | 72.1 | 25.7 | 0.7 | 1.6 | 14.9 | 100 |
| 52 | 48.8 | 48.8 | 0 | 2.3 | 13 | 100 |
| 54 | 59.2 | 40.1 | 0.7 | 0 | 15.2 | 100 |
| 56 | 55.1 | 42.4 | 0.3 | 2.2 | 15.8 | 100 |
| 58 | 56.3 | 43 | 0.3 | 0.7 | 11.3 | 100 |
| 60 | 61.2 | 38.2 | 0.3 | 0.3 | 14.3 | 100 |
| 62 | 73.8 | 26.3 | 0 | 0.3 | 11.3 | 100 |
| 64 | 64.4 | 34.7 | 1 | 0 | 14.6 | 100 |
| 66 | 72.4 | 27.1 | 0.9 | 0 | 13 | 100 |
| 68 | 66.7 | 32.1 | 0.3 | 0.7 | 14.4 | 100 |
| 70 | 78.3 | 21.1 | 0.3 | 0.3 | 16.5 | 100 |
| 72 | 76.7 | 22.6 | 0.6 | 0 | 12.5 | 100 |
| 74 | 85.5 | 13.6 | 0.6 | 0 | 14.1 | 100 |
| 76 | 87.5 | 11.9 | 0.9 | 0 | 14 | 100 |
| 78 | 85.4 | 13 | 1.3 | 0 | 14.1 | 100 |
| 80 | 85.9 | 13.4 | 0.6 | 0 | 11.1 | 100 |
| 82 | 81.8 | 17.3 | 0.6 | 0 | 11.5 | 100 |

Table B1 continued... the pollen groups (%) for Aguajal Agua Blanca.

| | | | | | | |
|-----|------|------|------|------|------|-----|
| 84 | 74.8 | 22.7 | 2.6 | 0 | 14.8 | 100 |
| 86 | 75.4 | 20.9 | 4 | 0 | 15.6 | 100 |
| 88 | 71.9 | 24.8 | 2.9 | 0 | 13.8 | 100 |
| 90 | 78 | 18 | 4 | 0 | 17.1 | 100 |
| 92 | 76.3 | 19.7 | 4.3 | 0 | 8.5 | 100 |
| 94 | 80.3 | 16.7 | 3 | 0 | 16.2 | 100 |
| 96 | 69 | 20.8 | 10.6 | 0 | 19.6 | 100 |
| 98 | 78.3 | 19.3 | 1 | 1.3 | 19.3 | 100 |
| 100 | 82.9 | 16.1 | 0 | 1 | 15.9 | 100 |
| 102 | 69.3 | 21.5 | 1 | 8.6 | 18.1 | 100 |
| 104 | 67.4 | 29.4 | 3 | 0 | 14 | 100 |
| 106 | 54.4 | 44.4 | 1.1 | 0 | 35.7 | 100 |
| 108 | 31.4 | 40.7 | 28.1 | 0 | 22.4 | 100 |
| 110 | 18.3 | 32.5 | 49.2 | 0 | 1.6 | 100 |
| 112 | 29 | 44.7 | 26.3 | 0 | 5 | 100 |
| 114 | 56.3 | 37.5 | 6.3 | 0 | 42.9 | 100 |
| 116 | 50 | 33.3 | 16.7 | 0 | 25 | 100 |
| 118 | 52.4 | 38.1 | 4.8 | 4.8 | 68.7 | 100 |
| 120 | 42.9 | 42.9 | 14.3 | 0 | 84.8 | 100 |
| 122 | 33.3 | 66.7 | 0 | 0 | 92.3 | 100 |
| 124 | 55.6 | 11.1 | 0 | 33.3 | 60.9 | 100 |
| 126 | 0 | 0 | 0 | 0 | 100 | 0 |
| 128 | 75 | 25 | 0 | 0 | 0 | 100 |
| 130 | 0 | 0 | 0 | 0 | 100 | 0 |
| 132 | 0 | 0 | 0 | 0 | 0 | 0 |
| 134 | 0 | 0 | 0 | 0 | 0 | 0 |
| 136 | 0 | 0 | 0 | 0 | 0 | 0 |
| 138 | 0 | 0 | 0 | 0 | 0 | 0 |
| 140 | 0 | 0 | 0 | 0 | 0 | 0 |
| 142 | 0 | 0 | 0 | 0 | 0 | 0 |
| 144 | 0 | 0 | 0 | 0 | 0 | 0 |
| 146 | 0 | 0 | 0 | 0 | 0 | 0 |
| 148 | 0 | 0 | 0 | 0 | 0 | 0 |
| 150 | 0 | 0 | 0 | 0 | 0 | 0 |

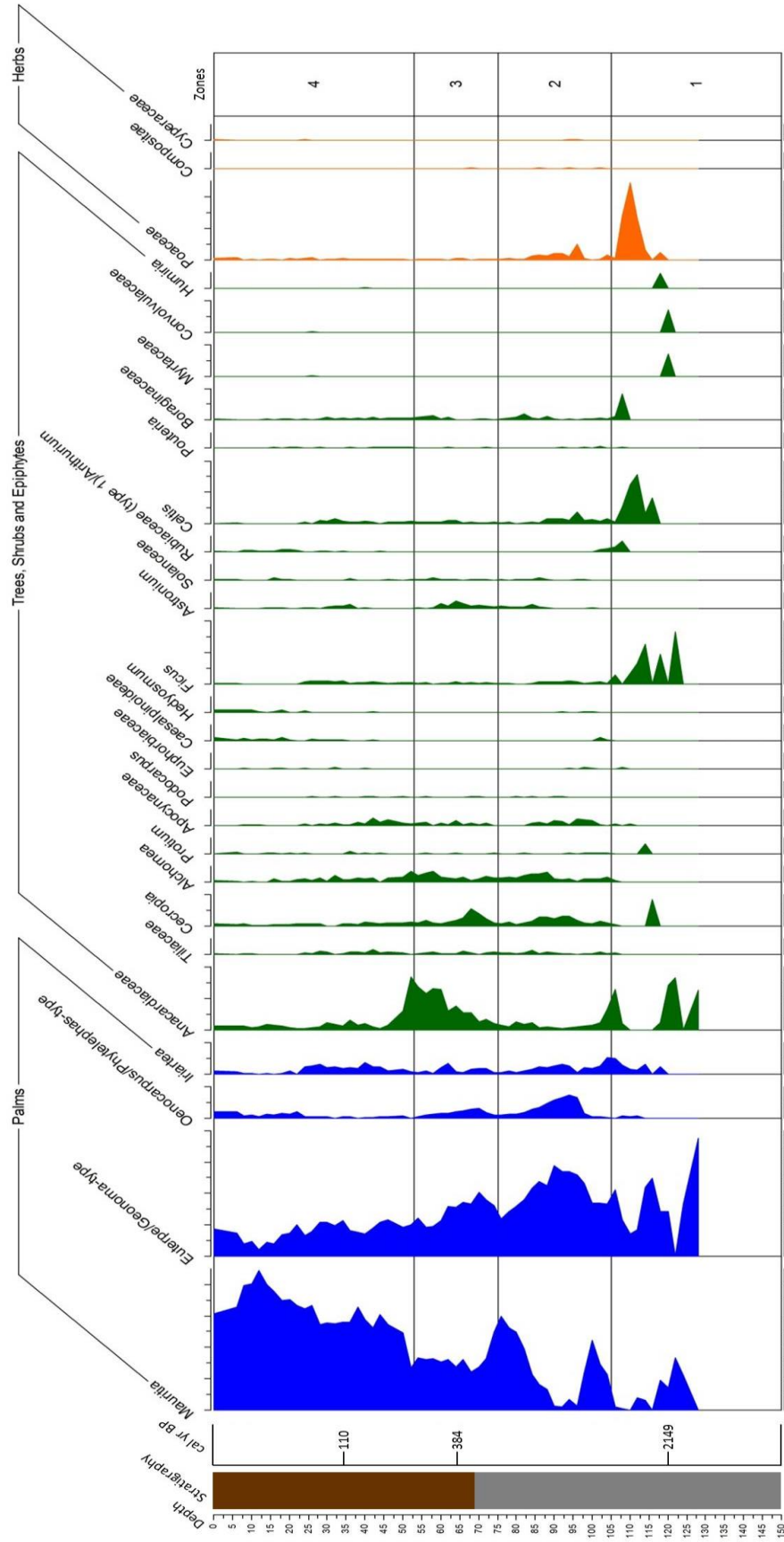


Figure B1. Percentage pollen diagram for Aguajal Agua Blanca displaying 28 of the most frequent taxa identified from the Aguajal Agua Blanca core. Source: Berrio, unpublished data.

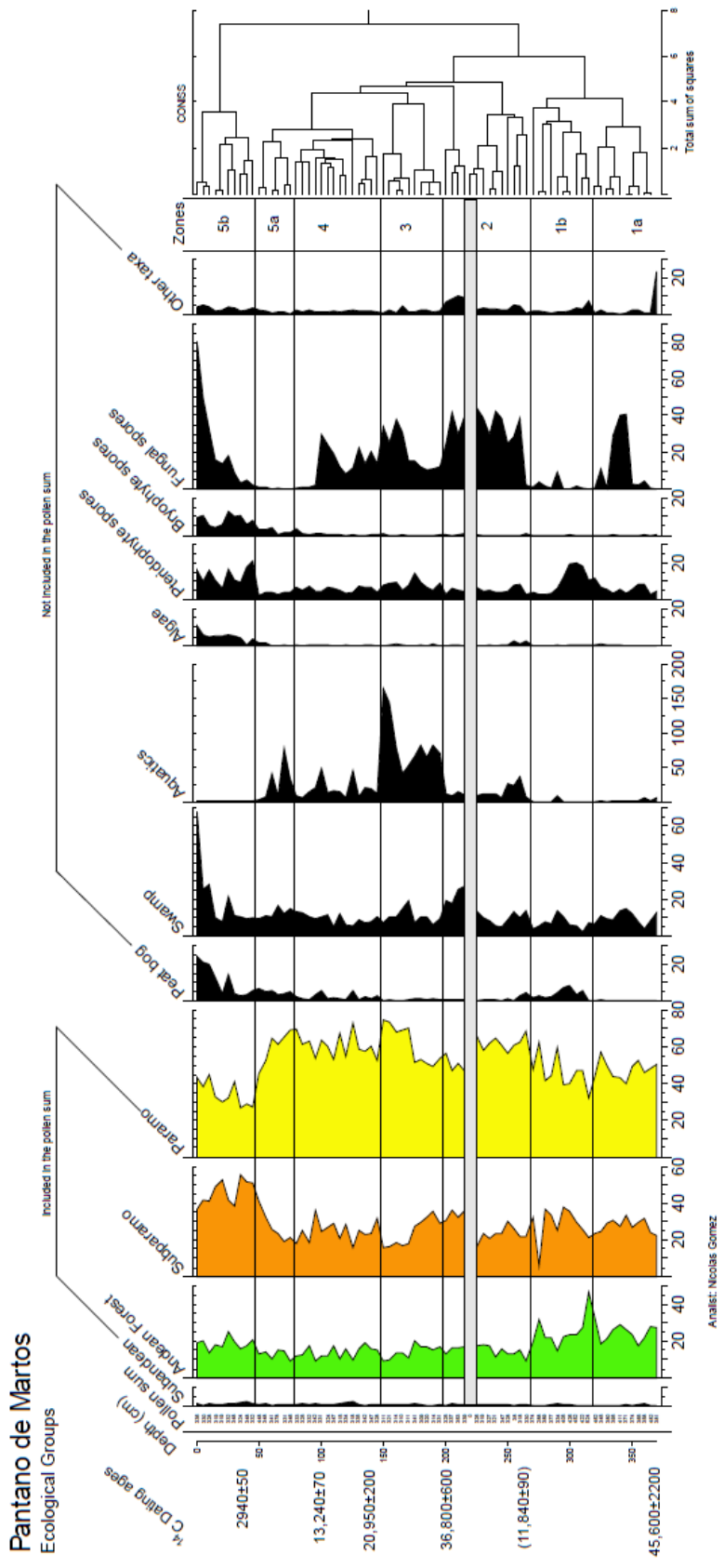


Figure B2. The ecological groups obtained from pollen data for the Pantano de Martos core. Source: Berrío, unpublished data.

References

- Abbot, M.B., Wolfe, B.B., Aravena, R., Wolfe, A.P. and Seltzer, G.O. (2000). Holocene hydrological reconstructions from stable isotopes and paleolimnology, Cordillera Real, Bolivia. *Quaternary Science Reviews*. 19. Pp. 1801 – 1820.
- Aggarwal, P.K., Alduchov, O.A., Froehlich, K.O., Araguas-Araguas, L.J., Sturchio, N.C. and Kurita, N. (2012). Stable isotopes in global precipitation: A unified interpretation based on atmospheric moisture residence time. *Geophysical Research Letters*. 39. Pp. 1-6.
- Aichner, B., Herzsuh, U., Wilkes, H., Vieth, A. and Bohner J. (2010). δD values of n-alkanes in Tibetan lake sediments and aquatic macrophytes – A surface sediment study and application to a 16 ka record from Lake Koucha. *Organic Geochemistry*. 41. Pp. 779–790.
- Alley, R.B. (2000). The Younger Dryas cold interval as viewed from central Greenland. *Quaternary Science Reviews*. 19. Pp. 213–226.
- Alley, R.B., Mayewski, P.A., Sowers, T., Stuiver, M., Taylor, K.C. and Clark, P.U. (1997). Holocene climatic instability: A prominent, widespread event 8200 yr ago. *Geology*. 25. Pp. 483–486.
- Andersson, R.A., Meyers, P., Hornibrook, E., Kuhry, P. and Morth, C-M. (2012). Elemental and isotopic carbon and nitrogen records of organic matter accumulation in a Holocene permafrost peat sequence in the East European Russian Arctic. *Journal of Quaternary Science*. 27(6). Pp. 545-552.
- Anstey, M.H.R. (2013). Climate change and health—what’s the problem?. *Globalisation and Health*. 9(4). Pp. 1-5.
- Apasegui, J., Cruz, F.W., Vuille, M., Fohlmeister, J., Espinoza, J.C., Sifeddine, A. et al. (2018). Precipitation changes over the eastern Bolivian Andes inferred from speleothem ($\delta^{18}O$) records for the last 1400 years. *Earth and Planetary Science Letters*. 494. Pp. 124-134.
- Appenzeller, C., Stocker, T.F. and Anklin, M. (1998). North Atlantic Oscillation Dynamics Recorded in Greenland Ice Cores. *Science*. 282(5388). Pp. 446-449.
- Araguas-Araguas, L., Froehlich, K. and Rozanski, K. (2000). Deuterium and oxygen-18 isotope composition of precipitation and atmospheric moisture. *Hydrological Processes*. 14. Pp. 1341–1355.

- Arbuszewski, J.A., deMenocal, P.B., Cleroux, C., Bradtmiller, L. and Mix, A. (2013). Meridional shifts of the Atlantic Intertropical Convergence Zone since the Last Glacial Maximum. *Nature Geoscience*. 6. Pp. 959-962.
- Arens, N. and Jahren, H. (2000). Carbon isotope excursion in the atmospheric CO₂ at the Cretaceous-Tertiary boundary: evidence from terrestrial sediments. *Palaios*, 15. Pp. 314-322.
- Arguez, A. (2007). State of the climate in 2006. *Bulletin of the American Meteorological Society*. 88(6). s1es135.
- Arking, A. (1991). The Radiative Effects of Clouds and their Impact on Climate. *Bulletin of American Meteorological Society*. 71. Pp. 795-813.
- Armstrong, H.A., Baldini, J., Challands, T.J., Grocke, D.R. and Owen, A.W. (2009). Response of the Inter-tropical Convergence Zone to Southern Hemisphere cooling during Upper Ordovician glaciation. *Palaeogeography, Palaeoclimatology, Palaeoecology*. 284. Pp. 227–236.
- Asada, T., Warner, B.G. and Aravena, R. (2005a). Nitrogen isotope signature variability in plant species from open peatland. *Aquatic Botany*. 82. Pp. 297-307.
- Avella, A.M., Torres, S.R., Gomez, W.A. and Pardo, M.P. (2014). Ecological characterization and conservation status of the páramos (moors) and high Andean forests of the Monquentiva and Martos wetlands (Guatavita, Cundinamarca). *Biota Colombiana*. 15 (1). Pp. 3-39.
- Baker, P.A., Seltzer, G.O., Fritz, S.C. et al. (2001). The History of South American Tropical Precipitation for the Past 25,000 Years. *Science*. 291. Pp. 640-643.
- Balascio, N.L., D’Andrea, W.J., Gjerde, M. and Bakke, J. (2018). Hydroclimate variability in the High Arctic Svalbard during the Holocene inferred from hydrogen isotopes of leaf waxes. *Quaternary Science Reviews*. 183. Pp. 177-187.
- Balslev, H., Copete, J-C., Pedersen, D., Bernal, P., Galeano, G., Duque, A., Berrio, J-C. and Sanchez, M. (2017). Palm Diversity and Abundance in the Colombian Amazon. In: Myster, R.W. *Forest structure, function, and dynamics in Western Amazonia*. Chichester, West Sussex: John Wiley & Sons. pp. 101-125.
- Barber, K.E. (1981). *Peat Stratigraphy and Climate Change: A Palaeoecological Test of the Theory of Cyclic Peat Bog Regeneration*. Balkema, Rotterdam.

- Barnola, J.M., Raynaud, D., Korotkevich, Y.S. and Lorius, C. (1987). Vostok ice core provides 160,000-year record of atmospheric CO₂. *Nature*. 329. Pp. 408-413.
- Basilier, K. (1980). Fixation and uptake of nitrogen in Sphagnum blue-green algal associations. *Oikos*. 34. Pp. 239–242.
- Bechtel, A., Sachsenhofer, R., Markic, M., Gratzner, R., Lucke, A. and Puttmann, W. (2003). Paleoenvironmental implications from biomarker and stable isotope investigations on the Pliocene Velenje lignite seam (Slovenia). *Organic Geochemistry*. 34. pp. 1277-1298.
- Beerling, D. and Royer, D. (2002). Fossil plants as indicators of the Phanerozoic global carbon cycle. *Annual Review of Earth and Planetary Sciences*. 30. pp. 527- 556.
- Behling, H. (2002). South and Southeast Brazilian grasslands during Late Quaternary times: a synthesis. *Palaeogeography, Palaeoclimatology, Palaeoecology*. 177. Pp. 19–27.
- Behling, H., Berrío, J.C. and Hooghiemstra, H. (1999). Late Quaternary pollen records from the middle Caqueta river basin in central Colombian Amazon. *Palaeogeography, Palaeoclimatology, Palaeoecology*. 145. Pp. 193 – 213.
- Belyea, L.W. and Clymo, R.S. (2001) Feedback control of the rate of peat formation. *Proceedings of the Royal Society B*. 268. Pp. 1315-1321.
- Bendle, J., Kawamura, K., Yamazaki, K. and Niwai, T. (2007). Latitudinal distribution of terrestrial lipid biomarkers and n-alkane compound-specific stable carbon isotope ratios in the atmosphere over the western Pacific and Southern Ocean. *Geochimica et Cosmochimica Acta*. 71. Pp. 5934-5955.
- Beniston, M. (2002). *Climatic Change: Implications for the Hydrological Cycle and for Water Management*. Dordrecht: Kluwer Academic Publishers. Pp. 1-40.
- Benner, R., Fogel, M., Sprague, E.K. and Hodson, R.E. (1987). Depletion of ¹³C in lignin and its implication for stable isotope studies. *Nature*. 329. Pp. 708–710.
- Berdugo-Lattke, M.E., Gonzalez, F., Rangel-Ch, J.O. and Gomez, F. (2016). P-type based dimensionality reduction for open contours of Colombian Páramo plant species. *Ecological Informatics*. 36. Pp. 1-7.
- Berman, A-L., Silvestri, G.E. and Tonello, M.S. (2016). Differences between Last Glacial Maximum and present-day temperature and precipitation in southern South America. *Quaternary Science Reviews*. 150. Pp. 221-233.

- Berrio, J.C., Boom, A., Botero, P.J. et al. (2001). Multidisciplinary evidence of the Holocene history of a cultivated floodplain area in the wetlands of Northern Colombia. *Vegetation History and Archaeobotany*. 10. Pp. 161-174.
- Bi, X.H., Sheng, G.Y. and Liu, X.H. et al. (2005). Molecular and carbon and hydrogen isotopic composition of n-alkanes in plant leaf waxes. *Organic Geochemistry*. 36. Pp. 1405–1417.
- Bianchi, T.S. and Canuel, E.A. (2011). *Chemical Biomarkers in Aquatic Ecosystems*. Princeton University Press, Princeton.
- Bierregaard, R.O., Gascon, C., Lovejoy, T.E. and Mesquita, C.G. (2001) *Lessons for Amazonia: the ecology and conservation of a fragmented forest*. Yale University Press, New Haven, CT.
- Bingham, E.M., McClymont, E.L., Valiranta, M., Mauquoy, D., Roberts, Z., Chambers, F.M., Pancost, R.D. and Evershed, R.P. (2010). Conservative composition of n-alkane biomarkers in Sphagnum species: Implications for palaeoclimate reconstruction in ombrotrophic peat bogs. *Organic Geochemistry*. 41. Pp. 214-220.
- Bird, B.W., Abbott, M.B., Vuille, M., Rodbell, D.T. Stansell, N.D. and Rosenmeier, M.F. (2011). A 2,300-year-long annually resolved record of the South American summer monsoon from the Peruvian Andes. *PNAS*. 108(21). Pp. 8583-8588.
- Bird, M.I., Ayliffe, L.K., Fifield, L.K., Turney, C.S.M., Cresswell, R.G., Barrows, R.G. and David, B. (1999). Radiocarbon dating of "old" charcoal using a wet oxidation, stepped-combustion procedure. *Radiocarbon*. 41(2). Pp. 127-140.
- Blaauw, M. and Christen, J.A. (2005). Radiocarbon Peat Chronologies and Environmental Change. *Journal of the Royal Statistical Society. Series C (Applied Statistics)*. 54(4). Pp. 805-816.
- Blaauw, M. and Christen, J.A. (2011). Flexible paleoclimate age-depth models using an autoregressive gamma process. *Bayesian Analysis*. 6. Pp. 457-474.
- Blaauw, M., Christen, J.A., Guilderson, T.P., Reimer, P.J. and Brown, T.A. (2005). The problems of radiocarbon dating. *Science*. 308(5728). Pp.1551–3.

- Blaauw, M., Heuvelink, G.B.M., Mauquoy, D., van der Plicht, J. and van Geel, B. (2003). A numerical approach to ^{14}C wiggle-match dating of organic deposits: best fits and confidence intervals. *Quaternary Science Reviews*. 22. Pp. 1485- 1500.
- Blockley, S.P.E., Blaauw, M., Bronk Ramsey, C. and van der Plicht, J. (2007). Assessing uncertainties in age modelling sedimentary records in the Lateglacial and early Holocene. *Quaternary Science Reviews*. 26. Pp. 1915–1926.
- Bolin, B., Doos, B.R., Jager, J. and Warrick, R.A. eds. (1986). *The Greenhouse Effect: Climate Change and Ecosystems*. Wiley, New York.
- Bond, G., Heinrich, H., Broecker, W., Labeyrie, L., McManus, J., Andrews, J., Huon, S. et al. (1992). Evidence for massive discharges of icebergs into the North Atlantic Ocean during the last glacial period. *Nature*. 360. Pp. 245-249.
- Bosnan, A.F., van der Molen, P.C., Young, R. and Cleef, A.M. (1993). Holocene mire development and climatic change from a high Andean *Plantago rigida* cushion mire. *Journal of Vegetation Science*. 4(5). pp. 633-640.
- Bouma, M.J., Poveda, G., Rojas, W., Chavasse, D. et al. (1997). Predicting high-risk years for malaria in Colombia using parameters of El Niño Southern Oscillation. *Tropical Medicine and International Health*. 2(12). Pp. 1122-1127.
- Bowen, G.J. (2008). Spatial analysis of the intra-annual variation of precipitation isotope ratios and its climatological corollaries. *Journal of Geophysical Research*. 113. doi:10.1029/2007JD009295.
- Bowen, G.J. and Revenaugh, J. (2003). Interpolating the isotopic composition of modern meteoric precipitation. *Water Resources Research*. 39(10). Pp. 1-9. doi:10.1029/2003WR002086
- Brader, A.V., Van Widnen, J.F., Bohncke, S.J.P., Betts, C.J., Reichart, G.J. and de Leeuw, J.W. (2010). Fractionation of hydrogen, oxygen and carbon isotopes in *n*-alkanes and cellulose of three *Sphagnum* species. *Organic Geochemistry*. 41. Pp. 1277-1284.
- Bray, E.E. and Evans, E.D. (1961). Distribution of *n*-paraffins as a clue to recognition of source beds. *Geochimica et Cosmochimica Acta*. 22(1). Pp. 2-15.

- Briant, R.M. and Bateman, M.D. (2009). Luminescence dating indicates radiocarbon age underestimation in late Pleistocene fluvial deposits from eastern England. *Journal of Quaternary Science*. 24(8). Pp. 916-927.
- Brienen, R.J., Helle, G., Pons, T.J., Guyot, J.L. and Gloor, M. (2012). Oxygen isotopes in tree rings are a good proxy for Amazon precipitation and El Niño Southern Oscillation variability. *PNAS*. 109(42). Pp. 16957-16962.
- Broccoli, A.J., Dahl, K.A. and Stouffer, R.J. (2006). Response of the ITCZ to Northern Hemisphere cooling. *Geophysical Research Letters*. 33. L01702.
- Brodie, C.R., Leng, M.J., Casford, J.S.L., Kendrick, C.P., Lloyd, J.M., Yongqiang, Z. and Bird, M.I. (2011). Evidence for bias in C and N concentrations and $\delta^{13}\text{C}$ composition of terrestrial and aquatic organic materials due to pre-analysis acid preparation methods. *Chemical Geology*. 282. Pp. 67-83.
- Burgoyne, T.W. and Hayes, J.M. (1998). Quantitative production of H_2 by pyrolysis of gas chromatographic effluents. *Annals in Chemistry*. 70. Pp. 5136–5141.
- Bush, M.B., Silman, M.R. and Listopad, C.M.C.S. (2007). A Regional Study of Holocene Climate Change and Human Occupation in Peruvian Amazonia. *Journal of Biogeography*. 34 (8). pp. 1342-1356.
- Bush, R.T. and McInerney, F.A. (2013). Leaf wax n-alkane distributions in and across modern plants: implications for paleoecology and chemotaxonomy. *Geochimica et Cosmochimica Acta*. 117. pp.161-179.
- Bush, R.T. and McInerney, F.A. (2015). Influence of temperature and C_4 abundance on n-alkane chain length distributions across central USA. *Organic Geochemistry*. 79. Pp. 65-73.
- Buytaert, W., Céleri, R., De Bièvre, B., Cisneros, F., Wyseure, G., Deckers, J. and Hofstede, R. (2006). Human impact on the hydrology of the Andean páramos. *Earth-Science Reviews*. 79. Pp. 53-72.
- Calvo, E., Pelejero, C., Logan, G.A. and De Dekker, P. (2004). Dust-induced changes in phytoplankton composition in the Tasman Sea during the last four glacial cycles. *Palaeoceanography and Paleoclimatology*. 19. (2). Pp. DOI: 10.1029/2003PA000992.

Cane, M.A. (2005). The evolution of El Niño, past and future. *Earth Planetary Science Letters*. 230. Pp.227–240.

CAR - Corporación Autónoma Regional de Cundinamarca. (2000). Esquema de Ordenamiento Territorial Guatavita Cundinamarca. Bogotá, Colombia.

Carr, A.S., Boom, A., Chase, B.M., Meadows, M.E. and Grimes, H.L. (2015). Holocene sea level and environmental change on the west coast of South Africa: Evidence from plant biomarkers, stable isotopes and pollen. *Journal of Paleolimnology*. 53 (4). Pp. 415-432.

Carr, A.S., Boom, A., Grimes, H.L., Chase, B.M., Meadows, M.E. and Harris, A. (2014). Leaf wax n-alkane distributions in arid zone South Africa: evidence from plant biomarkers, stable isotopes and pollen. *Journal of Paleolimnology*. 53(4). Pp. 415-432.

Casteneda, I.S., Wene, J.P., Johnson, T.C. and Filley, T.R. (2009). Late Quaternary vegetation history of southeast Africa: The molecular isotopic record from Lake Malawi. *Palaeogeography, Palaeoclimatology, Paleoecology*. 275. Pp. 100-112.

Chacón, J., Madrinán, S., Chase, M.W. and Bruhl, J.J. (2006). Molecular phylogenetics of *Oreobolus* (Cyperaceae) and the origin and diversification of the American species. *Taxon*. 55. Pp. 359–366.

Chahine, M.T. (1992). The hydrological cycle and its influence on climate. *Nature*. 359. Pp. 373-379.

Chen, J., Chen, F., Feng, S., Huang, W., Liu, J. and Zhou, A. (2015). Hydroclimatic changes in China and surroundings during the Medieval Climate Anomaly and Little Ice Age: spatial patterns and possible mechanisms. *Quaternary Science Reviews*. 107. Pp. 98-111.

Cheng, H., Fleitmann, D., Edwards, R.L., Wang, X., Cruz, F.W., Auler, A.S., Mangini, A., Wang, Y., Kong, X., Burns, S.J. and Matter, A. (2009). Timing and structure of the 8.2 kyr B.P. event inferred from $\delta^{18}\text{O}$ records of stalagmites from China, Oman, and Brazil. *Geology*. 37. (11). Pp. 1007-1010.

Cheng, H., Sinha, A., Cruz, F.W., Wang, X.W., Edwards, R.L., d’Horta, F.M., Ribas, C.C., Vuille, M., Stott, L.D. and Auler, A.S. (2013). Climate change patterns in Amazonia and biodiversity. *Nature Communications*. 4. (1411). Pp. 1-5.

- Chiang, J.C.H. and Bitz, C.M. (2005). Influence of high latitude ice cover on the marine Intertropical Convergence Zone. *Climate Dynamics*. 25. Pp. 477–496.
- Christen, J.A. (1994). Summarizing a set of radiocarbon determinations: a robust approach. *Applied Statistics - Journal of the Royal Statistical Society Series C*. 43(3). Pp. 489–503.
- Christen, J.A. and Pérez E.S. (2010). A new robust statistical model for radiocarbon data. *Radiocarbon*. 51. Pp. 1047-1059.
- Clark, I.D. and Fritz, P. (1997). *Environmental Isotopes in Hydrogeology*. CRC Press. New York.
- Clark, P.U., Dyke, A.S., Shakun, J.D., Carlson, A.E., Clark, J., Wohlfarth, B., Mitrovica, J.X., Hostetler, S.W. and McCabe, A.M. (2009). The Last Glacial Maximum. *Science*. 325. Pp. 710-714.
- Cleef, A.M. (1981). The vegetation of the Paramos of the Colombian Cordillera Oriental. *Dissertationes Botanicae*. 61.
- Cleef, A.M. (2012). Field information Colombia: Andean mires. Institute of Botany and Landscape Ecology, Grimmerstr, Germany. *International Mire Conservation Group Newsletter 1*. Pp. 7-10.
- Cleef, A.M. and Hooghiemstra, H. (1984). Present vegetation of the area of the high plain of Bogota. In: Hooghiemstra, H. Vegetational and climatic history of the high plain of Bogota, Colombia: a continuous record of the last 3.5 million years. *The Quaternary of Colombia*. 10.
- Climate-Data.org. (2019). *CLIMATE LETICIA*. Available: <https://en.climate-data.org/south-america/colombia/amazonas/leticia-3820/>. Last accessed 01/04/2019.
- Collins, J.A., Schefuss, E., Mulitza, S., Prange, M., Werner, M., Tharammal, T., Paul, A. and Wefer, G. (2013). Estimating the hydrogen isotopic composition of past precipitation using leaf-waxes from western Africa. *Quaternary Science Reviews*. 65. Pp. 88-101.
- Collins, J.M. (2009). Temperature Variability over South America. *Journal of Climate*. 22. Pp. 5854-5869.
- Conte, M.H. and Weber, J.C. (2002). Plant biomarkers in aerosols record isotopic discrimination of terrestrial photosynthesis. *Nature*. 417. Pp. 639-641.

- Cook, K., Sieh, J.S. and Hagos, S.M. (2004). The Africa–South America Intercontinental Teleconnection. *Journal of Climate*. 17. Pp. 2851–2865.
- Costa, M.H. and Foley, J.A. (1999). Trends in the hydrologic cycle of the Amazon basin, *Journal of Geophysical Research*. 104. (12). Pp. 14189 – 14198.
- Costa, M.H., Coe, M.T. and Guyot, J.L. (2009). Effects of climatic variability and deforestation on surface water regimes. In: *Amazonia and Global Change*. eds. Keller, M., Bustamante, M., Gash, J. and Silva Dias, P. (American Geophysical Union, Washington, DC). Monograph 186. pp 576.
- Craig, H. (1961). Standards for reporting concentrations of deuterium and oxygen-18 in natural waters. *Science*. 133. Pp. 1833–1834.
- Craig, H. and Gordon, L.I. (1965). Deuterium and Oxygen 18 variations in the Ocean and the marine atmosphere. Symposium on Marine Geochemistry, Narraganset Marine Laboratory, University of Rhode Island. Publication, Vo.3. pp. 277-374.
- Crann, C.A., Patterson, R.T., Macumber, A.L., Galloway, J.M., Roe, H.M., Blaauw, M., Swindles, G.T. and Falck, H. (2015). Sediment accumulation rates in subarctic lakes: Insights into age-depth modeling from 22 dated lake records from the Northwest Territories, Canada. *Quaternary Geochronology*. 27. Pp. 131-144.
- Cranwell P.A. (1981) Diagenesis of free and bound lipids in terrestrial detritus deposited in a lacustrine sediment. *Organic Geochemistry*. 3. Pp. 79–89.
- Cranwell, P.A. (1973). Chain-length distributions of n-alkanes from lake sediments in relation to post-glacial environmental change. *Freshwater Biology*. 3. Pp. 259-265.
- Criss, R.E. (1999). *Principles of Stable Isotope Distribution*. New York: Oxford University Press.
- Cross, S.L., Baker, P.A., Seltzer, G.O., Fritz, S.C. and Dunbar, R.B. (2001). Late Quaternary Climate and Hydrology of Tropical South America Inferred from an Isotopic and Chemical Model of Lake Titicaca, Bolivia and Peru. *Quaternary Research*. 51 (1). Pp. 1-9.
- Cross, S.L., Baker, P.A., Seltzer, G.O., Fritz, S.C. and Dunbar, R.B. (2000). A new estimate of The Holocene low-stand level of Lake Titicaca, central Andes, and implications for tropical palaeohydrology. *Holocene*. 10. Pp. 21 – 32.

- Cruz, F.W., Burns, S.J., Karmann, I., Sharp, W.D. and Vuille, M. (2006). Reconstruction of regional atmosphere circulation features during the late Pleistocene in subtropical Brazil from oxygen isotope composition of speleothems. *Earth, Planetary and Science Letters*. 248. Pp. 494–506.
- Cruz, F.W., Burns, S.J., Karmann, I., Sharp, W.D., Vuille, M., Cardoso, A.O., Ferrari, J.A., Silva Dias, P.L. and Viana Jr, O. (2005). Insolation-driven changes in atmospheric circulation over the past 116,000 years in subtropical Brazil. *Nature*. 434. Pp. 63–66.
- Cruz, F.W., Vuille, M., Burns, S.J., Wang, X., Cheng, H., Werner, M., Edwards, R.L., Karmann, I., Auler, A.S. and Nguyen, H. (2009). Orbitally driven east–west antiphasing of South American precipitation. *Nature Geoscience*. 2. Pp. 210-214.
- Cuevas, E. and Medina, E. (1988). Nutrient dynamics within Amazonian forests. II fine root growth, nutrient availability and leaf litter decomposition. *Oecologia*. 76. Pp. 222–235.
- Curtis, J.H., Brenner, M. and Hodell, D.A. (1999). Climate change in the Lake Valencia Basin, Venezuela, ~12600 yr BP to present. *The Holocene*. 9. (5). Pp. 609-619.
- Damsté, J.S.S., Verschuren, D., Ossebaer, J., Blokker, J., van Houten, R., van der Meer, M.T.J., Plessen, B. and Schouten, S. (2011). A 25,000-year record of climate-induced changes in lowland vegetation of eastern equatorial Africa revealed by the stable carbon-isotopic composition of fossil plant leaf waxes. *Earth and planetary Science Letters*. 302. Pp. 236-246.
- Daniels, W.C., Russell, J.M., Giblin, A.E., Welker, J.M., Klein, E.S. and Huang, Y. (2017). Hydrogen isotope fractionation in leaf waxes in the Alaskan Arctic Tundra. *Geochimica et Cosmochimica Acta*. 213. Pp. 216-236.
- Dansgaard, W. (1954). The O¹⁸ abundance in fresh water. *Geochimica et Cosmochimica Acta*. 6. Pp. 241-260.
- Dansgaard, W. (1964). Stable isotopes in precipitation. *Tellus*. 16. Pp. 436–468.
- Davidson, E.A. and Janssens, I.A. (2006). Temperature sensitivity of soil carbon decomposition and feedbacks to climate change. *Nature*. 440. Pp. 165– 173.
- Davis, M.E., Thompson, L.G., Mosley-Thompson, E., Lin, P-N., Mikhailenko, V.N. and Dai, J. (1995). Recent ice-core climate records from the Cordillera Blanca, Peru. *Annals of Glaciology*. 21. Pp. 225–230.

- Dawson, T.E. (1993). Water sources of plants as determined from xylem-water isotopic composition: perspectives on plant competition, distribution and water relations. In: Ehleringer, J.R., Happ, A.E. and Farquhar, G.D. (eds). *Stable Isotopes and Plant Carbon-Water Relations*. Academic Press, New York.
- Delgado, C., Coutourier, G. and Mejia, K. (2007). *Mauritia flexuosa* (Arecaceae: Calamoideae), an Amazonian palm with cultivation purposes in Peru. *Fruits*. 62. Pp. 157-169.
- Dickinson, R.E. (1987). *The Geophysiology of Amazonia: Vegetation and Climate Interactions*. Wiley: New York.
- Diefendorf, A.F., Freeman, K.H., Wing, S.L. and Graham, H.V. (2011). Production of n-alkyl lipids in living plants and implications for the geologic past. *Geochimica et Cosmochimica Acta*. 75. Pp. 7472-7485.
- Dirzo, R. and Raven, P.H. (2003) Global state of biodiversity and loss. *Annual Review of Environment and Resources*. 28. pp.137–167.
- Domínguez, C. (1985). Amazonia Colombiana: Visión General. Biblioteca Banco Popular. Bogotá, Colombia.
- Douglas, P.M.D., Pagani, M., Brenner, M., Hodell, D.A. and Curtis, J.H. (2012). Aridity and vegetation composition are important determinants of leaf-wax δD values in southeastern Mexico and Central America. *Geochimica et Cosmochimica Acta*. 97. Pp. 24–45.
- Draper, F.C., Roucoux, K.H., Lawson, I.T., Mitchard, E.T., Coronado, E.N.H., Lähteenoja, O., Montenegro, LT, Sandoval, EV, Zaráte, R. and Baker, TR. (2014). The distribution and amount of carbon in the largest peatland complex in Amazonia. *Environmental Research Letters*. 9 (12). 124017. Doi: <https://doi.org/10.1088/1748-9326/9/12/124017>.
- Eglinton, G. and Hamilton, R.J. (1967). Leaf epicuticular waxes. *Science*. 156 (3780). Pp. 1322–1335.
- Ehleringer, J.R. and Dawson, T.E. (1992). Water-uptake by plants – perspectives from stable isotope composition. *Plant Cell and Environment*. 15. Pp. 1073–1082.
- Ehleringer, J.R., Bowen, G.J., Chesson, L.A., West, A.G., Podlesak, D.W. and Cerling, T.E. (2008). Hydrogen and oxygen isotope ratios in human hair are related to geography. *PNAS*. 105 (8). Pp. 2788-2793.

- Eley, Y.L. and Hren, M.T. (2018). Reconstructing vapor pressure deficit from leaf wax lipid molecular distributions. *Nature Scientific Reports*. 8. (3967). Pp. 1-8. Doi: 10.1038/s41598-018-21959-w.
- Epstein, S., Thompson, P. and Yapp, C.J. (1977). Oxygen and Hydrogen Isotope Ratios in Plant Cellulose. *Science*. 198 (4323). Pp. 1209-1215.
- Farquhar, G., Ehleringer, J. and Hubick, K. (1989). Carbon isotope discrimination and photosynthesis. *Annual Review of Plant Physiology and Plant Molecular Biology*. 40. pp. 503-537.
- Farquhar, G.D., Cernusak, L.A. and Barnes, B. (2007). Heavy water fractionation during transpiration. *Plant Physiology*. 143. Pp. 11–18.
- Feakins, S.J. and Sessions, A.L. (2010). Controls on the D/H ratios of plant leaf waxes in an arid ecosystem. *Geochimica et Cosmochimica Acta*. 74. Pp. 2128-2141.
- Feakins, S.J., Bentley, L.P., Salinas, N. et al. (2016b). Plant leaf wax biomarkers capture gradients in hydrogen isotopes of precipitation from the Andes and Amazon. *Geochimica et Cosmochimica Acta*. 182. Pp. 155-172.
- Feakins, S.J., Peters, T., Wu, S.W., Shenkin, A., Salinas, N., Girardin, C.A.J., Bentley, L.P., Blonder, B. et al. (2016a). Production of leaf wax n-alkanes across a tropical forest elevation transect. *Organic Geochemistry*. 100. Pp. 89-100.
- Ferronsky, V.I. and Polyakov, V.A. (1982). *Environmental Isotopes in the Hydrosphere*. John Wiley and Sons, New York.
- Ficken, K.J., Li, B., Swain, D.L. and Eglinton, G. (2000). An n-alkane proxy for the sedimentary input of submerged/floating freshwater aquatic macrophytes. *Organic Geochemistry*. 31(7). Pp. 745-749.
- Flanagan, L.B. and Ehleringer, J.R. (1991). Stable isotope composition of stem and leaf water – applications to the study of plant water-use. *Functional Ecology*. 5. Pp. 270– 277.
- Flanagan, L.B., Bain, J.F. and Ehleringer, J.R. (1991). Stable oxygen and hydrogen isotope composition of leaf water in C3 and C4 plant species under field conditions. *Oecologia*. 88. Pp. 394-400.

- Flanagan, L.B., Comstock, J.P. and Ehleringer, J.R. (1991). Comparison of modelled and observed environmental influences on the stable oxygen and hydrogen isotope composition of leaf water in *Phaseolus vulgaris* L. *Plant Physiology*. 96. Pp.588–596.
- Flores, R.M. (2014). Chapter 3 - Origin of Coal as Gas Source and Reservoir Rocks. In: *Coal and Coalbed Gas*. Pp. 97-165. <https://doi.org/10.1016/B978-0-12-396972-9.00003-3>.
- Foley, J.A., Botta, A., Coe, M.T. and Costa, M.H. (2002). El Nino-Southern Oscillation and the climate, ecosystems and rivers of Amazonia. *Global Biogeochemical Cycles*. 16 (4). Pp. 1132.
- Fornace, K.L., Hughen, K.A., Shanahan, T.M., Fritz, S.C., Baker, P.A. and Sylva, S.P. (2014). A 60,000-year record of hydrological variability in the Central Andes from the hydrogen isotopic composition of leaf waxes in Lake Titicaca sediments. *Earth and Planetary Science Letters*. 408. Pp. 263-271.
- Fornace, K.L., Whitney, B.S., Galy, V., Hughen, K.A. and Mayle, F.E. (2016). Late Quaternary environmental change in the interior South American tropics: new insight from leaf wax stable isotopes. *Organic Geochemistry*. 438. Pp. 75-85.
- Friedman, I. (1953). Deuterium content of natural waters and other substances. *Geochimica et Cosmochimica Acta*. 4. Pp. 89-103.
- Fry, B. (2006). *Stable Isotope Ecology*. New York, NY: Springer. Pp. 1-270.
- Gagnon, A., Smoyer-Tomic, K. and Bush, A. (2002). The El Nino Southern Oscillation and malaria epidemics in South America. *International Journal of Biometeorology*. 46. Pp. 81-89.
- Gagosian, R.B. and Peltzer, E.T. (1986). The importance of atmospheric input of terrestrial organic material to deep sea sediments. *Organic Geochemistry*. 10. Pp. 661–669.
- Galeano, A., Urrego, L.E. and Penuela, M.C. (2015). Environmental drivers for regeneration of *Mauritia flexuosa* L.f. in Colombian Amazonian swamp forest. *Aquatic Botany*. 123. Pp. 47-53.
- Galimov, E. (1985). Isotopic composition of the carbon of organisms. In: *The Biological Fractionation of Isotopes*. Galimov, E. (ed.). Academic Press, Inc.: New York. Pp. 16–38.

- Gallego-Sala, A.V., Charman, D.J., Brewer, S., Page, S.E, Prentice, I.C. et al. (2018). Latitudinal limits to the predicted increase of the peatland carbon sink with warming. *Nature Climate Change*. 8. Pp. 907-913.
- Gao, L., Hou, J., Toney, J., MacDonald, D. and Huang, Y. (2011). Mathematical modelling of the aquatic macrophyte inputs of mid-chain n-alkyl lipids to lake sediments: Implications for interpreting compound specific hydrogen isotopic records. *Geochimica et Cosmochimica Acta*. 75. Pp. 3781–3791.
- Garcin Y., Schwab V.F., Gleixner G., Kahmen A., Todou G., Sene O., Onana J-M., Achoundong G. and Sachse D. (2012). Hydrogen isotope ratios of lacustrine sedimentary n-alkanes as proxies of tropical African hydrology: Insights from a calibration transect across Cameroon. *Geochimica et Cosmochimica Acta*. 79. Pp. 106–126.
- Gareaud, R.D., Vuille, M., Compagnucci, R. and Marengo, J. (2009). Present-day South American climate. *Palaeogeography, Palaeoclimatology, Palaeoecology*. 281. Pp. 180-195.
- Garreaud, R. (2007). Precipitation and circulation covariability in the extratropics. *Journal of Climate*. 20. Pp. 4789–4797.
- Gasse, F. (2000). Hydrological changes in the African tropics since the Last Glacial Maximum. *Quaternary Science Reviews*. 19. Pp. 189–211.
- Gat, J. (2010). *Isotope Hydrology: A Study of the Water Cycle*. London: Imperial College Press.
- Gat, J.R. (1980). The isotopes of hydrogen and oxygen in precipitation. In: Fritz, P., Fontes, J.Ch. (Eds.). *Handbook of Environmental Isotope Geochemistry*. Elsevier, Amsterdam.
- Gat, J.R. (1996). Oxygen and Hydrogen isotopes in the hydrological cycle. *Annual Review of Earth and Planetary Science*. 24. Pp. 225-262.
- Gat, J.R. (2000). Atmospheric water balance - the isotopic perspective. *Hydrological Processes*. 14. Pp.1357–1369.
- Gat, J.R. and Carmi, I. (1970). Evolution of the isotopic composition of atmospheric waters in the Mediterranean Sea area. *Journal of Geophysical Research*. 75. Pp. 3039-3048.
- Gat, J.R. and Gonfiantini, R. (1981). *Stable isotope hydrology. Deuterium and oxygen-18 in the water cycle*. International Atomic Energy Agency, Vienna.

Gat, J.R. and Matsui, T. (1991). Atmospheric water balance in the Amazon Basin: an isotopic evapotranspiration model. *Journal of Geophysical Research*. 96. Pp.13179–13188.

Gillespie, R. (1997). Burnt and unburnt carbon: dating charcoal and burnt bone from the Willandra Lakes, Australia. *Radiocarbon*. 39(3). Pp. 225-36.

Giorgi, F. and Mearns, L.O. (1991). Approaches to the simulation of regional climate change: A review. *Rev Geophysics*. 29. Pp. 191-216.

Gómez, C.L. and Rubio, D. (2003). El pantano de Martos: estudio histórico, cultural y geográfico. Academia de Historia de Cundinamarca y Secretaria del Medio Ambiente del departamento de Cundinamarca. 103 pp.

Gröcke, D. (2002). The carbon isotope composition of ancient CO₂ based on higher plant organic matter. *Philosophical Transactions of the Royal Society, London A*. 360. pp. 633-658.

Gupta, A.S. and England, S. (2006). Coupled ocean–atmosphere–ice response to variations in the southern annular mode. *Journal of Climate*. 19. Pp. 4457–4486.

Hahn, A, Miller, C., Bouimetarhan, I., Cawthra, H.C., Garzanti, E., Green, A.N., Radeff, G., Scheffus, E. and Zabel, M. (2018). The Provenance of Terrigenous Components in Marine Sediments along the East Coast of Southern Africa. *Geochemistry, Geophysics, Geosystems*. 19. Pp. 1946–1962.

Halinski, L.P., Szafranek, J. and Stepnowski, P. (2011). Leaf cuticular n-alkanes and markers in the chemotaxonomy of the eggplant (*Solanum Melongena* L.) and related species. *Plant Biology*. 13. Pp. 932-939.

Hamilton, S.K. and Lewis, W.M. (1992). Stable carbon and nitrogen isotopes in algae and detritus from the Orinoco River floodplain, Venezuela. *Geochimica et Cosmochimica Acta*. 56. Pp. 4237–4246.

Harwood, J.L. (1997). Plant Lipid Metabolism. In: Dey, P.M. and Harborne, J.B. (eds.). *Plant Biochemistry*. Academic Press, London.

Hastenrath, S. (1978). ‘On modes of tropical circulation and climate anomalies’. *Journal of Atmospheric Science*. 35. Pp. 2222-2231.

Hastenrath, S. (1991). *Climate Dynamics of the Tropics*. Kluwer, Dordrecht.

- Hatte, C., Morvan, J., Noury, C. and Paterne, M. (2001). Is classical acid–alkali– acid treatment responsible for contamination? An alternative proposition. *Radiocarbo*. 43. Pp. 177–182.
- Haug, G.H., Hughen, K.A., Sigman, D.M., Peterson, L.C. and Rohl, U. (2001). Southward migration of the Intertropical Convergence Zone through the Holocene. *Science*. 293. Pp. 1304-1308.
- Hayes, J. (2001). Fractionation of carbon and hydrogen isotopes in biosynthetic processes. In: Valley, J. and Cole, D. (ed). Stable isotope geochemistry. *Reviews in Mineralogy and Geochemistry*. 43. pp. 225-277.
- Hayes, J.M. (1993). Factors controlling ^{13}C contents of sedimentary organic compounds: principles and evidence. *Marine Geology*. 113. Pp. 111–125.
- Heine, K. (2000). Tropical South America during the Last Glacial Maximum: Evidence from glacial, periglacial and fluvial records. *Quaternary International*. 72(1). Pp. 7-21.
- Heinrich, H. (1988). Origin and consequences of cyclic ice rafting in the Northeast Atlantic Ocean during the past 130,000 years. *Quaternary Research*. 29. (2). Pp. 142-152.
- Henderson, A. (1995). *The Palms of the Amazon*. Oxford University Press, New York, USA
- Hendricks, M.B., De Paolo, D.J. and Cohen, R.C. (2000). Space and time variation of $\delta^{18}\text{O}$ and δD in precipitation: Can paleotemperature be estimated from ice cores? *Global Biogeochemical Cycles*. 14(3). Pp. 851-861.
- Hermann, N., Boom, A., Carr, A.S., Chase, B.M., West, A.G., Zabel, M. and Schefuss, E. (2017). Hydrogen isotope fractionation of leaf wax n-alkanes in southern African soils. *Organic Geochemistry*. 109. Pp. 1-13.
- Hoffmann, G., Ramirez, E., Taupin, J.D., Francou, B., Ribstein, P, Delmas, R., Durr, H., Gallaire, R., Simoes, J., Schotterer, U., Stievenard, M. and Werner, M. (2003). Coherent isotope history of Andean ice cores over the last century. *Geophysical Research Letters*. 30(4). Pp. 1-4. doi:10.1029/2002GL014870.
- Hogg, A.G., Hua, Q., Blackwell, P.G., Niu, M., Buck, C.E. et al. (2013). SHCAL13 Southern Hemisphere calibration, 0–50,000 years cal BP. *Radiocarbon*. 55(4). Pp. 1889-1903.
- Hoorn, C. and Wesselingh, F.P. (2010) *Amazonia: Landscape and Species Evolution: A look into the past*. Wiley-Blackwell, Oxford, UK.

- Horel, J. and Cornejo-Garrido, A. (1986). Convection along the coast of Northern Peru during 1983. Spatial and temporal variation of clouds and rainfall. *Monthly Weather Review*. 114. Pp. 2091–2105.
- Hornibrook, E.R.C. (2009). The stable carbon isotope composition of methane produced and emitted from northern peatlands. In: *Northern Peatlands and Carbon Cycling*. Baird, A., Belyea, L., Comas, X. et al. (eds). American Geophysical Union: Washington, DC. Pp. 187–203.
- Horning-Leoni, C.T. and Sosa, V. (2008). Morphological phylogenetics of Puya subgenus Puya (Bromeliaceae). *Botanical Journal of the Linnean Society*. 156. Pp. 93–110.
- Hostede, R.G.M. and Witte, H.J.L. (1993). An evaluation of the use of the dry – weight rank and the comparative yield biomass estimation methods in páramo ecosystem research. *Caldasia*. 17(2). Pp. 205 – 210.
- Hou, J., D’Andrea, W.J. and Huang, Y. (2008). Can sedimentary leaf waxes record D/H ratios of continental precipitation? Field, model, and experimental assessments. *Geochimica et Cosmochimica Acta*. 72. Pp. 3503–3517.
- Hou, J., D’Andrea, W.J., Macdonald, D. and Huang, Y. (2007). Evidence for water use efficiency as an important factor in determining the delta D values of tree leaf waxes. *Organic Geochemistry*. 38. Pp. 469-483.
- Hou, J., Tian, Q. and Wang, M. (2018). Variable apparent hydrogen isotopic fractionation between sedimentary n-alkanes and precipitation on the Tibetan Plateau. *Organic Geochemistry*. 122. Pp. 78-86.
- Howard, S., McInerney, F.A., Caddy-Retalic, S., Hall, P.A. and Andrae, J.W. (2018). Modelling leaf wax n-alkane inputs to soils along a latitudinal transect across Australia. *Organic Geochemistry*. 121. Pp. 126-137.
- Hoyos, N., Escobar, J., Restrepo, J.C., Arango, A.M. and Ortiz, J.C. (2013). Impact of the 2010-2011 La Niña phenomenon in Colombia, South America: The human toll of an extreme weather event. *Applied Geography*. 39. Pp. 16-25.
- Ingraham, N.L. and Taylor, B.E. (1991). Light stable isotope systematics of large-scale hydrological regimes in California and Nevada. *Water Resource and Research*. 27. Pp. 77-90.

Intergovernmental Panel on Climate Change, Climate Change (2001). The Science Basis (Cambridge Univ. Press, Cambridge, UK, 2001).

Intergovernmental Panel on Climate Change IPCC. (2007). Climate change 2007: The physical science basis. Contribution of working group I to the Fourth Assessment Report (AR4) of the Intergovernmental Panel on Climate Change. Cambridge New York: Cambridge University Press

IPCC. (2007). *Climate Change 2007: Impacts, Adaptation and Vulnerability. Contribution of Working Group II to the Fourth Assessment Report of the Intergovernmental Panel on Climate Change*. Parry, M.L., Canziani, O.F., Palutikof, J.P., van der Linden, P.J. and Hanson Eds., Cambridge University Press, Cambridge, UK.

IPCC. (2013). Summary for Policymakers. In: Climate Change 2013: The Physical Science Basis. Contribution of Working Group I to the Fifth Assessment Report of the Intergovernmental Panel on Climate Change [Stocker, T.F., D. Qin, G.-K. Plattner, M. Tignor, S. K. Allen, J. Boschung, A. Nauels, Y. Xia, V. Bex and P.M. Midgley (eds.)]. Cambridge University Press, Cambridge, United Kingdom and New York, NY, USA.

Ishiwatari, R. and Uzaki, M. (1987). Diagenetic changes of lignin compounds in a more than 0.6 million-year-old lacustrine sediment (Lake Biwa, Japan). *Geochimica et Cosmochimica Acta*. 51(2). Pp. 321-328.

Ishiwatari, R., Hirakawa, Y., Uzaki, M. et al. (1994). Organic geochemistry of the Japan Sea sediments. 1. Bulk organic matter and hydrocarbon analyses of core KH-79-3, C-3 from the Oki Ridge from paleoenvironment assessments. *Journal of Oceanography*. 50. Pp. 179-195.

IUPAC (1997). *Compendium of Chemical Terminology (the "Gold Book")*. 2nd ed. Oxford: Blackwell Scientific Publications. pp. 1132.

Jansen, B., Nierop, K.G.J., Hageman, J.A., Cleef, A.M. and Verstraten, J.M. (2006). The straight chain lipid biomarker composition of plant species responsible for the dominant biomass production along two altitudinal transects in the Ecuadorian Andes. *Organic Geochemistry*. 37. Pp. 1514–1536.

Jeng, W. (2006). Higher plant n-alkane average chain length as an indicator of petrogenic hydrocarbon contamination in marine sediments. *Marine Chemistry*. 102. Pp. 242-251.

- Jenks, M.A. and Ashworth, E.N., (1999). Plant epicuticular waxes: function, production, and genetics. *Horticultural reviews*. 23. pp. 1-68.
- Jetter, R., Kunst, L., Samuels, A.L. (2008). A composition of plant cuticular waxes. *Annual Plant Reviews, Biology of the Plant Cuticle*. 23. Pp. 145.
- Johnson, T.C., WERne, J.P., Brown, E.T., Abbott, A., Berke, M., Steinman, B.A., Halbur, J., Contreras, S., Grosshuesch, S., Deino, A., Lyons, R.P., Scholz, C.A., Schouten, S. and Sinninghe Damsté, J.S. (2016). A progressively wetter climate in southern East Africa over the past 1.3 million years. *Nature*. 537. Pp. 220-226.
- Jonasson, S. and Shaver, G.R. (1999). Within-stand nutrient cycling in Arctic and boreal wetlands. *Ecology*. 80. Pp. 2139– 2150.
- Jones, V.J., Stevenson, A.C., and Battarbee, R.W. (1989). Acidification of lakes in Galloway, southwest Scotland: a diatom and pollen study of the post-glacial history of the Round Loch of Glenhead. *Journal of Ecology*. 77. Pp. 1–23.
- Jouzel, J., Hoffman, G., Koster, R.D. and Masson, V. (2000). Water isotopes in precipitation: data/model comparison for present-day and past climates. *Quaternary Science Reviews*. 19. Pp. 363-379.
- Jouzel, J., Lorius, C., Petit, J.R. et al. (1987). Vostok ice core: a continuous isotope temperature record over the last climatic cycle (160,000 years). *Nature*. 329. Pp. 403-408.
- Junk, W.J., Piedade, M.T.F., Parolin, P. et al. (2010). *Amazonian Floodplain Forests: ecophysiology, biodiversity and sustainable management, Ecological Studies*. Springer-Verlag, Berlin.
- Kahmen, A., Hoffmann, B., Schefuss, E., Arndt, S.K., Cernusak, L.A., West, J.B. and Sachse, D. (2013b). Leaf water deuterium enrichment shapes leaf wax n-alkane δD values of angiosperm plants. II. Observational evidence and global implications. *Geochimica et Cosmochimica Acta*. 111. Pp. 50–63.
- Kahmen, A., Schefuss, E. and Sachse, D. (2013a). Leaf water deuterium enrichment shapes leaf wax n-alkane δD values of angiosperm plants I: Experimental evidence and mechanistic insights. *Geochimica et Cosmochimica Acta*. 111. Pp.39-49.

- Kanner, L.C., Burns, S.J., Cheng, H. and Edwards, R.L. (2012). High-Latitude Forcing of the South American Summer Monsoon During the Last Glacial. *Science*. 335 (6068). Pp. 570-573.
- Kendall, C. and McDonnell, J. J. (1993). Effect of intrastorm isotopic heterogeneities of rainfall, soil water and groundwater on runoff modeling. *Tracers in Hydrology. IAHS*. 215. Pp. 41– 48.
- Kendall, C. and McDonnell, J.J. (1998). *Isotope Tracers in Catchment Hydrology*. Elsevier Science. Amsterdam.
- Kennicutt, M.C., Barker, C., Brooks, J.M et al. (1987). Selected organic matter source indicators in the Orinoco, Nile and Changjiang Deltas. *Organic Geochemistry*. 11. Pp. 41-51.
- Klein, J., Lerman, J.C., Damon, P.E. and Ralph, E.K. (1962). Calibration and radiocarbon dates. *Radiocarbon*. 24(2). Pp. 103-150.
- Koch, K. and Ensikat, H.J. (2008). The hydrophobic coatings of plant surfaces: epicuticular wax crystals and their morphologies, crystallinity and molecular self-assembly. *Micron*. 39. (7). Pp. 759-772.
- Könönen, M., Jauhiainen, J., Laiho, R., Kusin, K. and Vasander, H. (2015). Physical and chemical properties of tropical peat under stabilised land uses. *Mires and Peat*. 16 (8). Pp. 1-13.
- Koolen, H.H. F., da Silva, F.M.A., Paz, W.H.P. and Bataglion, G.A. (2018). Buriti fruit—*Mauritia flexuosa*. *Exotic Fruits – Reference Guide*. <https://doi.org/10.1016/B978-0-12-803138-4.00004-6>.
- Kousky, V.E, Kagano, M.T. and Cavalcanti, I.F.A. (1984). A review of the Southern Oscillation - oceanic-atmospheric circulation changes and related rainfall anomalies. *Tellus*. 36. Pp. 490–504.
- Krishnamurthy, R.V., Syrup, K.A., Baskaran, M. and Long, A. (1995). Late glacial climate record of midwestern United States from the hydrogen isotope ratio of lake organic matter. *Science*. 269. Pp. 1565–1567.
- Kuhn, T.K., Krull, E.S., Bowater, A., Grice, K. and Gleixner, G. (2010). The occurrence of short-chain n-alkanes with an even over odd predominance in higher plants and soils. *Organic Geochemistry*. 41. Pp. 88–95.

Kuhry, P. and Vitt, D.H. (1996). Fossil carbon/nitrogen ratios as a measure of peat decomposition. *Ecology*. 77. Pp. 271–275.

Kurita, N. (2013). Water isotopic variability in response to mesoscale convective system over the tropical ocean. *Journal of Geophysical Research Atmospheres*. 118. Pp. 10376–10390.

Kurita, N., Ichiyanagi, K., Matsumoto, J. et al. (2009). The relationship between the isotopic content of precipitation and the precipitation amount in tropical regions. *Journal of Geochemical Exploration*. 102. Pp. 113-122.

Labat, D. (2006). Oscillations in land surface hydrological cycle. *Earth and Planetary Science Letters*. 242. Pp. 143-154.

Labraga, J.C., Frumento, O. and Lopez, M. (2000). The Atmospheric Water Vapor Cycle in South America and the Tropospheric Circulation. *American Meteorological Society*. 13. Pp. 1899-1915.

Lamb, A.L., Wilson, G.P. and Leng, M.L. (2006). A review of coastal palaeoclimate and relative sea-level reconstructions using $\delta^{13}\text{C}$ and C/N ratios in organic material. *Earth-Science Reviews*. 75. Pp. 27-57.

Lambeck, K., Rouby, H., Purcell, A., Sun, Y. and Sambridge, M. (2014). Sea level and global ice volumes from the Last Glacial Maximum to the Holocene. *PNAS*. 111. (43). Pp. 15296-15303.

Lampela, M., Jauhiainen, J. and Vasander, H. (2014). Surface peat structure and chemistry in a tropical peat swamp forest. *Plant and Soil*. 382. Pp. 329-347.

Ledru, M.P., Bertaux, J., Sifeddine, A. and Suguio, K. (1998). Absence of last glacial maximum records in lowland tropical forest. *Quaternary Research*. 49. Pp. 233-237.

Ledru, M.P., Ivo Soares Braga, P., Soubiès, F., Fournier, M., Martin, L., Suguio, K. and Turcq, B. (1996). The last 50,000 years in the neotropics (southern Brazil): Evolution of climate and vegetation. *Palaeogeography, Palaeoclimatology, Palaeoecology*. 123. Pp. 239–257.

Lee J.E., Johnson, K. and Fung, I. (2009). Precipitation over South America during the Last Glacial Maximum: an analysis of the ‘amount effect’ with a water isotope-enabled general circulation model. *Geophysical Research Letters*. 36. L19701.

Lee, J.E. and Fung, I. (2008). “Amount effect” of water isotopes and quantitative analysis of post-condensation processes. *Hydrological Process*. 22(1). Pp. 1–8.

- Lemke, P., Ren, J., Alley, R.B., Allison, I., Carrasco, J., Flato, G., Fujii, Y., Kaser, G., Mote, P., Thomas, R.H. and Zhang, T. (2007). Observations: changes in snow, ice and frozen ground. In: *Climate Change 2007: The Physical Science Basis. Contribution of Working Group I to the Fourth Assessment Report of the Intergovernmental Panel on Climate Change*. Solomon, S., Qin, D., Manning, M., Chen, Z., Marquis, M., Averyt, K.B., Tignor, M. and Miller, H.L. (eds). Cambridge University Press: Cambridge. Pp. 337–383.
- Lettau, H., Lettau, K. and Molion, L.C.B. (1979). Amazonias hydrologic cycle and the role of atmospheric recycling in assessing deforestation effects. *Monthly Weather Review*. 107. Pp. 227–238.
- Li, G., Li, L., Tarozo, R., Longo, W.M., Wang, K.J., Dong, H. and Huang, Y. (2018). Microbial production of long-chain n-alkanes: Implication for interpreting sedimentary leaf wax signals. *Organic Geochemistry*. 115. Pp. 24-31.
- Li, R., Luo, G., Meyers, P.A. et al (2012). Leaf wax n-alkane chemotaxonomy of bamboo from a tropical rainforest in southwest China. *Plant Systematics and Evolution*. 298(4). Pp. 731-738.
- Li, Y. and Glime, J.M. (1990). Growth and nutrient ecology of two Sphagnum species. *Hikobia* 10. Pp. 445–451.
- Li, Y. and Vitt, D.H. (1997). Patterns of retention and utilization of aerielly deposited nitrogen in boreal peatlands. *Ecoscience*. 4. Pp. 106–116.
- Li, Y., Zhang, H., Tu, C., Fu, C., Xue, Y. and Luo, Y. (2016). Sources and fate of organic carbon and nitrogen from land to ocean: Identified by coupling stable isotopes with C/N ratio. *Estuarine, Coastal and Shelf Science*. 181. Pp. 114-122.
- Liebmann, B., Kiladis, G.N., Marengo, J.A., Ambrizzi, T. and Glick, J.D. (1999). Submonthly Convective Variability over South America and the South Atlantic Convergence Zone. *Journal of Climate*. 12. Pp. 1877-1891.
- Limpens, J., Hejmans, M. and Berendse, F. (2006). The nitrogen cycle in boreal peatlands. In: *Boreal Peatland Ecosystems*. Wieder, R.K. and Vitt, D.H. (eds). Springer-Verlag Berlin and Heidelberg GmbH & Co. K: Berlin. Pp. 195–230.
- Lin, H-L., Peterson, L.C., Overpeck, J.T., Trumbore, S.E. and Murray, D.W. (1997). Late Quaternary climate change from 6180 records of multiple species of planktonic foraminifera: High-resolution records from the anoxic Cariaco Basin, Venezuela. *Paleoceanography*. 12. (3). Pp. 415-427.

- Lindzen, R.S. (1990). Some coolness concerning global warming. *Bulletin of American Meteorological Society*. 71. Pp. 288-299.
- Ling, Y., Zheng, M., Sun, Q. and Dai, X. (2017). Last deglacial climatic variability in Tibetan Plateau as inferred from *n*-alkanes in a sediment core from Lake Zabuye. *Quaternary International*. 454. Pp. 15-24.
- Liu, W., Yang, H. and Li, L. (2006). Hydrogen isotopic compositions of *n*-alkanes from terrestrial plants correlate with their ecological life forms. *Oecologia*. 150. Pp. 330– 338.
- Liu, Y., Wu, J., Shen, J., Liu, S., Wang, C., Chen, D., Huang, T. and Zhang, J. (2016). Soil microbial C:N ratio is a robust indicator of soil productivity for paddy fields. *Nature*. 6 (35266). Pp. 1-8.
- Liu, Z., Bowen, G.J. and Welker, J.M. (2010). Atmospheric circulation is reflected in precipitation isotope gradients over the conterminous United States. *Journal of Geophysical Research*. 115. D221210.
- Loisel, J., Garneau, M. and Helie, J-F. (2010). *Sphagnum* $\delta^{13}\text{C}$ values as indicators of paleohydrological changes in a peat bog. *The Holocene*. 20(2). Pp. 285-291.
- Londono, C., Cleef, A. and Madrinan, S. (2014). Angiosperm flora and biogeography of the páramo region of Colombia, Northern Andes. *Flora*. 209. Pp. 81-87.
- Lowe, J.J. and Walker, M.J.C. (1997). *Reconstructing Quaternary Environments*. 2nd ed. Harlow, England: Addison-Wesley Longman.
- Ludwiczuk, A., Skalicka-Woźniak, K. and Georgiev, M.I. (2017). Chapter 11 - Terpenoids. In: Badal, S. and Delgoda, R. *Pharmacognosy: Fundamentals, Applications and Strategies*. Oxford: Elsevier. pp. 233-266.
- Luo, P., Peng, P., Gleixner, G., Zheng, Z., Pang, Z. and Ding, Z. (2011). Empirical relationship between leaf wax *n*-alkane δD and altitude in the Wuyi, Shennongjia and Tianshan Mountains, China: implications for paleoaltimetry. *Earth and Planetary Science Letters*. 301. Pp. 285–296.
- Luteyn J. L., Cleef, A.M. and Rangel, J.O. (1992). Plant Diversity in Paramo: Towards a checklist of paramo and a generic flora in paramo. In: Balslev, H. and Luteyn, J.L. (Eds.). *Paramo: An Andean ecosystem under human influence*. Academic Press, San Diego. Pp. 71-84.

- Luteyn, J.L. (1999). *Páramos: A Checklist of Plant Diversity, Geographical Distribution, and Botanical Literature*. New York Botanical Garden Press, Brooklyn, NY.
- Luz, B., Barkan, E., Yam, R. and Shemesh, A. (2009). Fractionation of oxygen and hydrogen isotopes in evaporating water. *Geochimica et Cosmochimica Acta*. 73. Pp. 6697–6703.
- Madriñán, S., Cortés, A.J. and Richardson, J.E. (2013). Páramo is the world's fastest evolving and coolest biodiversity hotspot. *Frontiers in Genetics*. 4. Pp. 1–7.
- Maffei, M., Badino, S., and Bossi, S. (2004). Chemotaxonomic significance of leaf wax n-alkanes in the Pinales (Coniferales). *Journal of Biological Research*. 1. Pp. 3-19.
- Maffei, M., Meregalli, M. and Scannerini, S. (1997). Chemotaxonomic significance of surface wax n-alkanes in the Cactaceae. *Biochemical Systematics and Ecology*. 24(6). Pp. 241-253.
- Magrin, G.O., Marengo, J.A., Boulanger, J.-P., Buckeridge, M.S., Castellanos, E., Poveda, G., Scarano, F.R. and Vicuña, S. (2014). Central and South America. In: *Climate Change 2014: Impacts, Adaptation, and Vulnerability. Part B: Regional Aspects. Contribution of Working Group II to the Fifth Assessment Report of the Intergovernmental Panel on Climate Change*. [Barros, V.R., Field, C.B., Dokken, D.J., Mastrandrea, M.D., Mach, K.J., Bilir, T.E., Chatterjee, M., Ebi, K.L., Estrada, Y.O., Genova, R.C., Girma, B., Kissel, E.S., Levy, A.N., MacCracken, S., Mastrandrea, P.R. and White, L.L. (eds.)]. Cambridge University Press, Cambridge, United Kingdom and New York, NY, USA. pp. 1499-1566.
- Makou, M.C., Hughen, K.A., Xu, L., Sylva, S.P. and Eglinton, T.I. (2007). Isotopic records of tropical vegetation and climate change from terrestrial vascular plant biomarkers preserved in Cariaco Basin sediments. *Organic Geochemistry*. 38. Pp. 1680-1691.
- Mann, M.E., Zhang, Z., Bradley, R.S., Hughes, M.K., Shindell, D., Ammann, C., Faluvegi, G. and Ni, F. (2009). Global Signatures and Dynamical Origins of the Little Ice Age and Medieval Climate Anomaly. *Science*. 326. Pp. 1256-1260.
- Mantilla, G., Oliveros, H. and Barnston, A.G. (2009). The role of ENSO in understanding changes in Colombia's annual malaria burden by region, 1960-2006. *Malaria Journal*. 8(6). Pp. 1-11.
- Marchant, R. and Hooghiemstra, H. (2004). Rapid environmental change in African and South American tropics around 4000 years before present: a review. *Earth Science Reviews*. 66. Pp. 217-260.

- Marchant, R.A., Behling, H., Berrio, J.C., Cleef, A.M., Duivenvoorden, J., Hooghiemstra, H., Kuhry, P., Melief, A.B.M., van Geel, B., Van der Hammen, T., Van Reenen, G. and Wille, M. (2001). Mid- to late Holocene pollen based biome reconstructions for Colombia: a regional reconstruction. *Quaternary Science Reviews*. 20. Pp. 1289 – 1308.
- Marengo, J. (2004). Interdecadal and long-term rainfall variability in the Amazon basin. *Theoretical and Applied Climatology*. 78. Pp. 79–96.
- Marengo, J.A., Tomasella, J., Alves, L.M., Soares, W.R. and Rodriguez, D.A. (2011). The drought of 2010 in the context of historical droughts in the Amazon region. *Geophysical Research Letters*. 38(12). Pp. 1-5. (L12703).
- Marques, J., Santos, J.M., Villa Nova, N.A. and Salati, E. (1977). Precipitable water and water vapour flux between Belem and Manaus. *Acta Amazonica*. 7(3). Pp. 355-362.
- Martin, L., Bertaux, J., Correge, T. et al. (1997). Astronomical forcing of contrasting rainfall changes in tropical South America between 12,400 and 8800 cal yr B.P. *Quaternary Research*. 47. Pp. 117-122.
- Martinelli, L.A., Piccolo, M.C., Townsend, A.R., Vitousek, P.M., Cuevas, E., McDowell, W., Robertson, G.P., Santos, O.C. and Treseder, K. (1999). Nitrogen stable isotopic composition of leaves and soil: Tropical versus temperate forests. *Biogeochemistry*. 46. Pp. 45–65.
- Martinson, D.G; Pisias, N.G., Hays, J.D., Imbrie, J.D., Moore, T.C., Shackleton and Nicholas, J. (1987). (Table 2) SPECMAP stack of stable oxygen isotopes covering the last 300 000 years. *PANGAEA*. <https://doi.org/10.1594/PANGAEA.56039>.
- Marzi, R., Torkelson, B.E. and Olson, R.K. (1993). A revised carbon preference index. *Organic Geochemistry*. 20. Pp. 1303-1306.
- Mayewski, P.A., Rohling, E.E., Stager, J.C. et al. (2004). Holocene climate variability. *Quaternary Research*. 62. Pp. 243-255.
- McCarroll, D. and Loader, N.J. (2004). Stable isotopes in tree rings. *Quaternary Science Reviews*. 23. Pp. 771-801.
- McDermott, F., Schwarcz, H.P. and Rowe, P.J. (2006). Isotopes in speleothems. In: Leng, M.J. (Ed.). *Isotopes in Palaeoenvironmental Research, 10. Developments in Palaeoenvironmental Research*. Springer, Dordrecht, the Netherlands. Pp. 185–225.

- McInerney, F.A., Helliker, B.R. and Freeman, K.H. (2011). Hydrogen isotope ratios of leaf wax n-alkanes in grasses are insensitive to transpiration. *Geochimica et Cosmochimica Acta*. 75. Pp. 541–554.
- McKinney, C.R., McCrea, J.M., Epstein, S., Allen, H.A. and Urey, H.C. (1950). Improvements in mass-spectrometers for the measurement of small differences in isotope abundance ratios. *Review of Scientific Instruments*. 21. Pp. 724–30.
- McMullen, J.A., Barber, K.E. and Johnson, B. (2004). A paleoecological perspective of vegetation succession on raised bog microforms. *Ecological Monographs*. 74. Pp. 45–77.
- Melander, L. (1960). *Isotope Effects on Reaction Rates*. New York: Roland.
- Melillo, J.M., Houghton, R.A., Kicklighter, D.W. and McGuire, A.D. (1996). Tropical deforestation and the global carbon budget. *Annual Review of Energy and the Environment*. 21. pp.293-310.
- Menot, G. and Burns, S.J. (2001). Carbon isotopes in ombrogenic peat bog plants as climatic indicators: calibration from an altitudinal transect in Switzerland. *Organic Geochemistry*. 32. Pp. 233–245.
- Merah, O., Deleens, E., Souyris, I. and Monneveux, P. (2000). Effect of glaucousness on carbon isotope discrimination and grain yield in Durum wheat. *Journal of Agronomy and Crop Science*. 185. Pp. 259-265.
- Merlivat, L. and Jouzel, J. (1979). Global climatic interpretation of the deuterium-oxygen 18 relationship for precipitation. *Journal of Geophysical Research*. 84. Pp. 5029–5033.
- Meyers, P. (1997). Organic geochemical proxies of paleoceanographic, paleolimnologic and paleoclimatic processes. *Organic Geochemistry*. 27 (5/6). Pp. 213-250.
- Meyers, P.A. (1994). Preservation of elemental and isotopic source identification of sedimentary organic matter. *Chemical Geology*. 114. Pp. 289– 302.
- Mimura, M.R.M., Salatino, M.L.F., Salatino, A. and Baumgratz, J.F.A. (1998). Alkanes from foliar epicuticular waxes of *Huberia* species: Taxonomic implications. *Biochemical Systematics and Ecology*. 26. Pp. 581-588.
- Mix, A.C., Bard, E. and Schneider, R. (2001). Environmental processes of the ice age: Land, oceans, glaciers (EPILOG). *Quaternary Science Reviews*. 20. Pp. 627-658.

Molion, L.C.B. (1987). *Micro-meteorology of an Amazonian rain-forest. The Geo-Physiology of Amazonia; vegetation and climate interactions* (R. E. Dickinson, ed.). John Wiley for the U.N. University, New-York. Chapter 14: pp. 255–270.

Mook, W.G. (2001). Environmental Isotopes in the Hydrological Cycle: Principles and Applications. Volume 1. *International Atomic Energy Agency*. http://www-naweb.iaea.org/naweb/ih/documents/global_cycle/Environmental%20Isotopes%20in%20the%20Hydrological%20Cycle%20Vol%201.pdf.

Moore, M., Kuang, Z. and Blossey, P.N. (2014). A moisture budget perspective of the amount effect. *Geophysical Research Letters*. 41. Pp. 1329-1335.

Mora-Perez, H., Mencin, D.J., Molnar, P., Diederix, H., Cardona-Piedrahita, L., Palaez-Gavrida, J-R. and Corchelo-Cuervo, Y. (2016). GPS velocities and the construction of the Eastern Cordillera of the Colombian Andes. *Geophysical Research Letters*. 48. Pp. 8407–8416.

Moron, V., Bigot, S. and Roucou, P. (1995). Rainfall variability in subequatorial America and Africa and relationships with the main sea-surface temperature modes (1951–1990). *International Journal of Climatology*. 15. Pp. 1297–1322.

Mosblech, N.A.S., Bush, M.B., Gosling, W.D., Hodell, D., Thomas, L., van Calsteren, P. et al. (2012). North Atlantic forcing of Amazonian precipitation during the last ice age. *Nature Geoscience*. 5. Pp. 817-820.

Moura, A.D. and Shukla, J. (1981). On the dynamics of droughts in northeast Brazil - Observations, theory and numerical experiments with a general-circulation model. *Journal of Atmospheric Science*. 38. Pp. 2653–2675.

Myers, N., Mittermeier, R.A., Mittermeier, C.G., Da Fonseca, G.A. and Kent, J. (2000). Biodiversity hotspots for conservation priorities. *Nature*. 403. Pp. 853–858.

Myster, R.W. (2017). Introduction. In: Myster, R.W. *Forest structure, function, and dynamics in Western Amazonia*. Chichester, West Sussex: John Wiley & Sons. pp. 1-25.

Nadelhoffer, K.J. and Fry, B. (1988). Controls on natural Nitrogen-15 and Carbon-13 abundances in forest soil organic matter. *Soil Science Society of America*. 52. Pp. 1633–1640.

National Research Council (1986). *Global Change in the Geosphere-Biosphere*. 91. National Academy Press. Washington DC.

- Newell, R.E. and Gould-Stewart, S. (1981). A stratospheric fountain? *Journal of Atmospheric Science*. 38. Pp. 2789-2796.
- Nicholls, J., Booth, R.K., Jackson, S.T., Pendall, E.G. and Huang, Y. (2010). Differential hydrogen isotope ratios of Sphagnum and vascular plant biomarkers in ombrotrophic peatlands as a quantitative proxy for precipitation-evaporation balance. *Geochimica et Cosmochimica Acta*. 74. Pp. 1407-1416.
- Nichols J.E., Booth R.K., Jackson S.T., Pendall E.G. and Huang Y. (2006). Paleohydrologic reconstruction based on n-alkane distributions in ombrotrophic peat. *Organic Geochemistry*. 37. Pp. 1505– 1513.
- Nichols, J.E., Walcott, M., Bradley, R., Pilcher, J. and Huang, Y. (2009). Quantitative assessment of precipitation seasonality and summer surface wetness using ombrotrophic sediments from an Arctic Norwegian peatland. *Quaternary Research*. 72. Pp. 443–451.
- Niedermeier, E.M., Forrest, M., Beckmann, B. et al. (2016). The stable hydrogen isotopic composition of sedimentary plant waxes as quantitative proxy for rainfall in the West African Sahel. *Geochimica et Cosmochimica Acta*. 184. Pp. 55-70.
- Niedermeier, E.M., Schfuss, E., Sessions, A.L. et al. (2010). Orbital- and millennial-scale changes in the hydrologic cycle and vegetation in the western African Sahel: insights from individual plant wax δD and $\delta^{13}C$. *Quaternary Science Reviews*. 29. (23-24). Pp. 2996-3005.
- Nobre, P. and Shukla, J. (1996). Variations of sea surface temperature, wind stress and rainfall over the tropical Atlantic and South America. *Journal of Climate*. 9. Pp. 2464–2479.
- Nogues-Paegle, J. and Mo, K.C. (1997). Alternating wet and dry conditions over South America during summer. *Monthly Weather Review*. 125. Pp. 279-291.
- Nott, C.J., Xie, S., Avsejs, L.A., Maddy, D., Chambers, F.M. and Evershed, R.P. (2000). n-Alkane distributions in ombrotrophic mires as indicators of vegetation change related to climatic variation. *Organic Geochemistry*. 31. Pp. 321-235.
- O’Leary, M.H. (1988). Carbon isotopes photosynthesis – fractionation techniques may reveal new aspects of carbon dynamics in plants. *BioScience*. 38. Pp. 328–336.
- Oki, T. and Kanae, S. (2006). Global Hydrological Cycles and World Water Resources. *Science*. 313. pp. 1068-1072.

- Olsson, I.U. (1970). The use of Oxalic acid as a Standard. In: Olsson, IU. Ed. *Radiocarbon Variations and Absolute Chronology*. Nobel symposium, 12th Proc: New York, John Wiley & Sons.
- Page, S.E., Wust, R.A.J., Weiss, D., Riely, J.O., Shotyk, W. and Limin, S.H. (2004). A record of Late Pleistocene and Holocene carbon accumulation and climate change from an equatorial peat bog (Kalimantan, Indonesia): implications for past, present and future carbon dynamics. *Journal of Quaternary Science*. 19(7). Pp. 625-635.
- Pancost, R.D., Baas, M., van Geel, B. and Damsté, J.S.S. (2003). Response of an ombrotrophic bog to a regional climate event revealed by macrofossil, molecular and carbon isotopic data. *The Holocene*. 13(6). Pp. 921–932.
- Parnell, A., Haslett, J., Allen, J., Buck, C., and Huntley, B. (2008). A flexible approach to assessing synchronicity of past events using Bayesian reconstructions of sedimentation history. *Quaternary Science Reviews*. 27(19-20). Pp. 1872–1885.
- Pedentchouk, N., Sumner, W., Tipple, B. and Pagani, M. (2008). $\delta^{13}\text{C}$ and δD compositions of *n*-alkanes from modern angiosperms and conifers: an experimental set up in central Washington State, USA. *Organic Geochemistry*. 39. Pp. 1066–1071.
- Peters, K.E., Walters, C.C. and Moldowan, J.M. (2005). *The Biomarker Guide*. Cambridge University Press, Cambridge, UK.
- Peterson, L.C., Haug, G.H., Hughen, K.A. and Röhl, U. (2001). Rapid changes in the hydrologic cycle of the tropical Atlantic during the last glacial. *Science*. 290. Pp. 1947–1951.
- Petit, J.R., Jouzel, J., Raynaud, D., Barkov, N.I., Barnola, J.M. et al. (1999). Climate and atmospheric history of the past 420,000 years from the Vostok ice core, Antarctica. *Nature*. 399. Pp. 429-436.
- Pigati, J.S., Quade, J., Wilson, J., Jull, A.J.T. and Lifton, N.A. (2007). Development of low-background vacuum extraction and graphitization systems for ^{14}C dating of old (40–60 ka) samples. *Quaternary International*. 166. Pp. 4–14.
- Piotrowska, N., Blaauw, M., Mauquoy, D. and Chambers, F.M. (2011). Constructing deposition chronologies for peat deposits using radiocarbon dating. *Mires and Peat*. 7(10). Pp. 1-14.

- Poage, M.A. and Chamberlain, C.P. (2001). Empirical relationships between elevation and the stable isotope composition of precipitation and surface waters: considerations for studies of paleoelevation change. *American Journal of Science*. 301. Pp. 1-15.
- Polissar, P.J. and Freeman, K.H. (2010). Effects of aridity and vegetation on plant-wax δD in modern lake sediments. *Geochimica et Cosmochimica Acta*. 74. Pp. 5785-5797.
- Polissar, P.J., Abbott, M.B., Wolfe, A.P., Bezada, M., Rull, V. and Bradley, R.S. (2006). Solar modulation of Little Ica Age climate in the tropical Andes. *PNAS*. 103(24). Pp. 8937-8942.
- Polissar, P.J., Abbott, M.B., Wolfe, A.P., Vuille, M. and Bezada, M. (2013). Synchronous interhemispheric Holocene climate trends in the tropical Andes. *PNAS*. 110. (36). Pp. 14551-14556.
- Poveda G. and Mesa O.J. (1997). Feedbacks between hydrological processes in tropical South America and large-scale ocean atmospheric phenomena. *Journal of Climate*. 10. pp. 2690–2702.
- Poveda, G. and Mesa, O.J. (2000). On the existence of Llor (the rainiest locality on Earth): Enhanced ocean-atmosphere-land interaction by a low-level jet. *Geophysical Research Letters*. 27(11). Pp. 1675-1678.
- Poveda, G., Alvarez, D. M., and Rueda, O. (2011). A Hydro-climatic variability over the Andes of Colombia associated with ENSO: a review of climatic processes and their impact on one of the Earth's most important biodiversity hotspots, *Climate Dynamics*. 36. 2233–2249.
- Poveda, G., Jaramillo, A., Gil, M., Quiceno, N. and Mantilla, R. (2001). Seasonality in ENSO-related precipitation, river discharges, soil moisture, and vegetation index in Colombia. *Water Resources Research*. 37(8). Pp. 2169-2178.
- Poynter, J.G. and Eglinton, G. (1990). Molecular composition of three sediments from hole 717C: The Bengal Fan: In: Cochran, J.R., Stow, D.A.V. et al. (eds.). *Proceedings of the Ocean Drilling Program Scientific Results*. Vol. 116. Pp. 155-161.
- Poynter, J.G., Farrimond, P., Robinson, N., Eglinton, G. (1989). Aeolian-derived higher plant lipids in the marine sedimentary record: links with paleoclimate. In: Leinen, M., Sarnthein, M. (Eds.). *Paleoclimatology and Paleometeorology: Modern and Past Patterns of Global Atmospheric Transport*. Dordrecht (Kulwer Academic), Hingham, Mass. Pp. 435-462.

- Ramirez, E., Hoffmann, G., Taupin, J., Francou, B., Ribstein, P., Caillon, N., Ferron, F., Landais, A., Petit, J. and Pouyaud, B. (2003). A new Andean deep ice core from Nevado Illimani (6350 m), Bolivia. *Earth and Planetary Science Letters*. 212. Pp. 337–350.
- Rao, Z., Zhu, Z., Wang, S., Jia, G., Quiang, M. and Wu, Y. (2009). CPI values of terrestrial higher plant-derived long-chain n-alkanes: a potential paleoclimatic proxy. *Frontiers of Earth Science in China*. 3(3). Pp. 266-272.
- Rao, Z.G., Jia, G.D., Zhu, Z.Y., Wu, Y. and Zhang, J.W. (2008). Comparison of the carbon isotope composition of total organic carbon and long-chain n-alkanes from surface soils in eastern China and their significance. *Chinese Science Bulletin*. 53. Pp. 3921–3927.
- Rasmussen, S.O., Anderson, K.K., Svensson, A.M., Steffensen, J.P., Vinther, B.M., Clausen, H.B. et al. (2006). A new Greenland ice core chronology for the last glacial termination. *Journal of Geophysical Research*. 111(6). doi:10.1029/2005JD006079.
- Rasmusson, E.M. and Mo, K. (1993). Linkages between 200mb tropical and extratropical circulation anomalies during the 1986-1989 ENSO cycle. *Journal of Climate*. 6. Pp. 595-616.
- Raval, A. and Ramanathan, V. (1989). Observational determination of the greenhouse effect. *Nature*. 342. Pp. 758-761.
- Reimer, P.J., Bard, E., Bayliss, A., Beck, J.W., Blackwell, P.G., Bronk Ramsey, C., Buck, C.E., Edwards, R.L., Friedrich, M., Grootes, P.M., Guilderson, T.P., Hafliðason, H., Hajdas, I., Hatté, C., Heaton, T.J., Hoffmann, D.L., Hogg, A.G., Hughen, K.A., Kaiser, K.F., Kromer, B., Manning, S.W., Niu, M., Reimer, R.W., Richards, D.A., Scott, M.E., Southon, J.R., Turney, C.S.M., van der Plicht, J. (2013). IntCal13 and Marine13 radiocarbon age calibration curves 0-50,000 yr cal BP. *Radiocarbon* 55(4). Pp. 1869-1887.
- Restrepo, J.D. and Kjerfve, B. (2000). Magdalena river: interannual variability (1975-1995) and revised water discharge and sediment load estimates. *Journal of Hydrology*. 235. Pp. 137-149.
- Reuter, J., Stott, L., Khider, D. et al. (2009). A new perspective on the hydroclimate variability in northern South America during the Little Ice Age. *Geophysical Research Letters*. 36. (L21706). doi:10.1029/2009GL041051.
- Rice, S.K. (2000). Variation in carbon isotope discrimination within and among *Sphagnum* species in a temperate wetland. *Oecologia*. 123. Pp. 1–8.

- Riederer, M. (2006). Introduction: biology of the plant cuticle. In: Riederer, M. and Muller, C. *Biology of the Plant Cuticle*. Blackwell Publishing Ltd, Oxford.
- Rieley, G., Collier, R.J., Jones, D.M. and Eglinton, G. (1991). The biogeochemistry of Ellesmere Lake, UK— I: source correlation of leaf wax inputs to the sedimentary lipid record. *Organic Geochemistry*. 17. Pp. 901–912.
- Risi, C., Bony, S. and Vimeux, F. (2008). Influence of convective processes on the isotopic composition ($\delta^{18}\text{O}$ and δD) of precipitation and water vapor in the Tropics, Part 2: physical interpretation of the amount effect. *Journal of Geophysical Research*. 113. doi:10.1029/2008JD009943.
- Roden, J.S., Lin, G. and Ehleringer, J.R. (2000). A mechanistic model for interpretation of hydrogen and oxygen isotope ratios in tree-ring cellulose. *Geochimica et Cosmochimica Acta*. 64. Pp. 21–35.
- Rommerskirchen, F., Eglinton, G., Dupont, L., Gunter, U., Wenzel, C. and Rullkotter, J. (2003). A north to south transect of Holocene southeast Atlantic continental margin sediments: relationships between aerosol transport and compound-specific d^{13}C land plant biomarker and pollen records. *Geochemistry Geophysics Geosystems*. 4. Pp. 1–29.
- Ronchail J, Cochonneau G, Molinier M, Guyot JL, Chaves AGD, Guimaraes V, de Oliveira E (2002) Interannual rainfall variability in the Amazon basin and sea-surface temperatures in the equatorial Pacific and the tropical Atlantic Oceans. *International Journal of Climatology*. 22. Pp. 1663–1686.
- Ropelewski, C.F. and Halpert, M.S. (1987). Global and regional scale precipitation associated with the El-Nino southern oscillation. *Monthly Weather Review*. 115. Pp. 1606–1626.
- Rose, T.P., Davisson, M.L. and Criss, R.E. (1996). Radiocarbon in hydrologic systems containing dissolved magmatic carbon dioxide. *Science*. 273. Pp. 1367-1370.
- Rozanski, K., Araguas-Araguas, L. and Gonfiantini, R. (1993). Isotopic patterns in modern global precipitation. In: *Climate Change in Continental Isotopic Records, Geophysical Monograph*. American Geophysical Union, Washington DC.
- Rozanski, K., Sonntag, C. and Munnich, K.O. (1982). Factors controlling stable isotope composition of European precipitation. *Tellus*. 34. Pp. 142-150.

- Rubenstein, D.R. and Hobson, K.A. (2004). From birds to butterflies: animal movement patterns and stable isotopes. *Trends in Ecology and Evolution*. 19(5). Pp. 256-263.
- Rull, V. (1998). Biogeographical and evolutionary considerations of *Mauritia* (Arecaceae), based on palynological evidence. *Review of Palaeobotany and Palynology*. 100. Pp. 109–122.
- Rull, V. and Montoya, E. (2014). *Mauritia flexuosa* palm swamp communities: natural or human-made? A palynological study of the Gran Sabana region (northern South America) within a neotropical context. *Quaternary Science Reviews*. 99. Pp. 17-33.
- Rutherford, M.C., Mucina, L. and Powrie, L.W. (2006). Biomes and Bioregions of Southern Africa. *Trelitzia*. 19. Pp. 31-51.
- Sachse, D., Billault, I., Bowen, G.J., Chikaraishi, Y., Dawson, T.E., Feakins, S.J., Freeman, K.H., Magill, C.R., McInerney, F.A., van der Meer, M.T.J., Polissar, P., Robins, R.J., Sachs, J.P., Schmidt, H.-L., Sessions, A.L., White, J.W.C., West, J.B. and Kahmen, A. (2012). Molecular paleohydrology: interpreting the hydrogen-isotopic composition of lipid biomarkers from photosynthesizing organisms. *Annual Review of Earth and Planetary Sciences*. 40 (1). Pp. 221–249.
- Sachse, D., Gleixner, G., Wilkes, H. and Kahmen, A. (2010). Leaf wax n-alkane δD values of field-grown barley reflect leaf water δD values at the time of leaf formation. *Geochimica et Cosmochimica Acta*. 74. Pp. 6741–6750.
- Sachse, D., Kahmen, A. and Gleixner, G. (2009). Significant seasonal variation in the hydrogen isotopic composition of leaf-wax lipids for two deciduous tree ecosystems (*Fagus sylvatica* and *Acer pseudoplatanus*). *Organic Geochemistry*. 40. Pp. 732-742.
- Sachse, D., Radke, J. and Gleixner, G. (2004). Hydrogen isotope ratios of recent lacustrine sedimentary n-alkanes record modern climate variability. *Geochimica et Cosmochimica Acta*. 68. Pp. 4877-4887.
- Sachse, D., Radke, J. and Gleixner, G. (2006). δD values of individual n-alkanes from terrestrial plants along a climatic gradient—implications for the sedimentary biomarker record. *Organic Geochemistry*. 37. Pp. 469–83.
- Salati, E. (1985). The climatology and hydrology of Amazonia. In: Prance, G.T. and Lovejoy, T.E. (eds). *Amazonia*. Pergamon Press, Ltd, Oxford, UK, pp. 18–48.

- Salati, E., Dallolio, A., Matsui, E. and Gat J.R. (1979). Recycling of water in the Amazon Basin – isotopic study. *Water Resources Research*. 15. Pp. 1250–1258.
- Salati, E., Sylvester-Bradley, R. and Victoria, R.L. (1982). Regional gains and losses of nitrogen in the Amazon Basin. *Plant and Soil*. 67. Pp. 367–376.
- Sanchez, A., Posada, J.M. and Smith, W.K. (2014). Dynamic Cloud Regimes, Incident Sunlight, and Leaf Temperatures in *Espeletia grandiflora* and *Chusquea tessellata*, Two Representative Species of the Andean Páramo, Colombia. *Arctic, Antarctic and Alpine Research*. 46(2). Pp. 371-378.
- Santos, G.M., Moore, R.B., Southon, J.R., Griffin, S., Hinger, E. and Zhang, D. (2007). AMS ¹⁴C sample preparation at the KCCAMS/UCI facility: status report and performance of small samples. *Radiocarbon*. 49(2). Pp. 255-269.
- Sauer, P.E, Eglinton, T.I., Hayes, J.M., Schimmelmann, A. and Sessions, A.L. (2001). Compound-specific D/H ratios of lipid biomarkers from sediments as a proxy for environmental and climatic conditions. *Geochimica et Cosmochimica Acta*. 65. Pp. 213–222.
- Saurer, M., Robertson, I., Siegwolf, R. and Leuenberger, M. (1998). Oxygen isotope analysis of cellulose: an interlaboratory comparison. *Analytical Chemistry*. 70. Pp. 2074–2080.
- Saylor, J.E., Mora, A., Horton, B.K. and Nie, J. (2009). Controls on the isotopic composition of surface water and precipitation in the Northern Andes, Colombian Eastern Cordillera. *Geochimica et Cosmochimica Acta*. 73. Pp. 6999-7018.
- Schefuß, E., Kuhlmann, H., Mollenhauer, G., Prange, M. and Patzold, J. (2011). Forcing of south-east African wet phases during the last 17,000 years. *Nature*. 480(7378). Pp. 509-512
- Schefuss, E., Schouten, S. and Schneider, R.R. (2005). Climatic controls on central African hydrology during the past 20,000 years. *Nature*. 437(13). Pp. 1003-1006.
- Scheigl, W.E. (1972). Deuterium Content of Peat as a Paleoclimatic Recorder. *Science*. 175. Pp. 512-513.
- Scheigl, W.E. and Vogel, J.C. (1980). Deuterium content of organic matter. *Earth Planetary Science Letters*. 7. Pp. 307-313.

- Schellekens, J. and Buurman, P. (2011). *n*-Alkane distributions as palaeoclimatic proxies in ombrotrophic peat: The role of decomposition and dominant vegetation. *Geoderma*. 164. Pp. 112-121.
- Schemmel, F., Niedermeyer, E.M., Koutsodendris, A., Pross, J., Fiebig, J. and Mulch, A. (2017). Paleohydrological changes in the Eastern Mediterranean region during the early to mid-Holocene recorded in plant wax *n*-alkane distributions and $\delta^{13}\text{C}_{\text{TOC}}$ – New data from Tenaghi Philippon, NE Greece. *Organic Geochemistry*. 110. Pp. 100-109.
- Schiegl, W. and Vogel, J. (1970). Deuterium content of organic matter. *Earth and Planetary Science Letters*. 7. Pp. 307–313.
- Schiegl, W. E. and Vogel, J. C. (1970). Deuterium content of organic matter. *Earth and Planetary Science Letters*. 7. Pp. 307-313.
- Schimmelmann, A., Sessions, A.L. and Mastalerz, M. (2006). Hydrogen isotopic (D/H) composition of organic matter during diagenesis and thermal maturation. *Annual Review of Earth and Planetary Science*. 34. Pp. 501–533.
- Schmidt, G.A., Hoffmann, G., Shindell, D.T. and Hu, Y. (2005). Modelling atmospheric stable water isotopes and the potential for constraining cloud processes and stratosphere-troposphere water exchange. *Journal of Geophysical Research*. 110. doi:10.1029/2005JD005790.
- Schneider, S.H. (1972). Cloudiness as a global climate feedback mechanism: The effects on the radiation balance and surface temperature of variations in cloudiness. *Journal of Atmospheric Science*. 29. Pp. 1413-1422.
- Schongart, J., Piedade, M.T.F., Ludwigshausen, S. et al. (2002). Phenology and stem-growth periodicity of tree species in Amazonian floodplain forests. *Journal of Tropical Ecology*. 18. Pp. 581-597.
- Schrag, D.P., Adkins, J.F., McIntyre, K., Alexander, J.L., Hodell, D.A., Charles, C.D. and McManus, J.F. (2002). The oxygen isotopic composition of seawater during the Last Glacial Maximum. *Quaternary Science Reviews*. 21. Pp. 331–342.
- Schreuder, L.T., Stuut, J-B. W., Sinninghe Damse, J.S. and Schouten, S. (2008). Aeolian transport and deposition of plant wax *n*-alkanes across the tropical North Atlantic Ocean. *Organic Geochemistry*. 115. Pp. 113-123.

- Schwark, L., Zink, K. and Lechterbeck, J. (2002). Reconstruction of postglacial to early Holocene vegetation history in terrestrial Central Europe via cuticular lipid biomarkers and pollen records from lake sediments. *The Geological Society of America*. 30(5). Pp. 463-466.
- Seltzer, G., Rodbell, D. and Burns, S. (2000). Isotopic evidence for late Quaternary climatic change in tropical South America. *Geology*. 28(1). Pp. 35-38.
- Seltzer, G.O. (1990). Recent glacial history and paleoclimate of the Peruvian-Bolivian Andes. *Quaternary Science Reviews*. 9. Pp. 137–152.
- Seluchi, M.E., Saulo, C., Nicolini, M. and Satyamurty, P. (2003). The northwestern Argentinean Low: a study of two typical events. *Monthly Weather Review*. 131. Pp. 2361–2378.
- Sessions, A.L. (2006). Isotope-ratio detection for gas chromatography. *Journal of Separation Science*. 29 (12). Pp. 1946-1961.
- Sessions, A.L. (2016). Factors controlling the deuterium contents of sedimentary hydrocarbons. *Organic Geochemistry*. 96. Pp. 43-64.
- Sessions, A.L., Burgoyne, T.W. and Hayes, J.M. (2001). Correction of H₃ + Contributions in Hydrogen Isotope Ratio Monitoring Mass Spectrometry. *Analytical Chemistry*. 73. Pp. 192-199.
- Sessions, A.L., Burgoyne, T.W., Schimmelmann, A. and Hayes, J.M. (1999). Fractionation of hydrogen isotopes in lipid biosynthesis. *Organic Geochemistry*. 30. Pp. 1193-1200.
- Sharp, Z. (2007). *Principles of Stable Isotope Geochemistry*. Pearson Prentice Hall, Upper Saddle River, New Jersey.
- Shepherd, T. and Griffiths, D.W. (2006). The effects of stress on plant cuticular waxes. *New Phytologist*. 171. Pp. 469–499.
- Shepherd, T. and Griffiths, D.W. (2006). The effects of stress on plant cuticular waxes. *New Phytologist*. 171. pp. 469-499.
- Sifeddine, A., Wirrmann, D., Albuquerque, A.L.S., Turcq, B., Cordeiro, R.C., Gurgel, M.H.C. and Abrao, J.J. (2004). Bulk composition of sedimentary organic matter used in palaeoenvironmental reconstructions: examples from the tropical belt of South America and Africa. *Palaeogeography, Palaeoclimatology, Palaeoecology*. 214. Pp. 41-53.

Siffeddine, A., Spadano-Albuquerque, A-L., Ledru, M-P, Turcq, B., Knoppers, B., Martin, L., Zamboni de Mello, W., Passenau, H. et al. (2003). A 21,000 cal years paleoclimatic record from Caco Lake, northern Brazil: evidence from sedimentary and pollen analyses. *Palaeogeography, Palaeoclimatology, Palaeoecology*. 189. Pp. 24-34.

Silva, R.S., Ribeiro, L.M., Mercadante-Simoes, M.O., Nunes, Y.R.F. and Lopez, P.S. N. (2014). Seed structure and germination in buriti (*Mauritia flexuosa*), the Swamp palm. *Flora*. 209. Pp. 674-685.

Silva, R.S., Ribeiro, L.M., Mercadante-Simoes, M.O., Nunes, Y.R.F. and Lopez, P.S.N. (2014). Seed structure and germination in buriti (*Mauritia flexuosa*), the Swamp palm. *Flora*. 209. Pp. 674-685.

Silvestri, G.E. and Vera, C.S. (2003). Antarctic Oscillation signal on precipitation anomalies over southeastern South America. *Geophysical Research Letters*. 30(21). Pp. 1-4.

Simoneit, B.R.T., Sheng, G., Chen, X., Fu, J., Zhang, J. and Xu, Y. (1991). Molecular marker study of extractable organic matter in aerosols from urban areas in China. *Atmospheric Environment*. 25 (10). Pp. 2111-2129.

Sinninghe-Damste, J.S., Verschuren, D., Ossebaar, J., Blokker, J., van Houten, R., van der Meer, M.T.J., Plessen, B. and Schouten, S. (2011). A 25,000 year record of climate-induced changes in lowland vegetation of eastern equatorial Africa revealed by the stable carbon-isotopic composition of fossil plant leaf waxes. *Earth and Planetary Science Letters*. 302. Pp. 236-246.

Skrzypek, G., Jezierski, P. and Szyrkiewicz, A. (2010). Preservation of primary stable isotope signatures of peat-forming plants during early decomposition – observation along an altitudinal transect. *Chemical Geology*. 273. Pp. 238–249.

Skrzypek, G., Kaluzny, A., Wojtun, B. and Jedrysek, M-O. (2007). The carbon stable isotopic composition of mosses: A record of temperature variation. *Organic Geochemistry*. 38. Pp. 1770–1781.

Smith, B. and Epstein, S. (1970). Biogeochemistry of the stable isotopes of hydrogen and carbon in salt marsh biota. *Plant Physiology*. 46. Pp. 738–742.

Smith, F.A. and Freeman, K.H. (2006). Influence of physiology and climate on δD of leaf wax n-alkanes from C3 and C4 grasses. *Geochimica et Cosmochimica Acta*. 70. Pp. 1172–1187.

- Solman, S.A. (2013). Regional Climate Modelling over South America: A Review. *Advances in Meteorology*. Pp. 1-13.
- Sonibarea, M.A., Jayeolab, A.A. and Egunyomib, A. (2005). Chemotaxonomic significance of leaf alkanes in species of *Ficus* (Moraceae). *Biochemical Systematics and Ecology*. 33. Pp. 79-86.
- Stansell, N.D., Polissar, P.J. and Abbott, M.B. (2007). Last glacial maximum-equilibrium line altitude and paleo-temperature reconstructions for the Cordillera de Mérida, Venezuelan Andes. *Quaternary Research*. 67. Pp. 115-127.
- Sternberg, L., De Niro, M. and Savidge, R. (1986). Oxygen isotope exchange between metabolites and water during biochemical reactions leading to cellulose synthesis. *Plant Physiology*. 82. Pp. 423–427.
- Stevenson, F.J. (1966). Lipids in soil. *Journal of the American Oil Chemists' Society*. 43(4). Pp. 203-210.
- Stewart, M.K. (1975). Stable isotope fractionation due to evaporation and isotopic exchange of falling water drops: Applications to atmospheric processes and evaporation of lakes. *Journal of Geophysical Research*. 80 (9). Pp. 1133-1146.
- Stiles, G.F., Rosselli, L. and De La Zerda, S. (2017). Changes over 26 Years in the Avifauna of the Bogota Region, Colombia: Has Climate Change Become Important?. *Frontiers in Ecology and Evolution*. 5 (58). Pp. 1-21.
- Stocker, T. (2014). *Climate change 2013: the physical science basis: Working Group I contribution to the Fifth assessment report of the Intergovernmental Panel on Climate Change*. Cambridge University Press.
- Stuiver, M. and Polach, H.A. (1977). Radiocarbon – discussion of reporting ^{14}C data. *Radiocarbon*. 19(3). pp. 355-363.
- Stuiver, M., Reimer, P.J., and Reimer, R.W. (2018). CALIB 7.1 [WWW program] at <http://calib.org>. Accessed 2018-12-4.
- Sturm, C., Hoffmann, G. and Langmann, B. (2007). Simulation of the stable water isotopes in precipitation over South America: Comparing regional to global circulation models. *Journal of Climate*. 20. Pp.3730–3750.

- Summons, R.E., Freeman, K.H., Grice, K. and Pancost, R.D. (2008). Where would we be without the isotopes? *Organic Geochemistry*. 39. Pp. 483–484.
- Sun, Q., Xie, M., Shi, L., Zhang, Z., Lin, Y., Shang, W., Wang, K., Li, W., Liu, J., and Chu, G. (2013). Alkanes, compound-specific carbon isotope measures and climate variation during the last millennium from varved sediments of Lake Xiaolongwan, northeast China. *Journal of Paleolimnology*. 50. Pp. 331-344.
- Tao, X., Liu, Y., Wang, Y., Qiu, Y., Lin, J., Zhao, A., Su, M. and Jia, W. (2008). GC-MS with ethyl chloroformate derivatization for comprehensive analysis of metabolites in serum and its application to human uremia. *Analytical and Bioanalytical Chemistry*. 391. Pp. 2881-2889.
- Taylor, A.K., Benedetti, M.M., Haws, J.A. and Lane, C.S. (2018). Mid-Holocene Iberian hydroclimate variability and palaeoenvironmental change: molecular and isotopic insights from Praia Rei Cortico, Portugal. *Journal of Quaternary Science*. 33(1). Pp. 79-92.
- Tedesco, K., Thunell, R., Astor, Y. and Muller-Karger, F. (2007). The oxygen isotope composition of planktonic foraminifera from the Cariaco Basin, Venezuela: Seasonal and interannual variations. *Marine Micropaleontology*. 62. Pp. 180-193.
- ter Steege, H., Pitman, N.C.A., Sabatier, D., Baraloto, C., Salomao, R.P., Guevara, J.E., Phillips, O.L., Castilho, C.V., Magnusson, W.E., Molino, J-F., Monteagudo, A., Núñez Vargas, P., Montero, J.C., Feldpausch, T.R., Honorio Coronado, E.N., Killeen, T.J., Mostacedo, B., Vasquez, R., Assis, R.L., Terborgh, J., Wittmann, F. et al. (2013). Hyperdominance in the Amazonian tree flora. *Science*. 342. (1243092). Doi: <http://dx.doi.org/10.1126/science.1243092>.
- Thompson L.G. and Davis, M.E. (2007). ICE CORE RECORDS: South America. *Encyclopedia of Quaternary Science*. Pp. 1233-1242.
- Thompson, D.W.J. and Wallace, J.M. (2000). Annular modes in the extratropical circulation. Part I: month-to-month variability. *Journal of Climate*. 13. Pp. 1000–1016.
- Thompson, L.G., Moseley-Thompson, E., Vavis, M.E., Lin, P-N., Henderson, K.A., Cole-Dai, J., Bolzan, J.F. and Liu, K-B. (1995). Late Glacial Stage and Holocene Tropical Ice Core Records from Huascarán, Peru. *Science*. 269 (5220). Pp. 46-50.
- Thompson, L.G., Mosley-Thompson, E., and Henderson, K. (2000). Ice-core palaeoclimate records in tropical South America since the Last Glacial Maximum. *Journal of Quaternary Science*. 15(4). Pp. 377-394.

- Thompson, L.G., Mosley-Thompson, E., Davis, M.E., Lin, P.N., Henderson, K.A. and Mashiotta, T.A. (2003). Tropical glacier and ice core evidence of climate change on annual to millennial time scales. *Climatic Change*. 59. pp. 137–155.
- Thompson, L.G., Mosley-Thompson, E., Davis, M.E., Lin, P.N., Henderson, K.A., Cole-Dai, J., Bolzon, J.F. and Liu, K.B. (1995). Late glacial stage and Holocene tropical ice core records from Huascarán, Peru. *Science*. 269. Pp. 46–50.
- Thompson, L.G., Thompson, E.M., Dansgaard, W. and Groot, P.M. (1986). The Little Ice Age as recorded in the stratigraphy of the tropical Quelccaya Ice Cap. *Science*. 234. Pp. 361–364.
- Tierney, J.E., Russell, J.M. Huang, Y. (2010). A molecular perspective on Late Quaternary climate and vegetation change in the Lake Tanganyika basin, East Africa. *Quaternary Science Reviews*. 29. Pp. 787–800.
- Tierney, J.E., Smerdon, J.E., Anchukaitis, K.J. and Seager, R. (2013). Multidecadal variability in East African hydroclimate controlled by the Indian Ocean. *Nature*. 493. Pp. 389–392.
- Tipple B.J. and Pagani M. (2013). Environmental control on eastern broadleaf forest species' leaf wax distributions and D/H ratios. *Geochimica et Cosmochimica Acta*. 111. Pp. 64–77.
- Tipple, B.J. and Pagani, M. (2010). A 35 Myr North American leaf-wax compound-specific carbon and hydrogen isotope record: implications for C4 grasslands and hydrologic cycle dynamics. *Earth Planetary Science Letters*. 299. Pp. 250–262.
- Tipple, B.J., Berke, M.A., Doman, C.E., Khachatryan, S. and Ehleringer, J.R. (2013). Leaf-wax n-alkanes record the plant-water environment at leaf flush. *PNAS*. 110(7). Pp. 2659-2664.
- Trenberth, K. (1999). Atmospheric Moisture Recycling: Role of Advection and Local Evaporation. *Journal of Climate*. 12. Pp. 1368–1381.
- Trouet, V., Esper, J., Graham, N.E., Baker, A., Scourse, J.D. and Frank, D.C. (2009). Persistent Positive North Atlantic Oscillation Mode Dominated the Medieval Climate Anomaly. *Science*. 324. Pp. 78-80.
- Trouet, V., Esper, J., Graham, N.E., Baker, A., Scourse, J.D. and Frank, D.C. (2009). Persistent Positive North Atlantic Oscillation Mode Dominated the Medieval Climate Anomaly. *Science*. 324. Pp. 78-80.
- Tue, N.T., Hamaoka, H., Sogabe, A., Quy, T.D., Nhuan, M.T., Omori, K. (2011). The application of $\delta^{13}\text{C}$ and C/N ratios as indicators of organic carbon sources and

paleoenvironmental change of the mangrove ecosystem from Ba Lat Estuary, Red River, Vietnam. *Environmental Earth Science*. 64. Pp. 1475-1486.

Turney, C.S.M., Bird, M.I., Fifield, L.K., Kershaw, A.P., Cresswell, R.G., Santos, G.M., di Tada, M.L., Hausladen, P.A. and Youping, Z. (2001). Development of a robust ¹⁴C chronology for Lynch's Crater (North Queensland, Australia) using different pretreatment strategies. *Radiocarbon*. 43. Pp. 45–54.

Uppenbrink, J. (1999). Climate variability – the North Atlantic Oscillation. *Science*. 283(5404). Pp. 948-949.

Väliranta, M., Korhola, A., Seppä, H., Tuittila, E-S., Sarmaja-Korjonen, K., Laine, J. and Alm, J. (2007). High-resolution reconstruction of wetness dynamics in a southern boreal raised bog, Finland, during the late Holocene: a quantitative approach. *The Holocene*. 17. Pp. 1093–1107.

Van Breukelen, M.R., Vonhof, H.B., Hellstrom, J.C., Wester, W.C.G. and Kroon, D. (2008). Fossil dripwater in stalagmites reveals Holocene temperature and rainfall variation in Amazonia. *Earth and Planetary Science Letters*. 275. Pp. 54-60.

Van Wesenbeeck, B.K., van Mourik, T., Duivenvoorden, J.F. and Cleef, A.M. (2003). Strong effects of a plantation with *Pinus patula* on Andean subparamo vegetation: a case study from Colombia. *Biological Conservation*. 114. Pp. 207-218.

Vardy, S.R., Warner, B.G., Turunen, J. and Aravena, R. (2000). Carbon accumulation in permafrost peatlands in the Northwest Territories and Nunavut, Canada. *The Holocene*. 10. Pp. 273–280.

Vera, C., Higgins, W., Amador, J., Ambrizzi, T., Garreaud, R., Gochis, D., Gutzler, D., Lettenmaier, D., Marengo, J., Mechoso, C.R., Nogues-Paegle, J., Silva Diaz, P.L. and Zhang, C. (2006). Towards a unified view of the American Monsoon System. *Journal of Climate*. 19. Pp. 4977–5000.

Victoria, R., Martinelli, L.A., Mortatti, J. and Richley, J. (1991). Mechanisms of water recycling in the Amazon Basin: isotopic insights. *AMBIO A Journal of the Human Environment*. 20(8). Pp. 384-387.

Viera, S., Barbosa de Camargo, P., Selhorst, D. et al. (2004). Forest structure and carbon dynamics in Amazonian tropical rainforests. *Ecosystem Ecology*. 140. Pp. 468-479.

- Villacís, M., Vimeux, F. and Taupin, J.D. (2008). Analysis of the climate controls on the isotopic composition of precipitation ($\delta^{18}\text{O}$) at Nuevo Rocafuerte, 74.5°W, 0.9°S, 250m, Ecuador. *Comptes Rendus Geoscience*. 340(1). Pp. 1–9.
- Villadiego, K. and Velay-Dabat, M.A. (2014). Outdoor thermal comfort in a hot and humid climate of Colombia: A field study in Barranquilla. *Building and Environment*. 75. Pp. 142-152.
- Villar, J.C.E., Ronchail, J., Guyot, J.L., Cohonneau, G., Naziano, F., Lavado, W., De Oliveira, E., Pombosa, R. and Vauchel, P. (2009). Spatio-temporal rainfall variability in the Amazon basin countries (Brazil, Peru, Bolivia, Colombia, and Ecuador). *International Journal of Climatology*. 29. Pp. 1574-1594.
- Vimeux, F., Gallaire, R., Bony, S., Hoffmann, G., Chiang, J. and Fuertes, R. (2005). What are the climate controls on isotopic composition (δD) of precipitation in Zongo Valley (Bolivia)? Implications for the Illimani ice core interpretation. *Earth Planetary Science Letters*. 240. Pp. 205–220.
- Vimeux, F., Tremoy, G., Risi, C. and Gallaire, R. (2011). A strong control of the South American SeeSaw on the intra-seasonal variability of the isotopic composition of precipitation in the Bolivian Andes. *Earth and Planetary Science Letters*. 307. Pp. 47-58.
- Virapongse, A., Endress, B.A., Gilmore, M.P., Horn, C. and Romulo, C. (2017). Ecology, livelihoods, and management of the *Mauritia flexuosa* palm in South America. *Global Ecology and Conservation*. 10. Pp. 70-92.
- Visbeck, M.H., Hurrell, J.W., Polvani, L. and Cullen, H.M. (2001). The North Atlantic Oscillation: Past, present, and future. *PNAS*. 98(23) pp. 12876-12877.
- Vitt, D., Wieder, R., Halsey, L., and Turetsky, M. (2003). Response of *Sphagnum fuscum* to nitrogen deposition: a case study of ombrogenous peatlands in Alberta, Canada. *The Bryologist*. 106. Pp. 235–245.
- Vizy, E.K. and Cook, K.H. (2007). Relationship between Amazon and high Andes rainfall. *Journal of Geophysical Research*. 112. D07107.
- Vogts, A., Badewien, T., Rullkotter, J. and Schefuss, E. (2016). Near-constant apparent isotope fractionation between leaf-wax *n*-alkanes and precipitation in tropical regions: evidence from a marine sediment transect off SW Africa. *Organic Geochemistry*. 96. Pp. 18-27.

Vogts, A., Schefuss, E., Badewien, T. and Rullkotter J. (2012). *n*-Alkane parameters from a deep-sea sediment transect off southwest Africa reflect continental vegetation and climate conditions. *Organic Geochemistry*. 47. Pp. 109–119.

Vuille, M and Werner, M. (2005). Stable isotopes in precipitation recording South American summer monsoon and ENSO variability: Observations and model results. *Climate Dynamics*. 25 (4). Pp. 401–413.

Vuille, M. and Keimig, F. (2004). Interannual variability of summertime convective cloudiness and precipitation in the central Andes derived from ISCCP-B3 data. *Journal of Climate*. 17. Pp. 3334–3348.

Vuille, M., Bradley, R.S., Werner, M., Hardy, D.R., Thompson, L.G. and Keimig, F. (2003). Modeling $\delta^{18}\text{O}$ in precipitation over the tropical Americas: 2. Simulation of the stable isotope signal in Andean ice cores. *Journal of Geophysical Research*. 108(6). doi:10.1029/2001JD002039.

Vuille, M., Burns, S.J., Taylor, B.L., Cruz, F.W., Bird, B.W., Abbott, M.B., Kanner, L.C., Cheng, H. and Novello, V.F. (2012). A review of the South American Monsoon history as recorded in stable isotopic proxies over the past two millennia. *Climate of the Past Discussions*. 8. Pp. 637–668.

Walker, M., Johnsen, S., Rasmussen, S.O., Popp, T., Steffensen, J.P., Gibbard, P., Hoek, W., Lowe, J., Andrews, J., Björck, S., Cwynar, L. C., Hughen, K., Kershaw, P., Kromer, B., Litt, T., Lowe, D.J., Nakagawa, T., Newnham, R. and Schwander, J. (2009). Formal definition and dating of the GSSP (Global Stratotype Section and Point) for the base of the Holocene using the Greenland NGRIP ice core, and selected auxiliary records. *Journal of Quaternary Science*. 24. Pp. 3–17.

Walker, M.J.C., Berkelhammer, M., Björck, C., Cwynar, D., Fisher, D.A., Long, A.J. and Lowe, J.J. (2012). Formal subdivision of the Holocene Series/Epoch: a Discussion Paper by a Working Group of INTIMATE (Integration of ice-core, marine and terrestrial records) and the Subcommittee on Quaternary Stratigraphy (International Commission on Stratigraphy). *Journal of Quaternary Science*. 27. (7). Pp. 649-659.

Wang, M., Zhang, W. and Hou, J. (2015). Is average chain length of plant lipids a potential proxy for vegetation, environment and climate changes? *Biogeosciences Discuss*. 12. Pp. 5477-5501.

- Wang, X., Auler, A.S., Edwards, L.R., Cheng, H., Cristalli, P.S., Smart, P.L., Richards, D.A. and Shen, C-C. (2004). Wet periods in northeast Brazil over the past 210 kyr linked to distant climate anomalies. *Nature*. 432. Pp. 740–743.
- Wang, Y.V., Larsen, T., Leduc, G., Andersen, N., Blanz, T. and Schneider, R.R. (2013). What does leaf wax δD from a mixed C₃/C₄ vegetation region tell us?. *Geochimica et Cosmochimica Acta*. 111. Pp. 128–139.
- Weijers, J.W.H., Schouten, S., Schefuss, E. et al. (2009). Disentangling marine, soil and plant organic carbon contributions to continental margin sediments: A multi-proxy approach in a 20,000 year sediment record from the Congo deep-sea fan. *Geochimica et Cosmochimica Acta*. 73. Pp. 119-132.
- Wellock, M.L., Reidy, B., Laperle, C.M., Bolger, T. and Kiely, G. (2011). Soil organic carbon stocks of afforested peatlands in Ireland. *Forestry*. 84(4). Pp. 441-451.
- Wershaw, R.L., Friedman, I. and Heller, S.J. (1966). Hydrogen isotope fractionation in water passing through trees. In: Hobson, F., Speers, M. (Eds.). *Advances in Organic Geochemistry*. Pergamon, New York, pp. 55–67.
- Werth, M. and Kuzyakov, Y. (2010). ¹³C fractionation at the root-microorganisms-soil interface: a review and outlook for partitioning studies. *Soil Biology and Biochemistry*. 42. Pp. 1372–1384.
- West, A.G., February, E.C. and Bowen, G.J. (2014). Spatial analysis of hydrogen and oxygen stable isotopes (“isoscapes”) in ground water and tap water across South Africa. *Journal of Chemical Exploration*. 145. Pp. 213-222.
- West, J.B., Bowen, G.J., Cerling, T.E. and Ehleringer, J.R. (2006). Stable isotopes as one of nature's ecological recorders. *Trends in Ecology and Evolution*. 21. Pp. 408–414.
- West, J.B., Sobek, A. and Ehleringer, J.R. (2008). A Simplified GIS Approach to Modeling Global Leaf Water Isoscapes. *PLoS ONE*. 3(6). 2447. doi:10.1371/journal.pone.0002447.
- Wetherald, R.T. and Manabe, S.J. (1988). Cloud feedback processes in a general circulation model. *Journal of Atmospheric Science*. 45. Pp. 1397-1415.
- Winnick, M. J., Chamberlain, C.P., Caves, J.K. and Welker J.M. (2014). Quantifying the isotopic ‘continental effect’. *Earth and Planetary Science Letters*. 406. Pp. 123–133.

- Woodin, S.J. and Lee, J.A. (1987). The fate of some components of acidic deposition in ombrotrophic mires. *Environmental Pollution*. 45. Pp. 61–72.
- Worden, J., Noone, D., Bowman, K. et al. (2007). Importance of rain evaporation and continental convection in the tropical water cycle. *Nature*. 445. Pp. 528-532.
- Xia, Z.H., Xu, B.Q., Mugler, I., Wu, G.J., Gleixner, G., Sachse, D. and Zhu, L.P. (2008). Hydrogen isotope ratios of terrigenous *n*-alkanes in lacustrine surface sediment of the Tibetan Plateau record the precipitation signal. *Geochemistry Journal*. 42. Pp. 331–338.
- Xie, S., Guo, J., Huang, J. et al. (2004). Restricted utility of $\delta^{13}\text{C}$ of bulk organic matter as a record of paleovegetation in some loess-paleosol sequences in the Chinese Loess Plateau. *Quaternary Research*. 62. Pp. 86-93.
- Xie, S., Nott, C.J., Avsejs, L.A., Volders, F., Maddy, D., Chambers, F.M., Gledhill, A., Carter, J.F. and Evershed, R.P. (2000). Palaeoclimate records in compound-specific δD values of a lipid biomarker in ombrotrophic peat. *Organic Geochemistry*. 31. Pp. 1053–1057.
- Xie, S-P., Tanimoto, Y., Noguchi, H. and Matsuno, T. (1999). How and why climate variability differs between the tropical Atlantic and Pacific. *Geophysical Research Letters*. 26 (11). Pp. 1609-1612.
- Yang, H., Liu, W., Leng, Q. et al. (2011). Variation in *n*-alkane dD values from terrestrial plants at high latitude: Implications for paleoclimate reconstruction. *Organic Geochemistry*. 42. Pp. 283-288.
- Yao, Y. and Liu, W. (2014). Hydrogen isotopic composition of plant leaf wax in response to soil moisture in an arid ecosystem of the northeast Qinghai-Tibetan Plateau, China. *Journal of Arid Landscapes*. 6(5). Pp. 592-600.
- Yoneyama, T., Muraoka, T., Murakami, T. and Boonkerd, N. (1993). Natural abundance of ^{15}N in tropical plants with emphasis on tree legumes. *Plant and Soil*. 153. Pp. 295–304.
- Yoon, J. and Zeng, N. (2010). An Atlantic influence on Amazon rainfall. *Climate Dynamics*. 34. Pp. 249-264.
- Zeng, N., Yoon, J.H., Marengo, J.A., Subramaniam, A., Nobre, C.A., Mariotti, A. and Neelin, J.D. (2008). Causes and impacts of the 2005 Amazon drought. *Environmental Research Letters*. 3. Pp. 1-9.

Zhang, Y., Chiessi, C.M., Mulitza, S., Sawakuchi, A.O., Haggi, C., Zabel, M., Portilho—Ramos, R.C., Schefuss, E., Crivellari, S. and Wefer, G. (2017). Different precipitation patterns across tropical South America during Heinrich and Dansgaard-Oeschger stadials. *Quaternary Science Reviews*. 177. Pp. 1-9.

Zhang, Y., Chiessi, C.M., Mulitza, S., Sawakuchi, A.O., Haggi, C., Zabel, M., Portilho-Ramos, R.C., Schefuss, E., Crivellari, S. and Wefer, G. (2017). Different precipitation patterns across tropical South America during Heinrich and Dansgaard-Oeschger stadials. *Quaternary Science Reviews*. 177. Pp. 1-9.

Zhang, Y., Zhang, X., Chiessi, C.M., Mulitza, S., Zhang, X., Lohmann, G. et al. (2016). Equatorial Pacific forcing of western Amazonian precipitation during Heinrich Stadial 1. *Nature Scientific Reports*. 6(35866). Doi: 10.1038/srep35866.

Zhou, W., Zheng, Y., Meyers, P.A., Jull, A.J.T. and Xie, S. (2010). Postglacial climate-change record in biomarker lipid compositions of the Hani peat sequence, Northeastern China. *Earth and Planetary Science Letters*. 294. (1-2). Pp. 37-46.

Zwiers, F. and Karin, V. (1998). Changes in the extremes of climate simulated by CCC GMC2 under CO₂ doubling. *Journal of Climate*. 11. Pp. 2200-2222.